UNIVERSIDAD COMPLUTENSE DE MADRID

FACULTAD DE CIENCIAS QUÍMICAS
DEPARTAMENTO DE QUÍMICA ORGÁNICA I

TESIS DOCTORAL

Bioinspired electroactive supramolecular ensembles

Ensamblajes supramoleculares electroactivos bioinspirados

MEMORIA PARA OPTAR AL GRADO DE DOCTOR

PRESENTADA POR

Braulio Alberto Insuasty Chamorro

DIRECTORES

Nazario Martín León
Carmen María Atienza Castellanos

Madrid, 2017

UNIVERSIDAD COMPLUTENSE DE MADRID
FACULTAD DE CIENCIAS QUÍMICAS
Departamento de Química Orgánica I

BIOINSPIRED ELECTROACTIVE SUPRAMOLECULAR ENSEMBLES

ENSAMBLAJES SUPRAMOLECULARES ELECTROACTIVOS BIOINSPIRADOS

TESIS DOCTORAL

Braulio Alberto Insuasty Chamorro

MADRID, 2015

UNIVERSIDAD COMPLUTENSE DE MADRID
FACULTAD DE CIENCIAS QUÍMICAS
Departamento de Química Orgánica I

BIOINSPIRED ELECTROACTIVE SUPRAMOLECULAR ENSEMBLES

ENSAMBLAJES SUPRAMOLECULARES ELECTROACTIVOS BIOINSPIRADOS

Directores:

Prof. Nazario Martín León
Dra. Carmen Mª Atienza Castellanos

Memoria que para optar al grado de
DOCTOR EN CIENCIAS QUÍMICAS
Presenta

Braulio Alberto Insuasty Chamorro

MADRID, 2015

D. Nazario Martín León, Catedrático de Universidad del Departamento de Química Orgánica de la Universidad Complutense de Madrid, y **Dña. Carmen Mª Atienza Castellanos**, Investigadora Ramón y Cajal del Departamento de Química Orgánica de la Universidad Complutense de Madrid.

CERTIFICAN

Que la presente Memoria titulada "BIOINSPIRED ELECTROACTIVE SUPRAMOLECULAR ENSEMBLES" se ha realizado bajo su dirección en el Departamento de Química Orgánica de la Facultad de Ciencias Químicas de la Universidad Complutense de Madrid, por el Licenciado en Ciencias Químicas D. Braulio Alberto Insuasty Chamorro y autorizan su presentación para ser calificada como Tesis Doctoral.

Y para que conste firmo el presente certificado en Madrid a 14 de octubre de 2015.

Fdo. Dr. Nazario Martín León   Fdo. Dra. Carmen Mª Atienza Castellanos

Some of the results discussed within this thesis have been published in the following papers:

J. L. López, C. Atienza, A. Insuasty, J. López-Andarias, C. Romero-Nieto, D. M. Guldi and N. Martín "Concave vs Planar Geometries for the Hierarchical Organization of Mesoscopic 3D Helical Fibers" *Angew. Chem. Int. Ed.* **2012**, *51*, 3857-3861.

A. Insuasty, C. Atienza , J. L. López, J. Marco-Martínez1, S. Casado, A. Saha, D. M. Guldi and N. Martín "Supramolecular One-Dimensional n/p-Nanofibers" *Sci. Rep.* **2015**, *5*, 14154.

A. Insuasty, C. Atienza, J. L. López, N. Martín "Supramolecular pentapeptide-based fullerene nanofibers: effect of molecular chirality" *Chem. Commun.* **2015**, *51*, 10506-10509.

During the PhD, some of the results have been shown in scientific congresses and schools:

Toledo-Spain, 2011. The 1st Simposium on "Carbon Nanoforms" (Oral presentation).

Madrid-Spain, 2013. 3rd Early Stage Researchers Workshop-IMDEA Nanoscience (Oral presentation).

Santander-Spain, 2013. XXXIV Reunión Bienal de la Real Sociedad Española de Química (Oral presentation).

Madrid-Spain, 2013. Symposium on Carbon Nanoforms-IMDEA Nanoscience.

Madrid-Spain, 2014. Simposio Internacional: "Química: respuestas para un mundo mejor".

Madrid-Spain, 2015. 16th International Symposium on Novel Aromatic Compounds - ISNA-16 (2 Posters, Organizing Committee).

A mis padres
y a mi hermano

Abbreviations and acronyms

In addition to the standard abbreviations and acronyms in organic chemistry (as defined by the *J. Org. Chem.* Author Guidelines) the following terms have been used in this thesis:

AFM	Atomic force microscopy
Boc	*tert*-butoxycarbonyl
CD	Circular dichroism
DRC	Dendron rodcoil
DIPEA	*N,N*-Diisopropylethylamine
DSSC	Dye sensitized solar cells
exTTF	9,10-Di(1,3-dithiol-2-ylidene)-9,10-dihydroanthracene
Fmoc	9-Fluorenylmethoxycarbonyl
HBC	Hexabenzocoronene
HBTU	*O*-(benzotriazol-1-yl)-*N,N,N',N'*-tetramethyluronium hexafluorophosphate
HMTA	Hexamethylenetetramine
HOPG	Highly ordered pyrolytic graphite
HRTEM	High Resolution Transmission electron microscopy
ICD	Induced circular dichroism
MBHA	4-Methylbenzhydrylamine
MCH	Methylcyclohexane
NBS	*N*-Bromosuccinimide
NDI	Naphthalenediimide
TCE	1,1,2,2-Tetrachloroethane
TCNQ	Tetracyano-*p*-quinodimethane
TEG	Triethylene glycol
oPVs	Oligo(*p*-phenylenevinylene)s
PAs	Peptide Amphiphiles

PCBM	[6,6]-Phenyl-C_{61}-butyric acid methyl ester
PCC	Pyridinium chlorochromate
SEM	Scanning electron microscopy
STM	Scanning tunneling microscopy
SWNTs	Single-walled nanotubes
TFA	Trifluoroacetic acid
TEM	Transmission electron microscopy
XRD	X-ray diffraction

Table of contents

Summary

BIOINSPIRED ELECTROACTIVE ELECTROACTIVE ENSEMBLES

Introduction

In the 20th century, science and technology have enormously progressed with strong impact in the style and quality of human life. Nowadays, nanoscience and nanotechnology offer the new avenue for the development of new smart and applicable materials of ultra-small size (in the range of 1-100nm) (Figure S1).
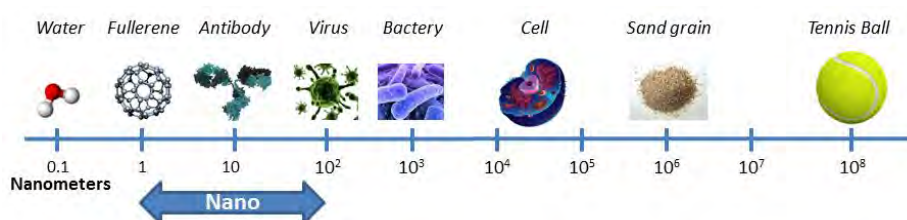
Figure S1. Size scale showing the range of what the word "*nano*" implies.

Thanks to the small size of nanomaterials, they can easily interact with biomolecules either on the cell's surface or inside them; as a consequence, these materials represent promising alternatives to detect and treat diseases in such a way that was unthinkable in a recent past. In order to achieve these nanomaterials, chemists have resorted to the *bottom-up* approach which consists in the self-assembly of small molecules that serves as scaffolds for the construction of nanostructures with tailored sizes, forms and properties.

In this context, the present thesis is framed on the study of bioinspired electroactive molecules that self-assemble giving rise to new functional nanomaterials. For this end, a variety of peptides functionalized with electroactive units such as π-extended TTF (exTTF), C_{60} and porphyrins were studied.

Objectives and results

Concave vs planar geometries for the hierarchical organization of mesoscopic helical fibers

As objective we planned the use of exTTF as electroactive non-planar unit, functionalized with a pentapeptide sequence for the growth of new supramolecular nanostructures at different length scales. Furthermore, a comparison with related but planar moieties aimed to determine morphological consequences was performed (Figure S2).
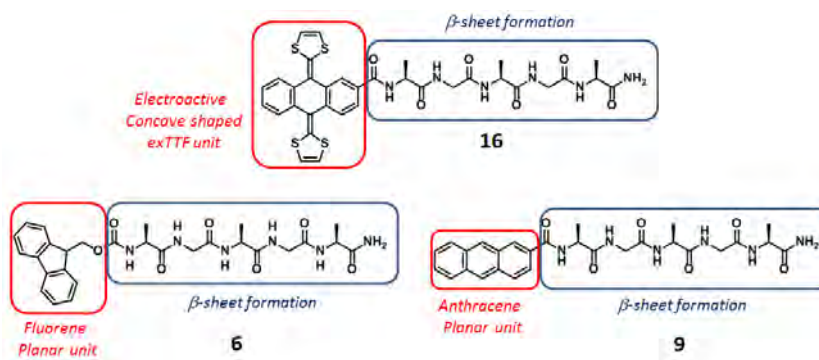
Figure S2. Pentapeptide derivatives based on exTTF, fluorene and anthracene moieties.

In TCE, planar derivatives (**6** and **9**) self-assemble by means of H-bonds and $\pi-\pi$ interactions into nanospheres or sheets (Figure S3 A-B), while exTTF derivative (**16**) self-assembles exclusively by H-bonds into a network of long chiral nanofibers with helical features (Figure S3 C). Importantly, exTTFs are not interacting with each other in the secondary structure.

In CHCl$_3$/MCH, the subsequent self-assembly of the secondary structure into a tertiary structure by means of a solvophobic collapse, gives rise to straight fibers in the case of planar derivatives and, helical mesostructures for the exTTF derivative **16** (Figure S3 B-C).
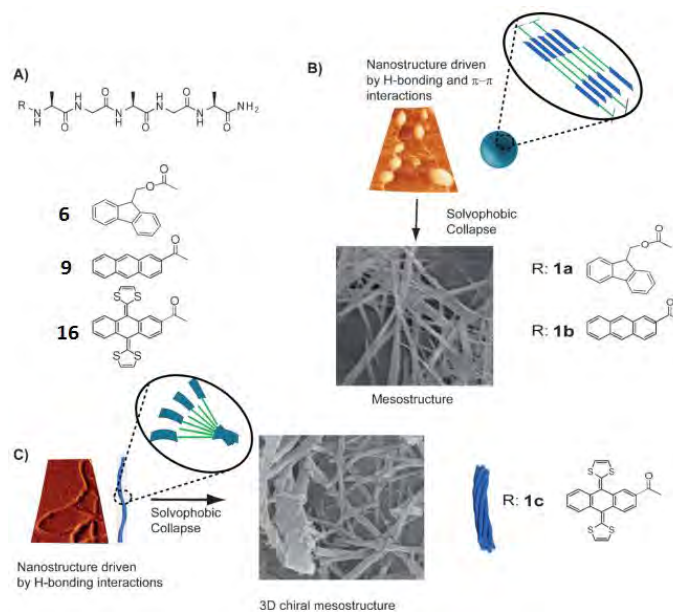
Figure S3. (A) Chemical structures of compounds **6**, **9** and **16**. Proposed models (B and C) of the supramolecular architectures.

Supramolecular one dimensional n/p nanofibers

Inspired by the results of the previous systems, we proposed the formation of 1D *n/p* nanohybrids. For this end, we combined our described exTTF-nanofibers **16** with electron acceptor molecules such as fullerene C_{60} and PCBM (Figure S4).
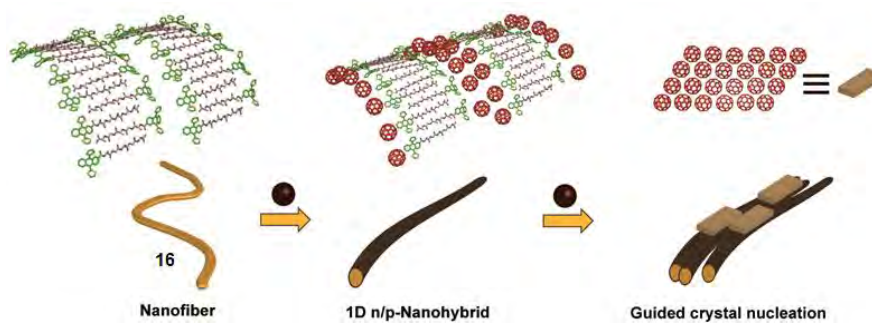
Figure S4. Schematic representation of nanohybrid formation and further crystal nucleation.

We found that the use of supramolecular exTTF nanofibers in TCE, in which exTTFs are not interacting between them, has led to the efficient formation of 1D n/p-nanohybrids through the concave-convex interaction between exTTFs and C_{60} units. Morevover, the high tendency of C_{60} to aggregate favors the evolution from an initial state, in which close packed columns of C_{60}/PCBM are intercalated between exTTF-fibers, into a final state, where the C_{60}/PCBM crystalize onto n/p-nanohybrids.

Supramolecular pentapeptide-based fullerene nanofibers: effect of molecular chirality

As objective we proposed the construction of fullerene nanofibers based on the use of pentapeptide moieties. Moreover, explore the effects on fiber's morphology stemming from the use of chiral and achiral pentapeptides linked to a PCBM moiety (compounds **24** and **25**) as well as the decrease in distance from the fullerene moiety to the β-sheet domain (compounds **24** and **29**, Figure 5S).
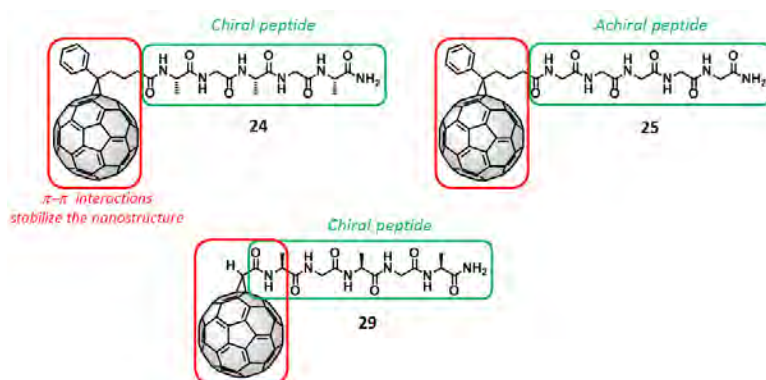
Figure S5. Molecular structures of compounds **24**, **25** and **29**.

We found that the these molecules can self-assemble in a mixture of TCE:DMSO giving rise to nanofibers stabilized through H-bonds along with $\pi-\pi$ interactions between C_{60} units (Figure S6). A study over nanofiber's morphology showed that there is a correlation between the nanofibers obtained and chirality of the peptide. Thus, using

a chiral peptide gives rise to twisted fibers, while the use of an achiral peptide with the same C_{60} moiety gives rise to straight fibers instead.
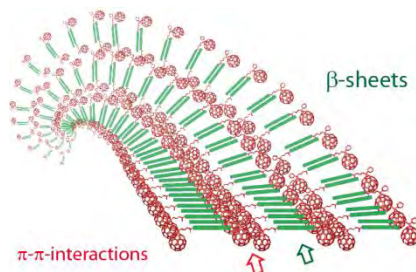
Figure S6. Proposed model of the supramolecular architecture.

Furthermore, we found that there is a correlation between the nanofibers and the distance from the peptide backbone and the C_{60} moiety. Thus, a short distance gives rise to straight, rigid and more aggregated fibers, while a larger distance affords twisted fibers instead.

Supramolecular porphyrin-C_{60} peptide dyads: morphology and chiral induction effects

We focused on study the formation of supramolecular porphyrin-C_{60} peptide dyads through strong hydrogen bonds interactions between a carboxylate-amidinium pair varying the peptide length (Figure S7).
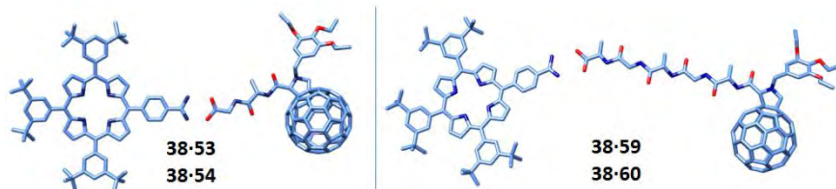
Figure S7. Supramolecular porphyrin-C_{60} dyads.

The study of supramolecular dyads in $CHCl_3$ showed that the formation of the amidinium-carboxylate pair was efficiently achieved. This interaction gives rise to an induced circular dichroic (ICD) signal that in the case of dipeptide complexes is mainly affected by the chiral center over the fulleropyrrolidine, while in the case of

pentapeptide complexes the ICD is mainly affected by the alanine units closer to the amidinium-carboxylate pair.

The study of supramolecular dyads in MCH showed that besides of the formation of the amidinium-carboxylate pair, $\pi-\pi$ interactions were also involved. In the case of dipeptide complexes such $\pi-\pi$ interactions occur between porphyrin and C_{60} units in an antiparallel fashion, while in the case of pentapeptide complexes such interactions are probably given, in one side, between porphyrin units, and in the other side, between C_{60} moieties like in a parallel fashion (Figure S8).

Figure S8. Schematic representation of supramolecular dipeptide (**38·53** and **38·54**) and pentapeptide (**38·59** and **38·60**) complexes in MCH.

Conclusions

This work has demonstrated how useful peptides are in order to create new nanostructures. Their high tendency to form β-sheets through H-bonds gives rise to very stables supramolecular architectures. In this sense, it has been demonstrated that the functionalization of the same peptide sequence with planar or non-planar units has considerable implications in the nanostructure obtained.

Moreover, we demonstrated that it is possible to create 1D *n/p* nanohybrids formed by the concave-convex interaction between exTTF and C_{60} units.

Furthermore, we observed that for a same fullerene moiety, peptide's chirality plays a critical role in the nanostructure obtained. In a similar way, for a same peptide

sequence which differs in distance to the fullerene unit, notably consequences can be noted.

Finally, we observed that for our supramolecular porphyrin-C_{60} peptide dyads, changing the solvent from $CHCl_3$ to MCH it is possible to favor $\pi-\pi$ interactions between the electroactive units with notable changes in morphology.

Resumen

ENSAMBLAJES SUPRAMOLECULARES ELECTROACTIVOS BIOINSPIRADOS

Introducción

En el siglo XX, la ciencia y la tecnología han progresado enormemente con una repercusión significativa en el estilo y calidad de vida humana. Hoy en día, la nanociencia y la nanotecnología ofrecen una nueva vía para el desarrollo de nuevos materiales inteligentes y aplicables de tamaño ultra-pequeño (en el intervalo de 1-100 nm) (Figura S1).
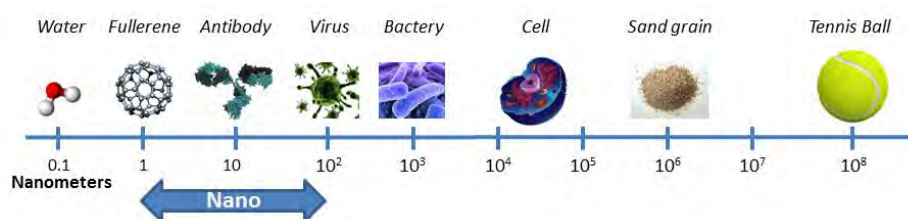
Figura S1. Escala de tamaño dando una idea de lo que la palabra "*nano*" implica.

Gracias al tamaño de los nanomateriales, estos pueden interactuar fácilmente con biomoléculas ya sea en la superficie de la célula o dentro de ellas; como consecuencia, estos materiales representan alternativas prometedoras para detectar y tratar enfermedades de una forma que, en un pasado reciente, era impensable. Con el propósito de obtener estos nanomateriales, los químicos han recurrido a la aproximación *bottom-up* que consiste en el auto-ensamblaje de moléculas pequeñas sintetizadas por métodos químicos convencionales, y que se emplean como bloques de construcción en la obtención de nanoestructuras con determinados tamaños, formas y propiedades.

En este contexto, la presente tesis se enmarca en el estudio de moléculas electroactivas bioinspiradas que se auto-ensamblan a nivel de la nanoescala dando lugar a la formación de nuevos nanomateriales funcionales. Para este fin, una

variedad de péptidos funcionalizados con moléculas electroactivas tales como TTF π-extendido (exTTF), C_{60} y porfirinas han sido estudiadas.

Objetivos y Resultados

Geometría cóncava vs plana para la organización jerárquica de fibras helicoidales mesoscópicas.

Como objetivo nos planteamos el uso del exTTF como unidad electroactiva no plana, funcionalizada con una secuencia pentapeptídica, para el crecimiento de nuevas arquitecturas supramoleculares a diferentes escalas de longitud. Además, se planteó llevar cabo un estudio comparativo sobre el efecto que produce en la morfología de las estructuras formadas el uso de unidades planas y no planas (Figura S2).
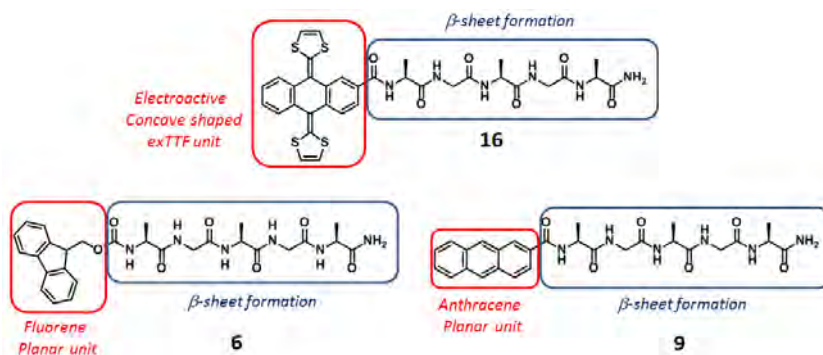
Figura S2. Derivados de pentapéptido basados en exTTF, fluoreno y antraceno.

En TCE, los derivados planos (**6** y **9**) se auto-ensamblan mediante enlaces de hidrógeno e interacciones $\pi-\pi$ formando nanoesferas u hojas (Figura S3 A-B), mientras que el derivado de exTTF (**16**) se autoensambla exclusivamente por medio de enlaces de hidrógeno en una red de nanofibras quirales con características helicoidales (Figura S3 C). Es importante destacar que, las unidades de exTTFs no están interactuando entre sí en la estructura secundaria.

En $CHCl_3$/MCH, se produce un colapso solvofóbico dando lugar a un auto-ensamblaje superior de la estructura secundaria en una estructura terciaria, proporcionando

fibras rectas en el caso de los derivados planos (**6** y **9**) y, mesoestructuras helicoidales para el derivado de exTTF **16** (Figura S3 B-C).
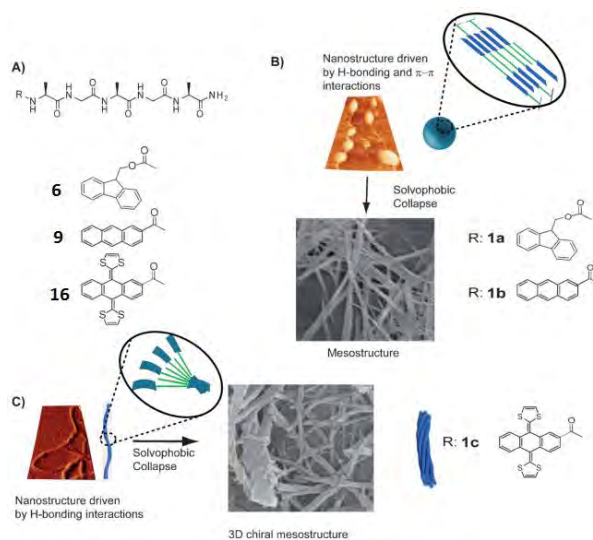
Figura S3. (A) Estructuras químicas de los compuestos **6**, **9** y **16**. (B) y (C) Modelos propuestos para las arquitecturas supramoleculares.

Nanofibras n/p supramoleculares en una dimensión

Inspirados por los resultados de los sistemas anteriores, nos propusimos la formación nanohíbridos 1D de tipo *n/p*. Para este fin, combinamos nuestras nanofibras de exTTF **16** con moléculas aceptoras de electrones como fullereno C_{60} y PCBM (Figura S4).
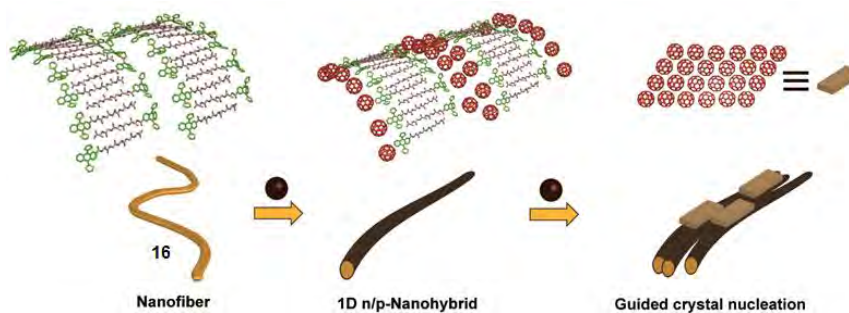
Figura S4. Representación esquemática de la formación del nanohíbrido y posterior nucleación cristalina sobre el nanohíbrido.

En este trabajo encontramos que el uso de nanofibras supramoleculares de exTTF en TCE, donde las unidades de exTTF no están interactuando entre ellas, lleva a la formación eficiente de nanohíbridos 1D de tipo *n/p* a través de la interacción cóncava-convexa entre las unidades de exTTF y C_{60}. De hecho, la gran tendencia del C_{60} a agregarse favorece la evolución desde un estado inicial, en el que columnas empaquetadas de C_{60}/PCBM están intercaladas entre las fibras de exTTF, hasta un estado final, donde el C_{60}/PCBM cristaliza sobre el nanohíbrido (Figura S4).

Nanofibras supramoleculares basadas en pentapéptidos: Efecto de la quiralidad molecular

Como objetivo nos planteamos la construcción de nanofibras basadas en fullereno mediante el uso de la secuencia peptídica previamente utilizada. En este caso, nos interesó explorar los efectos sobre la morfología de la fibra derivada del uso de pentapéptidos quirales y aquirales unidos a una unidad de PCBM (compuestos **24** y **25**, Figura S5), asi como el uso de un sistema flexible y uno más rígido, acortando la distancia entre la subunidad de fullereno y la lámina β (compuestos **24** y **29**, Figura S5).
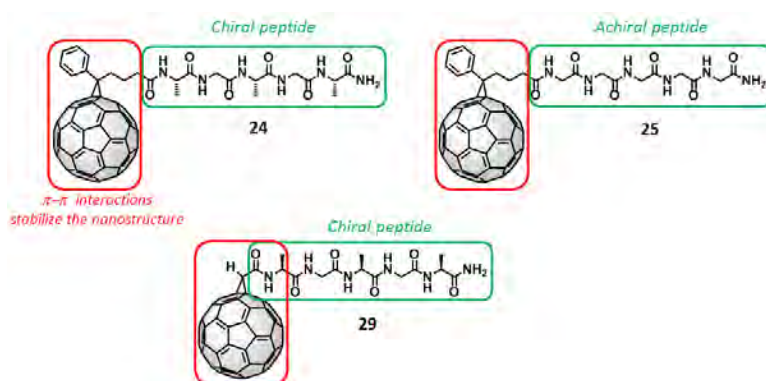
Figura S5. Estructuras moleculares de los compuestos **24**, **25** y **29**.

En esta parte encontramos que los derivados de fullereno se auto-ensamblan en una mezcla de disolventes de TCE:DMSO dando lugar a la formación de nanofibras que se

16

estabilizan a través de enlaces de hidrógeno junto con interacciones $\pi-\pi$ entre unidades de C_{60} (Figura S6). Un estudio sobre la morfología de las nanofibras demostró que existe una correlación entre las nanofibras obtenidas y quiralidad del péptido. Así pues, utilizando un péptido quiral se obtuvo fibras retorcidas, mientras que el uso de un péptido aquiral con la misma unidad de C_{60} dio lugar a fibras rectas.
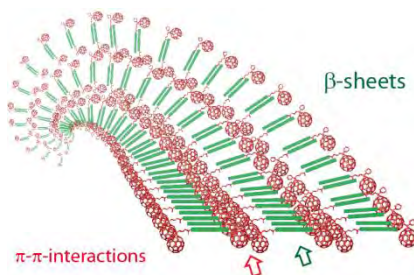
Figura S6. Modelo propuesto de la arquitectura supramolecular.

Además, observamos que existe una correlación entre las nanofibras y la distancia entre la cadena peptídica y la unidad de C_{60}. Se ha demostrado que, a una distancia corta se obtiene fibras rectas, rígidas y más agregadas, mientras que en el caso de una más grande proporciona fibras retorcidas.

Díadas supramoleculares de porfirina-C_{60} con péptidos: efectos en morfología e inducción quiral

En este trabajo nos planteamos el estudio de la formación de diadas supramoleculares de porfirina-C_{60} con péptidos a través de fuertes enlaces de hidrógeno entre el par amidinio-carboxilato variando la longitud del péptido (Figura S7).
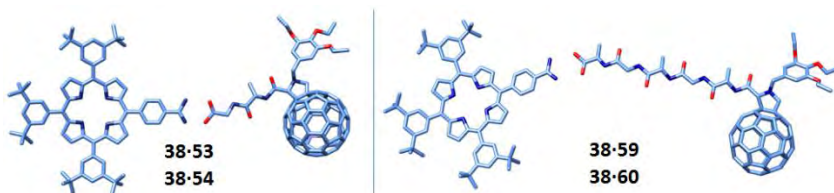
Figura S7. Diadas supramoleculares de porfirina-C_{60}.

El estudio de díadas supramoleculares en $CHCl_3$ mostró que la formación del par amidinio-carboxilato se logró de manera eficiente. Esta interacción da lugar a una señal dicroica circular inducida (DCI) que en el caso de los complejos de dipéptido se ve afectada principalmente por el centro quiral sobre la fulleropirrolidina, mientras que en el caso de los complejos de pentapéptido la DCI es afectada principalmente por la unidad de alanina más cercana al par amidinio-carboxilato.

El estudio de las díadas supramoleculares en MCH mostró que, además de la formación del par amidinio-carboxilato, también están involucradas interacciones $\pi-\pi$. En el caso de los complejos de dipéptido dichas interacciones se producen entre las unidades de porfirina y C_{60} de una manera antiparalela, mientras que en el caso de los complejos de pentapéptidos estas interacciones se dan, probablemente, entre las unidades de porfirina por un lado, y entre las unidades de C_{60} por el otro, de manera paralela (Figura S8).
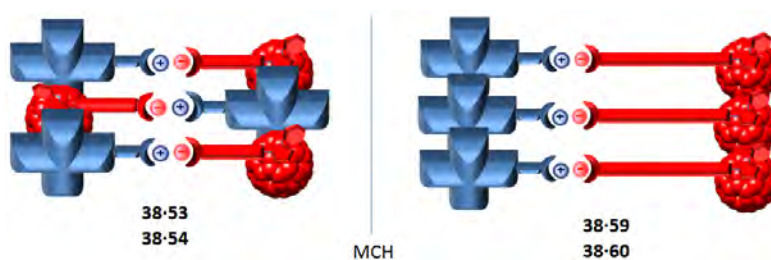
Figura S8. Representación esquemática de los complejos supramoleculares de dipéptido (**38·53** y **38·54**) y pentapéptido (**38·59** y **38·60**) en MCH.

Conclusiones

Este trabajo ha demostrado la utilidad de los péptidos para crear nanostructuras nuevas. Su tendencia a formar láminas β a través de enlaces de hidrógeno da lugar a arquitecturas supramoleculares muy estables. En este sentido, se ha demostrado que la funcionalización de la misma secuencia peptídica con unidades planas y no planas tiene considerables implicaciones en la nanoestructura obtenida.

Por otra parte, hemos demostrado que es posible crear nanohíbridos 1D de tipo *n/p* formados a partir de interacciones cóncava-convexa entre las unidades de exTTF y C_{60}.

Asimismo, se observó que para una unidad de fullereno, la quiralidad del péptido desempeña un papel crítico en la nanoestructura obtenida. De manera similar, una misma secuencia peptídica que difiere en distancia a la unidad de fullereno, puede dar lugar a consecuencias destacables.

Finalmente, se observó que para nuestras díadas supramoleculares de porfirina-C_{60} con péptidos, al cambiar el disolvente de $CHCl_3$ a MCH es posible favorecer interacciones $\pi-\pi$ entre las unidades electroactivas con cambios notables en la morfología obtenida.

1. Introduction

1. INTRODUCTION

The world has witnessed the tremendous progress undergone by science and technology during the 20th century as well as their strong impact in the style and quality of human life. The question that emerges in this new century is what is it coming up next? How further is it possible to go? The answer seems to be related with size and, in this sense, the word "*nano*" takes a relevant significance in the new promising branches of science: *Nanoscience and Nanotechnology*.

"*Nano*" is essentially referred to something ultra-small, a billionth part of a meter. In this regard, *Nanoscience* could be defined as the study of the performance of ultra-small structures, materials or devices usually in the range of 1-100 nm (Figure 1.1). Similarly, *Nanotechnology* could be considered as the creation of functional materials at nanometer scale.
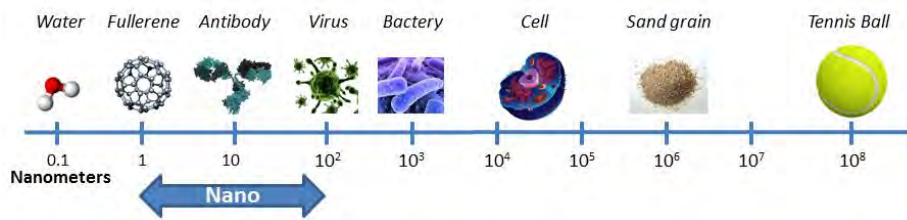
Figure 1.1 Size scale showing the range of what the word "*nano*" implies.

Nanotechnology is nowadays applied in any imaginable field, that is, electronics, magnetics, optics, information technology, materials development, biomedicine, among others. Thanks to the small size of nanomaterials, they can easily interact with biomolecules either on the cell's surface or inside them; as a consequence, these materials represent promising alternatives to detect and treat diseases in such a way that was unthinkable in a recent past.

In this regard, *Nanotechnology* strongly depends on the conversion of different areas such as chemistry, biology, physics and engineering; branches of science which are getting closer and closer moving to the field of the nanoscale (Figure 1.2).
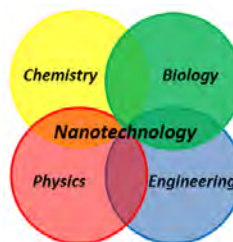
Figure 1.2 Nanotechnology as interdisciplinary science.

In order to achieve these nanomaterials, two different approaches can be distinguished:

- *Top-down* approach which consists in the creation of smaller devices by scaling down pieces of matter; this concept is more related to physicist and engineers that look for the manipulation of smaller pieces by lithographic techniques and related ones.
- *Bottom-up* approach which consists in the self-assembly of small molecules synthesized by conventional chemical methods, and that serves as scaffolds in the construction of nanostructures with tailored sizes, forms and properties (Figure 1.3). This concept is more related to chemists due to their ability to manipulate atoms and molecules; therefore chemists are in a perfect position for the development of *Nanotechnology* through this approach.
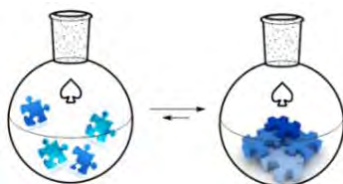
Figure 1.3 *Bottom-up* approach.

Traditionally, chemistry has worked out of the field of the construction of nanostructures. However, in last years, the huge advance of electron microscopy

techniques has let to chemists the self-assembly study of simple molecules under different conditions. In fact, during the last decade, the number of articles and patents related to *Nanotechnology* has increased exponentially. This abrupt behavior has been classified as the beginning of the third industrial revolution. The consequences of these new technologies will transform industries and subsequently society, in turn cheap energy, as well as improves in detection, prevention and treatment of new diseases will be developed. The wide spectrum of *Nanotechnology* applications will produce a social change and an increase in quality of life.

It is worth to note that the current technological development in the field of *Nanoscience* requires innovative materials; in this sense, *nature* presents infinity of biomolecular complexes performing lots of functions with considerable efficiencies. Thus, inspired by nature, scientists have designed new organic materials aimed to their use in a variety of applications. In this regard, photosynthesis is one of the representative examples that humans are trying to imitate. This process leads to near-unity charge separation quantum yield at ambient temperatures, becoming it the perfect machine to convert sunlight into chemical energy. As such, many attempts using biomolecules or bioinspired molecules are nowadays at the forefront of research (Figure 1.4).

Other examples such as the incorporation of a pigment-protein complex photosystem in photovoltaic devices (Figure 1.4 A)[1], the use of DNA in combination with nanomaterials (Figure 1.4 B)[2] or the employment of peptide nanostructures in regenerative medicine (Figure 1.4 C),[3] stem all inspired by nature to reach functional materials with similar effectiveness.

[1] A. Mershin, K. Matsumoto, L. Kaiser, D. Yu, M. Vaughn, M. K. Nazeeruddin, B. D. Bruce, M. Graetzel, S. Zhang, *Sci. Rep.* **2012**, *2*, 234-240.
[2] J. Liu, *Phys. Chem. Chem. Phys.* **2012**, *14*, 10485-10496.
[3] J. Boekhoven, S. I. Stupp, *Adv. Mater.* **2014**, *26*, 1642-1659.
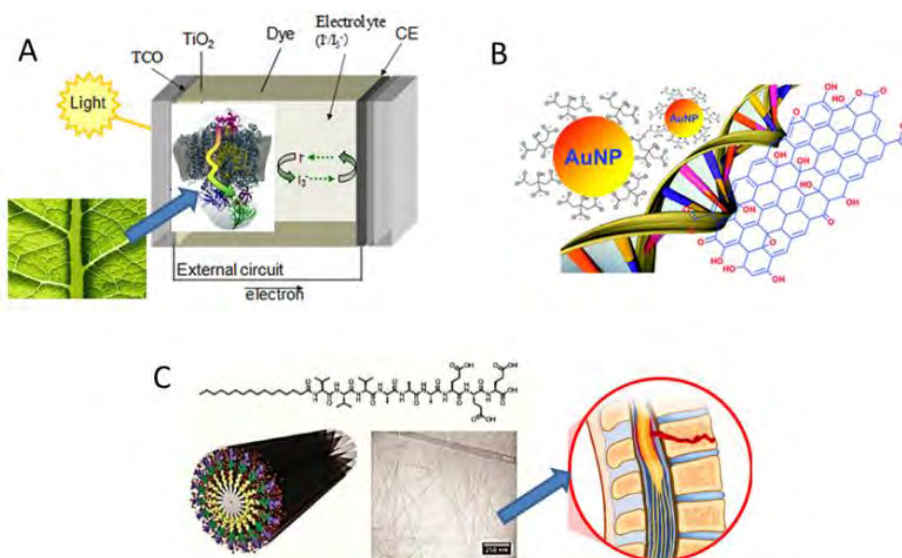
Figure 1.4 Bioinspired materials in nanotechnology applications.

The present thesis is framed in this context and focuses on the study of bioinspired electroactive molecules that self-assemble in the range of the nanoscale to create functional nanomaterials. Thus, the use of modern synthetic techniques has allowed the preparation of new molecules able to form more complex structures at the nanoscale by following the principles of supramolecular chemistry. Furthermore, the use of sophisticated spectroscopic and microscopic techniques as well as fluorescence and X-ray diffraction have allowed the thorough characterization of the created assembles.

2. Background

2. BACKGROUND

2.1. SUPRAMOLECULAR CHEMISTRY

While traditional organic chemistry focuses on the formation of covalent bonds, supramolecular chemistry goes beyond and explores weaker and reversible/non-covalent interactions between molecules. Such interactions comprise van der Waals forces, $\pi-\pi$ interactions, hydrogen bonds, electrostatic interactions, metal-ligand coordination and mechanical bonds. All these weak forces let the molecules interact between them in such a way that is necessary to talk about a new branch of chemistry called *supramolecular chemistry*. A concept that although had been perceived along the beginning of modern chemistry, was not defined until the early 90s by the Nobel Prize Jean-Marie Lehn as the "…chemistry beyond the molecule…"[4,5] (Scheme 2.1).
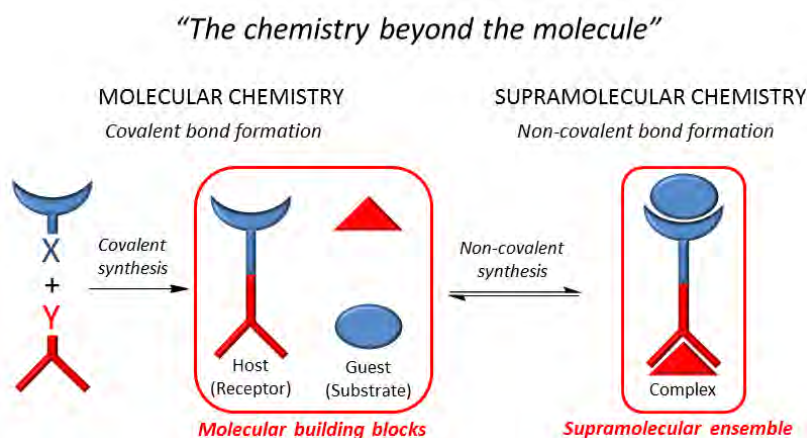
Scheme 2.1. Molecular chemistry and supramolecular chemistry.

---

[4] J.-M. Lehn, *Angew. Chem. Int. Ed.* **1990**, *29*, 1304-1319.

[5] a) J.-M. Lehn, *Supramolecular Chemistry. Concepts and Perspectives*, Wiley-VCH, Weinheim, **1995**; b) J.-M. Lehn, J. L. Atwood, J. E. D. Davies, D. D. Macnicol, F. Vögtle, *Comprehensive Supramolecular Chemistry, Vol. 1-11*, Pergamon/Elsevier, Oxford, **1996**; c) P. D. Beer, P. A. Gale, D. K. Smith, *Supramolecular Chemistry*, Oxford University Press, Oxford, **1999**; d) J. W. Steed, J. L. Atwood, *Supramolecular Chemistry*, 2nd ed., John Wiley & Sons, Wiltshire, **2009**; e) N. Martín, J.-F. Nierengarten, *Supramolecular Chemistry of Fullerenes and Carbon Nanotubes*, Wiley-VCH, Weinheim, **2012**; f) J. W. Steed, P. A. Gale, *Supramolecular Chemistry: From Molecules to Nanomaterials*, John Wiley & Sons, **2012**; g) C. A. Schalley, *Analytical Methods in Supramolecular Chemistry*, 2nd ed., Wiley-VCH, Weinheim, **2012**.

Supramolecular non-covalent forces were firstly described by van der Waals in 1873,[6] but it was not until 1894 when Fischer suggested that enzyme-substrate interactions would take the form of "*lock and key*",[7] seminal contribution which gave rise to a concept that seeded the supramolecular chemistry's philosophical roots. Later, pioneer scientific works describing the hydrogen bond,[8] allowed the non-covalent interactions to be understood in more detail. Eventually, the use of these principles led to a better understanding of protein structure and other biological processes such as the double helix of DNA which is strongly stabilized by means of hydrogen bonds.[9]

The aforementioned groundbreaking concepts paved the way to the creation of new systems such as crown ethers,[10] cryptands[11] and spherands,[12] compounds which were synthesized by Pedersen, Lehn and Cram, respectively, and that were awarded with the Nobel Prize in 1987 for the development of molecules with structure-specific interactions of high selectivity (Figure 2.1). More recently, a variety of complex and interesting systems such as catenanes or molecular knots developed by Sauvage[13] or the Borromean rings by Stoddart,[14] have also been synthesized. All these molecules have become benchmarks in supramolecular chemistry (Figure 2.1).

[6] J. D. van der Waals, *Over de Continuiteit van den Gas- en Vloeistoftoestand*, PhD thesis, Leiden, **1873**.

[7] E. Fischer, *Ber. Deutsch. Chem. Ges.* **1894**, *27*, 2985-2993.

[8] a) T. S. Moore, T. F. Winmill, *J. Chem. Soc., Trans.* **1912**, *101*, 1635-1676; b) W. M. Latimer, W. H. Rodebush, *J. Am. Chem. Soc.*, **1920**, *42*, 1419–1433.

[9] J. W. Watson, F. H. C. Crick, *Nature* **1953**, *171*, 737-738.

[10] C. J. Pedersen, *J. Am. Chem. Soc.* **1967**, *89*, 7017-7036.

[11] B. Dietrich, J. M. Lehn, J. P. Sauvage, *Tetrahedron Lett.* **1969**, *10,* 2885-2888.

[12] D. J. Cram, T. Kaneda, R. C. Helgeson, G. M. Lehn, *J. Am. Chem. Soc.* **1979**, *101*, 6752-6754.

[13] M. Cesario, C. O. Dietrich-Buchecker, J. Guilhem, C. Pascard and J. P. Sauvage, *Chem. Commun.* **1985**, 244-247.

[14] K. S. Chichak, S. J. Cantrill, A. R. Pease, S.-H. Chiu, G. W. V. Cave, J. L. Atwood, J. F. Stoddart, *Science* **2004**, *304*, 1308-1312.

Crown ether

Pedersen, **1967**

Cryptand

Lehn, **1969**

Spherand

Cram, **1979**

Catenane

Sauvage, **1985**

Borromean ring

Stoddart, **2004**
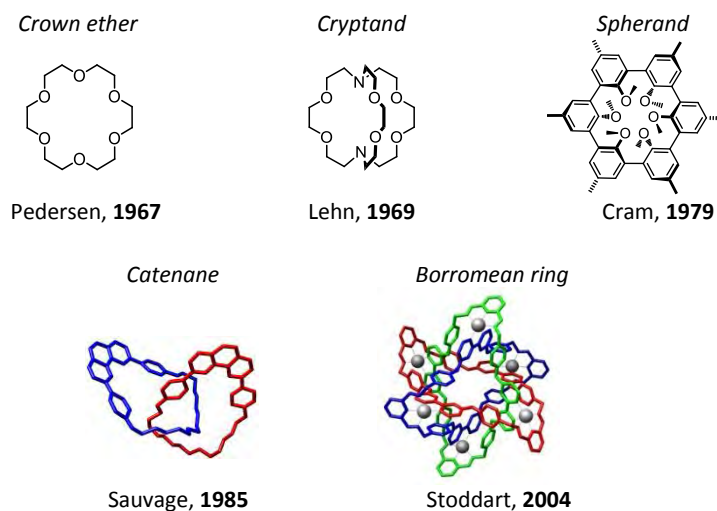
Figure 2.1 Benchmark molecules in supramolecular chemistry.

The study of supramolecular interactions is fundamental for the comprehension of several biological processes since living systems make extensive use of non-covalent forces for structure and function. In cell cytoskeleton, for instance, long ordered filaments of protein monomers form (fold) and depolymerize (unfold) dynamically for vital cell function.

2.2 SUPRAMOLECULAR POLYMERS OF ORGANIC MATERIALS

During the second half of 20th century, organic materials were obtained mainly from covalent polymerization chemistry, especially after acceptance of the Staudinger's hypothesis about macromolecules.[15] However, at the beginning of 21st century, based on the broad amount of literature concerning organic materials, their construction especially relied on the use of supramolecular chemistry and self-assembling as efficient tools to give rise to new organic materials at different length scales.[16] In this sense, pioneer works of J. M. Lehn gave rise to the concept of supramolecular chemistry and its relation to functional structures.[4] Subsequently, Whitesides developed the concept of self-assembly of molecules for the construction of nanoscale structures[17] and Samuel Stupp led the concept of *self-assembly* of designed molecules for functional materials in bulk.[18] In this regard, *molecular self-assembly* could be defined as the process in which ordered or patterned systems are obtained by spontaneous association of monomers through non-covalent interactions. These monomers should be properly designed in order to give rise to their spontaneous association.

From molecular self-assembly stems a new field, that is, "*supramolecular polymers*"; this focuses on the generation of ordered 1D nanostructures which have found a broad variety of applications with highly promising results.[16] In this context, there are at least two types of supramolecular polymers based on their formation mechanisms:[19]

- In one side, there are *random-coil supramolecular polymers* which do not present any internal order or structure. These polymers resemble to normal

[15] H. Staudinger, *Berichte der deutschen chemischen Gesellschaft* **1920**, *53*, 1073-1085.

[16] T. Aida, E. W. Meijer, S. I. Stupp, *Science* **2012**, *335*, 813-817.

[17] a) G. Whitesides, J. P. Mathias, C. T. Seto, *Science* **1991**, *254*, 1312-1319; b) C. T. Seto, G. Whitesides, *J. Am. Chem. Soc.* **1993**, *115*, 905-916.

[18] a) S. I. Stupp, S. Son, H. C. Lin, L. S. Li, *Science* **1993**, *259*, 59-63; b) S. I. Stupp, V. LeBonheur, K. Walker, L. S. Li, K. E. Huggins, M. Keser, A. Amstutz, *Science* **1997**, *276*, 384-389.

[19] a) T. F. A. De Greef, M. M. J. Smulders, M. Wolffs, A. P. H. J. Shenning, R. P. Sijbesma, E. W. Meijer, *Chem. Rev.* **2009**, *109*, 5687-5754; b) Z. Chen, A. Lohr, C. R. Saha-Moller, F. Würthner, *Chem. Soc. Rev.* **2009**, *38*, 564-584.

covalent polymers and are formed by an isodesmic polymerization, that is, each monomer interacts with another one with the same association constant, similar to a stepwise polymerization of macromolecules characterized by a high polydispersity (Figure 2.2).

- In the other side, there are *ordered supramolecular polymers* which present ordered internal structures and determined shapes. These polymers are formed, in contrast, by a nucleation-elongation (cooperative) mechanism, that is, a non-favored thermodynamic process forms a nucleus that further grows with a higher association constant affording a higher degree of polymerization with less polydispersity (Figure 2.2).
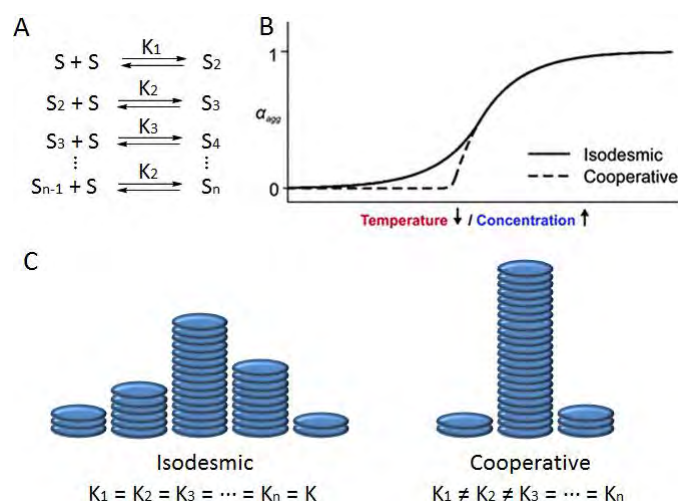
Figure 2.2 A) General scheme of the formation of a supramolecular polymer showing successive equilibrium constants. B) Schematic representation showing the degree of polymerization as a function of temperature and concentration in isodesmic or cooperative polymerizations. C) Schematic representation of polydispersity and degree of polymerization according to the type of mechanism and relation between constants of the successive equilibria.

In a supramolecular polymer, when the lifetime, τ, of non-covalent bonds that hold together the monomers is too short ($\tau < 1$ μs) a permanent polymer does not form, while a long life time ($\tau > 1$ min) generates materials without interesting dynamic behavior. However, within a medium range (1 μs $< \tau < 1$ min) new properties arise, such as, adaptability, sensibility, self-repair, novel recycling possibilities, ease of

biodegradation, among others.[20] Hence, due to the non-covalent/reversible nature of bonds and in contrast to covalent polymers, supramolecular polymers permit the access to a variety of interesting properties with astonishing new functions and persistence.[16,21,22]

Taking into account the non-covalent forces that govern the self-assembly, supramolecular polymers might have physical properties resembling to those of covalent polymers. An example of the latter is a polymer obtained by Meijer *et al.* using ureidopyrimidone derivatives, whose stabilization is governed by a quadrupole hydrogen bonding motif (Figure 2.3, left).[23] The unidirectional design of the binding sites prevents uncontrolled multidirectional polymerization. Moreover, the addition of end capping molecules (Figure 2.3, left and middle) lead to the formation of polymers with virtual molecular weights of 500.000 Daltons. This approach gives rise to a random-coil supramolecular polymer (Figure 2.3, right) that behaves as macromolecules with mechanical properties similar to covalent polymers at room temperature and low viscosity when heated.

Figure 2.3 Ureidopyrimidone end capping molecules (left and middle) added upon linear polymerization (right).

However, the importance of obtaining 1D structures with internal structure is of key importance since interesting properties can emerge from them. In this sense, in the context of organic materials, some examples of 1D assemblies are described from now on. In close similarity to the above mentioned molecules bearing strong donor-

[20] P. Cordier, F. Tournilhac, C. Soulié-Ziakovic, L. Leibler, *Nature* **2008**, *451*, 977-980.

[21] J. Hill, W. Jin, A. Kosaka, T. Fukushima, H. Ichihara, T. Shimonura, K. Ito, T. Hashizume, N. Ishii, T. Aida, *Science* **2004**, *304*, 1481-1483.

[22] S. I. Stupp, C. Palmer, *Chem. Mater*. **2014**, *26*, 507-518.

[23] R. P. Sijbesma, F. H. Beijer, L. Brunsveld, B. J. Folmer, J. H. Hirschberg, R. F. Lange, J. K. Lowe, E. W. Meijer, *Science* **1997**, *278*, 1601-1604.

acceptor H-bonding motifs of small molecules, it is possible to obtain 1D nanostructures with ureido-s-triazine derivatives. Meijer *et al.* synthesized a series of hydrogen-bonded oligo(*p*-phenylenevinylene)s (oPVs) composed by long aliphatic chains, chiral side chains and ureido-s-triazine H-bonding motif (Figure 2.4 A).[24] These compounds form firstly hydrogen-bonded dimers that further stacks by $\pi-\pi$ interactions between oPVs moieties, giving rise to cylindrical nanostructures with a defined helicity due to the chiral chains (Figure 2.4, A to C). Concentration and temperature studies showed that stability of the nanostructures formed increases with the conjugation length due to more favored $\pi-\pi$ interactions.
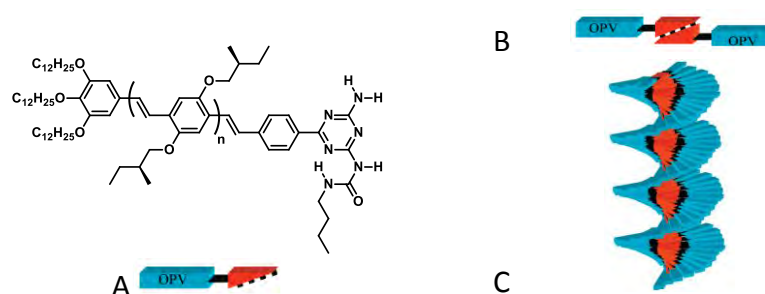
Figure 2.4 Oligo(*p*-phenylenevinylene)s (left, A) forming a dimer through H-bonds (B) and the subsequent $\pi-\pi$ stacking forming nanostructures with induced helicity (C).

Further studies of these nanostructures showed that upon irradiation efficient energy transfer from shorter to longer oligomers can take place in.[25] Moreover, the rate of the energy transfer of these compounds can be controlled by chromophore arrangements. Studies using ordered and disordered oPVs assemblies showed that fast energy transfer occurred within ordered assemblies, while energy transfer dynamics for disordered assemblies occurred in longer time scales assigned to weak electronic coupling between chromophore moieties.[26] Due to the interesting

[24] P. Jonkheijm, F. J. M. Hoeben, R. Kleppinger, J. van Herrikhuyzen, A. P. H. J. Schenning, E. W. Meijer, *J. Am. Chem. Soc.* **2003**, *125*, 15941-15949.

[25] F. J. M. Hoeben, L. M. Herz, C. Daniel, P. Jonkheijm, A. P. H. J. Schenning, C. Silva, S. C. J. Meskers, D. Beljonne, R. T. Phillips, R. H. Friend, E. W. Meijer, *Angew. Chem. Int. Ed.* **2004**, *43*, 1976-1979.

[26] F. J. M. Hoeben, A. P. H. J. Schenning, E. W. Meijer, *ChemPhysChem* **2005**, *6*, 2337-2342.

properties that emerge from ordered patterns, a great variety of interesting systems comprising oPVs has been studied.[27]

Other interesting approach which indeed emerges at the early stage of 1D nanostructures attainment, consisted of designed molecules with a dendritic domain located at the end of a rod segment, referred as dendron rodcoil (DRC, Figure 2.5-left).[28] Stupp *et al.* found that these molecules could self-assemble giving rise to nanoribbons as shown in figure 2.5. The driving force for the formation of these structures relies on the head-to-head hydrogen-bonds between dendrons and $\pi-\pi$ interactions between the rod (aromatic) segments of molecules (Figure 2.5, middle). These molecules form consistent gels which usually suggest the formation of 1D assemblies creating 3D networks (Figure 2.5, right). However, a systematical study with slight modifications in each DRC part showed that gelation process could be dramatically affected. For instance, bigger dendrons hinder the self-assembly and molecules remain soluble. In the same line, the length of rod segments affects dramatically the self-assembly: the presence of only one biphenyl ester unit do not lead to the formation of a gel and two units give rise to a weak one, while three or four units form consistent gels. Furthermore, different coils (alkyl end chains), such as diblock coils gives high solubility and gel formation is not achieved. In a similar way, the lack of a coil generates an amorphous insoluble material.
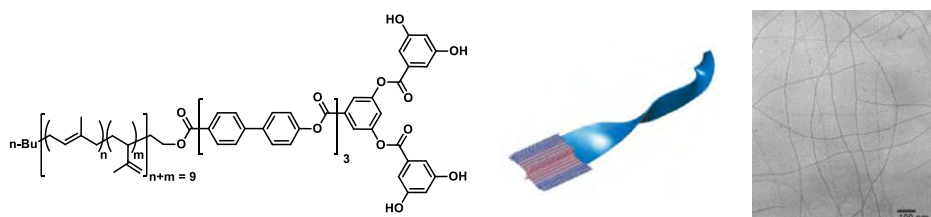
Figure 2.5 Dendron rodcoil structure (left), self-assembly (middle) and transmission electron microscopy (TEM) image (scale bar = 100 nm) showing the fibers obtained upon self-assembly.

In order to introduce functionality into the system, chemical modifications can be performed. Such modifications consist in changing the rod aromatic biphenyl ester for

[27] V. K. Praveen, C. Ranjith, E. Bandini, A. Ajayaghosh, N. Armaroli, *Chem. Soc. Rev.* **2014**, *43*, 4222-4242.
[28] E. R. Zubarev, M. U. Pralle, E. D. Sone, S. I. Stupp, *J. Am. Chem. Soc.* **2001**, *123*, 4105-4106.

oPVs or oligothiophene groups, giving rise to systems that show much higher conductivity in the assembled state when compared to the conductivity obtained in the unassembled state.[29] Again, highly ordered systems result in the generation of new and interesting properties and, therefore, these findings reveal the importance of creating 1D nanostructures.

Some other interesting examples of supramolecular polymers are based on extended π-conjugated motifs which let to achieve high charge mobilities. In this sense, Aida *et al.* worked with hexabenzocoronene (HBC) (molecular graphene) functionalizing it, on one side with triethylene glycol (TEG) chains and dodecyl chains in the other, giving to the molecule a marked amphiphilic nature (Figure 2.6).[21,30] In polar media, these molecules self-assemble into hollow nanotubes with a wall thickness of 3 nm which is assigned to the formation of a bilayer wall whose interior and exterior surfaces consist of hydrophilic triethylene glycol chains (see Figure 2.6). Furthermore, these nanotubes showed an electrical conductivity of 2.5 megaohms across a 180-nm-gap electrode, demonstrating its promising applications as conductive materials.
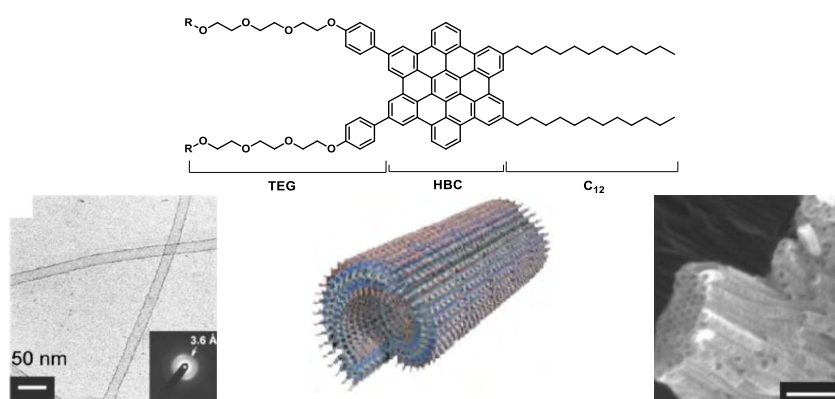
Figure 2.6 Molecular structure of hexabenzocoronene derivative (top). Cartoon showing the self-assembly (bottom-middle). Transmission electron microscopy (TEM) image (below-left) and scanning electron microscopy (SEM) image (bottom-right) showing the hollow nanotubes upon HBC self-assembly. (Scale bar in SEM image: 100 nm).

[29] B. W. Messmore, J. F. Hulvat, E. D. Sone, S. I. Stupp, *J. Am. Chem. Soc.* **2004**, *126*, 14452-14458.

[30] a) W. Jin, T. Fukushima, A. Kosaka, M. Niki, N. Ishii, T. Aida, *J. Am. Chem. Soc.* **2005**, *127*, 8284-8285; b) W. Zhang, W. Jin, T. Fukushima, A. Saeki, S. Seki, T. Aida, *Science* **2011**, *334*, 340-343.

It has been observed that the introduction of a chiral center at the end of TEG chains gives nanotubes with one-handed helicity highlighting the versatility of these systems.[31] Further studies of these graphitic nanotubes and similar derivatives showed that these self-assembled molecules can be easily processed using a glass hook producing macroscopic fibers (few centimeters) where the nanotubes are aligned unidirectionally along the fibers axis. The subsequent doping with iodine displayed a clear anisotropic conduction in the oriented self-assembled material.[32]

Taking advantage of the high order within the self-assembled molecules in the HBC nanotubes, it is possible to create photoconductive materials by introducing electron acceptor moieties at the end of TEG chains (Figure 2.6, top). In such materials, it is very important to have ordered donor and acceptor arrays with the aim that the photogenerated holes and electrons travel efficiently toward the electrodes through the ordered donor and acceptor domains. In this sense, HBC nanotubes functionalized with electron acceptor units such as trinitrofluorenone give rise to highly ordered coaxial *n/p* heterojunctions.[33] The nanotubes formed consist then in a molecular layer of the electron acceptor trinitrofluorenone laminating an electron donor HBC graphitic layer. The coaxial nanostructure allows the photogeneration of spatially separated charge carriers and fast photoconductive response. Other electron acceptor units such as fullerene can be also implemented giving rise to coaxial *n/p* heterojunctions as well. Such structures showed an ambipolar charge-carrier transport profile and displayed a photovoltaic response upon light irradiation (this example will be discussed further in section 2.4.1).[34]

A very important approach in supramolecular polymers relies on the use of peptides. Stupp pioneered this approach discovering a class of peptide amphiphiles (PAs) that

[31] W. Jin, T. Fukushima, M. Niki, A. Kosaka, N. Ishii, T. Aida, *Proc. Natl. Acad. Sci.* **2005**, *102*, 10801-10806.
[32] Y. Yamamoto, T. Fukushima, W. Jin, A. Kosaka, T. Hara, T. Nakamura, A. Saeki, S. Seki, S. Tagawa, T. Aida, *Adv. Mater.* **2006**, *18*, 1297-1300.
[33] Y. Yamamoto, T. Fukushima, Y. Suna, N. Ishii, A. Saeki, S. Seki, S. Tagawa, M. Taniguchi, T. Kawai, T. Aida, *Science* **2006**, *314*, 1761-1764.
[34] Y. Yamamoto, G. Zhang, W. Jin, T. Fukushima, N. Ishii, A. Saeki, S. Seki, S. Tagawa, T. Minari, K. Tsukagoshi, T. Aida, *Proc. Natl. Acad. Sci.* **2009**, *106*, 21051-21056.

can self-assemble to generate 1D nanostructures in water.[35] PAs consist of a lipid-like hydrophobic segment (e.g. palmitoyl, Figure 2.7 A1) covalently linked to the N-terminus of a charged peptide segment with high tendency to form β-sheets as secondary structure (Figure 2.7 B). In water, upon charge screening (pH-dependent) these molecules self-assemble into cylindrical micelles in which the alkyl chains are packed in the center of the cylinder leaving the peptide segment in contact with the aqueous environment. The self-assembly is driven by the hydrophobic collapse of the alkyl chains together with the hydrogen bonding interactions through the peptide sequences giving rise to high aspect ratio nanofibers with defined diameters and lengths up to micrometers (Figure 2.7 B). Furthermore, this molecule is able to direct mineralization of hydroxyapatite along the nanofibers (Figure 2.7 C). For this end, the molecule's design is explained in terms of the following features: *i*) fibers must be robust; thus, four consecutive cysteine units are placed in the peptide sequence leading the possibility of a covalent linkage through the formation of disulfide bonds upon oxidation (Figure 2.7 A2) *ii*) glycine units give flexibility to the hydrophilic head group from the rigid cross-linked region (cysteine units) (Figure 2.7 A3) *iii*) phosphorylated serine residue interacts strongly with calcium ions and helps to direct mineralization of hydroxyapatite (Figure 2.7 A4) *iv*) for biomedical applications, fibers should be able to promote the adhesion and growth of cells on their surfaces, process which is promoted by the sequence Arg-Gly-Asp (Figure 2.7 A5). The authors found that upon effective crystallization over the fibers, the c axes of hydroxyapatite crystals are co-aligned with the long axes of the fibers (see Figure 2.7 C).[35] This phenomenon is also observed between collagen fibrils and hydroxyapatite crystals in bone.

[35] J. D. Hartgerink, E. Beniash, S. I. Stupp, *Science* **2001**, *294*, 1684-1688.
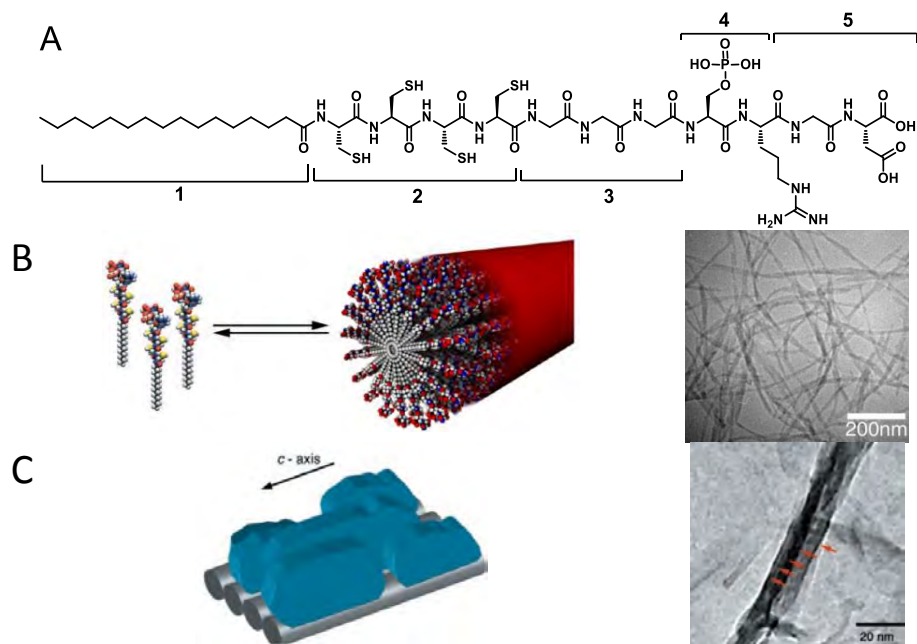
Figure 2.7 Molecular structure of peptide amphiphile (A). Cartoon of self-assembly of PAs in water at a pH below 4 and TEM image showing the fibers obtained (B). Cartoon and TEM image showing the oriented hydroxyapatite crystals along the fibers axes (C).

On the basis of the presented chemical structure for PAs, changes in the peptide sequences can be made in order to obtain defined bio-specific functions. In this regard, PAs materials have shown to be highly bioactive in events such as regeneration of axons in injured spinal cord,[36] the growth of blood vessels[37] and the regeneration of bone and cartilage.[38,39] For instance, epitope IKVAK can be incorporated into the peptide sequence giving rise to bioactive supramolecular nanofibers. This hydrophilic epitope is known to play a key role in signaling neurons, as such, these supramolecular nanofibers were used as a therapy in a mouse model of

[36] V. M. Tysseling-Mattiace, V. Sahni, K. L. Niece, D. Birch, C. Czeisler, M. G. Fehlings, S. I. Stupp, J. A. Kessler, *J. Neurosci.* **2008**, *28*, 3814-3823.

[37] K. Rajangam, H. A. Behanna, M. J. Hui, X. Han, J. F. Hulvat, J. W. Lomasney, S. I. Stupp, *Nano Lett.* **2006**, *6*, 2086-2090.

[38] A. Mata, Y. Geng, K. J. Henrikson, C. Aparicio, S. R. Stock, R. L. Satcher, S. I. Stupp, *Biomaterials* **2010**, *31*, 6004-6012.

[39] R. N. Shaha, N. A. Shahc, M. M. Del Rosario Lim, C. Hsieha, G. Nubere, S. I. Stupp, *Proc. Natl. Acad. Sci.* **2010**, *107*, 3293-3298.

spinal cord injury.[36] The results showed that these bioactive nanofibers displaying high densities of neuroactive epitopes on their surfaces, helped to inhibit glial scar formation and promote regeneration after injury. In fact, authors described that these densities are reduced by nanofiber bundling, lowering the effective concentration of bioactive epitopes on the surface. In this sense, bundling can be suppressed by electrostatic repulsions among the nanofibers with the incorporation of charged aminoacids such as glutamic acid (E) in the region between the β-sheet aminoacid sequence (VVAA) and the epitope region (IKVAK) (Figure 2.8).[40]

Palmitoyl-VVAA-**EE**-GIKVAV-COOH   Palmitoyl-VVAA-**EEEE**-GIKVAV-COOH
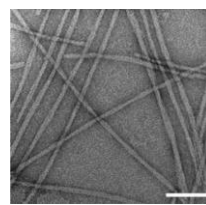
Figure 2.8 TEM images showing bundling of fibers upon incorporation of glutamic acid units (scale bars = 100 nm).
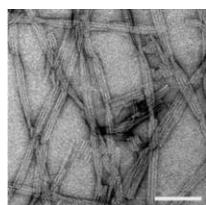
The role of hydrogen bonding in PAs was evaluated studying the effects of N-methylating the amide nitrogens at each glycine (G) position of a defined PA sequence (C_{16}-GGGGGGG-ERGDS).[41] Results showed that even a small *N*-methyl group notably affects the nanostructures obtained. Such effects have stronger impact as the *N*-methylations occur close to the core, that is, the alkyl C_{16} chain. In a similar way, a PA (C_{16}-GVVVAAAEEE) with a 2-nitrobenzoyl photocleavage group linked to the nitrogen of the closest amino acid to the central core (G) was studied.[42] This PA bearing the photocleavage group gives rise to the formation of quadrupole helical fibers (Figure 2.9, top). However, upon irradiation at 350 nm, and hence the subsequent photochemical cleavage, there is a conversion into single fibers (Figure 2.9, bottom). Authors hypothesize that a torsional strain is produced by the bulky 2-nitrobenzoyl

[40] J. E. Goldberg, E. J. Berns, R. Bitton, C. J. Newcomb, S. I. Stupp, *Angew. Chem. Int. Ed.* **2011**, *50*, 6292-6295.
[41] S. E. Paramonov, H. W. Jun, J. D. Hartgerink, *J. Am. Chem. Soc.* **2006**, *128*, 7291-7298.
[42] T. Muraoka, H. Cui, S. I. Stupp, *J. Am. Chem. Soc.* **2008**, *130*, 2946-2947.

group, which is released when the photocleavage group is released. This approach could be useful to create photoresponsive functional materials in sensing or actuation using external stimuli such as light.
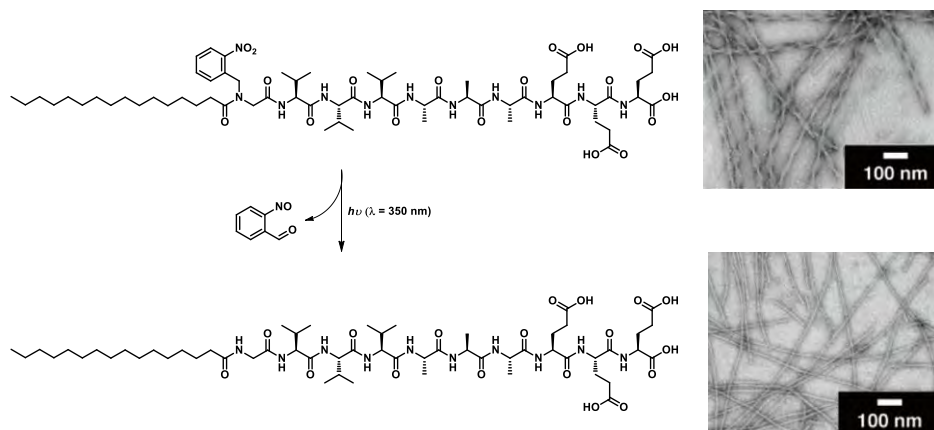
Figure 2.9 Molecular structures of PA bearing a 2-nitrobenzoyl group linked to the N of the glycine unit and TEM image of its self-assembly giving rise to quadrupole helical structures (top). Chemical photocleavage upon irradiation at 350 nm and TEM image of the single nanofibers obtained (bottom).

As it has been presented above, peptides are versatile scaffolds in the construction of supramolecular nanostructures with highly promising applications. In this regard, this thesis is fully dedicated to the use of peptides and its functionalization with electroactive units. Therefore, it is important to refer some interesting approaches that have been made in the peptide self-assembly of organic materials.

2.2.1 *Peptide self-assembly of organic materials*

Peptide self-assembly is a very useful strategy to create functional optoelectronic materials since it is possible to insert π-conjugated functions into defined peptide sequences that further self-assemble affording highly organized π-nanostructures with a variety of applications.[22,43] An advantage of using peptides relies on that employing the proper amino acid units, the chemistry of a peptide can be custom

[43] J. D. Tovar, *Acc. Chem. Res.* **2013**, *46*, 1527-1537.

designed. Both the amino acid composition and the length of the peptides will determine the assembly of the peptides. In this sense, some representative examples will be presented from now on.

Ulijn *et al.* synthesized a library of fluorenylmethoxycarbonyl (Fmoc) dipeptides in which the Fmoc moiety is covalently linked to the N-terminus of different dipeptide sequences made up of combinations of four amino acids: glycine (Gly), alanine (Ala), leucine (Leu) and phenylalanine (Phe) covering then, a range of hydrophobicities (Figure 2.10).[44] The self-assembly of these molecules is driven by hydrogen bonding and $\pi-\pi$ interactions between Fmoc units giving rise to hydrogels consisting of a network of nanofibers with variations in fiber diameters depending on the nature of the dipeptide used. Furthermore, these fibrous hydrogels were found to be capable of supporting cell culture of chondrocytes, demonstrating its biocompatibility. A similar work using series of dipeptides but functionalized with naphthalene units at the N-terminus showed the formation of fibrous hydrogels with a marked biocompatibility as well.[45]
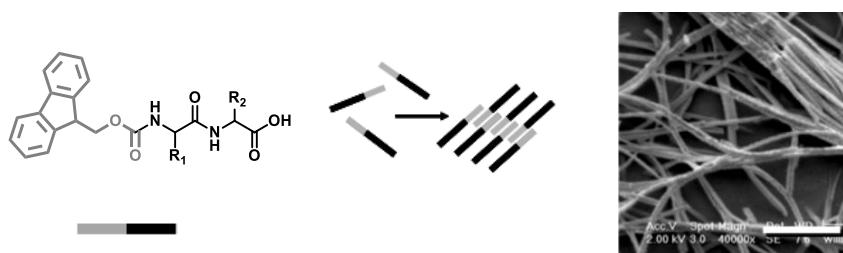
Figure 2.10 Molecular structure of Fmoc-dipeptides (left). R groups correspond to Gly, Ala, Leu and Phe. Cartoon showing the self-assembly process of Fmoc-dipeptides which is stabilized by H-bonds and $\pi-\pi$ interactions between Fmoc units (middle). SEM image showing the nanofibers obtained from the hydrogels upon self-assembly (right) (scale bar = 1µm).

Longer peptides are also good candidates for the construction of supramolecular 1D nanostructures. Meijer *et al.* reported the synthesis of a π-conjugated oPV coupled to the N-terminus of a silk-inspired β-sheet (Gly-Ala-Gly-Ala-Gly) pentapeptide

[44] V. Jayawarna, M. Ali, T. A. Jowitt, A. F. Miller, A. Saiani, J. E. Gough, R. V. Ulijn, *Adv. Mater.* **2006**, *18*, 611-614.
[45] Z. Yang, G. Liang, M. Ma, Y. Gao, B. Xu, *J. Mater. Chem.* **2007**, *17*, 850-854.

sequence.[46] As shown in figure 2.11 the peptide backbone forms an antiparallel β-sheet structure held together by six hydrogen bonds among β-strands. Scanning tunneling microscopy (STM) studies showed the formation of supramolecular ensembles composed by bilayer-like structures (Figure 2.11); each bilayer consists in three rows: a bright domain that corresponds to the oPV moieties, a less bright domain corresponding to the peptide backbone and a dark zone attributed to the long alkyl chains. In fact, the latter has a variation in width as can be discerned in STM image. This can be understood presumably to differences in interactions between the alkyl chains, that is, being fully, partially or not interdigitated. Then, it is observed that the supramolecular structure is mainly directed by the peptide segments. In the same line, oPVs functionalized with even longer peptides (Gly-Ala-Asn-Pro-Asn-Ala-Ala-Gly) give rise to defined 1D nanostructures showing the versatility of using peptides for creating organized materials.[46]
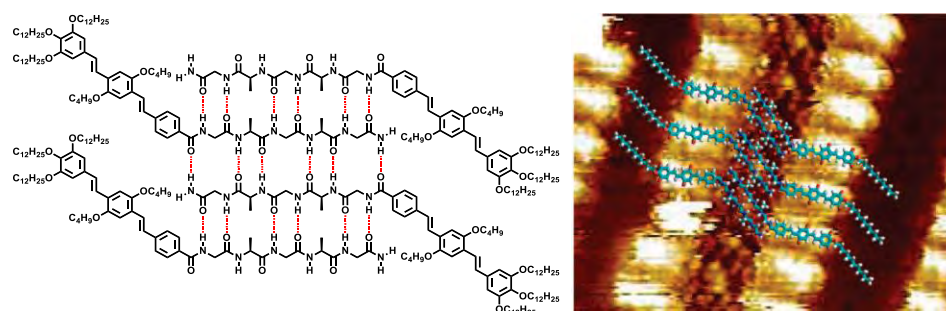
Figure 2.11 Molecular structure of oPV-peptide derivative showing an antiparallel β-sheet conformation (left). STM image obtained from the interface of a solution of the oPV-peptide in 1-octanoic acid and the HOPG surface (for simplicity, not all alkyl chains are shown) (right).

A systematic study of a library of pentapeptide epitopes comprising at the N-terminus π-conjugated moieties such as pyrene, fluorene or naphthalene has also been reported. The studies showed that most of the synthesized derivatives form bioactive

[46] R. Matmour, I. D. Cat, S. J. George, W. Adriaens, P. Leclère, P. H. H. Bomans, N. A. J. M. Sommerdijk, J. C. Gielen, P. C. M. Christianen, J. T. Heldens, J. C. M. van Hest, D. W. P. M. Löwik, S. D. Feyter, E. W. Meijer, A. P. H. J. Schenning, *J. Am. Chem. Soc.* **2008**, *130*, 14576-14583.

fibrous hydrogels stabilized by hydrogen bonding and π–π interactions between the aromatic units.[47]

Other interesting approach consists in embedding π-conjugated molecules directly into the peptide backbone. Tovar *et al.* pioneered these "peptide-π-peptide" triblock molecules which self-assemble mainly through hydrogen bonding giving rise to uniform 1D nanostructures in which there is a strong electron coupling between the π-conjugated units (Figure 2.12).[48] A diverse range of π-conjugated systems such as oPVs, perylene diimides and oligothiophenes can be successfully incorporated forming 1D assemblies. This "peptide-π-peptide" molecular design and its self-assembly through the formation of a *β*-sheet in which several hydrogen bonding interactions are implied, forces the π-conjugated units to be arranged into co-facial π-π interactions. This co-facial π-electron overlap is commonly associated to H-aggregates which are not usually favorable, thus, affecting the final semiconductor behavior.

Figure 2.12 Molecular structure of "peptide-dithiophene-peptide" triblock molecule (top). Cartoon depicting the self-assembly and AFM image showing the 1D nanostructures obtained (bottom).

[47] M. Ma, Y. Kuang, Y. Gao, Y. Zhang, P. Gao, B. Xu, *J. Am. Chem. Soc.* **2010**, *132*, 2719-2728.
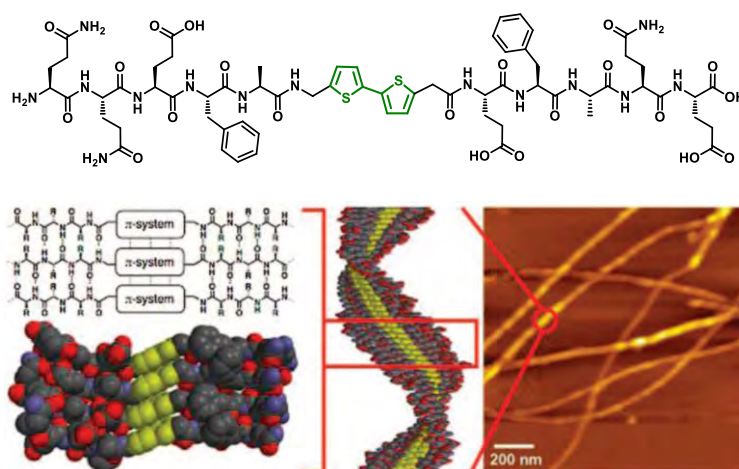[48] S. R. Diegelmann, J. M. Gorham, J. D. Tovar, *J. Am. Chem. Soc.* **2008**, *130*, 13840-13841.

Taking advantage of this molecular design, it is possible to preorganize reactive diphenyl butadiyne moieties with the aim of promoting topochemical polymerization into conjugated polydiacetylenes inside the nanostructures.[49] This kind of polymerizations requires strict geometric specifications necessary for successful reactivity becoming these systems attractive platforms to reach this goal.[50]

In contrast to a functionalization at the N- or C- termini as described above, other type of functionalization with π-conjugates molecules can be made at the side chains of the peptide backbone. Parquette and coworkers synthesized dilysine peptides functionalized with a naphthalenediimide (NDI) chromophore that serves as a good electron acceptor moiety, giving rise to *n*-type 1D nanostructures.[51] The designed peptides consist of opposite positions of NDI units and free amine groups (Figure 2.13 A and B). The self-assembly of these dipeptides is driven by hydrogen bonding of the β-sheet, $\pi-\pi$ interactions between NDI units and electrostatic repulsions among adjacent protonated lysines. Unlike the relative small changes in molecular structures between the two peptides, marked changes in the self-assembly and morphology of the nanostructures were observed. While one of the dipeptides gives the formation of flatten and twisted nanoribbons, the other gives helical nanofibers (see Figure 2.13). Charge transfer among NDI units within these ordered 1D nanostructures was found to be more effective in comparison with a similar disordered system, remarking again the importance of having π-stacked chromophores in ordered domains for nanoscale optoelectronics applications.

[49] S. R. Diegelmann, N. Hartman, N. Markovic, J. D. Tovar, *J. Am. Chem. Soc.* **2012**, *134*, 2028-2031.
[50] L. Tian, R. Szilluweit, R. Marty, L. Bertschi, M. Zerson, E.-C. Spitzner, R. Margerle, H. Frauenrath, *Chem. Sci.* **2013**, *3*, 1512-1521.
[51] H. Shao, T. Nguyen, N. C. Romano, D. A. Modarelli, J. R. Parquette, *J. Am. Chem. Soc.* **2009**, *131*, 16374-16376.
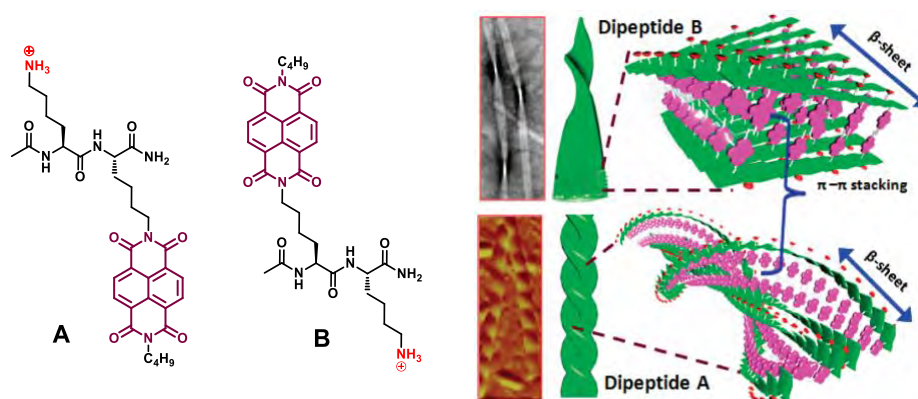
Figure 2.13 Molecular structures of NDI-dipeptides (left) and proposal of the self-assembly (right).

Cyclic peptides are also versatile systems that lead to organized 1D nanostructures.[52] Their molecular structure form substantially a flat ring in which C=O and N-H groups are oriented narrowly perpendicular to the ring plane and its side chains radiating outward (Figure 2.14). Furthermore, this design permits a control over the internal diameter and external surface properties, making these molecules good candidates for the fabrication of ion channels.[53] Moreover, electroactive units can be placed in the outer parts giving rise to organized electroactive nanotubes.[54]
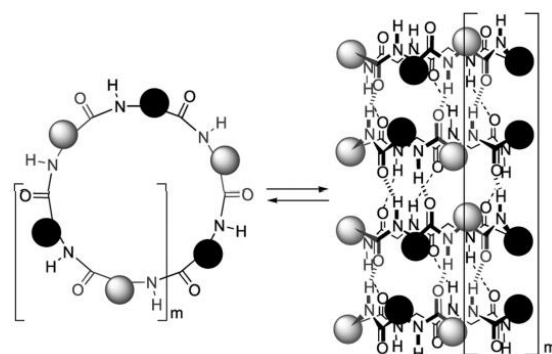
Figure 2.14 Molecular structures of cyclic peptides and their self-assembly process.

[52] D. T. Bong, T. D. Clark, J. R. Granja, M. R. Ghadiri, *Angew. Chem. Int. Ed.* **2001**, *40*, 988-1011.

[53] J. Montenegro, M. R. Ghadiri, J. R. Granja, *Acc. Chem. Res.* **2013**, *46*, 2955-2965.

[54] R. J. Brea, L. Castedo, J. R. Granja, M. A. Herranz, L. Sánchez, N. Martín, W. Seitz, D. M. Guldi, *Proc. Natl. Acad. Sci.* **2007**, *104*, 5291-5294.

2.3.   π-EXTENDED TTF (exTTF)

Upon the synthesis of tetrathiafulvalene (TTF),[55] it was found that this electroactive unit in combination with a strong electron-acceptor molecule, such as tetracyano-*p*-quinodimethane (TCNQ), forms a charge-transfer complex exhibiting remarkable conducting properties. This observation gave rise to a new series of compounds called "organic or synthetic metals".[56,57] Since then, several chemical modifications including substituents on the outer carbon atoms or the separation of the 1,3 dithiol rings through a *p*-quinoid system or even larger π-conjugated systems have been performed.[58]   Among these systems, 9,10-di(1,3-dithiol-2-ylidene)-9,10-dihydroanthracene (exTTF) has been widely studied in our group.

In contrast to TTF, which exhibits two well-separated one-electron oxidation processes at relatively low oxidation potential values (E_{ox}^1 = 0.37 V and E_{ox}^2 = 0.67 V *vs* SCE, in dichloromethane), exTTF shows a two-electron oxidation process to form a dication species (E_{ox}^1 = 0.44 V *vs* SCE, in dichloromethane). Furthermore, the two-electron oxidation process forming the dication species is accompanied by a gain in aromaticity together with a geometrical change from a butterfly shaped in the neutral state to a planar dicationic structure, where aromatic dithiolium rings are perpendicular to the aromatic anthracene skeleton (Figure 2.15).
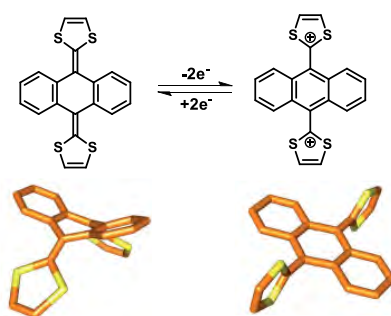

Figure 2.15 Changes in geometry of exTTF upon oxidation.

[55] F. Wudl, G. M. Smith, E. J. Hufnagel, *J. Chem. Soc. D* **1970**, 1453-1454.
[56] J. Ferraris, D. O. Cowan, V. Walatka, J. H. Perlstei, *J. Am. Chem. Soc.* **1973**, *95*, 948-949.
[57] N. Martín, *Chem. Commun.* **2013**, *49*, 7025-7029.
[58] M. Bendikov, F. Wudl, D. F. Perepichka, *Chem. Rev.* **2004**, *104*, 4891-4995.

Taking into account the strong electron-donor character of exTTF and its peculiar butterfly shape geometry, several works in diverse fields such as organic electronics and supramolecular chemistry have been reported.[59] In the field of organic electronics, a variety of dyads and triads using exTTF as electron-donor and fullerene as electron-acceptor moieties have been synthesized, showing efficient electron transfer processes through molecular wires with long lifetimes of charge-separated states;[60] therefore, these systems mimic photosynthetic processes and are appealing for their use in photovoltaic devices (Figure 2.16).[61] In addition, exTTF has been used in the construction of photoactive nanoconjugates[62] as well as in dye sensitized solar cells (DSSCs) showing significant conversion efficiencies (Figure 2.16).[63]

Figure 2.16 Some applications of exTTF in organic molecular electronics.

[59] F. G. Brunetti, J. L. López, C. Atienza, N. Martín, *J. Mater. Chem.* **2012**, *22*, 4188-4205.

[60] a) M. Wielopolski, C. Atienza, T. Clark, D. M. Guldi, N. Martín, *Chem. Eur. J.* **2008**, *14*, 6379-6390; b) A. Molina-Ontoria, G. Fernandez, M. Wielopolski, C. Atienza, L. Sánchez, A. Gouloumis, T. Clark, N. Martín, D. M. Guldi, *J. Am. Chem. Soc.* **2009**, *131*, 12218-12229.

[61] a) L. Sánchez, I. Pérez, N. Martín, D. M. Guldi, *Chem. Eur. J.* **2003**, *9*, 2457-2468; b) S. Castellanos, A. A. Vieira, B. M. Illescas, V. Sacchetti, C. Schubert, J. Moreno, D. M. Guldi, S. Hecht, N. Martín, *Angew. Chem. Int. Ed.* **2013**, *52*, 13985-13990.

[62] M. A. Herranz, N. Martín, S. Campidelli, M. Prato, G. Brehm, D. M. Guldi, *Angew. Chem. Int. Ed.* **2006**, *45*, 4478-4482.

[63] S. Wenger, P. A. Bouit, Q. L. Chen, J. Teuscher, D. Di Censo, R. Humphry-Baker, J. E. Moser, J. L. Delgado, N. Martín, S. M. Zakeeruddin, M. Grätzel, *J. Am. Chem. Soc.* **2010**, *132*, 5164-5169.

On the other hand, exTTF has also been used in supramolecular chemistry, and due to the interest of the present thesis in this matter it has been developed in the following section.

2.3.1 *Supramolecular chemistry of exTTF and fullerene C_{60}*

In our group, it has been described how the concave π-surface of exTTF molecule serves as a recognizing motif for the convex π-surface of C_{60}.[64,65] This interaction is thermodynamically driven by a concave-convex complementarity which involves electronic interactions and charge transfer. A noteworthy example that attests this supramolecular interaction is based on molecular tweezers where two exTTF moieties are separated through an isophthalic ester as spacer (Figure 2.17).[64]
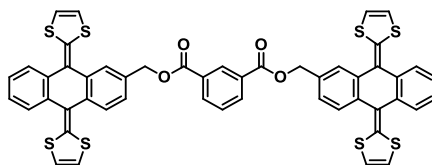
Figure 2.17 exTTF-tweezer for C_{60} recognition.

UV-Vis titrations of exTTF tweezer with C_{60} in chlorobenzene, showed a depletion of the maximum (λ = 434 nm) in simultaneous action with the appearance of a new band at 483 nm that was assigned to the exTTF-tweezer·C_{60} complex (Figure 2.18). The presence of an isosbestic point together with Job plots analyses suggests a 1:1 stoichiometry. Mathematical treatments for this process afforded a binding constant of 2.98 x 10^3 M^{-1}. Surprisingly, the complexation behavior was notably different in a mixture of $CHCl_3$/CS_2 where complex stoichiometries with cooperative effects were observed.[64a]

[64] a) E. M. Pérez, L. Sánchez, G. Fernández, N. Martín, *J. Am. Chem. Soc.* **2006**, *128*, 7172-7173; b) S. S. Gayathri, M. Wielopolski, E. M. Pérez, G. Fernández, L. Sánchez, R. Viruela, E. Ortí, D. M. Guldi, N. Martín, *Angew. Chem. Int. Ed.* **2009**, *48*, 815-819.
[65] a) E. M. Pérez, N. Martín, *Chem. Soc. Rev.* **2008**, *37*, 1512-1519; b) D. Canevet, E. M. Pérez, N. Martín, *Angew. Chem. Int. Ed.* **2011**, *50*, 9248-9259; c) E. M. Pérez, N. Martín, *Chem. Soc. Rev.* **2015**, *44*, 6425-6433.
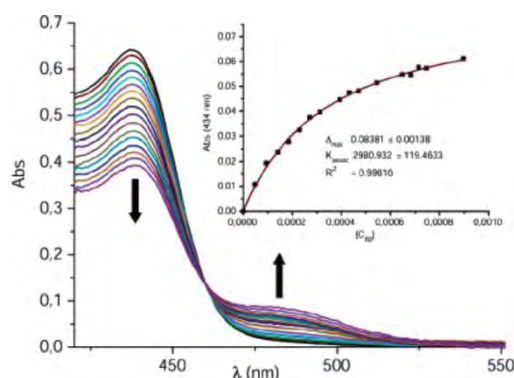
Figure 2.18 Absorption spectral changes of exTTF tweezer upon addition of C$_{60}$ in chlorobenzene. The inset shows the fit of Abs (434 nm) to a 1:1 binding isotherm.

With the aim of improving the complexation of the above mentioned tweezer with C$_{60}$, a more sophisticated system was synthesized.[66] Such system differs from the above mentioned exTTF-tweezer in the incorporation of an alkyl linker providing preorganization and a source of van der Waals interactions (exTTF-macrocyle, Figure 2.19, left). Consequently, due to the macrocyclation effect, a 1:1 complex (Figure 2.19, middle and right) with a higher binding constant (1.1 x 10^6 M^{-1}) was obtained.
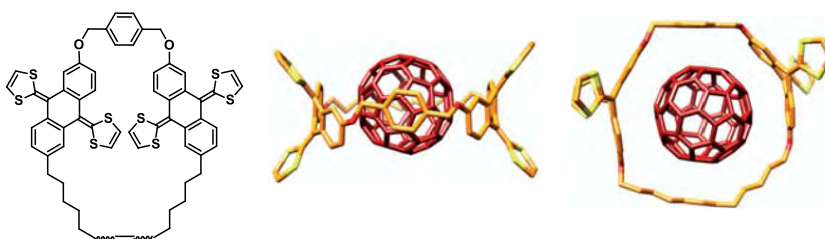
Figure 2.19 Structure of exTTF-macrocyle (left). Side (middle) and top (right) view of the exTTF-macrocyle·C$_{60}$ complex.

In order to demonstrate the weighting of non-covalent forces and the key role of the exTTF molecule in the molecular recognition of C$_{60}$, a series of four different tweezers bearing related recognition units were synthesized and evaluated (Figure 2.20).[67] Their molecular recognition ability towards C$_{60}$ significantly depended on shape

[66] H. Isla, M. Gallego, E. M. Pérez, R. Viruela, E. Ortí, N. Martín, *J. Am. Chem. Soc*. **2010**, *132*, 1772-1773.
[67] E. M. Pérez, A. L. Capodilupo, G. Fernández, L. Sánchez, P. M. Viruela, E. Ortí, M. Bietti, N. Martín, *Chem. Commun.* **2008**, 44, 4567-4569.

(concave or planar), aromaticity and the electronic character as describe in figure 2.20. As a result, the sum of all these factors makes exTTF-tweezer the more suited molecule for molecular recognition of C_{60}.

Concave
5 aromatic rings
Rich electron character
Log Ka = 3.5

Concave
5 aromatic rings
Very poor electron character
Log Ka = 3.1

Planar
1 aromatic ring
Rich electron character
Log Ka = very low

Planar
5 aromatic rings
Poor electron character
Log Ka = 2.9
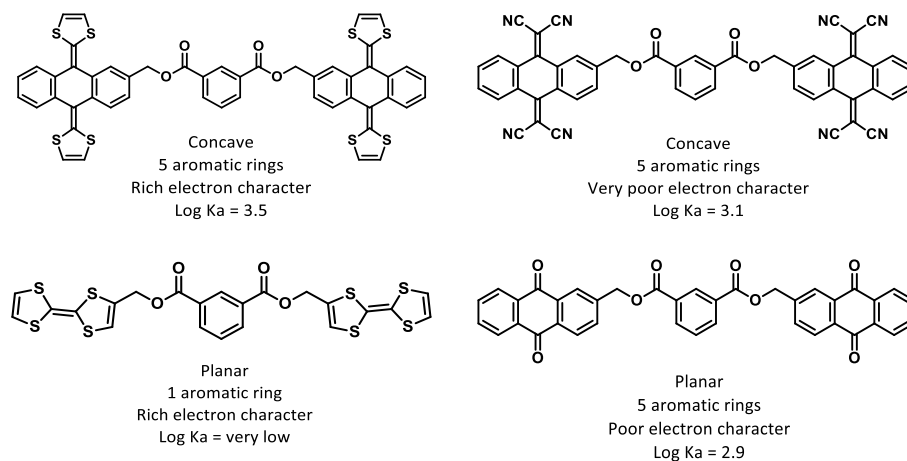
Figure 2.20 Structures of tweezers and binding constants for molecular recognition of C_{60}.

Inspired by the strong complexation between these tweezers and C_{60}, a supramolecular polymer based on a monomer that comprises exTTF and C_{60} at once was prepared (Figure 2.21).[68] The design of this monomer relies on the use of the exTTF tweezer covalently linked to a C_{60} derivative such as PCBM, chosen with the aim of increasing the solubility of the system. The monomer self-assembles in a head-to-tail fashion giving rise to a linear supramolecular polymer (Figure 2.21).
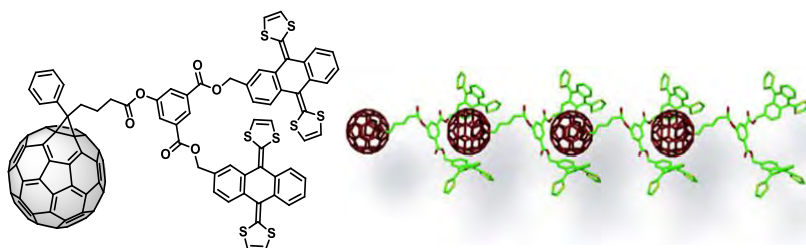
Figure 2.21 Monomer based on exTTF and C_{60} (left). Supramolecular polymer in a head-to-tail fashion (right).

[68] a) G. Fernández, E. M. Pérez, L. Sánchez, N. Martín, *Angew. Chem. Int. Ed.* **2008**, *47*, 1094-1097; b) H. Isla, E. M. Pérez, N. Martín, *Angew. Chem. Int. Ed.* **2014**, *53*, 5629-5633.

2.3.2 *Supramolecular chemistry of exTTF and Carbon Nanotubes (SWNTs)*

The concave-convex complementarity can be extended to another curved carbon nanoforms such as single wall carbon nanotubes (SWNTs).[69,70,71,72] exTTF serves again as a recognizing motif for SWNTs, in which the complementarity is based on $\pi-\pi$ interactions and the electron coupling between both components.

A water-soluble exTTF-tweezer endowed with a second generation polar dendron that carries carboxylic acids was synthesized and used for their binding to SWNTs in aqueous media (Figure 2.22).[69] Nanohybrid formation was characterized by AFM, TEM, UV-Vis, NIR, Raman and transient absorption spectroscopy showing a good electronic communication between the electroactive components with lifetimes of the radical pairs in the range of several hundreds of picoseconds.
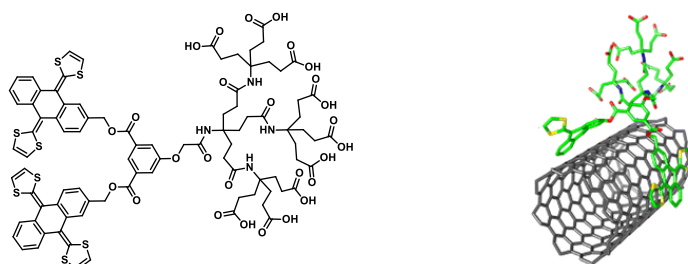

Figure 2.22 Polar exTTF-tweezer structure used for supramolecular functionalization of SWNTs.

In other approach, an exTTF unit covanlently linked to an alanyl-glycine dipeptide bearing a polyethylenglycol dendrimer was obtained to attain a supramolecular functionalization of SWNTs in aqueous media (Figure 2.23, top).[70] In fact, this molecule enables the formation of a *n/p* type nanohybrids with a marked

[69] C. R Nieto, R. García, M. A. Herranz, C. Ehli, M. Ruppert, A. Hirsch, D. M. Guldi, N. Martín, *J. Am. Chem. Soc.* **2012**, *134*, 9183-9192.

[70] F. G. Brunetti, C. R. Nieto, J. López-Andarias, C. Atienza, J. L. López, D. M. Guldi, N. Martín, *Angew. Chem. Int. Ed.* **2013**, *52*, 2180-2184.

[71] J. López-Andarias, J. L. López, C. Atienza, F. G. Brunetti, C. R. Nieto, D. M. Guldi, M. Martín, *Nat. Commun.* **2014**, *5*, 3763.

[72] A. de Juan, Y. Pouillon, L. Ruiz-Gonzalez, A. Torres-Pardo, S. Casado, N. Martín, Á. Rubio, E. M. Pérez, *Angew. Chem. Int. Ed.* **2014**, *53*, 5394-5400.

supramolecular organization from the nano- to the meso- scale in which the alignment of nanohybrids was efficiently achieved (Figure 2.23, bottom). This approach is a representative example of short and long-range organization by a short peptide sequence comprising an exTTF unit.
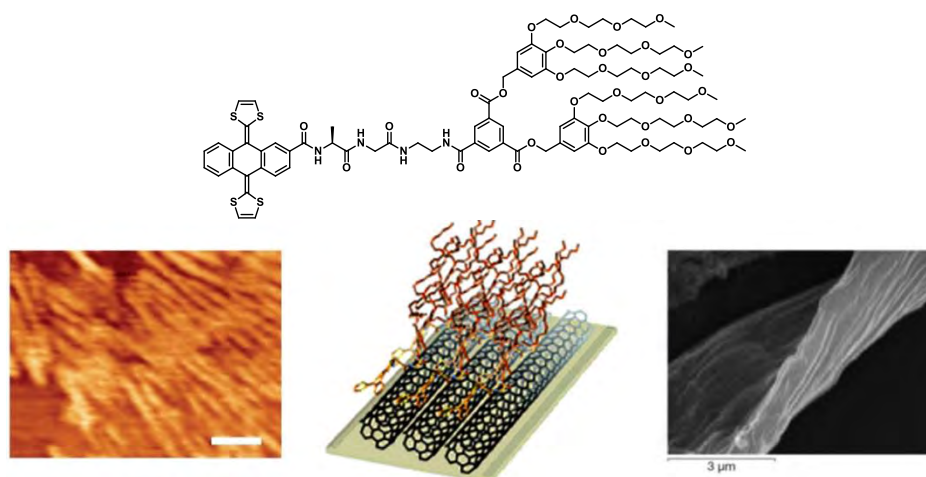
Figure 2.23 Molecular structure of exTTF derivative comprising a dipeptide sequence and ethylenglycol chains (top). AFM image in HOPG showing the aligned nanohybrids at nanoscale (bottom, left) (scale bar = 300 nm). Cartoon of the molecular assembly of the nanohybrids showing the height of nanohybrids which is corroborated by AFM height profiles (bottom, middle). SEM image showing the aligned SWNTs nanohybrids at mesoscale (below, right).

2.3.3 *Hierarchical structures based on exTTF*

As mentioned at the beginning of this background, the organization of electroactive units in 1D nanostructures through the self-assembly of properly designed molecules is quite interesting since new properties can arise from the organized structures. In this sense, exTTF units have been used for the growing of hierarchical nanostructures.[73,74]

A complementary complex made up by a cyanurate derivative which is a versatile hydrogen bonding motif and a diamino-s-triazine functionalized with a π-conjugated

[73] J. L. López, C. Atienza, W. Seitz, D. M. Guldi, N. Martín, *Angew. Chem. Int. Ed.* **2010**, *49*, 9876-9880.
[74] J. López-Andarias, M. J. Rodríguez, C. Atienza, J. L. López, T. Mikie, S. Casado, S. Seki, J. L. Carrascosa, N. Martín, *J. Am. Chem. Soc.* **2015**, *137*, 893-897.

p-phenylenevinylene linked to a exTTF unit, was used as building block for the construction of well-organized quaternary structures (Figure 2.24).[73]
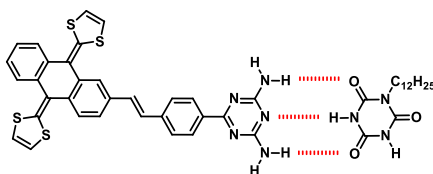
Figure 2.24 Molecular structure of the complementary complex based on exTTF.

UV studies showed that when a solution of the complex in methylcyclohexane (MCH) was aged, a bathochromic shift of the exTTF band from 450 nm to 500 nm ($\Delta\lambda$ = 50 nm) takes place. This shift attests a new electronic state steming from the $\pi-\pi$ interaction between exTTF units and, in fact, this was the first time that such interaction could be evaluated. SEM analysis showed the formation of self-assembled and homogenous fibers which are composed of multilayered nanoribbons entwined without any preference in a clockwise or anticlockwise handedness (Figure 2.25). In such assembly, $\pi-\pi$ interactions between exTTF units play a critical role in the stabilization of the nanostructures obtained (see cartoon in Figure 2.25).
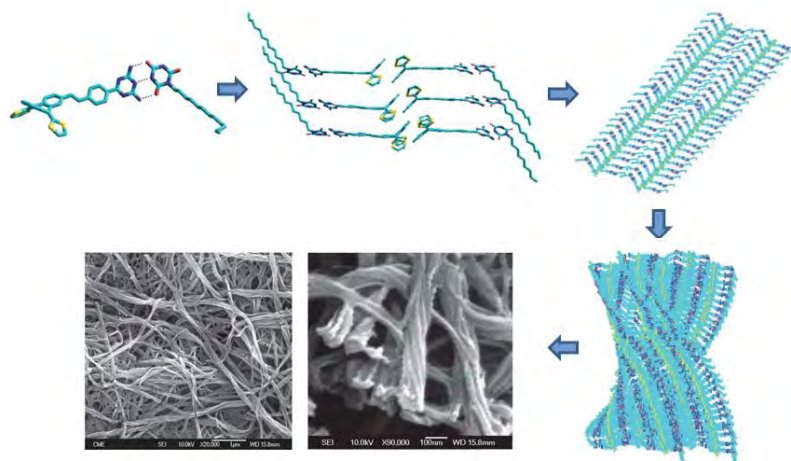
Figure 2.25 Evolution from primary to quaternary supramolecular structures based on the complementary complex. SEM images showing the nanofibers obtained upon aging in MCH.

2.4.   FULLERENE C$_{60}$

Fullerenes are a family of closed carbon cages discovered in 1985 by Kroto, Curl and Smalley during experiments aimed to understand the mechanisms by which long carbon chains molecules are formed in space.[75] In such experiments graphite was vaporized by laser irradiation, generating remarkably stable clusters consisting mainly of 60 carbon atoms. Since then, fullerene C$_{60}$ has become one of the most studied carbon nanomaterials due to their excellent redox and optoelectronic properties.[76]

The structure of fullerene C$_{60}$ consists in a truncated icosahedron (I_h) with 20 hexagons and 12 pentagons (resembling a soccer ball) in which all carbon atoms are sp^2-hybridized. Fullerene C$_{60}$ has a diameter of 7.1 Å and presents two types of bonds: those between two hexagons, the [6-6], measuring 1.38 Å and presenting a double bond character and those between a pentagon and a hexagon, the [5-6], measuring 1.45 Å and a simple bond character (Figure 2.26).
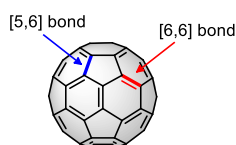
Figure 2.26 Structure of fullerene C$_{60}$.

Fullerene C$_{60}$ has a low reduction potential, able to accept up to 6 electrons, with a first reduction potential (E$^o_{red}$) comparable to those of benzoquinones due to a triply degenerated LUMO orbital (Figure 2.27).[77] Furthermore, C$_{60}$ presents various absorption bands between 190 and 410 nm due to allowed $^1T_{1u}$-^{1}Ag transitions and weak transitions between 410 and 620 nm from singlet-singlet forbidden transitions due to the high symmetry of C$_{60}$.[78] The latter are responsible for its purple color.

[75] H. W. Kroto, J. R. Heath, S. C. O'Brien, R. F. Curl, R. E. Smalley, *Nature* **1985**, *318*, 162-163.

[76] a) *Fullerenes. Chemistry and reactions.*, (Ed. A. Hirsch, M. Brettreich), Wiley-VCH, **2005**; b) D. M. Guldi and N. Martin, *Fullerenes: From Synthesis to Optoelectronic Properties*, Springer, **2002**.

[77] Q. Xie, E. Pérez-Cordero, L. Echegoyen, *J. Am. Chem. Soc.* **1992**, *114*, 3978-3980.

[78] H. Ajie, M. M. Alvarez, S. J. Anz, R. D. Beck, F. Diederich, K. Fostiropoulos, D. R. Huffman, W. Kraetschmer, Y. Rubin, K. E. Schriver, D. Sensharma, R. L. Whetten, *J. Phys. Chem.* **1990**, *94*, 8630-8633.
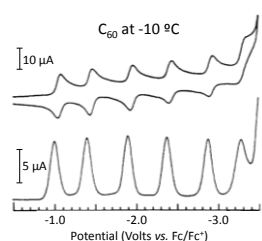
Figure 2.27 Cyclic voltammogram showing the reduction of C_{60} in PhMe/MeCN 5:1 at -10°C (100 mV/s).

Fullerene C_{60} shows low reorganization energies in electron transfer reactions, implying that upon reduction the charge is stabilized over the whole three-dimensional carbon framework.[79] Thus, the charge density in each carbon in $C_{60}^{\bullet-}$ is much smaller than it would be in other electron acceptors, such as benzoquinone, therefore reducing the value of the intramolecular reorganization energy.

The above mentioned remarkable properties of fullerene has led to extended studies aimed to its use as electroactive material for organic electronic devices such as field effect transistors and solar cells.[80,81,82] Several dyads, triads and polyads carring C_{60} and a variety of electron donor moieties with remarkable charge transfer and charge transport features have been developed.[83,84]

Efforts focused on understanding the importance of ordering fullerenes at nano- and macroscopic scales rendered in an organized morphology have proved to be influential in device performances.[80,85,86,87] In fact, supramolecular architectures with

[79] I. Hiroshi, H. Kiyoshi, A. Tsuyoshi, A. Masanori, T. Seiji, O. Tadashi, S. Masahiro and S. Yoshiteru, *Chem. Phys. Lett.* **1996**, *263*, 545-550.
[80] B. C. Thompson, J. M. J. Frechet, *Angew. Chem. Int. Ed.* **2008**, *47*, 58-77.
[81] a) J. L. Delgado, P. A. Bouit, S. Filippone, M. A. Herranz, N. Martín, *Chem. Commun.* **2010**, *46*, 4853-4865; b) J. E. Anthony, A. Facchetti, M. Heeney, S. R. Marder, X. Zhan, *Adv. Mater.* **2010**, *22*, 3876-3892.
[82] Y. Zhang, M. Wang, S. D. Collins, H. Zhou, H. Phan, C. Proctor, A. Mikhailovsky, F. Wuld, T.-Q. Nguyen, *Angew. Chem. Int. Ed.* **2014**, *53*, 244-249.
[83] D. M. Guldi, B. M. Illescas, C. Atienza, M. Wielopolski, N. Martín, *Chem. Soc. Rev.* **2009**, *38*, 1587-1597.
[84] A. S. Konev, A. F. Khlebnikov, P. I. Prolubnikov, A. S. Mereschenko, A. V. Povolotskiy, O. V. Levin, A. Hirsch, *Chem. Eur. J.* **2015**, *21*, 1237-1250.
[85] Y. Huang, E. J. Kramer, A. J. Heeger, G. C. Bazan, *Chem. Rev.* **2014**, *114*, 7006-7043.
[86] S. A. Mauger, L. Chang, S. Friedrich, C. W. Rochester, D. M. Huang, P. Wang, A. J. Moulé, *Adv. Funct. Mater.* **2013**, *23*, 1935-1946.
[87] S. S. Babu, H, Möhwald, T. Nakanishi, *Chem. Soc. Rev.* **2010**, *39*, 4021-4035.

highly organized domains and their applications in photovoltaic devices attest the importance of self-assembly of C_{60} with better device performances.[88,89]

2.4.1 *Supramolecular assemblies of fullerenes*

One of the most widely used methods for the construction of nanoarchictectures is based on the use of amphiphilic molecules in which a controlled balance between two competing interactions takes place. The advantage of this method is that through a suitable functionalization of C_{60} gives rise to the possibility of solubilizing hydrophobic C_{60} in polar media. In this sense, in our group, amphiphilic dendrofullerenes endowed with several carboxylic groups at the periphery have been synthesized (Figure 2.28).[90] These systems self-assemble resulting in the formation of nanorods in which the hydrophobic fullerene moieties are located in the inner part of the rod, while the carboxylic acids are stabilized in the outer part (Figure 2.28). Furthermore, it was observed that these systems form micelles or hollow vesicles depending on the concentration and on the solid surface.
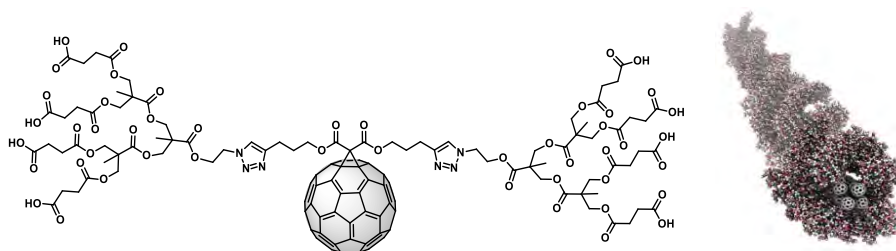
Figure 2.28 Molecular structure of dendrofullerenes and their self-assembly forming nanorods.

Other appealing approaches rely on the use of uncommon amphiphilic systems. This method is based on the construction of self-assembled arrays of alkylated fullerenes in solution and on surfaces.[91] In contrast to the common amphiphilic systems

[88] R. Bhosale, J. Misek, N. Sakai, S. Matile, *Chem. Soc. Rev.* **2010**, *39*, 138-149.

[89] Y. Hizume, T. Tashiro, R. Charvet, Y. Yamamoto, A. Saeki, S. Seki, T. Aida, *J. Am. Chem. Soc.* **2010**, *132*, 6628-6629.

[90] A. Muñoz, B. M. Illescas, M. Sánchez-Navarro, J. Rojo, N. Martín, *J. Am. Chem. Soc.* **2011**, *133*, 16758-16761.

[91] T. Nakanishi, *Chem. Commun.* **2010**, *46*, 3425-3436.

(hydrophobic-hydrophilic), the union of C_{60} ($\pi-\pi$) and aliphatic chains (van der Waals), namely "hydrophobic amphiphilicity", allows the control of supramolecular features with applications aimed toward photo-energy conversions.[92,93] Nakanishi *et al.* synthesized a series of fullerene derivatives with a multi(alkoxy) phenyl group that self-assemble into 1D nanowires on highly oriented pyrolytic graphite (HOPG) surface with tailored features (Figure 2.29).[94] In such systems, alkyl chains serve as insulating barriers, which spatially separate the fullerene nanowires and whose separation can be controlled at nanometer level by using longer or shorter alkyl chains. The self-assembly of these molecules is favored by the interaction of alkyl chains with HOPG surface together with $\pi-\pi$ interactions between C_{60} in a zigzag-type fashion giving rise to the 1D nanowires observed by AFM and STM (Figure 2.29).
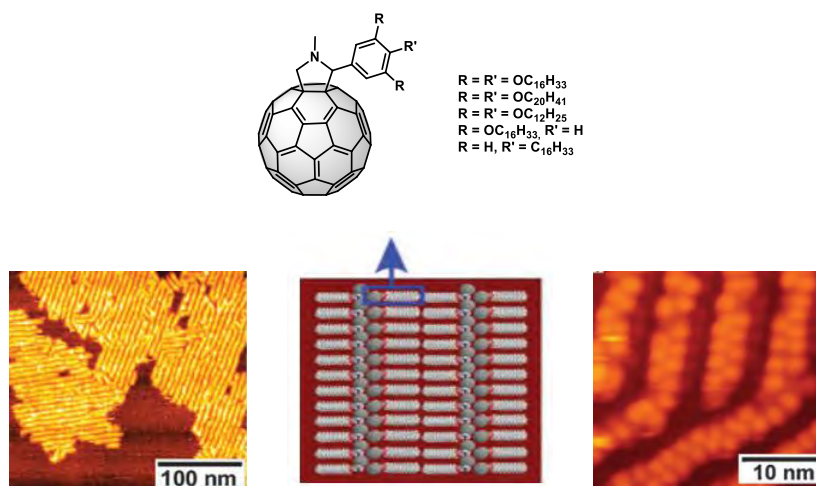
Figure 2.29 Molecular structure of alkyl-conjugated derivatives (top). AFM (bottom-left) and STM (bottom-right) images on HOPG surface from a solution of compound with R = R' = $OC_{16}H_{33}$ in $CHCl_3$. Schematic illustration shows the supramolecular organization.

[92] S. S. Babu, A. Saeki, S. Seki, H. Möhwald, T. Nakanishi, *Phys. Chem. Chem. Phys.* **2011**, *13*, 4830-4834.

[93] Y. Shen, T. Nakanishi, *Phys. Chem. Chem. Phys.* **2014**, *16*, 7199-7204.

[94] T. Nakanishi, N. Miyashita, T. Michinobu, Y. Wakayama, T. Tsuruoka, K. Ariga, D. G. Kurth, *J. Am. Chem. Soc.* **2006**, *128*, 6328-6329.

Polarized optical microscopy showed that this kind of compounds present birefringent optical textures comparable to those of smectic phases of liquid crystals.[95] Furthermore, X-ray diffraction showed the presence of multiple peaks indicating a long-range ordered lamellar mesophase in a head-to-head configuration. Moreover, the electron mobility of these systems ($\sim$3 x 10^{-3} $cm^2V^{-1}s^{-1}$) was found to be comparable with other organic semiconductors of smectic liquid-crystalline phases indicating a dense packing of fullerenes carrying the charges.

Bassani *et al.* synthesized a fullerene derivative comprising a solubilizing 3,4-di-*tert*-butylbenzene group linked to a barbituric acid which is a hydrogen-bonding motif (Figure 2.30).[96] Crystalline solids obtained from this compound showed the existence of fullerene hydrogen-bonding tapes in which the electronic interactions between fullerene units is large. Such interactions were examined by probing the polarization of the fluorescence emission arising from fullerene excimer-like emitting states, showing very strong polarization of *p* = 0.78, which is indicative of a high degree of anisotropy in accordance with the presence of fullerene hydrogen-bonded tapes. Consequently, a low polarization value of around *p* = 0.11 for pristine C_{60} crystals from chloroform solutions was observed.
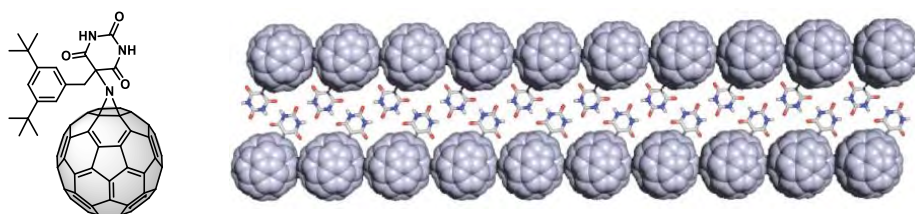
Figure 2.30 Molecular structure of a fullerene derivative comprising a barbituric acid (left). Fullerene hydrogen-bonded tapes observed in the crystalline structure (right).

Aida *et al.* synthesized an amphiphilic dyad comprising a fullerene unit with a chiral center and porphyrin moieties functionalized with triethylene glycol chains as shown

[95] T. Nakanishi, Y. Shen, J. Wang, S. Yagai, M. Funahashi, T. Kato, P. Fernandes, H. Möhwald, D. G. Kurth, *J. Am. Chem. Soc.* **2008**, *130*, 9236-9237.
[96] C.-C. Chu, G. Raffy, D. Ray, A. D. Guerzo, B. Kauffmann, G. Wantz, L. Hirsch, D. M. Bassani, *J. Am. Chem. Soc.* **2010**, *132*, 12717-12723.

in figure 2.31 (top).[89] Authors found that a suspension of the racemic mixture gave rise to the formation of spheres with uniform size (Figure 2.31, bottom-left). This kind of assembly is not as promising as 1D nanostructures for long-range charge-carrier transport. In this sense, essays with a suspension of the enantiopure compound under the same conditions resulted in the formation of bundles of long nanofibers (Figure 2.31, bottom right). These nanofibers presented photoconductivity with a very good electron (μ_e) and hole (μ_h) mobilities (μ_e = 0.14 cm^{2}V^{-1}s^{-1}, μ_h = 0.10 cm^{2}V^{-1}s^{-1}) far better than those obtained for the spherical aggregates (μ_e = not detected, μ_h = 1.5 x 10^{-4} cm^{2}V^{-1}s^{-1}). Therefore, the importance of chirality and having enantiomeric pure compounds is evidenced in the nanostructures obtained and, in turn, in their electric properties.[89]
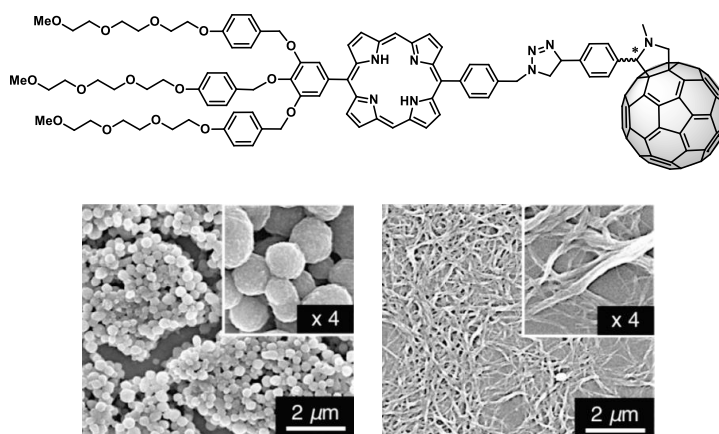
Figure 2.31 Molecular structure of dyad based on fullerene and porphyrin (top). SEM images obtained for racemic mixture (bottom-left) and the enantiopure compound (bottom-right).

Recently, studies using zinc-porphyrin and fullerene dyads with very similar structures to the above presented were synthesized.[97] These dyads are composed by the same hydrophilic chains but changing the triazole linker for ester and acetylene moieties giving rise to nanotubes with different dimensional and geometrical features from another differing, as well, in photoconductivity measurements.[97]

---

[97] R. Charvet, Y. Yamamoto, T. Sasaki, J. Kim, K. Kato, M. Takata, A. Saeki, S. Seki, T. Aida, *J. Am. Chem. Soc.* **2012**, *134*, 2524-2527.

Another example of amphiphilic dyads comprising a zinc phtalocyanine (ZnPc) as electron-donor and fullerene C_{60} as electron-acceptor was reported.[98] The salt obtained self-assembles into 1D nanotubes in polar solvents (Figure 2.32). The system showed a very efficient electron transfer process with a lifetime of τ = 1.4 ms, that is, six orders of magnitude longer in comparison with that obtained for the monomer (τ = 3 ns).
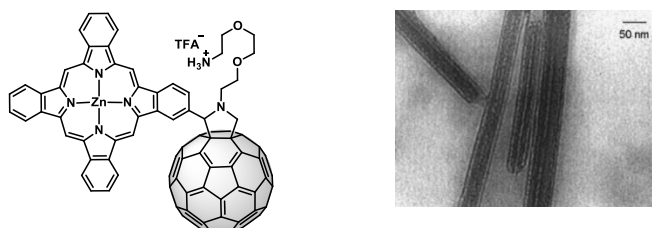
Figure 2.32 Molecular structure of the dyad ZnPc-C_{60} and TEM of nanotubes obtained.

In the same line, donor-acceptor amphiphilic compounds based on hexabenzocoronene (HBC) functionalized on one side with dodecyl chains and triethylene glycol (TEG) chains bearing a fullerene unit on the other have been synthesized.[34] These molecules self-assemble resulting in coaxial nanotubes with a π-stacked HBC array in which an outer layer of C_{60} covering the nanotube was obtained (Figure 2.33). The formed nanotubes presented an ambipolar charge carrier mobility and photovoltaic response upon light illumination. Interestingly, the coassembled nanotube containing 10 mol % of HBC-C_{60} (Figure 2.33, bottom-left) showed an intratubular hole mobility of 2.0 cm^{-2} V^{-1} s^{-1}, which is a value closer to the intersheet mobility in graphite measured by flash-photolysis time-resolved microwave conductivity (FP-TRMC).[34]

---

[98] D. M. Guldi, A. Gouloumis, P. Vázquez, T. Torres, V. Georgakilas, M. Prato, *J. Am. Chem. Soc.* **2005**, *127*, 5811-5813.
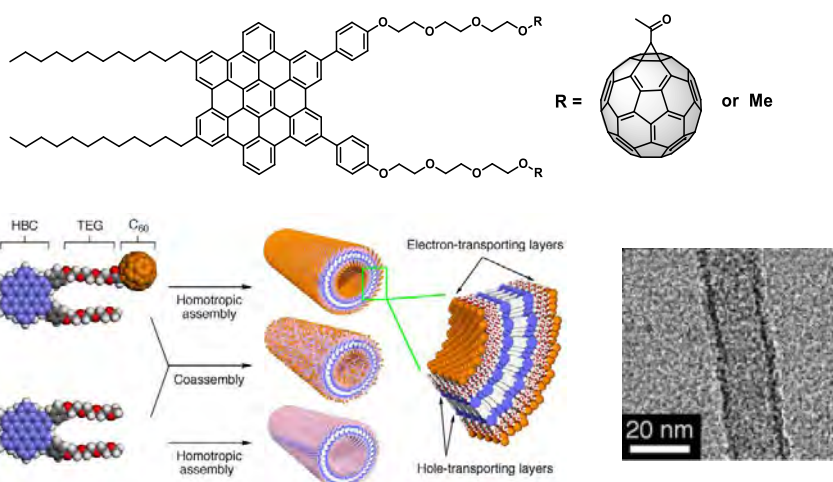
Figure 2.33 Molecular structure of HBC derivatives (top). Schematic representation of the formation of homotropic and coassembled nanotubes (bottom-left). TEM image of the nanotubes obtained (bottom-right).

An interesting approach using amphiphilic block copolymers was demonstrated by Ariga *et al.*[99] The co-polymer consists of hydrophilic electron-donor porphyrin (endowed with TEG chains) and hydrophobic electron-acceptor C_{60} placed at the side chains of the polymer (Figure 2.34). As a result, photoconductive films of domain-segregated self-assembled nanowires were obtained. The nanowires consist of alternating domains arranged perpendicular to the fiber axis as shown in TEM images (Figure 2.34). Having in mind the amphiphilic nature of this block co-polymer, it self-assembles into disks with porphyrins and C_{60} units segregated respectively above and below the disks' planes. This arrangement further stacks into well-ordered nanofibers through self-recognition giving rise to *n/p* heterojunctions exhibiting high charge carrier mobilities ($\mu_e = 3 \times 10^{-3}$ cm^{2}V^{-1}s^{-1}, $\mu_h = 3.7 \times 10^{-2}$ cm^{2}V^{-1}s^{-1}).[99]

[99] R. Charvet, S. Acharya, J. P. Hill, M. Akada, M. Liao, S. Seki, Y. Honsho, A. Saeki, K. Ariga, *J. Am. Chem Soc.* **2009**, *131*, 18030-18031.
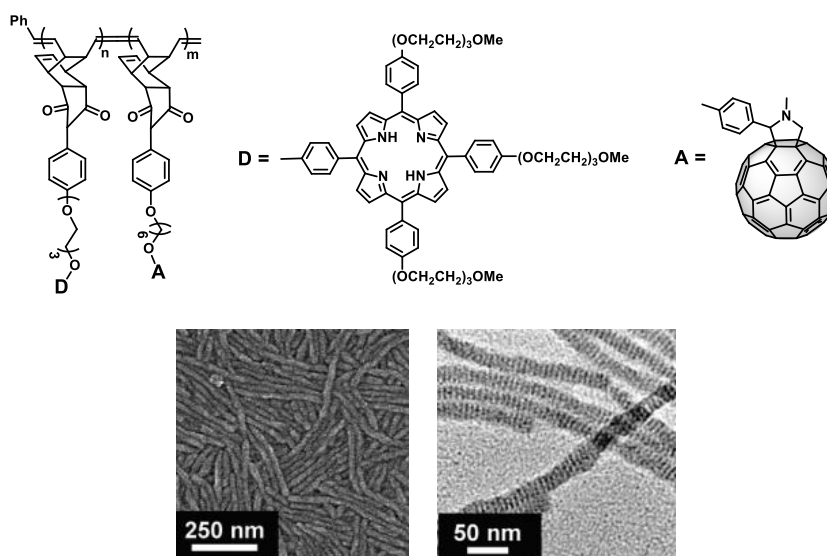
Figure 2.34 Copolymer struture showing donor (D) and acceptor (A) moieties at the side chains (top). SEM (bottom-left) and TEM (bottom-right) images showing the ordering within 1D nanostructures.

2.4.2 *Supramolecular co-assemblies of fullerenes*

The assembly of well separated structures (co-assembly) has emerged as an interesting approach for the construction of electroactive *n/p* heterojuntions. The self-assembly of C_{60} with polymers or π-conjugated molecules such as naphthalendiimides (NDI) or porphyrins to form well-defined nanostructures at different length scales, has been stablished as a promising method to achieve highly ordered functional assemblies. In this sense, an advantage of using pristine C_{60} among these co-assembled systems is that optoelectronic properties of fullerene C_{60} can be retained.

Sanders *et al.* reported the synthesis of NDI derivatives functionalized with α-amino acids that self-assemble into hydrogen bonded helical nanotubes with a cavity of 12.4 Å, which is well-suited to accommodate C_{60} molecules (Figure 2.35 A).[100]

[100] G. D. Pantos, J.-L. Wietor, J. K. M. Sanders, *Angew. Chem. Int. Ed.* **2007**, *46*, 2238-2240.

Complexation studies in UV-Vis showed that upon addition of C_{60} to a solution of NDI nanotubes in $CHCl_3$ the appearance of a broad band centered around 452 nm was observed, band which is attributed to interactions between fullerenes (Figure 2.35 B). Furthermore, the insertion of C_{60} molecules inside the nanotube was confirmed by a significant Cotton effect at 595 and 663 nm in circular dichroism (CD) measurements which are assigned to C_{60} absorptions (Figure 2.35 B).
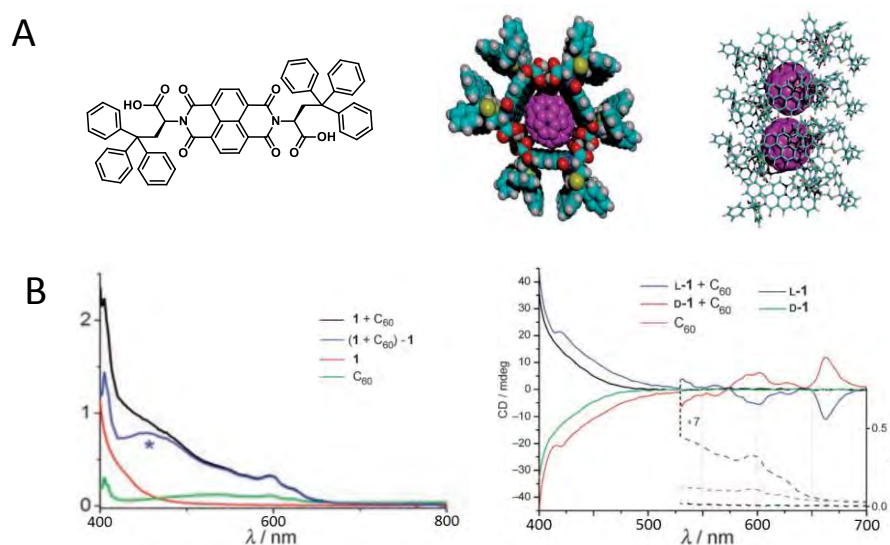
Figure 2.35 (A) Molecular structures of NDI derivative (left). Schematic representations of nanotubes complexing C_{60} inside, top (middle) and side (right) views. (B) (left) UV-Vis spectra of NDI α-amino acids derivative (1), C_{60}, 1+C_{60} and the C_{60} contribution to the 1+C_{60} solution (blue) in $CHCl_3$. (right) CD spectra of $CHCl_3$ solutions of NDI α-amino acids derivatives (L-1 and D-1) in the presence (blue and red) and the absence (black and green) of C_{60}.

In other cases, the formation of water-soluble toroids with a hydrophobic cavity formed by the co-assembly of laterally grafted *p*-phenylene rod amphiphiles was achieved. The latter further stack into tubular nanostructures triggered by the encapsulation of C_{60} molecules (Figure 2.36).[101] The formed toroids have a hydrophilic outer part (due to the TEG chains) with a diameter around 10 nm and a hydrophobic inner part with a diameter of 2 nm which is well-suited for the encapsulation of C_{60} molecules. Toroids are formed by the co-assembly of an 80% of

[101] E. Lee, J.-K. Kim, M. Lee, *J. Am. Chem. Soc.* **2009**, *131*, 18242-18243.

the monofunctionalized *p*-phenylene (Figure 2.36, top-left) in order to increase the volume fraction of hydrophobic segments and favor the encapsulation of C_{60} molecules.
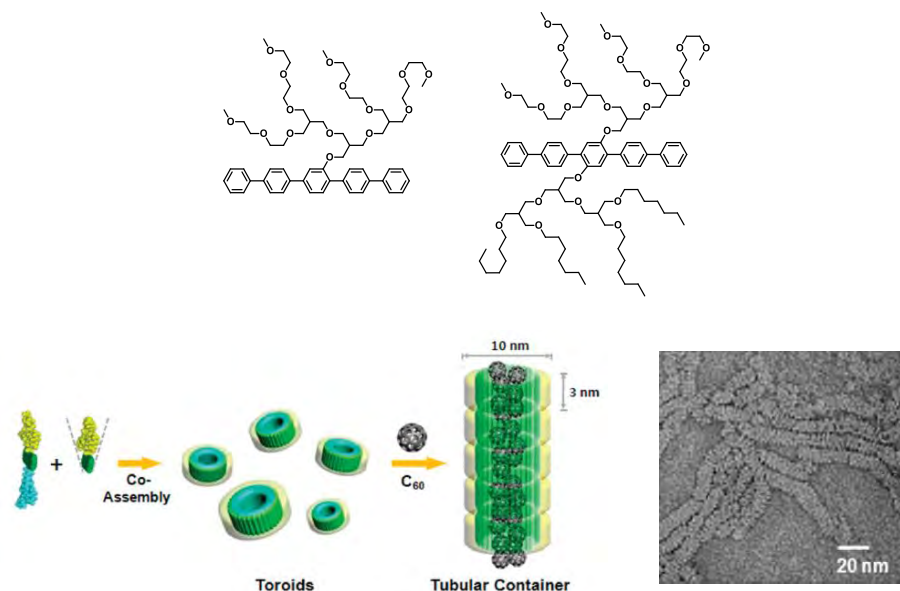
Figure 2.36 Molecular structures of oligo *p*-phenylene rod amphiphiles (Top). Schematic representation of molecular self-assembly forming toroids and their further stack into tubular nanostructures (below-left). TEM image showing the tubular sructures upon encapsulation of fullerene C_{60}.

Other similar approaches in which fullerene molecules are encapsulated within polymers have also been explored. A syndiotactic poly(methylmethacrylate) polymer (st-PMMA) forms an organogel after thermal treatments with C_{60} resulting in a 1D alignment of these molecules encapsulated within helical nanostructures (Figure 2.37).[102] In fact, authors found that preferred-handed helical nanostructures can be formed if the gel is formed using an optically active aromatic alcohol such as (*R*) or (*S*) 1-phenylethanol.

---

[102] T. Kawaguchi, J. Kumaki, A. Kitaura, K. Okoshi, H. Kusanagi, K. Kobayashi, T. Sugai, H. Shinohara, E. Yashima, *Angew. Chem. Int. Ed.* **2008**, *47*, 515-519.

Figure 2.37 Encapsulation of C_{60} using a st-PMMA polymer.

Furthermore, π-conjugated polymers comprising porphyrin moieties were found to be versatile in the organization of C_{60} giving rise to single-crystalline C_{60} microspheres composed of nanoplates with a face cubic centered (fcc) structure.[103] In addition, molecular composites based on fullerene encapsulated within porphyrin nanorods were reported.[104] The composite comprising zinc *meso*-tetra(4-pyridyl)porphyrin and C_{60} which is prepared with the aid of a surfactant, forms highly organized nanorods which showed a significant enhancement in solar energy conversion. Moreover, interesting multiresponsive fluorescent nanorods were fabricated through the co-assembly of C_{60} units and anthracene-ended hyperbranched polyetheramide.[105] The supramolecular nanorods obtained can be further cross-linked through a photodimerization of anthracene moieties giving rise to a supramolecular nanostrutre whose fluorescence is responsive to temperature and pH.

[103] X. Zhang, M. Takeuchi, *Angew. Chem. Int. Ed.* **2009**, *48*, 9646-9651.
[104] T. Hasobe, A. S. D. Sandanayaka, T. Wadac, Y. Arakic, *Chem. Commun.* **2008**, *44*, 3372-3374.
[105] Z. Su, B. Yu, X. Jiang, J. Yin, *Macromulecules* **2013**, *46*, 3699-3707.

2.5. PORPHYRINS

Porphyrins are aromatic heterocyclic macrocycles composed of four interconnected pyrrole moieties. Porphyrin functionalization can be performed in three different positions, two of them at the periphery, the *meso* and β-pyrrolic positions, and the other in the central part of the porphyrin, that is, the NH positions, where it is possible to coordinate a metal cation (Figure 2.38). As it has been described during this background, porphyrins are very good electron donors and, as such, they have been employed in a variety of donor-acceptor systems due to their remarkable properties, namely strong UV absorption bands, tunable oxidation potential and a long live singlet excited state.
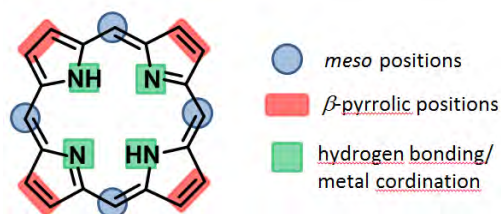
Figure 2.38 Porphyrin structure showing functionalization positions.

The typical UV absorption profile shows an intense band around 380-420 nm, named the Soret band, which is attributed to π-π* transitions from the ground state to the second excited singlet state and a series of weak bands in the 480-700 nm region, named the Q-bands, assigned to π-π* transitions from the ground state to the first excited singlet state. Free base porphyrin presents four Q bands, whereas metalated porphyrins only have 2 due to their higher symmetry. Furthermore, it is possible to modify the oxidation potential of porphyrins in a long range (>0.5 V) by changing their substituents[106] or the metal atom in the central core.[107] Moreover, porphyrins

---

[106] S. I. Yang, J. Seth, J.-P. Strachan, S. Gentemann, D. Kim, D. Holten, J. S. Lindsey, D. F. Bocian, *J. Porphyrins Phthalocyanines* **1999**, *3*, 117-147.
[107] J. H. Fuhrhop, D. Mauzerall, *J. Am. Chem. Soc.* **1969**, *91*, 4174-4181.

present a long lived singlet excited state, in the range of nanoseconds, which is beneficial in electron transfer processes.[108]

2.5.1 *Supramolecular porphyrin-C$_{60}$ complexes*

Having in mind the aforementioned remarkable properties of fullerenes and porphyrins, efforts in combining these two entities in donor-acceptor systems have been done. New interesting properties stemming from 1D-nanostructured dyads such as high charge carrier mobilities and long lifetime of charge separated states, among others, have been described in the past section. Now, some supramolecular porphyrin-C$_{60}$ complexes and the interactions that hold them together are described.

Porphyrin-C$_{60}$ attraction was firstly evidenced in the crystal structure of a fulleropyrrolidine dyad. Such attraction is stabilized by $\pi-\pi$ interactions between porphyrin and C$_{60}$ units in a dimeric form in which an intermolecular distance of 2.75 Å was observed (Figure 2.39).[109]
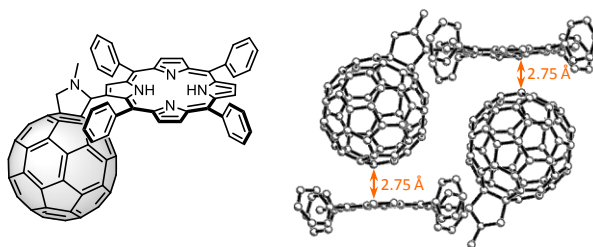
Figure 2.39 Molecular structure of the porphyrin dyad (left) and its crystal structure (right).

It is worth to mention that in solution these $\pi-\pi$ interactions between porphyrin and C$_{60}$ units are considerably weak and, therefore, exceptional examples in which a single porphyrin held together to a fullerene unit driven only by $\pi-\pi$ interactions are rarely

[108] a) A. Harriman, G. Porter , N. Searle, *J. Chem. Soc., Faraday Trans. 2* **1979**, *75*, 1515-1521; b) R. A. Reed, R. Purrello, K. Prendergast, T. G. Spiro, *J. Phys. Chem.* **1991**, *95*, 9720-9727.
[109] Y. Sun, T. Drovetskaya, R. D. Bolskar, R. Bau, P. D. W. Boyd, C. A. Reed, *J. Org. Chem.* **1997**, *62*, 3642-3649.

described.[110] More frequent systems are those composed of various porphyrin units together, combined in an opened or closed manner through different linker moieties.[111] As representative examples, Reed *et al.* synthesized a "porphyrin jaws" host which is an opened system for fullerene complexation where $PdCl_2$ serves as a linker between porphyrin units (Figure 2.40, left).[112] In the other hand, Aida *et al.* designed a closed cyclic compound in which pophyrins are sandwiching a fullerene molecule (Figure 2.40, right).[113]

Figure 2.40 Molecular opened (left) and closed (right) hosts for fullerene complexation.

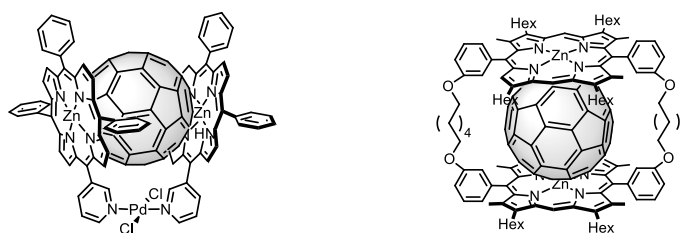In these cases, UV-Vis titration experiments showed a decrease and a red shift of the porphyrin Soret band upon addition of fullerene, indicating a less energetic π-π* transition from a charge transfer process. This phenomenon is widely used as a proof of π-π interaction between them.[114]

Other interesting approach relies on the use of metal-ligand coordination, based in a Lewis acid-base reaction for the formation of porphyrin-fullerene complexes. Pyridine and imidazole molecules are the most common moieties to form stable complexes with zinc porphyrins. In fact, imidazole coordination is around one order of magnitude stronger in comparison with pyridine, indicating that basicity is related with the

[110] M. Kimura, Y. Saito, K. Ohta, K. Hanabusa, H. Shirai, N. Kobayashi, *J. Am. Chem. Soc.* **2002**, *124*, 5274-5275.

[111] a) J. Song, N. Aratani, H. Shinokubo and A. Osuka, *J. Am. Chem. Soc.* **2010**, *132*, 16356-16357; b) W. Meng, B. Breiner, K. Rissanen, J. D. Thoburn, J. K. Clegg, J. R. Nitschke, *Angew. Chem. Int. Ed.* **2011**, *50*, 3479-3483.

[112] D. Sun, F. S. Tham, C. A. Reed, L. Chaker, P. D. W. Boyd, *J. Am. Chem. Soc.* **2002**, *124*, 6604-6612.

[113] K. Tashiro, T. Aida, J.-Y. Zheng, K. Kinbara, K. Saigo, S. Sakamoto, K. Yamaguchi, *J. Am. Chem. Soc.* **1999**, *121*, 9477-9478.

[114] a) A. Hosseini, S. Taylor, G. Accorsi, N. Armaroli, C. A. Reed and P. D. W. Boyd, *J. Am. Chem. Soc.* **2006**, *128*, 15903-15913; b) Z.-Q. Wu, X.-B. Shao, C. Li, J.-L. Hou, K. Wang, X.-K. Jiang, Z.-T. Li, *J. Am. Chem. Soc.* **2005**, *127*, 17460-17468.

stability of the complex formed.[115] D'Souza *et al.* synthesized a supramolecular triad which consists of the axial coordination of an imidazole-fulleropyrrolidine unit to the zinc center of a covalently linked zinc porphyrin-boron dipyrrin dyad (Figure 2.41). The entire system mimics a photosynthetic antenna-reaction center in which the selective excitation of the boron dipyrrin unit creates a singlet excited zinc porphyrin state capable of producing the subsequent efficient electron transfer to the fullerene, giving rise to a charge-separated state with a lifetime of around 4.7 ns in *o*-dichlorobenzene.[116]
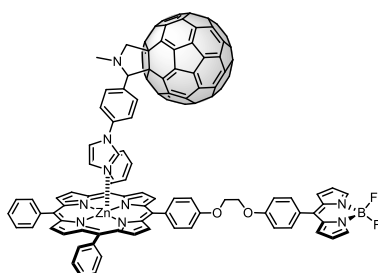

Figure 2.41 Molecular structure of a supramolecular triad based on imidazole coordination.

As it has previously been mentioned, hydrogen bonding interactions have shown to be useful in the creation of supramolecular assemblies. This is explained taking into account that hydrogen bond provides high directionality, sensitivity and efficiency in the electronic communication which is even larger than that found in comparable σ or π bonds.[117] In this sense, a remarkable example was developed by Martín *et al.* who used a two-point amidinium-carboxylate interaction to obtain a supramolecular dyad (Figure 2.42).[118] This interaction is particularly stable, even in solvents of high polarity, due to the synergy of hydrogen bonds and electrostatic interactions.[119] As a result, a relative strong association constant around 10^7 M^{-1} was determined for the

[115] A. Satake, Y. Kobuke, *Tetrahedron* **2005**, *61*, 13-41.

[116] F. D'Souza, P. M. Smith, M. E. Zandler, A. L. McCarty, M. Itou, Y. Araki, O. Ito, *J. Am. Chem. Soc.* **2004**, *126*, 7898-7907.

[117] a) J. L. Sessler, B. Wang, A. Harriman, *J. Am. Chem. Soc.* **1993**, *115*, 10418-10419; b) P. de Rege, S. Williams, M. Therien, *Science* **1995**, *269*, 1409-1413.

[118] L. Sánchez, M. Sierra, N. Martín, A. J. Myles, T. J. Dale, J. Rebek, W. Seitz, D. M. Guldi, *Angew. Chem. Int. Ed.* **2006**, *45*, 4637-4641.

[119] a) J. P. Kirby, J. A. Roberts, D. G. Nocera, *J. Am. Chem. Soc.* **1997**, *119*, 9230-9236; b) N. H. Damrauer, J. M. Hodgkiss, J. Rosenthal, D. G. Nocera, *J. Phys. Chem. B* **2004**, *108*, 6315-6321.

supramolecular dyad. Furthermore, strong electronic communication stemming from the linearity of the system and in turn faster, more efficient and longer lived formation of the radical-ion-pair state (in the order of 1 µs) in comparison to the covalent analogous was observed.
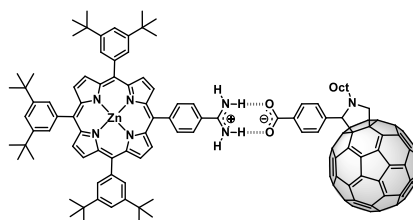

Figure 2.42 Porphyrin amidinium – carboxylate C_{60} supramolecular dyad.

It is worth to mention that the use of a single non-covalent interaction might give rise to relatively unstable complexes and, as a result, weak binding constants. In this sense, the use of multiple interactions might lead to more stable complexes. A representative example consists in the combination of ammonium-crown ether interaction and π−π stacking between porphyrin and C_{60} units, developed by Nierengarten *et al.* (Figure 2.43, right).[120] As a result of these combined interactions, the binding constant increases in two orders of magnitude (log K_a = 5.6) in comparison with the complex obtained with the malonate fullerene derivative and crown ether (log K_a = 3.3) (Figure 2.43, left).[121]
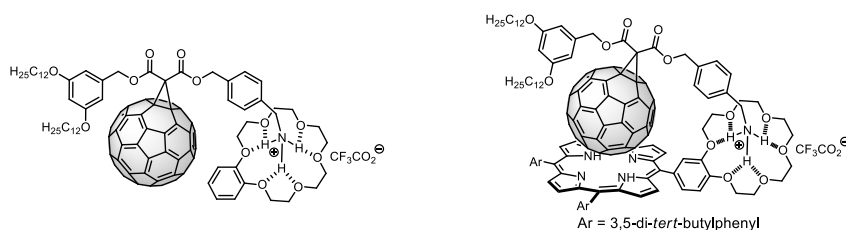
Figure 2.43 Molecular complexes showing a single (left) and two supramolecular interactions (right) resulting in more stable complexes.

[120] a) N. Solladié, M. E. Walther, M. Gross, T. M. F. Duarte, C. Bourgogne, J.-F. Nierengarten, *Chem. Commun.* **2003**, 2412-2413; b) L. Moreira, J. Calbo, B. M. Illescas, J. Aragó, I. Nierengarten, B. D. Nicot, E. Ortí, N. Martín, J.-F. Nierengarten, *Angew. Chem. Int. Ed.* **2015**, *54*, 1255-1260.
[121] N. Solladié, M. E. Walther, H. Herschbach, E. Leize, A. V. Dorsselaer, T. M. F. Duarte, J.-F. Nierengarten, *Tetrahedron* **2006**, *62*, 1979-1987.

Another interesting example relies on the use of a porphyrin-appended foldamers in which the combination of two noncovalent interactions take place in.[122] The foldamer binds to N ligand-C_{60} adducts through the cooperation of two noncovalent interacions: metal ligand coordination and $\pi-\pi$ stacking (Figure 2.44). This system, in contrast to relative smaller oligomers, leads to a larger binding constant with more dramatic shifts in UV-Vis (decrease and red shifting of the Soret band) and circular dichroism measurements in which a chiral induction from the chiral fullerene derivative to the achiral foldamer was efficiently achieved.

Figure 2.44 Porphyrin-appended foldamer complexing a chiral fullerene derivative.
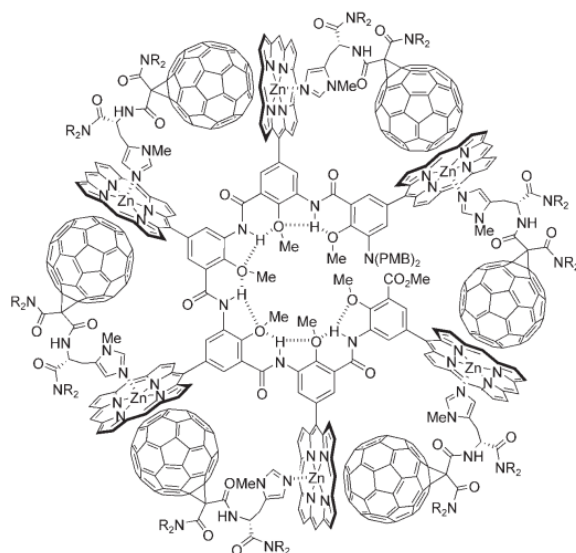
[122] J.-L. Hou, H.-P- Yi, X.-B. Shao, C. Li, Z.-Q. Wu, X.-K. Jiang, L.-Z. Wu, C.-H. Tung, Z.-T. Li, *Angew. Chem. Int. Ed.* **2006**, *45*, 796-800.

3. Objectives

3. OBJECTIVES

The aim of this work is focused on the use of peptides as an important class of biomolecules with remarkable ability to organize through H-bonds, for the construction of supramolecular ensembles endowed with electroactive species. For this purpose, a variety of electroactive systems, namely C_{60}, porphyrin, exTTF and different planar π-conjugated systems have been considered. Thus, the objectives of this thesis have been classified in the following topics:

1. *Concave vs planar geometries for the hierarchical organization of mesoscopic helical fibers.*

The main goal is directed to synthesize and characterize bioinspired pentapeptide derivatives comprising non-planar (exTTF) and planar (fluorene and anthracene) moieties. We also plan to study their self-assembly and analyze the influence of these moieties over morphology.
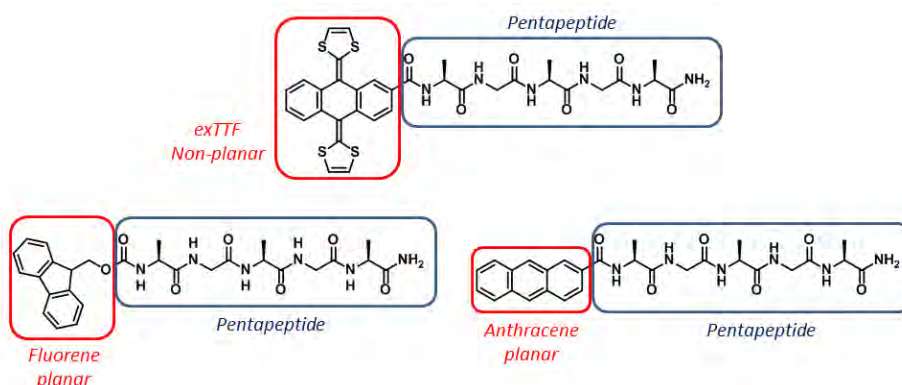
2. Supramolecular one dimensional n/p nanofibers.

Inspired by the results of the previous systems, we will combine the exTTF-fibers with electron acceptor units such as pristine C_{60} and PCBM in order to explore the formation of 1D *n/p*-nanohybrids.
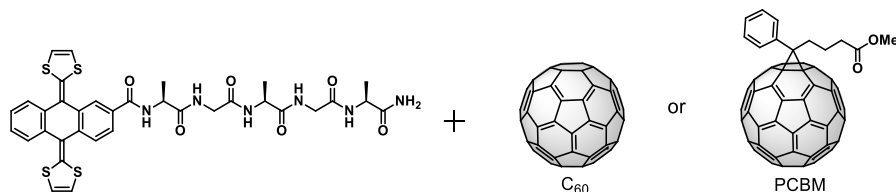
77

3. Supramolecular pentapeptide-based fullerene nanofibers: effect of molecular chirality.

The goal is to synthesize and characterize pentapeptide derivatives comprising C_{60} fullerene units. Further studies aimed to demonstrate morphological consequences when the pentapeptide backbone is changed and the fullerene moiety is closer to it will complement this issue.
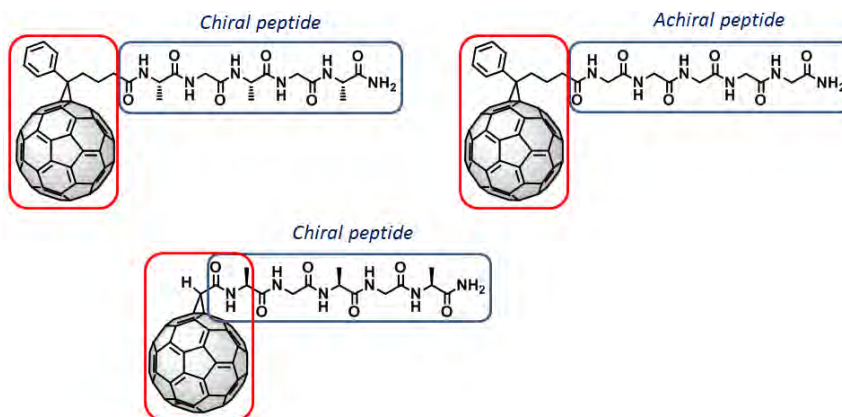
4. Supramolecular porphyrin-C_{60} peptide dyads: morphology and chiral induction effects.

In this particular topic, the ultimate goal is to synthesize, characterize and study the formation of supramolecular porphyrin-C_{60} peptide dyads through strong hydrogen bonds interactions between an amidinium-carboxylate pair varying the peptide length. The impact on the morphology obtained as well as chiral induction effects will be studied in the search for unprecedented ensembles.
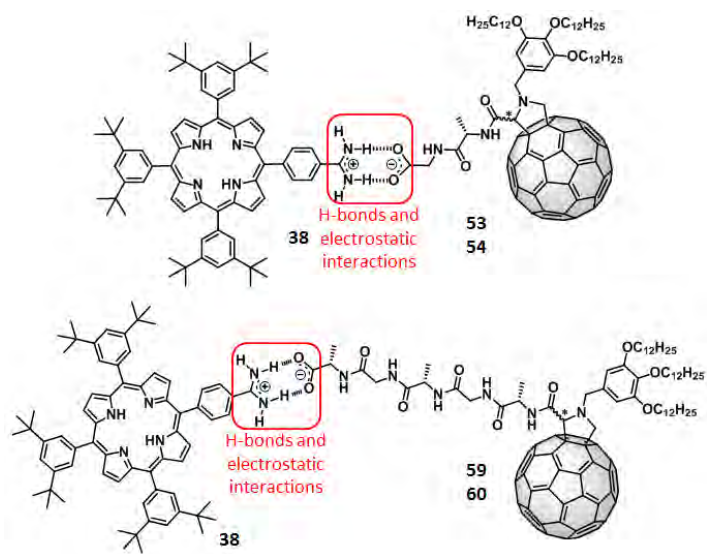
4. Results and discussion

SECTION 4.1

CONCAVE *vs* PLANAR GEOMETRIES FOR THE HIERARCHICAL ORGANIZATION OF MESOSCOPIC HELICAL FIBERS

4. RESULTS AND DISCUSSION

4.1. CONCAVE *vs* PLANAR GEOMETRIES FOR THE HIERARCHICAL ORGANIZATION OF MESOSCOPIC HELICAL FIBERS

In this part, we focused on the use of a bioinspired pentapeptide sequence (Ala-Gly-Ala-Gly-Ala-NH$_2$) with high tendency to form β-sheets. This pentapeptide was functionalized with an electroactive non-planar unit such as exTTF – with its concave shape – for the growth of new supramolecular architectures at different length scales. Furthermore, a comparison with related but planar moieties aimed to determine morphological consequences was performed (Figure 4.1).
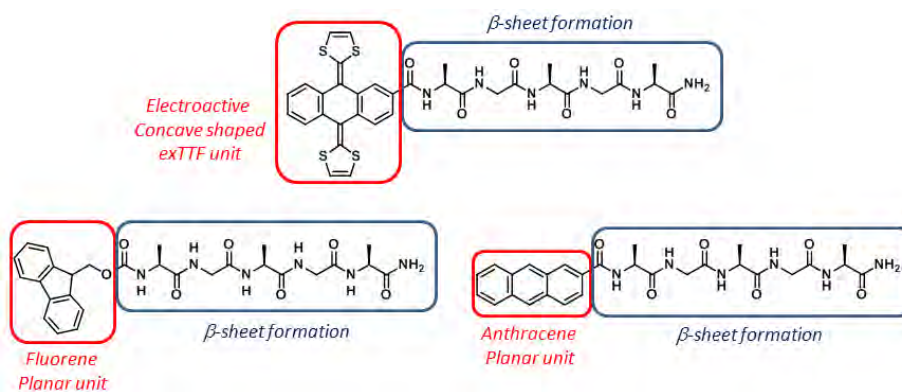
Figure 4.1 Pentapeptide derivatives based on exTTF, fluorene and anthracene moieties.

4.1.1. *General synthesis of pentapeptide derivatives*

The general representation of the synthesis of the pentapeptide derivatives is shown in scheme 4.1. A very important tool that led to the synthesis of these derivatives relied on the use of solid phase peptide synthesis (SPPS) technique; which consists in successive coupling-deprotection steps performed on a resin affording long peptide chains with relative ease. The advantage of the SPPS technique is that the normal and probably tedious purification protocols arising from standard liquid phase couplings are reduced to only filtrations and cycles of washing.

Thus, once pentapeptide L-alanyl-glycyl-L-alanyl-glycyl-L-alanine **5** was obtained, it was coupled by amidation reactions with anthracene-COOH **8** and exTTF-COOH **15** yielding the desired peptide derivatives **9** and **16**, respectively. The synthesis of the final product **6** was achieved directly from the SPPS process (this will be explained in detail below).
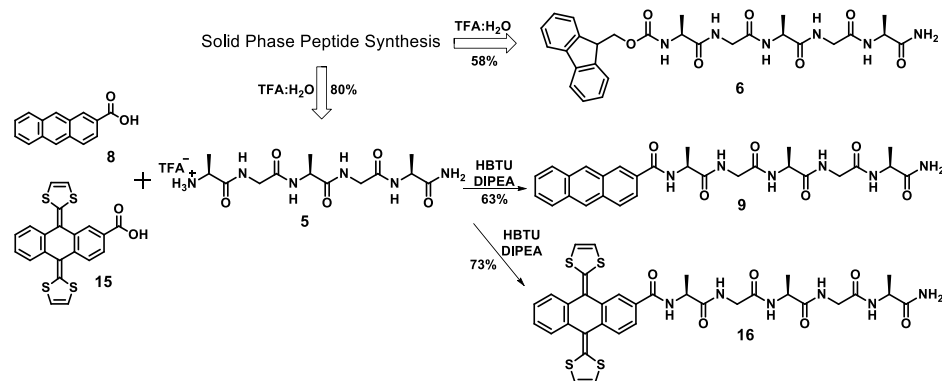
Scheme 4.1 Representative scheme of the synthesis of target products.

- *4.1.1.1* Synthesis of the pentapeptide Ala-Gly-Ala-Gly-Ala-NH$_2$ (5)

Pentapeptide **5** was obtained by means of standard solid-phase peptide synthesis (SPPS) employing an Fmoc (9-fluorenylmethoxycarbonyl) chemistry on a 4-methyl-benzhydrylamine (MBHA) resin. The first amino acid attached to the resin was Fmoc-L-alanine **1** in presence of the coupling reagents *O*-(benzotriazol-1-yl)-*N,N,N',N'*-tetramethyluronium hexafluorophosphate (HBTU) and *N,N'*-diisopropylethylamine (DIPEA) in *N,N*-dimethylformamide (DMF) (Scheme 4.2). The subsequent Fmoc-deprotection was accomplished by a solution of piperidine (20%) in DMF yielding the free amine group ready for the next coupling (Scheme 4.2). These coupling and deprotection steps were checked by a Kaiser test which consists on submerging and heating few beads of resin on a solution of ninhydrin in ethanol. Free amines react with ninhydrin leading to a characteristic purple color. Thus, Kaiser test upon Fmoc deprotection should give rise to the purple color; conversely, upon a coupling step test Kaiser should not lead to any change in color. If the Kaiser test result is not the

expected, coupling or deprotection step was repeated until complete reaction was observed.
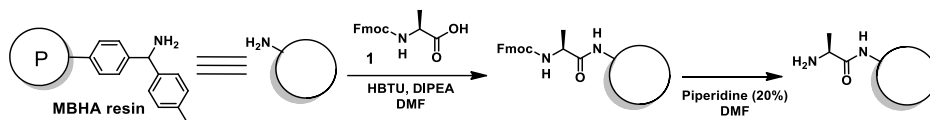
Scheme 4.2 First amino acid coupling and subsequent Fmoc-deprotection.

The second amino acid coupled to the resin was Fmoc-glycine **2** in presence of HBTU and DIPEA giving rise to a Fmoc-dipeptide moiety shown in scheme 4.3. From this unit, repetitive reaction steps were performed, that is, Fmoc deprotection of the peptide attached to the resin and the subsequent coupling of the corresponding Fmoc-protected amino acid as shown in scheme 4.3. Once the Fmoc-pentapeptide **3** was obtained a final deprotection was performed giving rise to pentapeptide **4**. The cleavage of the pentapeptide from the resin was performed by a mixture of trifluoroacetic acid (TFA) and water (95:5) affording the pentapeptide final product **5** with amine and amide groups at the N- and C- terminal positions, respectively (Scheme 4.3).
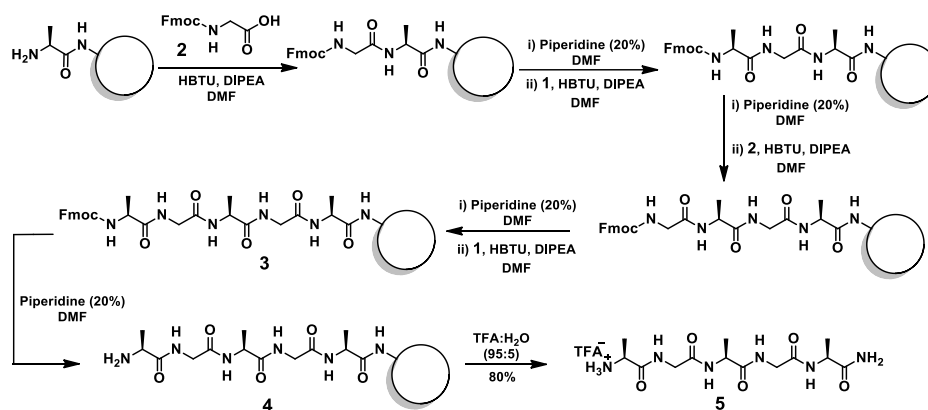
Scheme 4.3 Synthetic pathway followed in SPPS for obtaining pentapeptide **5**.

- ### *4.1.1.2 Synthesis of the Fmoc-pentapeptide derivative (6)*

As it has been previously mentioned, the synthesis of compound **6** was performed directly from SPPS. For this purpose, once compound **3** was achieved in the resin (see scheme 4.3), the subsequent Fmoc-deprotection to achieve pentapeptide **4** was not performed, and a cleavage with TFA:H$_2$O (95:5) at this point was carried out instead, affording the final product **6** (Scheme 4.4).
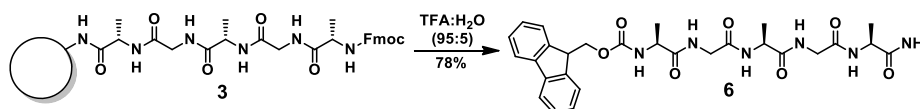
Scheme 4.4 Cleavage of compound **3** yielding the final compound **6**.

- ### *4.1.1.3 Synthesis of the anthracene-pentapeptide derivative (9)*

The synthesis of anthracene-pentapeptide **9** was performed in first place by a reduction of 2-anthraquinone carboxylic acid **7** with zinc and NH$_4$OH giving rise to the corresponding anthracene carboxylic acid **8**. Afterwards, an amidation reaction with pentapeptide **5** in presence of coupling reagents (HBTU and DIPEA) yielded product **9** (Scheme 4.5).
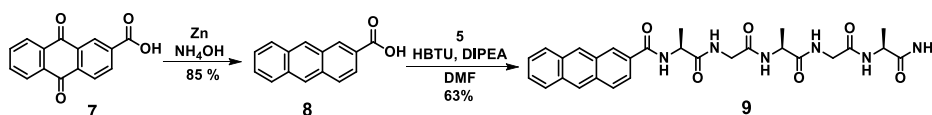
Scheme 4.5 Synthesis pathway of antharacene-pentapeptide derivative.

- ### *4.1.1.4 Synthesis of the exTTF-pentapeptide derivative (16)*

The synthesis of exTTF-pentapeptide **16** was performed firstly obtaining the required dimethyl (1,3-dithiol-2-yl)phosphonate **14** which is used for the synthesis of exTTF-COOH **15** through a Horner-Wadsworth-Emmons reaction. The phosphonate **14** was synthesized in a four steps procedure well stablished in our group.[123] For this end, commercially available vinylene trithiocarbonate **10** was methylated with Me$_2$SO$_4$,

[123] S. González, N. Martín, D. M. Guldi, *J. Org. Chem.* **2002**, *68*, 779-791.

reduced with NaBH$_4$ and treated with HBF$_4$ to produce the respective intermediates **11**, **12** and **13**. Final treatment of **13** with P(OMe)$_3$ gave rise to the desired phosphonate **14** in very good yield. The addition of *n*-BuLi over phosphonate **14** led to a very reactive anion which reacted readily with anthraquinone **7** to form the exTTF derivative **15**. Then, an amidation reaction with the pentapeptide **5** in presence of coupling reagents (HBTU and DIPEA) gave rise to the final compound **16** (Scheme 4.6).
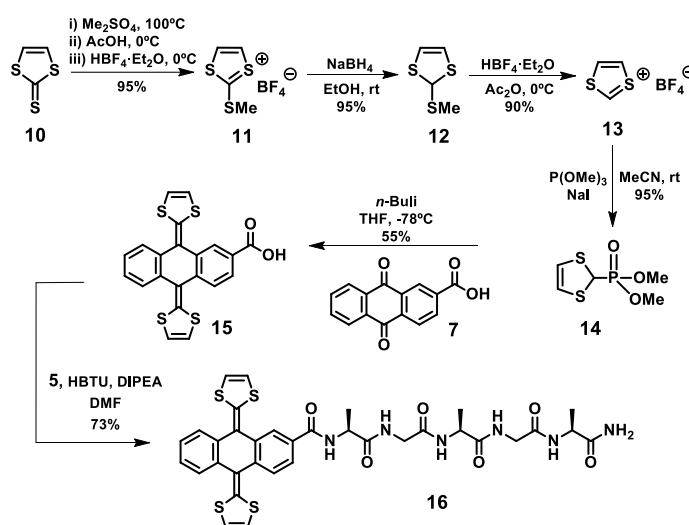
Scheme 4.6 Synthetic pathway for the preparation of exTTF-pentapeptide derivative.

All these products were fully characterized by standard spectroscopic techniques such as ^{1}H-NMR, ^{13}C-NMR, FTIR, Mass Spectrometry and UV-Vis spectroscopy. A detailed description of the synthesis is described in the Experimental Section.

4.1.2. Formation and characterization of supramolecular assemblies

As mentioned above, the design of molecule **16** was based on the following features: *i*) the pentapeptide Ala-Gly-Ala-Gly-Ala moiety was chosen due its high tendency to form *β*-sheets.[46,124] This repetitive unit (Ala-Gly) was found to be the most important repeated sequence in *Bombyx mori* silk, forming crystalline domains of *β*-sheets. *ii*)

---

[124] J. C. M. van Hest, D. A. Tirell, *Chem. Commun.* **2001**, 1897-1904.

The use of exTTF with its particular shape, facilitates the formation of 3D supramolecular assemblies.[73] Taking into account these features we expect that the different moieties presented in compounds **6**, **9** and **16**, that is, planar cores (**6** and **9**) *versus* concave one (**16**) give rise to remarkable differences in morphology.

To start our studies, we prepared solutions of compound **16** (1mg/1mL) in halogenated solvents such as $CHCl_3$ or 1,1,2,2-tetrachloroethane (TCE) and methanol (MeOH) as polar solvent. We tested halogenated solvents because they usually do not disrupt hydrogen bonding and the formation of supramolecular assemblies might be reasonably given, while in the case of MeOH such interactions are usually disrupted. Absorption essays showed a small bathochromic shift of around 5 and 10 nm in $CHCl_3$ or TCE with respect to MeOH (Figure 4.2 A). These shifts are far from what has previously been observed as an attest for $\pi-\pi$ interactions between exTTFs.[73] However, the small shift does not imply that supramolecular aggregates based on hydrogen bonding might not be given, therefore additional optical studies were carried out. In this sense, circular dichroism (CD) measurements were performed; in MeOH no CD signal was observed, but, in TCE, CD spectrum displayed a notable negative dichroic signal in the range of exTTF absorptions (Figure 4.2 B). Such observation is in agreement with the existence of supramolecular aggregates, in which a transfer of chirality occurs from the peptide to the exTTF unit. This transfer of chirality when molecules are aggregated has also been observed in related systems.[48,51]
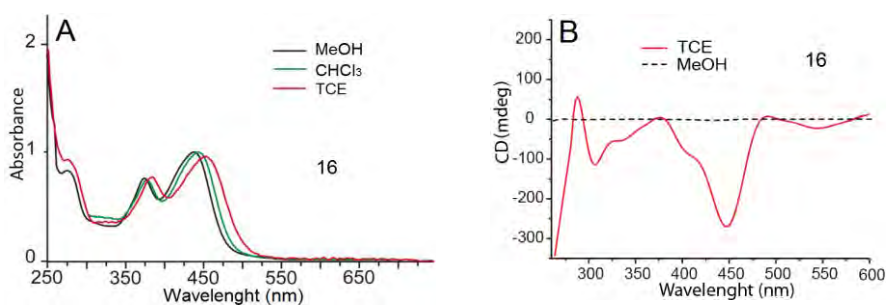
Figure 4.2 Absorption (A) and circular dichroism (B) spectra of compound **16** in different solvents.

In a similar way, absorption experiments for compounds **6** and **9** comprising planar moieties, in TCE, showed a bathochromic shift with respect to that observed in MeOH in which H-bonds are disrupted (Figure 4.3). These observations are in agreement with the existence of supramolecular aggregates in halogenated solvents.[125]
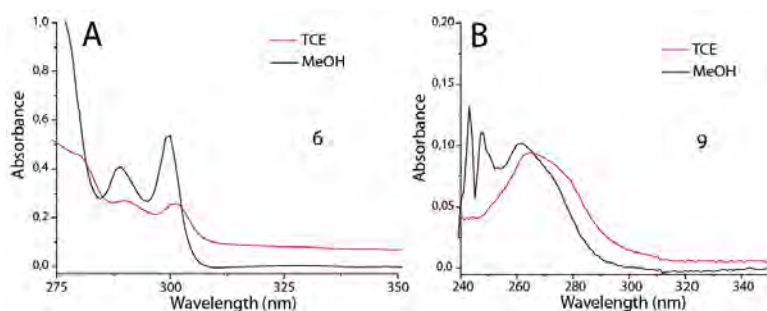
Figure 4.3 Absorption spectra of compounds **6** (A) and **9** (B) in TCE and MeOH.

Then, in order to confirm the existence of H-bonds in halogenated solvents Fourier Transform Infrared spectroscopy (FTIR) of respective compounds in TCE was performed. In fact, this technique shed light on the secondary structure adopted by the peptide backbone analyzing the $\nu_{C=O}$ vibration modes. The IR spectra for compounds **6**, **9** and **16** featured intense peaks for amide I ($\nu_{C=O}$) around 1629 cm^{-1} together with a weak shoulder around 1690 cm^{-1} (Figure 4.4 A-C), indicating the existence of intermolecular β-sheets in the peptide backbone in which the peptide units are interacting in an antiparallel mode (Figure 4.4 D and E). [46,47,126]

[125] K. J. Channon, G. L. Devlin, S. W. Magennis, C. E. Finlayson, A. K. Tickler, C. Silva, C. E. MacPhee, *J. Am. Chem. Soc.* **2008**, *130*, 5487-5491.

[126] a) A. Barth, C. Zscherp, *Q. Rev. Biophys.* **2002**, *35*, 369-430; b) Y. Cordeiro, J. Kraineva, M. P. B. Gomes, M. H. Lopes, V. R. Martins, L. M. T. R. Lima, D. Foguel, R. Winter, J. L. Silva, *Biophys. J.* **2005**, *89*, 2667–2676; c) H. Shao, J. R. Parquette, *Chem. Commun*. **2010**, *46*, 4285-4287.
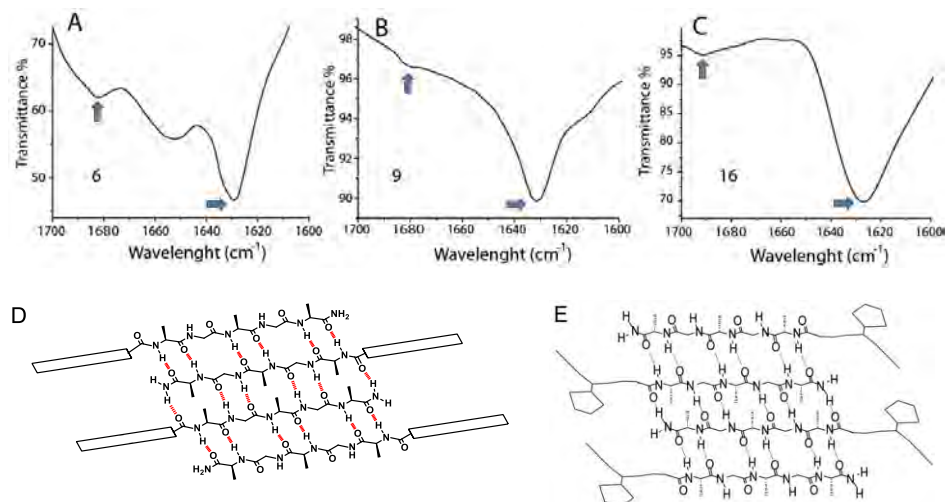
Figure 4.4 ATR-FTIR spectra of compounds **6** (A), **9** (B) and **16** (C) in TCE. Schematic representations of β-sheets for **6** and **9** (D) and **16** (E) interacting in an antiparallel fashion.

In order to gain insight about the morphology of the aggregated formed, Atomic Force Microscopy (AFM) measurements were performed. This technique lets to see the topography of a sample deposited over a substrate in the solid state with nanometer resolution. In this regard, a diluted solution of exTTF-pentapeptide **16** in TCE was drop-casted onto a mica surface. Inspection of selected areas showed the presence of predominately curved ropelike fibers with diameters ranging from 3 to 10 nm with helical features (Figure 4.5).
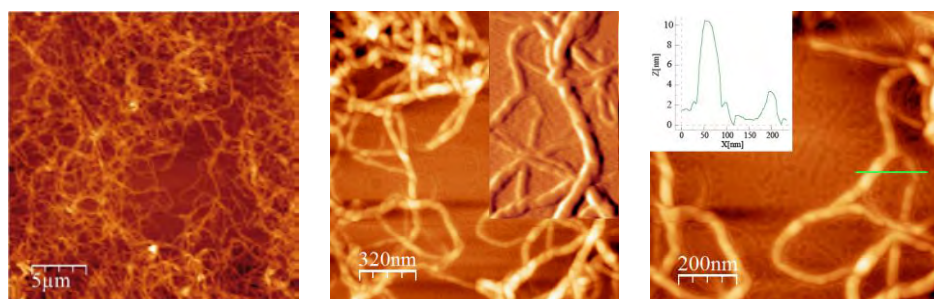
Figure 4.5 AFM height images of compound **16** from a solution of TCE (2 x 10^{-4} M) drop-casted on a mica surface at different zooms. Inset in the image at the middle shows the helical feature of fibers obtained. Inset in the image at the right indicates the height profile of the highlighted fibers.

In the case of compounds **6** and **9** under the same conditions to that of **16**, the presence of flat sheets with thicknesses of about 8-10 nm and homogenous nanospheres with diameters ranging from 20 to 30 nm were observed (Figure 4.6).
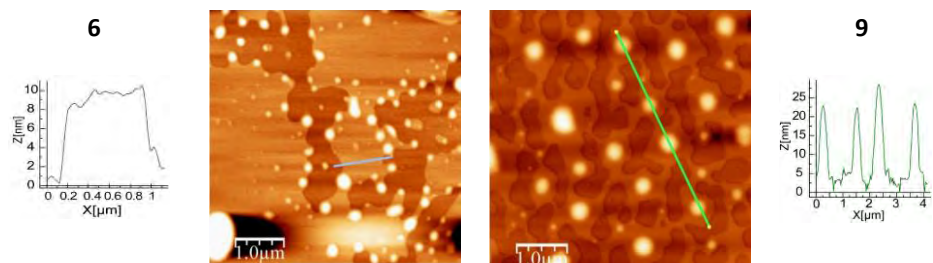
Figure 4.6 AFM height image of a TCE solution of **6** (2 x 10^{-4} M) on a mica surface and height profile of the section highlighted in blue (left). AFM height image of a CHCl$_3$ solution of **9** (2 x 10^{-4} M) on a mica surface and height profile of the section highlighted in green (right).

Considering these results, we believe that these observations can be explained on the hypothesis that the introduction of bulky exTTF in compound **16**, with its concave central core near to the β-sheet-forming peptide sequence, induces torsional strains in the secondary H-bonded nanostructure. In fact, the consequences of the latter are twofold: firstly, a maximum intermolecular H-bonding within the peptide backbone is preserved and secondly, mutual $\pi-\pi$ interactions between exTTFs are avoided. In turn, 1D helical nanostructures are formed at the nanoscale driven exclusively by H-bonding (Figure 4.4 D and figure 4.7 A). On the contrary, less-bulky planar aromatic cores, such as fluorene **6** and/or anthracene **9**, near the β-sheet forming peptide sequence, reduce the torsional strains in the nanostructures obtained and indeed, permit the interlocking of β-sheets through $\pi-\pi$ interactions between the aromatic cores.[44] As a consequence, nanospheres or sheets are obtained instead (Figure 4.4 E and Figure 4.7 B) which are normal nanostructures derived from the assembly of peptides derivatives.[127]

---

[127] a) M. Zelzer, R. V. Ulijn, *Chem. Soc. Rev.* **2010**, *39*, 3351-3357; b) E. De Santis, M. G. Radnov, *Chem. Soc. Rev.* **2015**, DOI: 10.1039/c5cs00470e.
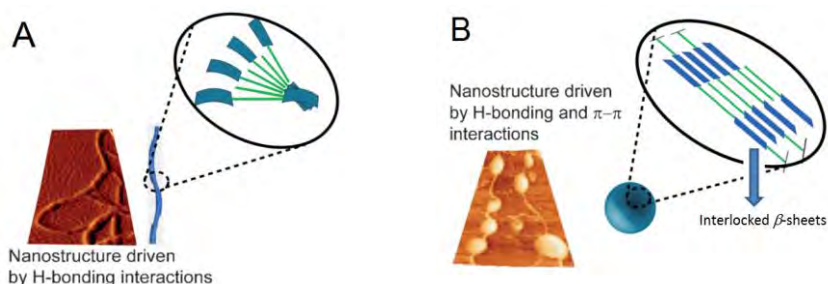
Figure 4.7 Schematic representation of the nanostructures obtained for concave-bulky core **16** (A) and planar cores **6** and **9** (B).

In this regard, evidences that help to support the fact that nanostructures obtained for compounds **6** and **9** are stabilized through $\pi-\pi$ interactions forming interlocked β-sheets, were provided by fluorescence assays. A strong fluorescence quenching in TCE with respect to that in MeOH was observed (Figure 4.8). This result suggests the existence of aromatic-aromatic ($\pi-\pi$) interactions in TCE. Moreover, these observations have also been described in other aromatic peptides derivatives, where strong $\pi-\pi$ interactions between aromatic units in the β-sheet secondary structure take place in.[44,125] In the case of **16**, due to the low fluorescence of exTTF moiety, these experiments could not be performed, however, the lack of interactions between exTTF units can be derived from absorption experiments in which the exTTF band is far from what has previously been observed as an attest for $\pi-\pi$ interacting exTTFs (Figure 4.2 A).[73]
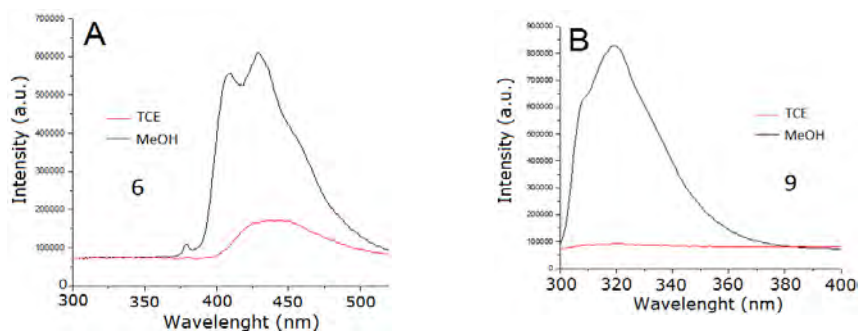
Figure 4.8 Fluorescence spectra for compounds **6** (A) and **9** (B) in TCE and MeOH (λ_{exc} = 270 nm).

In order to gain additional insight about supramolecular nanostructure, X-ray diffraction (XRD) studies were performed. Powder XRD of a dried precipitated obtained from **6** in TCE, showed a pattern displaying reflections of the (001) to (006) planes, which indicates a long-range ordered lamellar structure (Figure 4.9 A). Furthermore, XRD pattern showed a "*d*-spacing" at 8.4 Å that is in accordance with the repetitive distance through the axis of H-bonds in which the molecules are arranged in an antiparallel fashion (Figure 4.9 C). Similarly, the intra-strand distance ranging at 4.1 Å and the $\pi-\pi$ interactions distance between aromatic rings at 3.4 Å were also observed. This pattern suggests that the nanostructures formed are composed of several interlocked β-sheet arrangements (Figure 4.9 C) and is similar to those previously observed for related systems.[45,51,125,128] Unfortunately, XRD studies for compound **16** in TCE did not show any long-range detectable pattern (Figure 4.9 B).
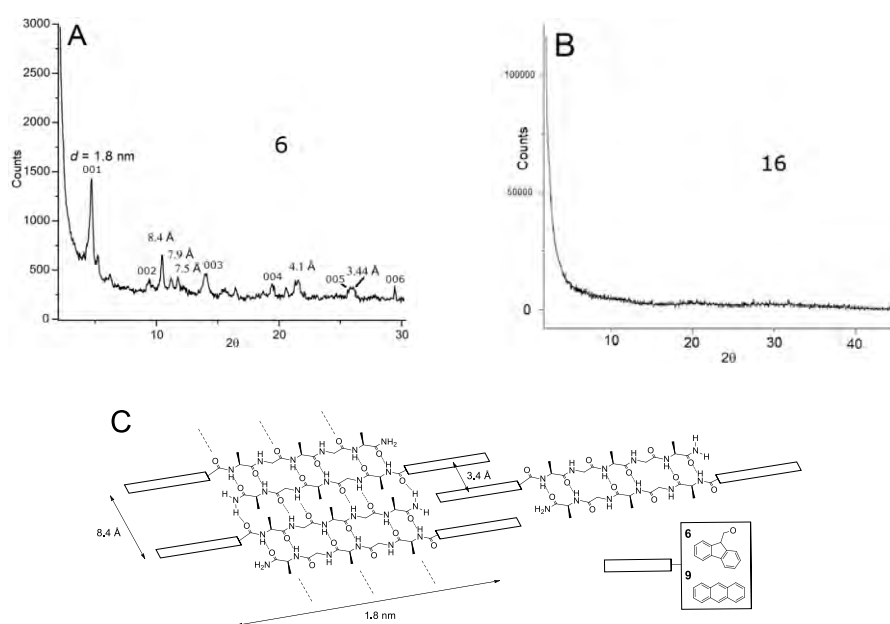
Figure 4.9 Powder XRD studies of dried precipitates of compounds **6** (A) and **16** (B). Proposal model for the nanostructure with the distances observed in XRD for **6** (C).

[128] A. M. Smith, R. J. Williams, C. Tang, P. Coppo, R. F. Collins, M. L. Turner, A. Saiani, R. V. Ulijn, *Adv. Mater.* **2008**, *20*, 37-41.

So far and in summary, the supramolecular growth of **6** and **9** (bearing less-bulky planar aromatics rings) at the nanoscale length in halogenated solvents is mainly governed by H-bonding and $\pi-\pi$ interactions as it has been demonstrated. On the contrary, for **16** (bearing bulky non-planar exTTFs) the nanostructure growth is a consequence of exclusively intermolecular H-bonding interactions between peptide units. The latter seems to be susceptible to a subsequent self-assembly process at mesoscopic length scales. In this regard, we tested the peculiar non-planar shape of exTTF as a means to create tertiary structures, that is, mesoscopic nanoarchitectures.[73] We rationalized that the solvophobic collapse of the nanometric ropelike fibers formed in halogenated solvents would promote intermolecular $\pi-\pi$ interactions between exTTFs. The latter would be the inception to assemble these fibers into mesoscopic helical materials, in which the helical handedness is controlled by the peptides.

To this end, we aged **16** in a solvent mixture of $CHCl_3$ and methylcyclohexane (MCH) (1:1 v/v). After one week of aging, a change of color was observed. This observation was corroborated by absorption essays which showed a large bathochromic shift of the lower energy band from 450 to 500 nm and a concomitant decrease of the initial absorption band (Figure 4.10 A). Such a bathochromic shift of around 50 nm is similar to a previously reported system in our group that attest $\pi-\pi$ interactions between exTTFs in the newly supramolecular ensemble.[73] It is worth to mention that after adding few drops of MeOH to the aged solution of **16**, resulted in a recovery of the initial exTTF absorptions. These observations point to the overall reversibility of the process (Figure 4.10 B).
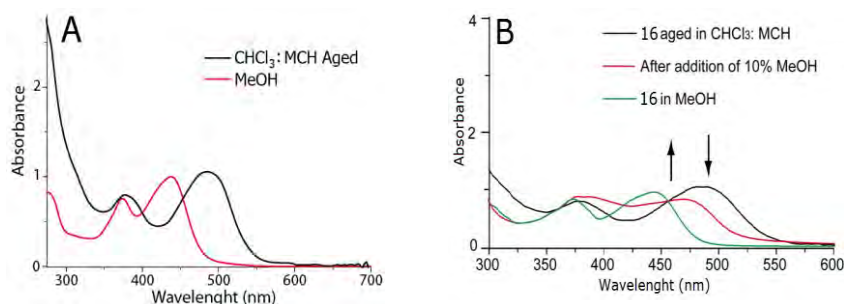
Figure 4.10 (A) UV-Vis spectra of an aged solution of **16** in CHCl₃:MCH and in MeOH. (B) UV-Vis spectra showing the addition of few drops of MeOH to an aged solution of **16** in the mixture CHCl₃:MCH.

With the aim to obtain information about the structural morphology of the dispersion obtained for **16** in the aged mixture CHCl₃:MCH, scanning electron microscopy (SEM), transmission electron microscopy (TEM) and X-ray diffraction (XRD) studies were performed. SEM provides information about the sample's surface topography at nano- and micrometer scales. For this end, a drop of the dispersion was deposited over a glass substrate and further recovered with Au film prior to observation. Inspection through this technique showed the formation of mesoscopic helical fibers as can be observed in figure 4.11. It is important to remark how the fibers are twisted along different areas (see white arrows).
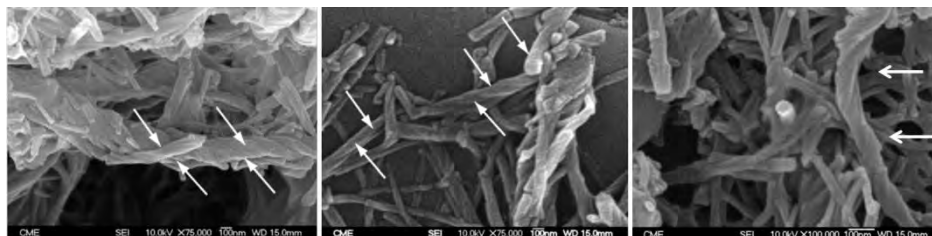
Figure 4.11 SEM images of a dispersion of aged **16** (8×10^{-4} M) in CHCl₃:MCH. Arrows indicate selected areas in which twisting is more clear.

These helical fibers are composed of several tightly entwined fibrils, possibly as a consequence of a solvophobic collapse promoted in the solvents used for the aging. These results suggest favorable interactions between adjacent supramolecular fibrils (previously formed by H-bonds) driven by efficiently $\pi-\pi$ interacting exTTFs. Low

97

amplification SEM images showed the growth of several nanofibers with sizes over 100 nm (Figure 4.12 A and B). TEM enables to examine fine details at nanometer scales; studies performed with this technique indicated that the nanofibers observed are formed by several stripes separated by a periodic distance of ~3 nm (Figure 4.12 C). This is in accordance with AFM observations (Figure 4.5).
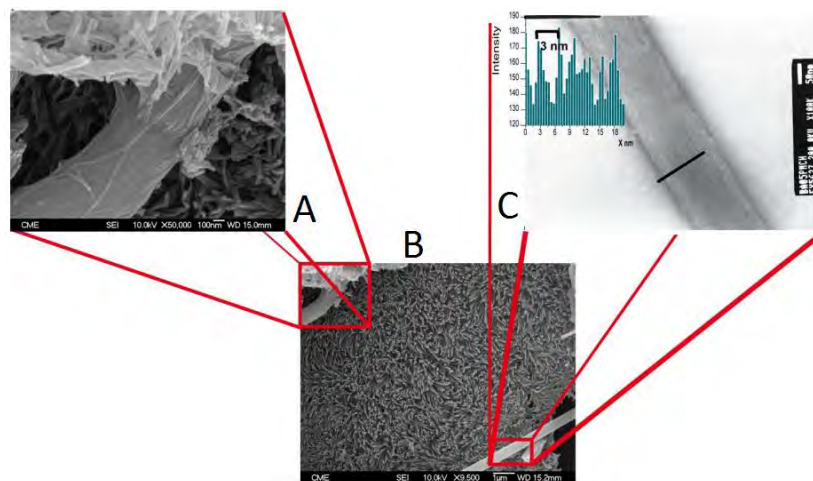
Figure 4.12 SEM (A and B) and TEM (C) images obtained from a dispersion of **16** (8 x 10^-4 M) in a mixture of CHCl$_3$:MCH. TEM sample was stained with an aqueous solution of uranyl acetate 2% (scale bar in C = 50 nm).

XRD studies of a precipitate obtained from the aged dispersion of **16** showed a number of sharp reflections at *d* spacings of 9.5, 8.98 and 3.3 Å (Figure 4.13 A). The two former *d* spacings are similar to those observed for supramolecular β-sheet arrangements in other chromophore-peptide systems.[47,51] Here the lack of the typical shorter interstrand reflections at *d* spacings in the range of 4-5 Å (i.e., 2θ values between 18 and 22°) is in accordance with our model of antiparallel β-sheet arrangements and in agreement with our experimental FTIR results. In this type of supramolecular arrangements in which antiparallel β-sheet fashion predominates, the repetitive distance is usually at around 0.9 nm, which is in accordance with our results.[129] Furthermore, it is worth to mention that the XRD pattern shows clearly a

[129] E. D. T. Atkins, in *Supramolecular and Colloidal Structures in Biomaterials and Biosubtrates*, Wordscientific, UK, **1999**.

distance of 3.3 Å, which we assigned to $\pi-\pi$ distances between exTTFs in the nanostructure. In fact, this value is in good agreement with previous calculations for $\pi-\pi$ interacting exTTFs in supramolecular systems.[73] Notably, this is the first time that $\pi-\pi$ distances between interacting exTTFs have been experimentaly determined for supramolecular nanoarchitectures. The XRD pattern also shows an intense and sharp reflection at 2.9 Å (Figure 4.13 A, see asterisk) which is probably originated from co-crystallized solvent molecules used for the growth of the nanostructures.
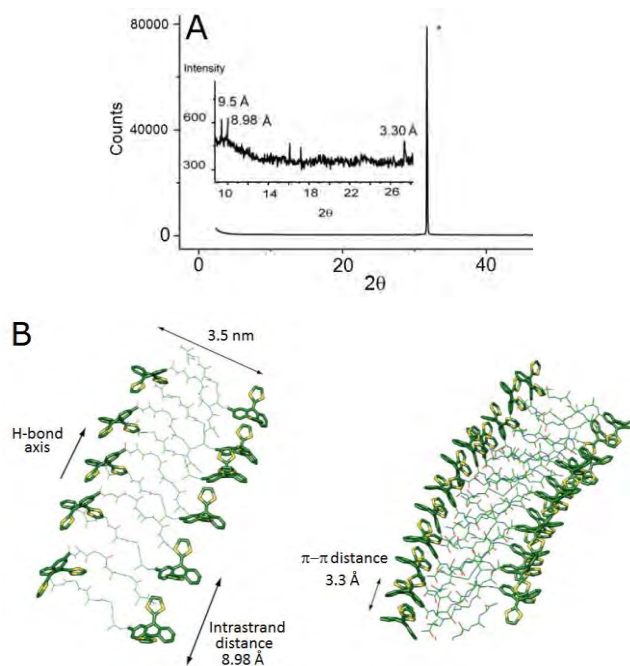
Figure 4.13 (A) Powder X-ray pattern obtained from a dispersion of aged **16** in CHCl$_3$:MCH. Asterisk represents the peak originated from co-crystallized solvent molecules used for the growth of the nanostructures. (B) Proposed tertiary structure (stacks of β-sheets) of the fibers obtained from the solvent mixture CHCl$_3$:MCH.

In contrast to the above findings, aging of solutions of **6** and **9** under the same experimental conditions and concentrations used for **16** resulted in the formation of white crystalline solids. Inspections by SEM showed the presence of long and straight fibers for **6** and planar leaves for **9** (Figure 4.14). In agreement with AFM results the observed nanoarchitectues did not show any helical signature.

99
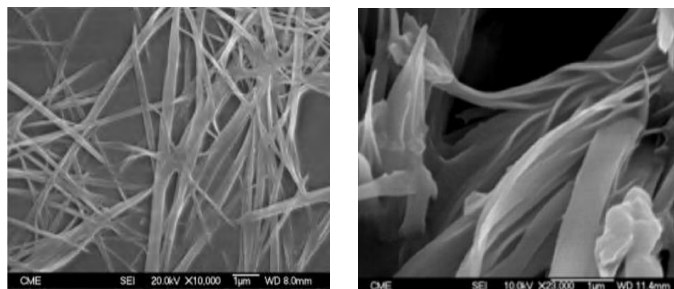
Figure 4.14 SEM images obtained for **6** (left) and **9** (right) (8 x 10^{-4} M) from a mixture of CHCl$_3$/MCH (8 x 10^{-4} M).

As a complement, transient absorption measurements of **16** in MeOH (Figure 4.15) and CHCl$_3$/MCH (Figure 4.16) were performed. In particular, 387 nm photoexcitation of **16** in MeOH leads to the instantaneous formation of transient species that features a strong minimum at 440 nm, a strong maxima at 500 nm and a series of weaker maxima at 730, 805, 930, 1000, 1035 and 1150 nm. Notable is that the 440 nm minimum is a good match of the exTTF-centered absorption seen in the ground state. With a rate of 6.6 x 10^{11} s^{-1} all of the above features have decayed into a new and weak transition that maximizes around 550 nm. The latter decays with rate constant of 8.1 x 10^9 s^{-1} during which the ground state is completely reinstated. Implicit are ultrafast deactivations of excited states that are centered exclusively at exTTF. The presence of sulfur atoms is responsible for a second-order spin orbit couplings.

The transient absorption changes with aged **16** in CHCl$_3$:MCH upon excitation at 387 nm are quite different. Firstly, two minima – instead of just one – are discernable, namely at 455 and 560 nm, which again reflect the ground-state absorption of **16**. Secondly, in the visible only a 495 nm maximum is seen, whereas the near-infrared is best characterized by a rather broad feature that spans from around 600 nm all the way to 1200 nm. Thirdly, the kinetics in the visible range give rise to a fast (i.e., 1.8 x 10^{11} s^{-1}) and a slow (i.e., 1.2 x 10^9 s^{-1}) process to yield a stable transient, whereas the kinetics in the near-infrared range show only evidence for the fast (i.e., 2.3 x 10^{11} s^{-1}) and the slow (i.e., 1.1 x 10^9 s^{-1}) processes without giving rise to the stable transient. A

plausible rationale implies the delocalization of the exTTF-centered excited state in aged **16**.
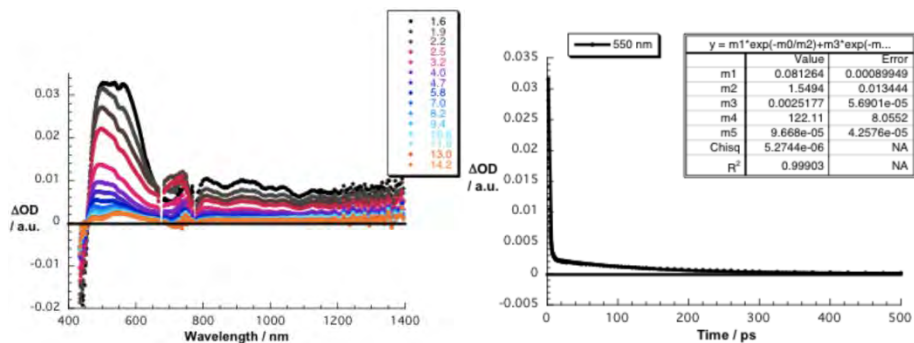
Figure 4.15 (Left) Differential absorption spectra (visible and near-infrared) obtained upon femtosecond flash photolysis (387 nm, 150 ns) of **16** in methanol with several time delays between 0 and 14.2 ps at room temperature – see figure legend for time evolution. (Right) time-absorption profile of the spectra at 550 nm, monitoring the excited state decay.
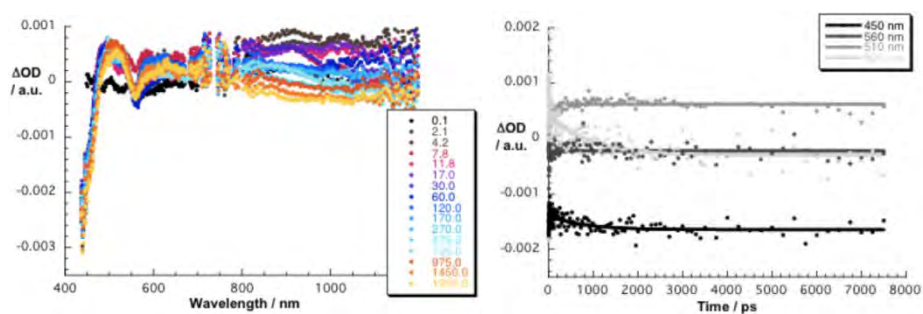
Figure 4.16 (Left) Differential absorption spectra (visible and near-infrared) obtained upon femtosecond flash photolysis (387 nm, 150 ns) of **16** in CHCl$_3$:MCH with several time delays between 0 and 1950 ps at room temperature – see figure legend for time evolution. (Right) time-absorption profiles of the spectra at 460, 510, 560, and 920 nm, monitoring the excited state decay.

Finally, a back transformation of aged solution **16** in MCH into **16** in MeOH, which is induced by dissolving aged **16** in pure MeOH, leads in line with steady-state absorption measurements to exactly the same transient spectra that were recorded upon photoexcitation of **16** in MCH, namely a fast decaying exTTF-centered transient. Importantly, when employing mixtures of CHCl$_3$:MCH and MeOH evidence for both species emerged.

SECTION 4.2

SUPRAMOLECULAR ONE DIMENSIONAL *N/P* NANOHYBRIDS

4.2. SUPRAMOLECULAR ONE DIMENSIONAL *N/P* NANOHYBRIDS

As mentioned in the objectives, this section is focused on the formation of 1D *n/p* nanohybrids. For this, we use the exTTF-nanofibers **16** described previously and we combine them with electron acceptor molecules such as fullerene C_{60} (**17**) and phenyl-C_{61}-butyric acid methyl ester (PCBM, **21**). The latter is a widely used electroactive molecule in photovoltaic devices.[80]

4.2.1. Synthesis of building blocks

The synthesis of compound **16** was already described in the previous chapter. Fullerene C_{60} (**17**) is commercially available and PCBM **21** was synthesized using the methodology described in the literature (Scheme 4.7).[130]
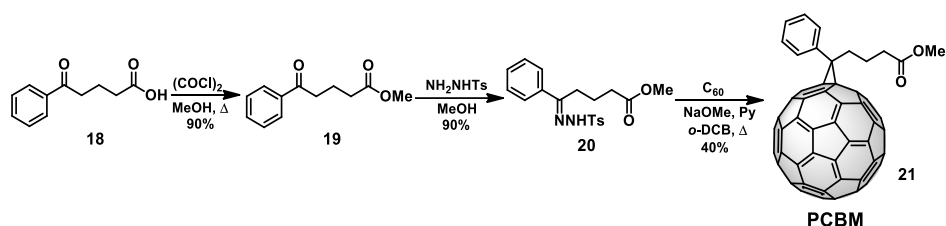
Scheme 4.7 Synthesis of PCBM.

An esterification of 4-benzoyl butyric acid **18** using oxalyl chloride in MeOH gave rise to compound **19** which was further treated with tosylhydrazine to produce the respective tosylhydrazone derivative **20**. Then, the Schiff base **20** in presence of sodium methoxide generates *in situ*, through a Bamford-Steven reaction, a diazoderivative that rapidly reacts with C_{60} by means of a 1,3-dipolar cycloaddition and extrusion of N_2 affording PCBM (**21**). Detailed description of the synthesis is described in the Experimental Section.

---

[130] J. C. Hummelen, B. W. Knight, F. LePeq, F. Wudl, *J. Org. Chem*. **1995**, *60*, 532-538.

4.2.2. Formation and characterization of supramolecular 1D n/p nanohybrids

We started this study fabricating exTTF-nanofibers **16** in TCE followed by the addition of C_{60} or PCBM. In this approach, it is important to take into account three key issues: *i*) the supramolecular structure of the exTTF-nanofibers formed in TCE is based only on hydrogen bonds in which exTTF units are not interacting between them, *ii*) the addition of C_{60} or PCBM to the exTTF-nanofibers would lead to the formation of 1D *n/p*-nanohybrids through non-covalent $\pi-\pi$ interactions between exTTF and C_{60}/PCBM units,[64,66,68,131] iii) the susceptibility of C_{60} or PCBM to aggregate itself, favors the crystallization of C_{60}/PCBM over the formed nanohybrid. As a matter of fact, we reasoned that these features ensure an efficient interfacing between C_{60} or PCBM and exTTF-fibers as a means of facilitating the growth of 1D *n/p*-nanohybrids. It is worth to note that our approach does not involve covalent chemical modifications, demonstrating the versatility of our system for nanostructuring electroactive fullerene derivatives.

As indicated above, we started these studies forming exTTF-nanofibers **16** in TCE (1mg/1mL) followed by the addition of equivalent amounts of C_{60} or PCBM. The characterization of the nanohybrids (**16:C$_{60}$** and **16:PCBM**) was performed through a variety of techniques such as UV-Vis, circular dichroism, AFM, TEM, SEM, Raman, FTIR, XRD and transient absorption spectroscopy.

The first evidence of nanohybrid formation was obtained by UV-Vis and circular dichroism spectroscopies. Initially, absorption studies of the mixtures did not show remarkable changes, however, upon aging the solutions for at least 5 days notable changes could be observed. UV-Vis spectra of an aged solution of **16:C$_{60}$** gave rise to a depletion and a red-shifting of the initial exTTF-fibers absorptions from 449 to 456 nm; this accompanied by an increase in the absorption in the region > 470 nm (Figure

[131] a) G. Fernández, E. M. Pérez, L. Sánchez, N. Martín, *J. Am. Chem. Soc.* **2008**, *130*, 2410-2411; b) G. Grimm, J. Santos, B. M. Illescas, A. Muñoz, D. M. Guldi, N. Martín, *J. Am. Chem. Soc.* **2010**, *132*, 17387-17389.

4.17 A-top). These features are assigned to π-π interactions between exTTF and C_{60}.[64,66,68,131] Similar results were obtained for the mixture with PCBM (Figure 4.17 B-top).
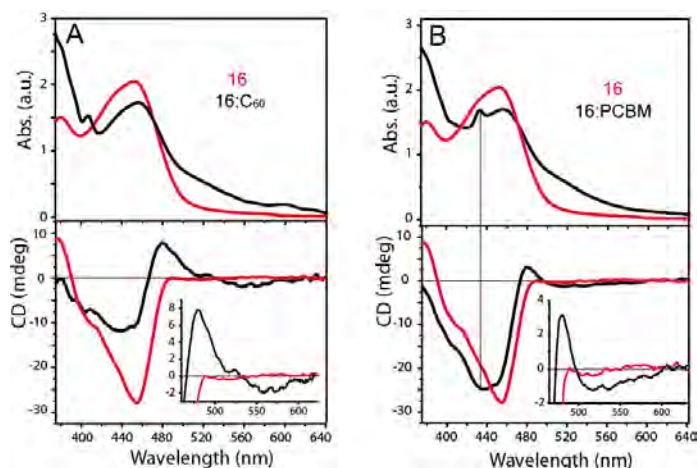
Figure 4.17 UV-Vis (top) and circular dichroism (bottom) spectra for exTTF-fibers **16** (red lines) and *n/p*-nanohybrids **16:C$_{60}$** (A) and **16:PCBM** (B) (black lines).

However, more pronounced were the changes noted in circular dichroism (CD) assays, in which the mixture **16:C$_{60}$** resulted in a positive dichroic signal at 483 nm and a negative signal at 439 nm (Figure 4.17 A-bottom). In line with previous reports, the signal at 483 nm is attributed to π-π interactions between C_{60} and exTTF in the new supramolecular helical arrangements.[64,66,68,131] Furthermore, an additional dichroic signal was observed in the 500-600 nm region, which is due to the fact that C_{60} is placed in a chiral environment owing to the lack of absorbance of the exTTF-nanofibers in this spectral region (Figure 4.17 A-bottom, inset).[100,102] Similarly, CD experiments with **16:PCBM** showed a positive signal at 480 nm and a negative one at 432 nm, which matches the typical absorptions of C_{60} monoadducts (Figure 4.17 B-bottom). Likewise, the new broad negative signal in the 500-600 nm region was also observed (Figure 4.17 B-bottom, inset). These findings point to the formation of chiral *n/p*-nanohybrids in which electron acceptor units (C_{60} and PCBM) have been inserted within the exTTF-fibers nanostructure through π–π interactions.

The formation of the *n/p*-nanohybrids was also investigated by Raman experiments. These studies were performed for pristine C_{60} and PCBM as references, and the *n/p*-nanohybrids formed from the respective mixtures (**16:C₆₀** and **16:PCBM**). In the case of pristine C_{60}, the characteristic $A_g(2)$ pentagonal pinch mode at 1466 cm^{-1} was observed.[93] In stark contrast, the $A_g(2)$ mode for the nanohybrid **16:C₆₀** gave rise to a slight shift towards lower frequencies, that is, 1461 cm^{-1} (Figure 4.18 A). As such, interactions between exTTF-fibers and C_{60} are inferred. Similar trends were noticed for nanohybrid **16:PCBM** respect to PCBM (Figure 4.18 B).
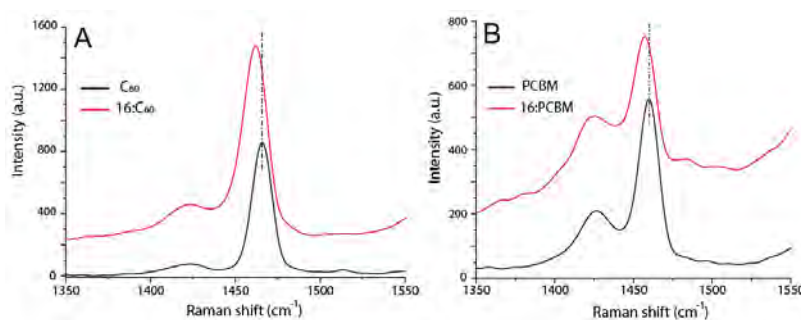
Figure 4.18 Raman spectra (λ_{exc} = 532 nm) of C_{60} and PCBM as references (black spectrum) and *n/p*-nanohybrids **16:C₆₀** (A) and **16:PCBM** (B) (red spectrum) on glass microscope slide.

With the aim of observing the possible morphological changes upon *n/p*-nanohybrid formation, AFM, SEM, TEM and XRD experiments were performed. AFM studies from the aged mixtures (**16:C₆₀** and **16:PCBM**) revealed the presence of bigger and more straight fibers (Figure 4.19) in comparison to the initial exTTF-fibers which are smaller and more entangled (Figure 4.5). AFM height profiles showed that the new fibers are higher (14-22 nm) than those obtained from only **16** (3-10 nm) (see insets in Figure 4.19). Such an increase in size, points to the *n/p*-nanohybrids formation. Furthermore, it is possible to discern C_{60} and PCBM saturated domains over the fibers (see arrows in Figure 4.19), presumably indicating the selective crystallization guided by the nanohybrid and triggered by the local saturation and high tendency of C_{60} and PCBM to aggregate as mentioned at the beginning of this section. The latter observation was further corroborated with TEM and SEM techniques which will be presented below.
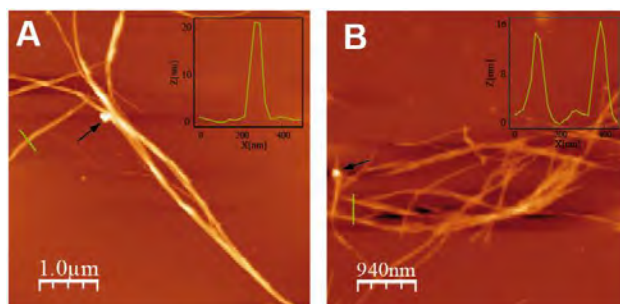
Figure 4.19 AFM images of aged solutions of **16:C$_{60}$** (A) and **16:PCBM** (B) (1.5 x 10^{-4} M) drop-casted on mica. Insets: height profiles of the respective green lines in A and B. Black arrows indicate C$_{60}$ (A) or PCBM (B) domains over the fibers.

TEM experiments carried out for **16:C$_{60}$** showed the presence of large straight fibers, in which C$_{60}$ crystal nuclei over the fibers are discernable (Figure 4.20 A-B, red arrows). In a similar way to that observed in biomimetic mineralization processes, the crystals grow along the fiber's axis (Figure 2.7).[35] SEM experiments corroborate also the oriented C$_{60}$ crystal growth exclusively on fiber's surfaces (Figure 4.20 D-E, black arrows). Furthermore, this tendency was also observed for **16:PCBM**, where PCBM domains grow along the fiber's axis (Figure 4.20 C and F).
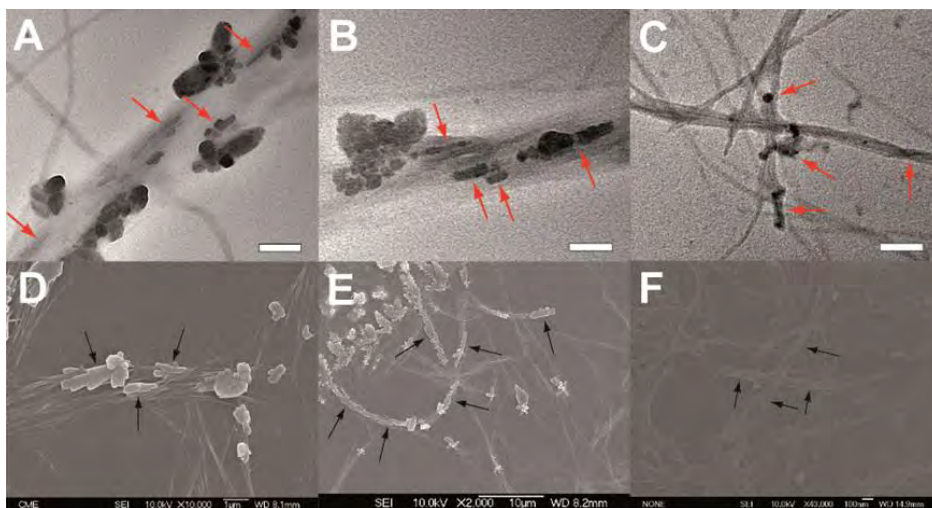
Figure 4.20 TEM images of nanohybrids **16:C$_{60}$,** (A and B) and **16:PCBM** (C) (1.5 x 10^{-4} M), red arrows remark the presence of C$_{60}$ or PCBM domains along the fiber's axis. Scale bars: 200 nm. SEM images of nanohybrids **16:C$_{60}$,** (D and E) and **16:PCBM** (F) (4.3 x 10^{-4} M), black arrows show the lengthening of C$_{60}$ and PCBM domains in the axial direction of the fibers.

To shed light on the formation of C_{60} crystals over the fibers, high resolution TEM (HRTEM) measurements were performed. A high inspection over these domains showed clearly C_{60} crystal lattices with a distance around 1.1 nm (Figure 4.21).
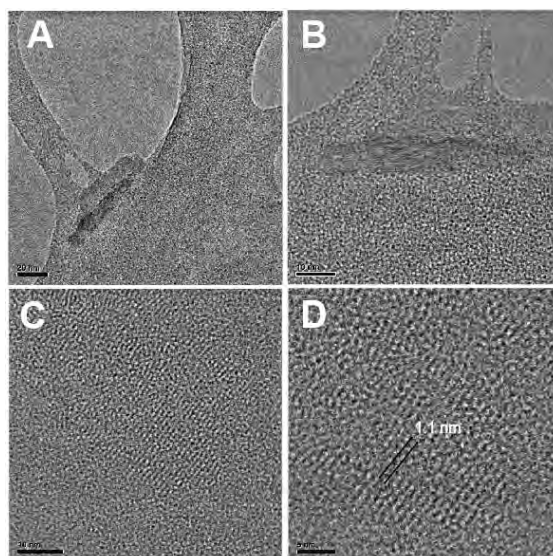
Figure 4.21 HRTEM images obtained from the mixture **16:C$_{60}$** in TCE (1.5 x 10^{-4} M).

In general terms, we believe that upon addition of fullerenes to the exTTF-nanofibers a new supramolecular structure is achieved (Figure 4.22, left-middle) and that nucleation of C_{60} or PCBM crystals on the surface of nanohybrids is followed (Figure 4.22, right). This process is analogous to peptide mineralization in which hydroxyapatite crystals grow along the axis of peptide nanofibers.[35] To the best of our knowledge, the use of supramolecular nanostructures as seeds for ordering "electroactive molecules" such as C_{60} or PCBM at the nanoscale is unprecedented.
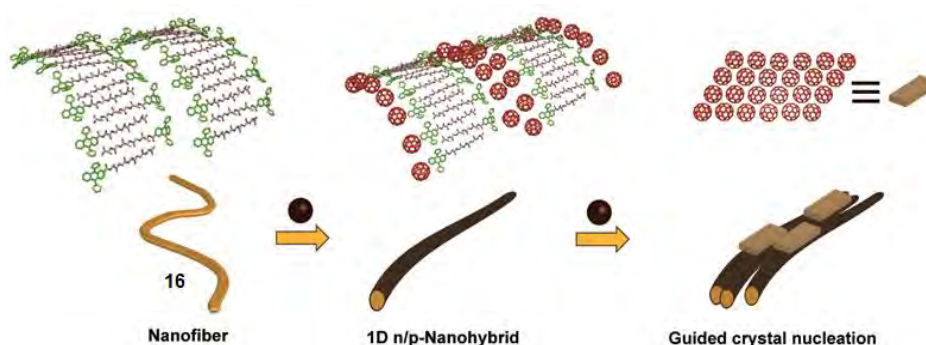
Figure 4.22 Schematic representation of nanohybrid formation and further guided crystallization on top of them. Brown circles refer to C_{60} or PCBM molecules.

In order to probe the key role of exTTF units in the guided growth of C_{60}/PCBM domains over the fibers, we performed control experiments in which we used a planar system such as compound **6** (Fmoc-Ala-Gly-Ala-Gly-Ala) from the previous section for such crystallization. Although compound **6** does not give rise to fibers in TCE, we fabricated them in the mixture $CHCl_3$:MCH (Figure 4.14). Then, the solvent was evaporated until dryness and a solution of C_{60} in TCE was added which was aged for 5 days trying to simulate similar conditions to that of nanohybrids based on **16**. An inspection by SEM showed the presence of C_{60} domains together with some small nanofibers. It can be tentatively said that C_{60} crystals are discerned over the nanofibers but most of them evolved in domains that lack any fiber (Figure 4.23, red squares), however this insight remains intuitive and any clear conclusion can be derived.
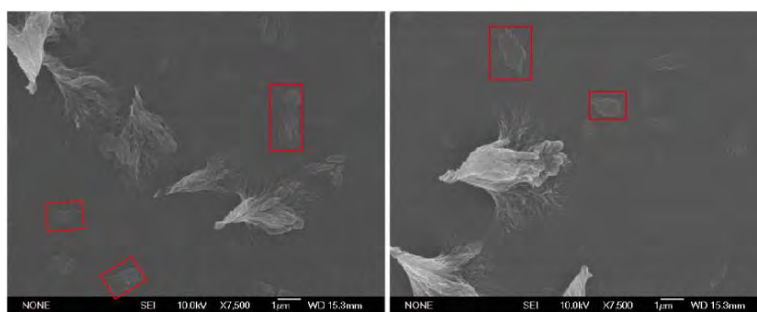
Figure 4.23 SEM images obtained from the mixture of **6:C_{60}** aged for 5 days (4.3 x 10 $^{-4}$ M). Red squares correspond to C_{60} domains out of the nanofibers domains.

111

To gain insight about the supramolecular structure of nanohybrids XRD and FTIR studies were performed. XRD studies for the nanohybrid **16:C$_{60}$** showed a new set of long range order with *d*-spacings at 4.6, 2.3, and 1.5 nm (Figure 4.24 A). Such a new set was associated with lamellar packing originated from exTTF-fibers within the newly formed *n/p*-nanohybrids. The lamellar pattern with a *d*-spacing of 4.6 nm relative to 3.6 nm for exTTF-fibers (obtained from a dispersion **16** in TCE:toluene, Figure 4.24 B) infers an increase of about 1 nm which is attributed to the insertion of C$_{60}$ within the nanostructure as shown in figure 4.24 C. Furthermore, two signals with *d*-spacings of 1.03 and 0.87 nm were observed (denoted as h$_{full}$, Figure 4.24 A, inset), which could be assigned to close packed columns of C$_{60}$ intercalated between exTTFs and in agreement with the crystals lattices observed in HRTEM measurements (Figure 4.24 C).[71,94,132]
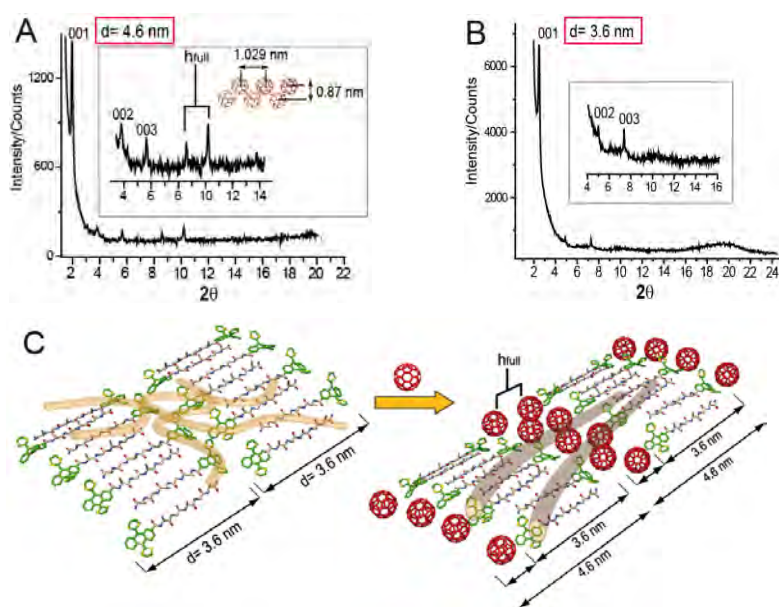
Figure 4.24 A) XRD pattern for **16** obtained from a dispersion of exTTF-fibers in a mixture TCE:toluene. B) XRD pattern for **16:C$_{60}$** nanohybrid. In the inset, "h$_{full}$" denotes the observed C$_{60}$ reflections in the 2θ region between 8 and 11. C) Cartoon showing the molecular packing observed for the exTTF-fibers and for **16:C$_{60}$** nanohybrid.

[132] a) J. Lenoble, N. Maringa, S. Campidelli, B. Donnio, D. Guillon, R. Deschenaux, *Org. Lett.* **2006**, *8*, 1851-1854; b) M. Makha, A. Purich, C. L. Raston, A. N. Sobolev, *Eur. J. Inorg. Chem*. **2006**, 507–517.

In the case of **16:PCBM**, despite XRD did not show a clear pattern as **16:C$_{60}$**, a broad signal with *d*-spacing of about 1 nm (2θ region between 8 and 11) supports the notion of close packed columns of PCBMs (Figure 4.25).
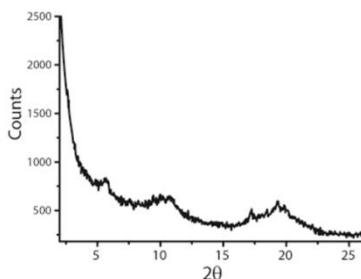
Figure 4.25 XRD experiment carried out for nanohybrid **16:PCBM** in TCE.

In order to confirm the proposed model for the n/p-nanohybrids FTIR experiments were performed. The results showed that intermolecular β–sheets in the peptide backbone are retained within the internal structure of the nanohybrids (Figure 4.26). In both cases an intense amide I peak at around 1627 cm^{-1} together with a weak shoulder at around 1680 cm^{-1} confirmed the existence of β–sheets in an antiparallel mode (Figure 4.26).[46,47,126]
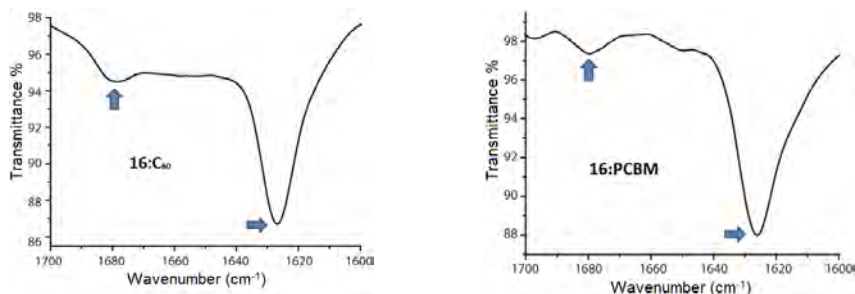
Figure 4.26 ATR-FTIR of n/p-nanohybrids **16:C$_{60}$** (left) and **16:PCBM** (right).

With the aim of studying the electron transfer process, photophysical studies were performed. Initially, reference experiments with exTTF, C$_{60}$ and PCBM in solution were probed. To this end, exTTF reveals upon radiation at 480 nm a short lived excited state spectrum with features that include transient maxima at 695 nm. From multi-wavelength analyses a lifetime of 0.075 ± 0.015 ns was determined, by which the

113

photoexcited exTTF decays to the singlet ground state. An efficient second order spin coupling is responsible for this fast process. In stark contrast, for C_{60}/PCBM a much slower deactivation – on the order of 1.5 ± 0.2 ns – of the singlet excited state transients is noted. Products are, however, the triplet excited states, which are formed in any of the cases nearly quantitatively. The most notable transient features of the singlet and triplet excited states are for C_{60} maxima at 965 and 750 nm, respectively. For PCBM, these maxima are shifted towards 960 and 690 nm.

Pump probe experiments with the aged **16:C$_{60}$** *n*/*p*-nanohybrid let immediately upon photoexcitation (480 nm) to differential absorption spectra, which are sound in agreement with the features of the C_{60} singlet excited state. These decays, however, in contrast to what has been seen in the reference experiments on the time scale of less than 100 ps, give rise to new species. The latter resembles with transient maxima at 700 and 1030 nm those seen upon the one electron oxidation of exTTF and the one electron reduction of PCBM, respectively (Figure 4.27). In the case of C_{60}, the near-infrared maximum evolved at around 1080 nm (Figure 4.27). As such, we conclude that photoexcitation of the self-assembled nanohybrids proceeds via a transient excited state into a charge separated state. A kinetic analysis across the visible and near-infrared assisted in gathering the rate constants for charge separation and charge recombination. In particular, for C_{60} and PCBM the values were 2.6×10^{10} / 1.1×10^{9} and 1.2×10^{11} / 8.1×10^{8} s^{-1}, respectively. Interesting is that in these cases only one long lived transient is discernable after the conclusion of the charge recombination, namely the triplet excited state of either C_{60} or its derivatives.
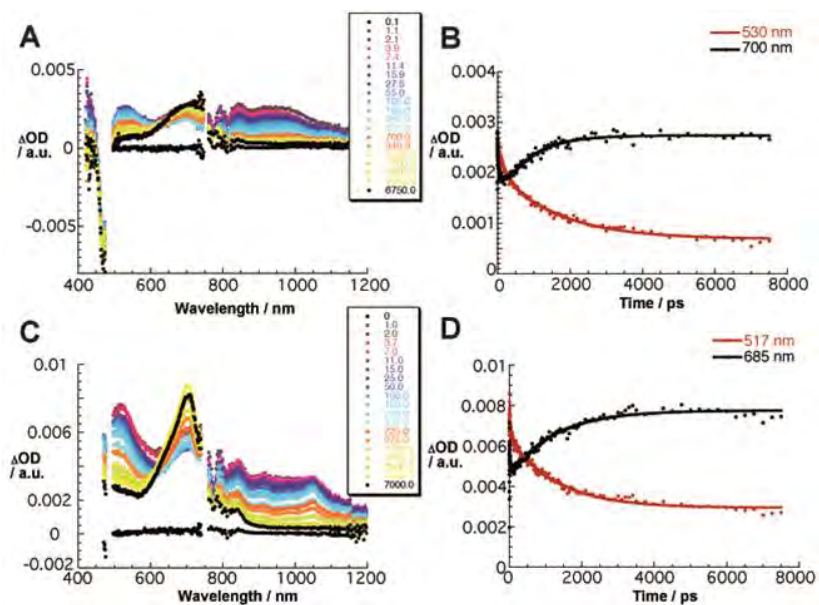
Figure 4.27 A) Differential absorption spectra (visible and near-infrared) obtained upon femtosecond flash photolysis (480 nm) of **16:C$_{60}$** in TCE with several time delays between 0.1 and 6750.0 ps at room temperature. B) Time-absorption profiles of the spectra at 530 and 700 nm, monitoring the charge separation / charge recombination. C) Differential absorption spectra (visible and near-infrared) obtained upon femtosecond flash photolysis (480 nm) of **16:PCBM** in TCE with several time delays between 0 and 7000.0 ps at room temperature. D) Time-absorption profiles of the spectra at 517 and 685 nm, monitoring the charge separation / charge recombination.

SECTION 4.3

SUPRAMOLECULAR PENTAPEPTIDE-BASED FULLERENE NANOFIBERS: EFFECT OF MOLECULAR CHIRALITY

4.3. SUPRAMOLECULAR PENTAPEPTIDE-BASED FULLERENE NANOFIBERS: EFFECT OF MOLECULAR CHIRALITY

In this section we have focused on the construction of fullerene nanofibers based on their functionalization with pentapeptide moieties. We try to exploit the effects on fiber's morphology stemming from *i*) the use of chiral and achiral pentapeptides linked to a PCBM moiety (referred to compounds **24** and **25**, Figure 4.28) and *ii*) the use of a flexible and a more rigid system through the shortening of distance from the fullerene moiety to the β-sheet domain (referred to compounds **24** and **29**, Figure 4.28).

Two main issues have been considered in the molecular design of compounds **24**, **25** and **29**: *i*) the presence of the peptide ensures the formation of the β-sheet as a secondary structure which stabilizes the nanostructure formed, and *ii*) the use of non-planar 3D units such as fullerene C_{60} allows stabilizing, through intermolecular $\pi-\pi$ interactions, the obtained nanostructures (Figure 4.28). Furthermore, fullerenes are in turn excellent n-type organic semiconductors of interest for a variety of purposes as indicated in the background.[81]
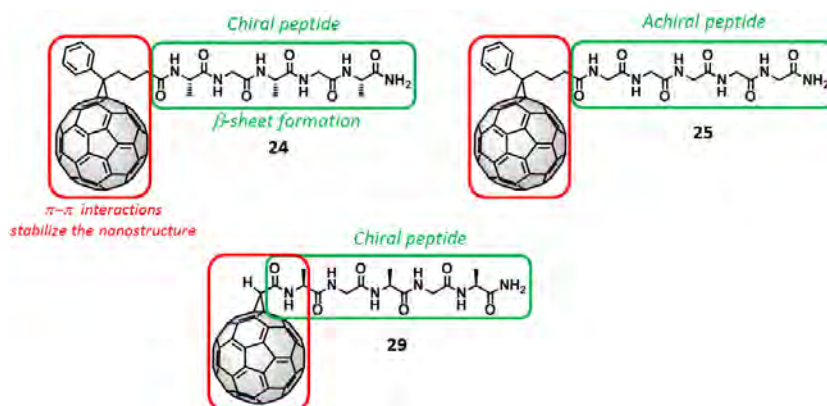
Figure 4.28 Molecular structures of compounds **24**, **25** and **29** indicating the points of interactions that stabilize the nanostructures obtained.

4.3.1. General synthesis of fullerene-pentapeptide derivatives

A general representation of the synthesis of the fullerene derivatives is shown in scheme 4.8. The synthesis of the pentapeptide Ala-Gly-Ala-Gly-Ala-NH$_2$ **5** was accomplished by solid phase peptide synthesis (SPPS) technique and was already described in section 4.1. Using the same technique, the pentapeptide based on glycine units Gly-Gly-Gly-Gly-Gly-NH$_2$ **22** was also synthesized. These pentapeptides were further coupled to the carboxylic acid of PCBM **23** giving rise to chiral **24** and achiral **25** PCBM derivatives. Moreover, a carboxy methano fullerene derivative **28** was coupled to peptide **5** yielding compound **29** as shown in scheme 4.8.
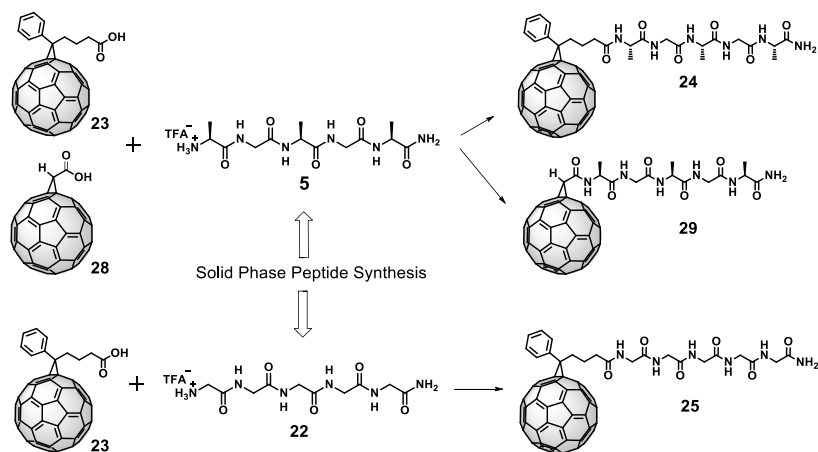
Scheme 4.8 Synthetic routes for obtaining the fullerene derivatives **24**, **25** and **29**.

- ### 4.3.1.1 Synthesis of the pentapeptide Gly-Gly-Gly-Gly-Gly-NH$_2$ (22)

The synthesis of this pentapeptide is quite similar to that explained in section 4.1.1.1. It was synthesized by means of standard solid-phase peptide synthesis (SPPS) employing an Fmoc chemistry on a MBHA resin. The only difference is that Fmoc-glycine **2** was used in all the coupling steps. Such couplings were performed using HBTU and DIPEA and the deprotection of the Fmoc group was carried out in the presence of piperidine. Once the pentapeptide moiety was achieved and the Fmoc group was removed, the cleavage of the peptide from the resin was performed by a

mixture of TFA:H$_2$O (95:5) giving rise to the desired achiral pentapeptide **22** with amine and amide groups at the N- and C- terminal positions, respectively (Scheme 4.9).
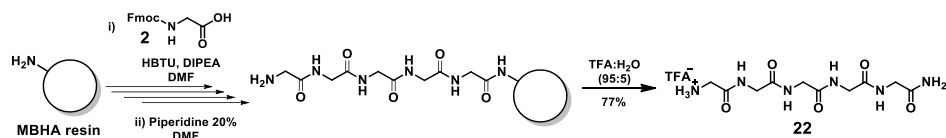
Scheme 4.9 Synthesis of the pentapeptide Gly-(Gly)$_3$-Gly-NH$_2$

- *4.3.1.2 Synthesis of PCBM pentapeptide derivatives (24 and 25)*

The synthesis of PCBM **21** was already described in section 4.2.1. The carboxylic acid of PCBM **23** (PCBA) was synthesized by hydrolysis of PCBM under acidic conditions using HCl and acetic acid (Scheme 4.10).[130] Then, amidation reactions with the chiral **5** and the achiral **22** pentapeptides lead to the formation of the desired products **24** and **25**.
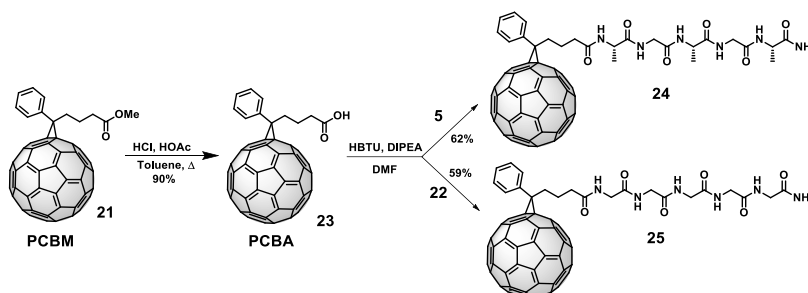
Scheme 4.10 Synthetic pathway for the synthesis of PCBM derivatives **24** and **25**.

- *4.3.1.3 Synthesis of the carboxymethano fullerene pentapeptide derivative (29)*

Cycloaddition of *tert*-butyldiazoacetate **26** with fullerene C$_{60}$ under thermal conditions lead to the formation of the *tert*-butyl ester carboxymethano fullerene **27**, the subsequent deprotection of the ester in acidic conditions using trifluoroacetic acid

(TFA) gave rise to the corresponding carboxylic acid **28**.[133] Finally, the coupling between **28** and pentapeptide **5** yielded the desired fullerene derivative **29** (Scheme 4.11).
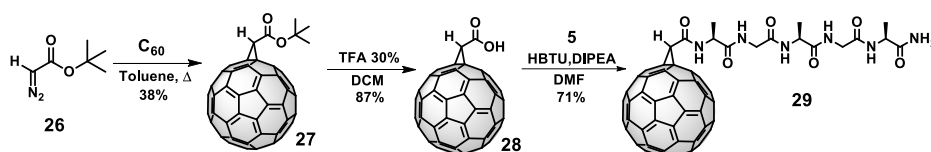
Scheme 4.11 Synthetic route of compound **29**.

4.3.2. Formation and characterization of supramolecular nanofibers

After several solubility essays, it was found that these compounds showed only good solubility in dimethyl sulfoxide (DMSO). In halogenated solvents such as TCE, the solubility was poor. Therefore, we prepared mixtures of TCE and DMSO (10% v/v) and we proceed to explore by different optical and microscopic techniques in order to follow the formation of possible supramolecular aggregates.

Initially, absorption experiments in DMSO and in the mixture TCE:DMSO (10% v/v) were performed. In DMSO, which is a solvent where molecules are solvated, the spectra showed the typical fullerene bands at 330 and 430 nm, the latter associated to the saturation of a C-C double bond in fullerene monoadducts.[134] However, UV-Vis spectra in the mixture TCE:DMSO (10% v/v) revealed a depletion of the band at 330 nm together with an increase in absorbance around ~450 nm (see red arrows in Figure 4.29 A-C). It is worth to mention that this trend has also been observed in fullerene aggregates,[135] films[136] or C_{60} molecules packed within constrained channels[137] and

[133] L. Isaacs, A. Wehrsig, F. Diederich, *Helv. Chim. Acta*, **1993**, *76*, 1231-1250.

[134] a) E. E. Maroto, S. Filippone, A. Martín-Domenech, M. Suárez, N. Martín, *J. Am. Chem. Soc.* **2012**, *134*, 12936–12938; b) K. Swai, Y. Takano, M. Izquierdo, S. Filippone, N. Martín, Z. Slanina, N. Mizorogi, M. Waelchli, T. Tsuchiya, T. Akasaka, S. Nagase, *J. Am. Chem. Soc.* **2011**, *133*, 17746-17752.

[135] R. V. Bensasson, E. Bienvenue, M. Dellinger, S. Leach, P. Seta, *J. Phys. Chem.* **1994**, *98*, 3492-3500.

[136] W. Kratschmer, L. D. Lamb, K. Fostiropoulos, D. R. Huffmann, *Nature* **1990**, *347*, 354-358.

[137] G. Dan Pantos, J. L. Wietor, J. K. M. Sanders, *Angew. Chem. Int. Ed.* **2007**, *46*, 2238-2240.

has been attributed to interactions between C_{60} units,[138] thus, being indicative of the aggregation of fullerene moieties. In the case of compound **29**, the broadening is more significant than the other compounds, losing the feature band at 430 nm (Figure 4.29 C). This observation could be in accordance with the higher packing of C_{60} moieties due to the more rigid nature of this system when compared to **24** and **25**.

Figure 4.29 UV-Vis spectra for compounds **24** (A), **25** (B) and **29** (C) in DMSO (black lines) and the mixture TCE:DMSO (10% v/v, red lines).

The self-assembly of compounds **24**, **25** and **29** was also monitored by circular dichroism (CD) measurements in DMSO and the mixture TCE:DMSO (10% v/v). The CD spectra in DMSO showed no optical activity for compounds **24** and **25**, and a weak dichroic signal for compound **29** as shown in figure 4.30 A-C (black lines). Here, it is important to remark that despite compounds **24** and **29** are covalently bonded to a chiral peptide, dichroic signal was solely observed for compound **29**. This effect has been previously observed in our group for different fullerene derivatives,[139] and has been attributed to the proximity effect of the first chiral center (Ala) when compared to molecule **24**, in which its chiral center is farther from the π-cloud of the fullerene. These low CD responses could be in agreement with the presence of disaggregated compounds.[48,51] However, CD studies for **24** and **29** in TCE:DMSO exhibited a notable negative dichroic signals in the range of fullerene absorptions (Figure 4.30 A and C,

[138] F. Diederich, J. Effing, U. Jonas, L. Jullien, T. Plesnivy, H. Ringsdorf, C. Thilgen, D. Weinstein, *Angew. Chem. Int. Ed.* **1992**, *31*, 1599-1602.

[139] a) J. Coro, H. Rodríguez, D. G. Rivera, M. Suárez, D. Molero, M. A. Herranz, R. Martínez-Álvarez, S. Filippone, N. Martín, *Eur. J. Org. Chem.* **2009**, *28*, 4810-4817; b) A. Ruiz, J. Coro, L. Almagro, J. A. Ruiz, D. Molero, E. E. Maroto, S. Filippone, M. A. Herranz, R. Martínez-Álvarez, J. C. Sancho-García, F. D. Meo, M. Suárez, N. Martín, *J. Org. Chem.* **2013**, *78*, 2819-2826.

red lines). These experimental findings resemble to that observed for related systems when the molecules are assembled.[51,48] Thus, the results support the existence of supramolecular aggregates in which a transfer of chirality occurs from the peptide to the fullerene. It is worth to mention that in the case of compound **29** the response in CD measurements is higher when compared with compound **24**. This outcome could be accounted for by the proximity effect of the peptide backbone to the C_{60} sphere when compared to compound **24**. As a matter of fact, in the case of compound **25** the lack of chirality in the peptide backbone does not trigger any response in CD measurements in any case, neither disaggregated (DMSO) nor assembled (TCE:DMSO) (Figure 4.30 B).
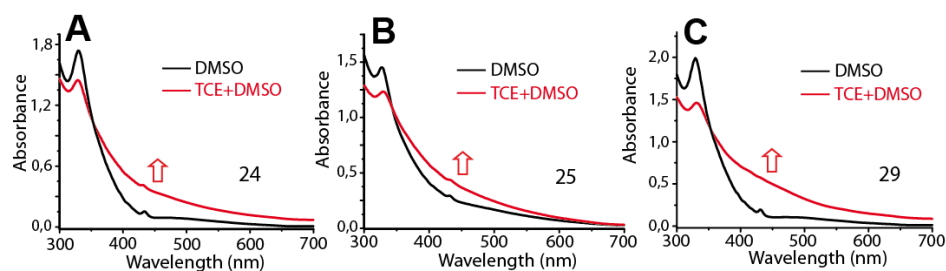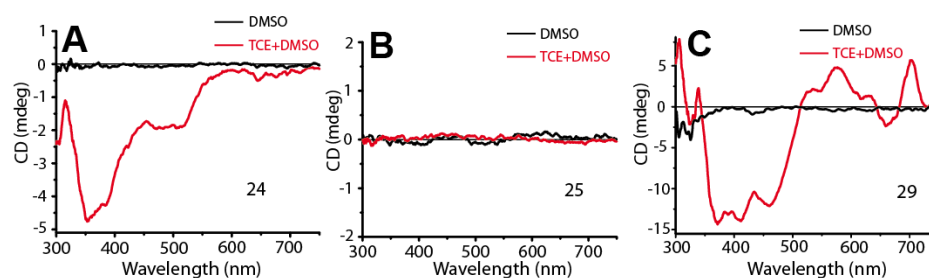

Figure 4.30 Circular dichroism (CD) spectra for compounds **24** (A), **25** (B) and **29** (C) in DMSO (black lines) and the mixture TCE:DMSO (10% v/v, red lines).

Taking into account the results, we proceeded to explore the morphology of the aggregates obtained in the mixture TCE:DMSO (10%, v/v). In this regard, TEM performed for compounds **24**, **25** and **29** showed the formation of nanofibers with several micrometers long in all cases (Figures 4.31-4.33). As expected, it was possible to appreciate differences between all compounds. In the case of compound **24**, figure 4.31 shows clearly how the fibers are twisted in some points along the fiber (see white arrows) while in the case of compound **25** straight fibers are obtained instead (Figure 4.32). At this point, it is important to remark that it is very difficult to correlate the chirality to the nanostructure obtained. As it has been described in the literature, two important aspects should be consider: *i*) chiral peptides endowed with planar

units, could lead or not to twisted arrangements at nano and mesoscale,[44,46,140] and *ii*) achiral molecules, could give rise to twisted arrangements.[73,141] Nevertheless, we believe that the nanostructural differences observed in our cases could be accounted for by the role of peptide's chirality.
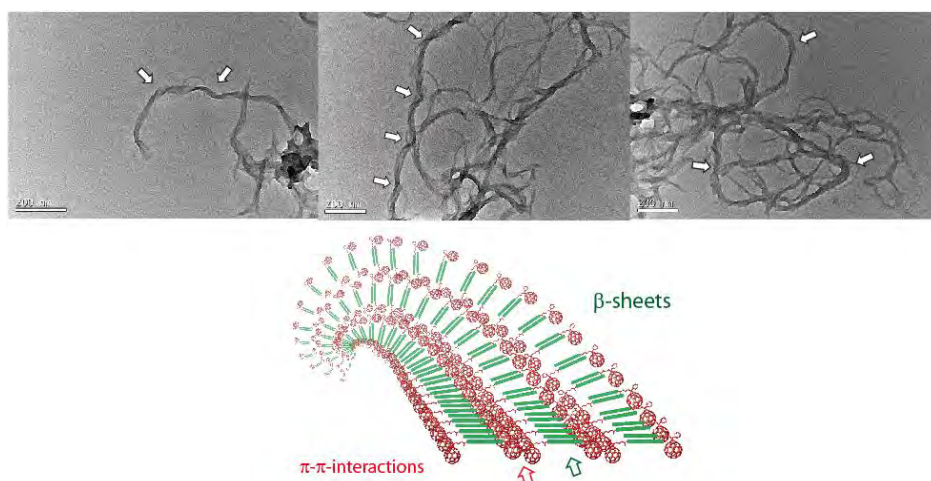
Figure 4.31 TEM images obtained from compound **24** in the mixture TCE:DMSO (10% v/v, 2.0 x 10^{-4} M). Arrows indicate twisting of fibers (top) (scale bar: 200 nm). Cartoon depicting the self-assembly of molecules showing β-sheets and $\pi-\pi$ interactions between C_{60} units stabilizing the formed nanostructure (bottom).

Figure 4.32 TEM images obtained from compound **25** in the mixture TCE:DMSO (10% v/v, 2.0 x 10^{-4} M). Inspection over several areas shows the presence of straight fibers (scale bar: 200 nm).

In the case of compound **29** the fibers formed seemed to be straighter, shorter and more aggregated than those obtained from compounds **24** and **25** (Figure 4.33). We believe that these features might be presumably attributed to the suppression of the

[140] V. Castelletto, I. W. Hamley, *J. Phys. Chem. B* **2010**, *114*, 8002-8008.
[141] F. Aparicio, E. Matesanz, L. Sánchez, *Chem. Eur. J.* **2014**, *20*, 14599-14603.

alkyl chain of three carbon atoms of the PCBM, becoming **29** a more rigid system when compared to **24** and **25**. This more rigid system in **29** allows a higher packing between β-sheets strands through $\pi-\pi$ interactions between C_{60} molecules, whereas in **24** and **25** systems, C_{60} moieties have a higher degree of freedom with respect to the β-sheet owed to the presence of the alkyl chain, in turn less packing of fibers can be observed.
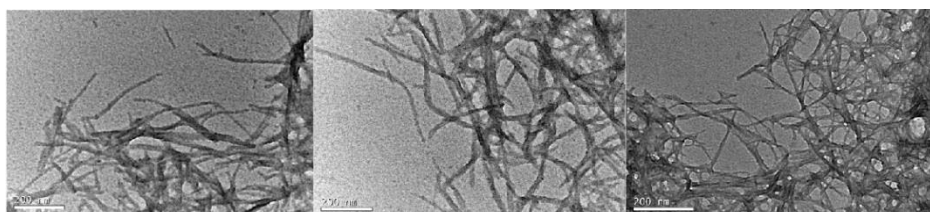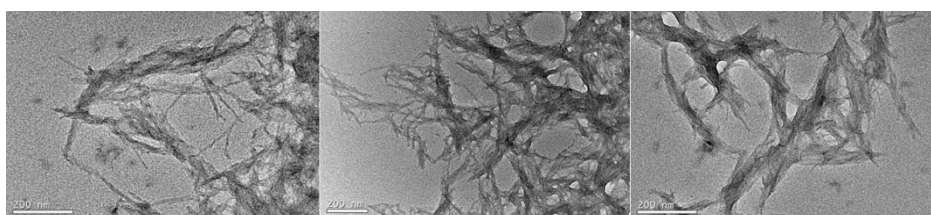

Figure 4.33 TEM images obtained from compound **29** in the mixture TCE:DMSO (10% v/v, 2.0 x 10^{-4} M). Inspection over several areas shows the presence of shorter, straighter and more aggregated fibers (scale bar: 200 nm).

Additional studies about the supramolecular structure were performed by atomic force microscopy (AFM). The images showed very similar trends to those observed in TEM regarding morphological features as it can be discerned in figure 4.34 A-C. Formation of long fibers and agglomerated structures were observed in all cases. Furthermore, inspection in heights over the nanofibers revealed that the smaller ones correspond to the expected heights for one (~3.4 nm), two (~7 nm) or three (~10 nm) strands of β-sheets as shown in the height profiles in figure 4.34 D-E. The agglomerated structures should consist of several packed strands, which are stabilized by $\pi-\pi$ interactions between C_{60} units.

In order to confirm the formation of β-sheets as secondary structure, Fourier-transform infrared (FTIR) spectroscopy measurements were performed. A strong amide I ($v_{C=O}$) band at 1630 cm^{-1} together with a weak shoulder around 1690 cm^{-1} were observed, which is in agreement with the existence of intermolecular β-sheets (Figure 4.35). These features, as it has been previously indicated, correspond to

peptide units interacting in an antiparallel mode.[46,47,126] In some cases the band at 1650 cm^{-1} was barely observed which indicates the existence of random aggregates.
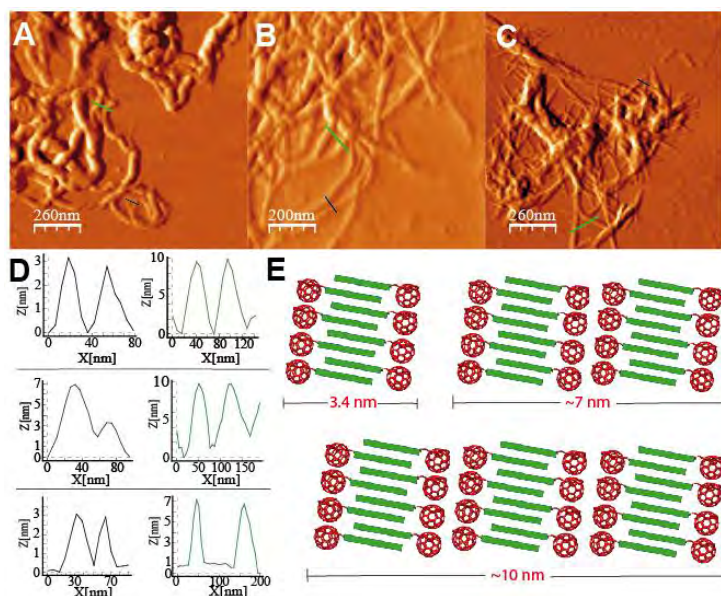
Figure 4.34 AFM images obtained by drop casting over mica. (A), (B) and (C) correspond to the nanofibers obtained from compounds **24**, **25** and **29** in the mixture TCE:DMSO (2.0 x 10^{-4} M), respectively. (D) Height profiles corresponding to the lines marked in figures A-C. Top, middle and bottom parts correspond to figures A, B and C, respectively. (E) Cartoon accounting for the height profiles observed in AFM corresponding to one, two and three strands of β-sheets.
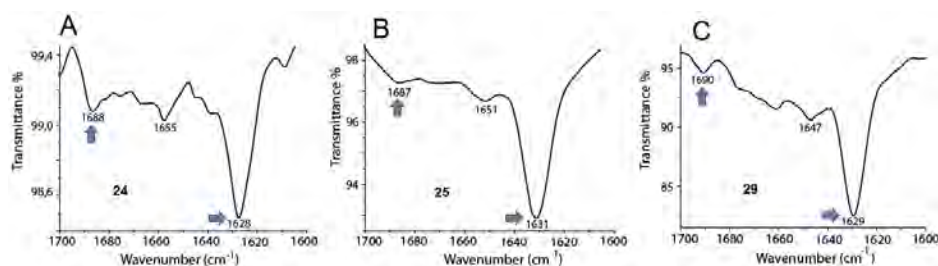
Figure 4.35 ATR-FTIR of compounds **24** (A), **25** (B) and **29** (C) in the mixture TCE:DMSO (10% v/v).

Furthermore, fluorescence studies in DMSO and the mixture TCE:DMSO were also performed. The fluorescence intensity of C$_{60}$ with maxima at ~709 nm decreased and shifted slightly in the mixture TCE:DMSO compared to that obtained in DMSO (Figure

4.36). However, these fluorescence changes are very weak in all cases to draw any clear conclusion.
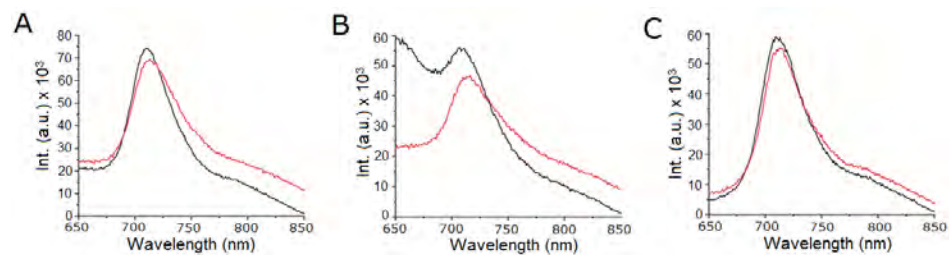
Figure 4.36 Fluorescence spectra (λ_{exc}= 463 nm) of compounds **24** (A), **25** (B) and **29** (C) in DMSO (black lines) and the mixture TCE:DMSO (10% v/v) (red lines).

SECTION 4.4

SUPRAMOLECULAR PORPHYRIN-C$_{60}$ PEPTIDE DYADS: MORPHOLOGY AND CHIRAL INDUCTION EFFECTS

4.4. SUPRAMOLECULAR PORPHYRIN-C$_{60}$ PEPTIDE DYADS: MORPHOLOGY AND CHIRAL INDUCTION EFFECTS

In this section, we have studied the formation of supramolecular porphyrin-C$_{60}$ peptide dyads through strong hydrogen bond interactions based on a carboxylate-amidinium pair (Figure 4.37). In this regard, the molecular design of the supramolecular dyads is based on the following features: *i*) porphyrin **38** is endowed with an amidine group that serves as anchoring unit in the formation of the amidinium-carboxylate pair; such interaction is known to favors the electronic communication through this interface.[118] Moreover, the functionalization with *tert*-butyl groups gives good solubility in a variety of solvents facilitating further studies; *ii*) enantiopure fullerene derivatives **53**, **54**, **59** and **60** have been functionalized with di- (**53** and **54**) and penta- (**59** and **60**) peptide sequences with tendency to form β-sheets as it has previously been described.[44,46]
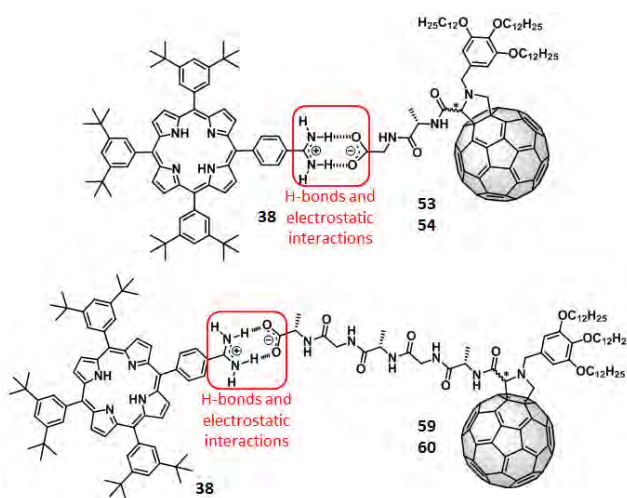
Figure 4. 37 Supramolecular porphyrin-C$_{60}$ dyads.

These peptides were chosen with the aim of analyzing the consequences of spatially separating both electroactive units and are functionalized with a carboxylic acid group at the end of the peptide backbone which serves as anchor unit in the formation of

the amidinium-carboxylate interaction. Finally, these fullerene derivatives are functionalized with long alkyl chains (-OC$_{12}$H$_{25}$) aimed not only to give solubility but also to stabilize a possible supramolecular structure through van der Waals interactions.[91-95]

As mentioned in the background of this thesis, it is important to work with enantiomerically pure compounds because it could affect the nanostructures obtained and their electronic properties.[89] In this sense, diastereoisomers **53**-**54** and **59**-**60** were efficiently isolated and characterized.

4.4.1. Synthesis of building blocks

- #### 4.4.1.1 Synthesis of the porphyrin-amidine derivative (38)

The complete synthesis of porphyrin **38** is described in scheme 4.12.[142] 3,5-Di-*tert*-butylbenzaldehyde **32** was prepared by a Sommelet oxidation of compound **31**, which was obtained in turn by bromination of commercially available 3,5-di-*tert*-butyltoluene **30**.[143] Then, a condensation reaction of aldehydes **32** and **33** and pyrrol **34** under Lindsey conditions afforded free base porphyrin **35**. The subsequent metallation of **35** with Ni(OAc)$_2$ gave rise to metalloporphyrin **36**, whose treatment with AlMe$_3$ and NH$_4$Cl led to **37** functionalized with the amidine group. Finally, demetallation of **37** under acidic conditions yielded the desired free base porphyrin **38** (Scheme 4.12).

[142] J. Otsuki, K. Iwsaki, Y. Nakano, M. Itou, Y. Araki, O. Ito, *Chem. Eur. J.* **2004**, *10*, 3461-3466.
[143] M. S. Newman, L. F. Lee, *J. Org. Chem.* **1972**, *37*, 4468-4469.
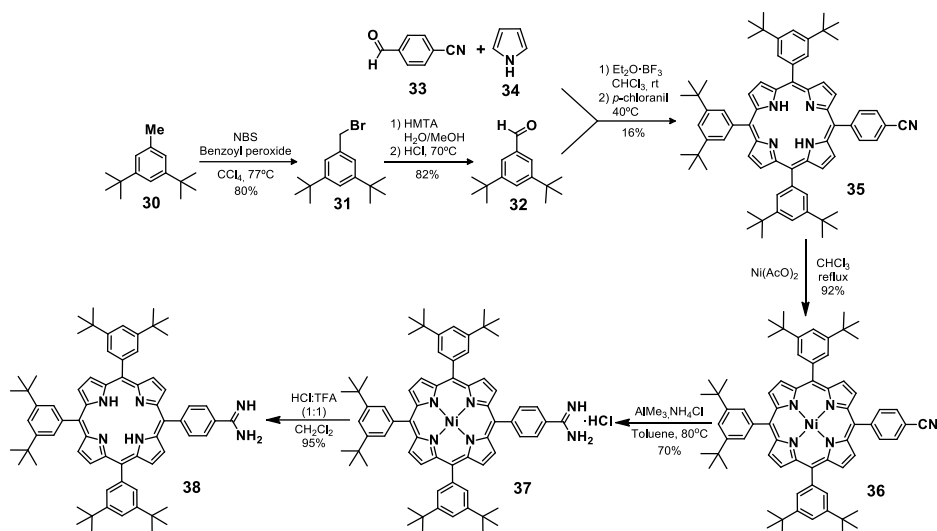
Scheme 4.12 Synthetic route for the preparation of porphyrin-amidine compound **38**.

- ## *4.4.1.2* Synthesis of enantiopure fullerene dipeptide derivatives (53 and 54)

The synthesis started, in first place, affording the dipeptide moiety in liquid phase as shown in scheme 4.13. An amidation reaction between *N*-(*tert*-butoxycarbonyl)-L-alanine (Boc-L-Alanine) **39** and glycine methyl ester (Gly-OMe) **40** gave rise to dipeptide **41**. Treatment of the latter under acid conditions using TFA yielded the deprotected dipeptide **42** with a free amine group ready for further couplings.
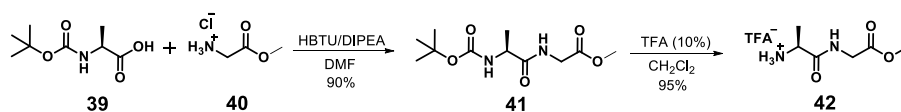
Scheme 4.13 Synthesis of dipeptide **42**.

In second place, we focused on the synthesis of the fulleropyrrolidine-carboxylic acid unit **50**, which is suitably functionalized for the coupling with dipeptide **42** (Scheme 4.14). For this, we performed the alkylation of methyl 3,4,5-trihydroxybenzoate **43** with dodecyl chains yielding **44**. Then, a reduction of the ester group with LiAlH₄ and

subsequent oxidation in presence of PCC gave rise to aldehyde **46** in good yields. Further treatment of **46** with glycine *tert*-butyl ester afforded imine **47**, which was reduced using NaBH$_3$CN yielding amine **48**. With the latter in hands, a 1,3-dipolar cycloaddition with formaldehyde and C$_{60}$ gave rise to the monoadduct **49** that was further deprotected under acid conditions using TFA generating the fullerene-carboxylic acid **50** (Scheme 4.14).
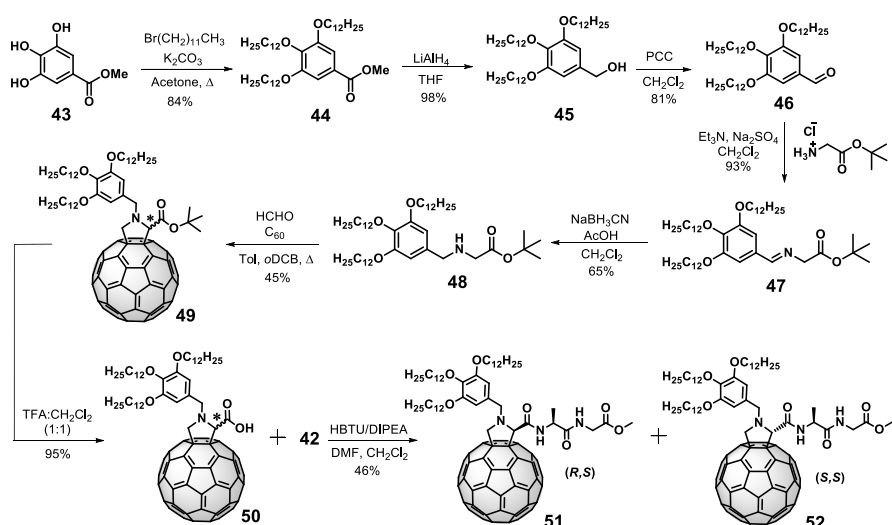
Scheme 4.14 Synthetic route for the preparation of fullerene dipeptide derivatives.

The amidation reaction between racemic fullerene-carboxylic acid **50** and dipeptide-amine **42** in presence of coupling reagents (HBTU and DIPEA) gave rise to the formation of diastereoisomers **51** and **52** as shown in scheme 4.14. These compounds could be well-separated and purified by preparative thin layer chromatography using a mixture of CH$_2$Cl$_2$:MeOH (100:1) as eluent. These diastereoisomers were obtained in a 1:1 ratio with a yield of 46% for each diastereoisomer. HPLC of the isolated diastereoisomers (**51** and **52**) in a non-chiral column (Buckyprep), showed different retention times as expected (Figure 4.38).
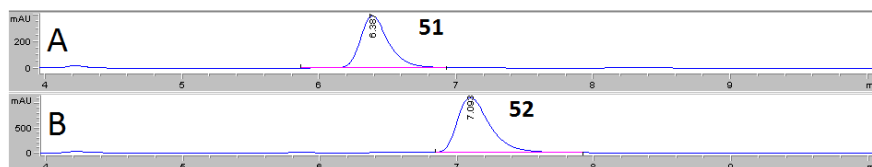
Figure 4.38 HPLC chromatograms for **51** (A) and **52** (B). HPLC conditions: Buckyprep column (4.6 × 250 mm), solvents: toluene:acetonitrile (70:30), flow rate: 1.0 mL/min, λ = 320 nm.

In order to determine the absolute configuration of each diastereoisomer, CD measurements were performed. Based on the sector rule for fullerenes, which has been used as an empirical way to assign the absolute configuration of chiral fullerenes derivatives, it was possible to determine the absolute configuration of **51** and **52**.[144] Thus, based on the dichroic signal of the monoadduct band (~432 nm) of each diastereoisomer and placing the bulkier group on the respective sector, the absolute configuration for diastereoisomer **52**, for instance, would be assigned as follows: *i*) diastereoisomer **52** showed a negative dichroic signal at 432 nm (Figure 4.39 A, green line), therefore *ii*) the bulkier group should be placed in a negative sector which in this case corresponds to the peptide backbone because the benzylic substituent of the N atom is placed in the plane that goes through the 6-6 bond as shown in figure 4.39 B. Under these considerations an *S* configuration was accounted for the chiral center of fulleropyrrolidine moiety. Taking into account that L-alanine was used in the synthesis of the dipeptide unit, the absolute configuration of compound **52** correspond to the *S,S* diastereoisomer. Consequently, the *R,S* configuration was assigned to diastereoisomer **51**.

[144] J. Marco-Martínez, V. Marcos, S. Reboredo, S. Filippone, N. Martín, *Angew. Chem. Int. Ed.* **2013**, *52*, 5115-5119.
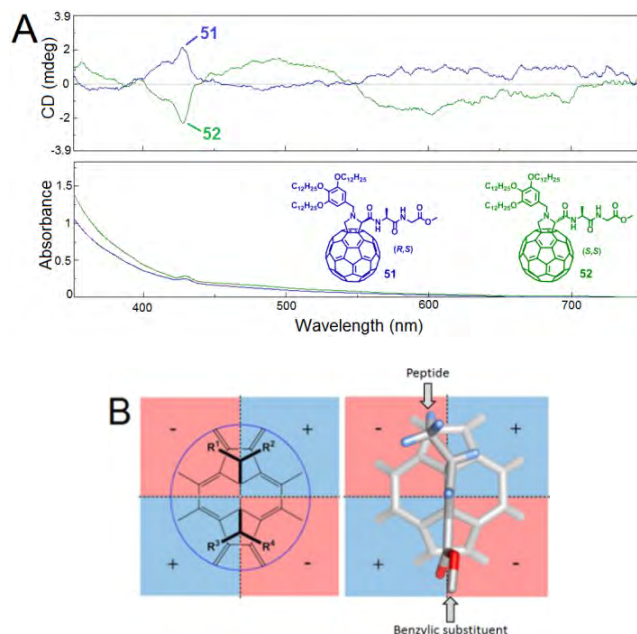
Figure 4.39 (A) Circular dichroism and UV-Vis spectra for diastereoisomers **51** and **52** in CHCl₃ (6.0 x 10⁻⁴ M). (B) Sector rule for the assignment of absolute configuration of chiral fullerenes derivatives. A plane tangent to the C₆₀ sphere at the 6–6 single bond is divided in four sectors by two other planes: one that goes through the 6–6 bond (placed in the vertical axis) and the second one which bisects the 6–6 single bond. A negative sign is assigned to the top-left and bottom-right sectors. For clarity of the cartoon, peptide and benzylic substituent do not correspond with the chemical structure shown.

Finally, once diastereoisomers **51** and **52** were isolated and characterized, a treatment under acidic conditions with HCl/TFA gave rise to the corresponding carboxylic acids **53** and **54** as shown in scheme 4.15.
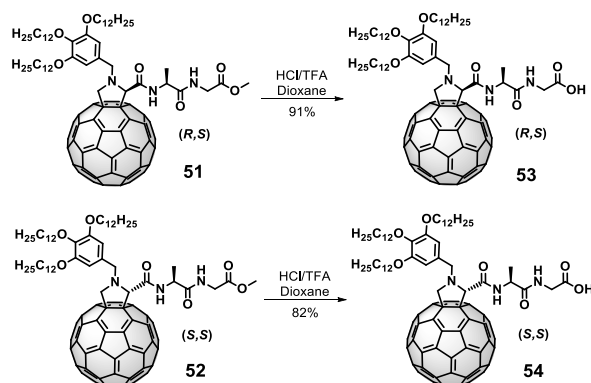
Scheme 4.15 Synthesis of carboxylic acid derivatives **53** and **54** under acidic conditions.

- *4.4.1.3.* **Synthesis of enantiopure fullerene-pentapeptide derivatives (59 and 60)**

For the synthesis of the pentapeptide moiety, we used the SPPS technique employing an Fmoc chemistry as described in previous sections. However, in this case we used an Fmoc-L-Ala-Wang resin (Fmoc-L-Ala-*p*-alkoxybenzyl alcohol resin) (Scheme 4.16). This resin already had the L-alanine unit attached to the resin, thus, reducing the coupling steps in comparison to the MBHA resin, and upon cleavage procedure, enables to obtain the pentapeptide product with amine and carboxylic acid groups at the N- and C- terminal positions, respectively.

In this regard, the synthesis of the pentapeptide using the Fmoc-L-Ala-Wang resin proceeds with the deprotection of the Fmoc group followed by the coupling of the Fmoc-glycine aminoacid **2** as shown in scheme 4.16.
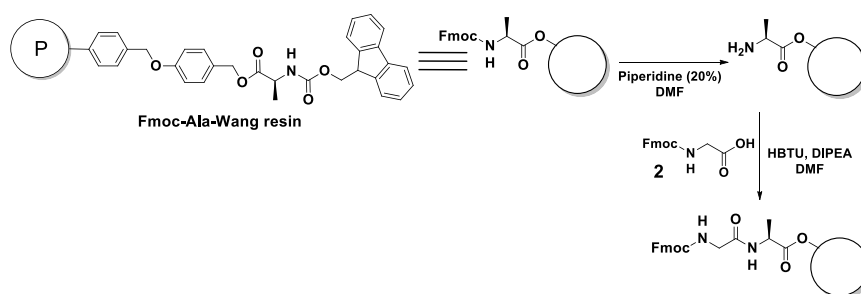
Scheme 4.16 Fmoc-deprotection and subsequent first amino acid coupling.

Employing the methodology described in previous sections, successive Fmoc deprotection and coupling reactions with the corresponding aminoacid were performed (Scheme 4.17). The cleavage from the resin using a mixture of TFA:H_2O (95:5) gave rise to the desired pentapeptide **55**.
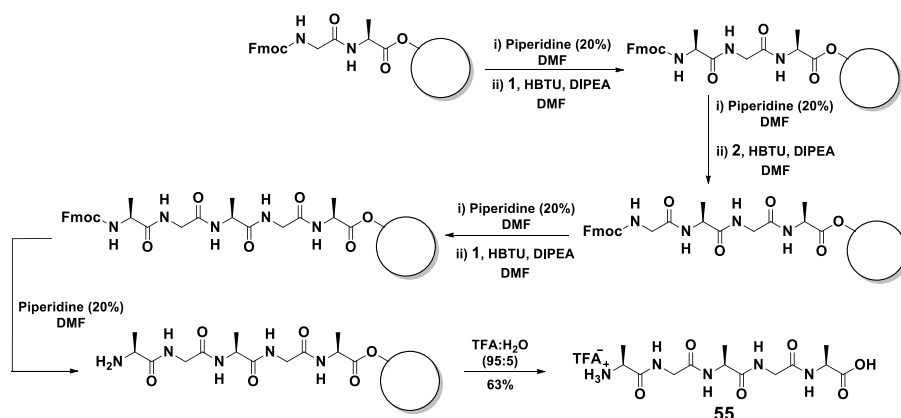
Scheme 4.17 Synthetic pathway followed in SPPS for the preparation of pentapeptide **55**.

Once the pentapeptide **55** was obtained, an esterification reaction of the acid group using trimethylsilyldiazomethane in methanol led to compound **56** (Scheme 4.18). Then, an amidation reaction between fullerene-carboxylic acid **50** and pentapeptide **56** in presence of HBTU and DIPEA, gave rise to the formation of diastereoisomers **57** and **58**, which were isolated by preparative thin layer chromatography using a mixture of CH$_2$Cl$_2$:MeOH (30:1) as eluent. HPLC profiles for diastereoisomers **57** and **58** in a non-chiral column (Buckyprep), showed different retention times as expected (Figure 4.40).
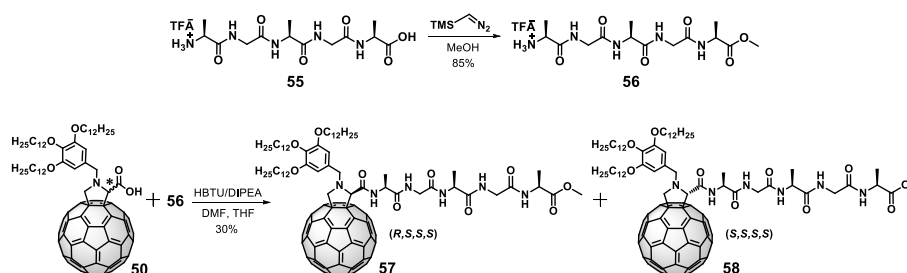
Scheme 4.18 Synthetic route for the preparation of fullerene pentapeptide derivatives.

138
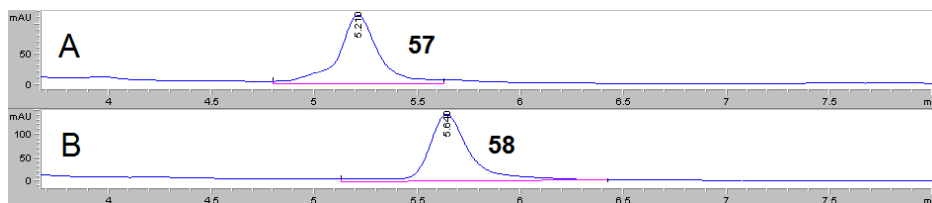
Figure 4.40 HPLC chromatograms for diastereoisomers **57** (A) and **58** (B). HPLC conditions: Buckyprep column (4.6 × 250 mm), solvents: toluene:acetonitrile:methanol (70:28:2), flow: 1.0 mL/min, λ = 320 nm.

In a similar way to that followed in the elucidation of the absolute configuration for dipeptide analogues **51** and **52**, that is, taking into account the circular dichroism spectra of compounds **57** and **58** (Figure 4.41) and the sector rule, their absolute configuration was assigned as *R,S,S,S* for **57** and *S,S,S,S* for **58**.
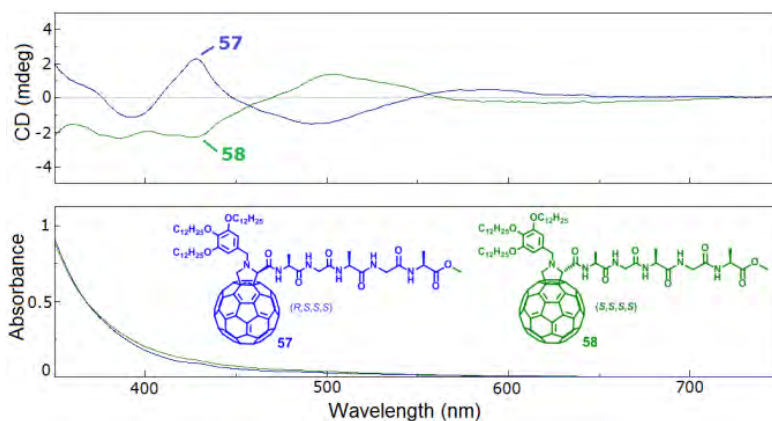
Figure 4.41 Circular dichroism and UV-Vis spectra for **57** and **58** in CHCl$_3$ (5.6 x 10^{-4} M).

Finally, we carried out a deprotection reaction under acid conditions with HCl/TFA affording carboxylic acids **59** and **60** as shown in scheme 4.19. Detailed description of the synthesis of all the above described derivatives can be found in the Experimental Section.
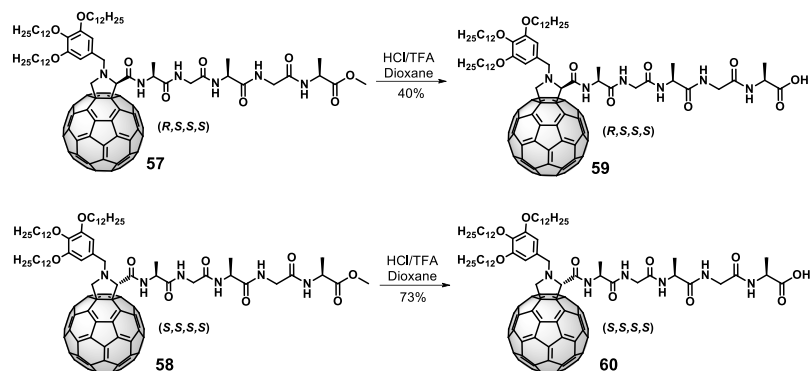
Scheme 4.19 Synthesis of carboxylic acid derivatives **59** and **60** under acidic conditions.

4.4.2. Formation and characterization of supramolecular dyads

Once the final products were obtained, we studied the formation of supramolecular dyads through different techniques such as NMR, UV-Vis, circular dichroism, fluorescence spectroscopy and AFM. The first evidence of the supramolecular interaction of the amidinium-carboxylate pair was obtained by ^{1}H-NMR spectroscopy. As a representative example, we studied the mixture of **38·53** (1:1) in CDCl$_3$ (Figure 4.42). It is worth to mention that for compound **38** in CDCl$_3$, the amidine protons are not observable. However, upon complexation with **53** these protons can be discerned as downfield resonances at 11.2 ppm (Figure 4.42),[118] which is consistent with the formation of the amidinium-carboxylate pair. Furthermore, upon the formation of the complex **38·53**, the *ortho* amidine protons shifted downfield, these observations are in agreement with the formation of the amidinium-carboxylate pair as it has been previously reported (see inset in Figure 4.42).[118]
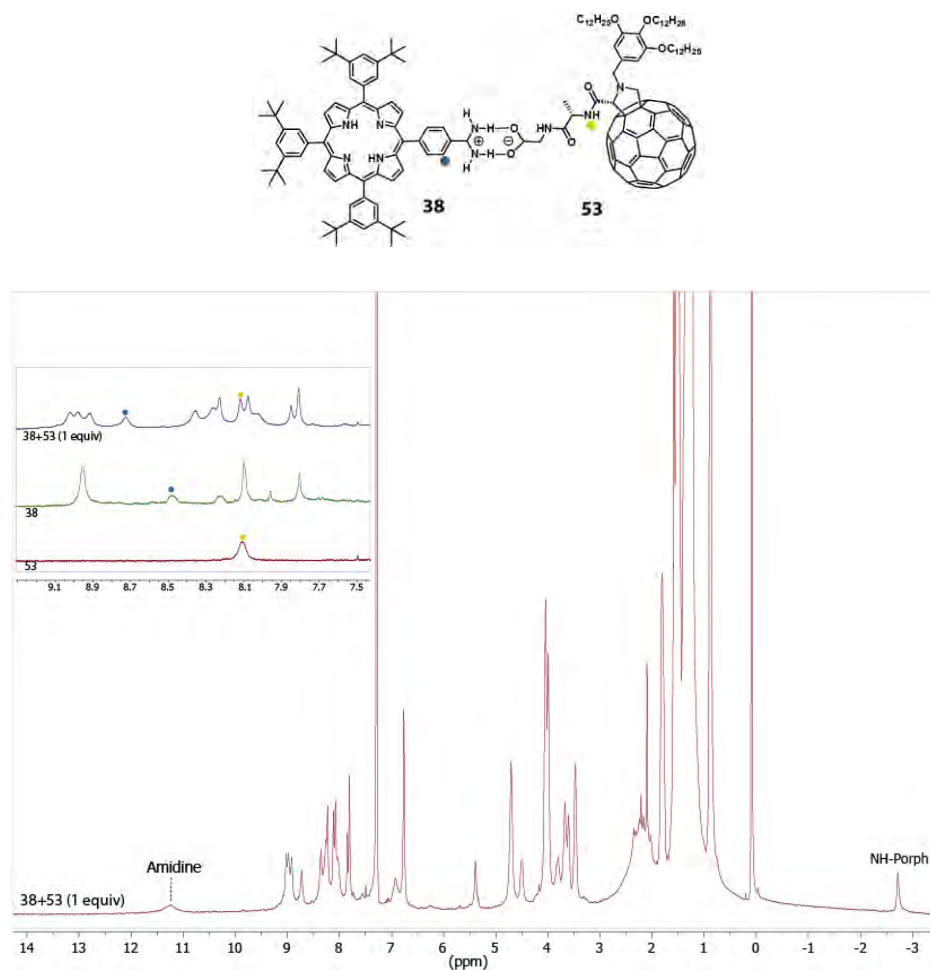
Figure 4.42 ¹H-NMR spectra of **38·53** (2.53 x 10⁻³ M) in CHCl₃ at 278 K. Spectra recorded on a Bruker 500. Inset shows the shifting of the *ortho* amidine protons (see blue circles) upon adition of **53**. The yellow circle indicates the NH-Ala proton of compound **53** as reference.

The supramolecular interaction between porphyrin **38** and fullerene derivative **53** was also investigated through UV-Vis titrations experiments. For this end, to solutions of **38** (2.01 x 10⁻⁵ M) in CHCl₃, increasing amounts of **53** (0 - 7.04 x 10⁻⁵ M) were added. Figure 4.43 A shows how the Soret band of the porphyrin (423 nm) decreased upon addition of **53**. This fact could be in agreement with the formation of the complex **38·53** through the amidinium-carboxylate interaction as it has been previously confirmed by NMR. A similar behavior was observed in the UV-Vis titrations when

diastereoisomer **54** was added to solutions of **38** (Figure 4.43 B). In fact, very similar trends were also observed in the case of complexes based on fullerene pentapeptide derivatives **38·59** and **38·60** as shown in figure 4.44 A and B, respectively.
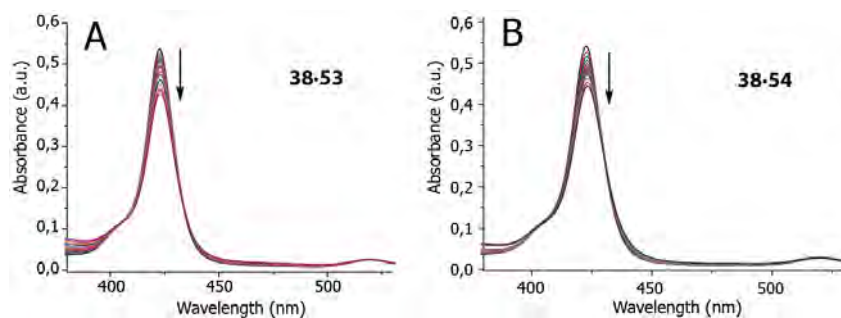
Figure 4.43 UV-Vis spectra of **38** (2.01 x 10^{-5} M) and variable concentration of **53** (A) and **54** (B) (0 - 7.04 x 10^{-5} M) in CHCl$_3$.
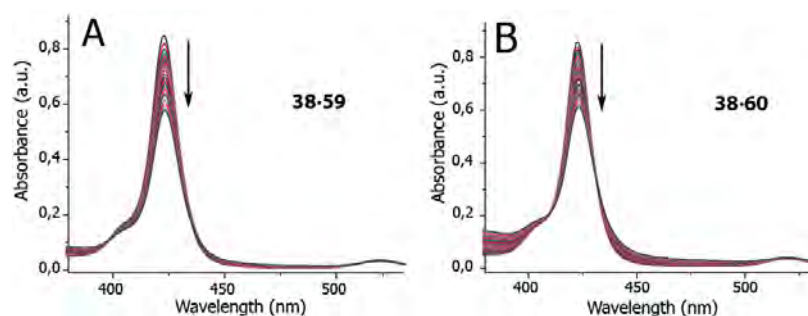
Figure 4.44 UV-Vis spectra of **38** (3.05 x 10^{-5} M) and variable concentration of **59** (A) and **60** (B) (0 - 1.22 x 10^{-4} M) in CHCl$_3$.

The formation of the supramolecular dyads was also followed by circular dichroism (CD) spectroscopy. CD measurements for **38·53** in CHCl$_3$ showed an induced circular dichroism (ICD) signal due to a transmission of chirality from the enantiopure fullerene derivative **53** to the achiral porphyrin **38** through the amidinium-carboxylate pair (Figure 4.45 A). Such ICD signal has a negative dichroic signal at longer wavelength (430 nm), a positive signal at shorter wavelength (419 nm) and a zero crossing point at 423 nm. The latter, matches with the Soret band of porphyrin at 423 nm as shown in figure 4.43 A. Conversely, measurements for **38·54** showed an ICD

signal with a positive dichroic signal at longer wavelength (430 nm) which is the opposite to that obtained for **38·53** (Figure 4.45 B).
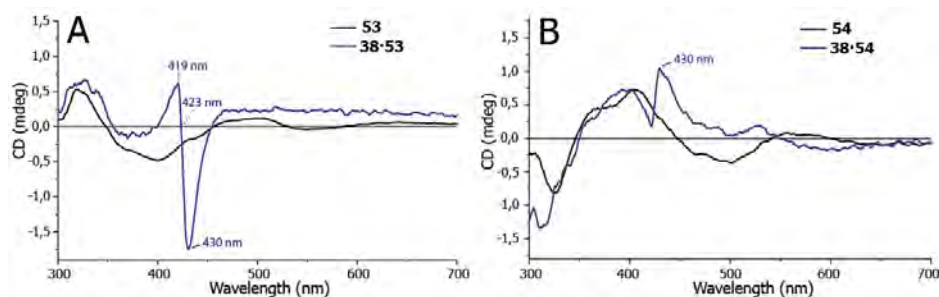
Figure 4.45 Circular dichroism (CD) spectra for complexes **38·53** (A) and **38·54** (B) in CHCl$_3$ (9.05 x 10^{-5} M, blue lines). Spectra of the respective fullerene derivatives **53** and **54** as references are also represented (9.05 x 10^{-5} M, black lines).

These ICD signals observed are produced by the interaction of porphyrin **38** with the respective diastereoisomers **53** and **54** through the amidine-carboxylate pair. Interestingly, despite the closer proximity of the chiral center of L-alanine to the porphyrin, we believe that the transmission of chirality is mainly affected by the chiral center of the fulleropyrrolidine moiety. This statement is based on the fact that, otherwise, the same ICD signal should be obtained for both complexes due to the effect of the L-alanine unit. In order to corroborate this hypothesis, a control CD experiment using porphyrin **38** and dipeptide **61**, in which fullerene unit has been removed, was carried out (Figure 4.46). CD spectra for complex **38·61** showed an ICD signal with a positive signal at longer wavelength (429 nm), a negative signal at shorter wavelength (415 nm) and a zero crossing point at 422 nm. This ICD signal is influenced exclusively by the presence of L-alanine unit. Therefore, based on these results, ICD signals for complexes **38·53** and **38·54** in CHCl$_3$ are mainly affected by the chiral center of the fulleropyrrolidine moiety.
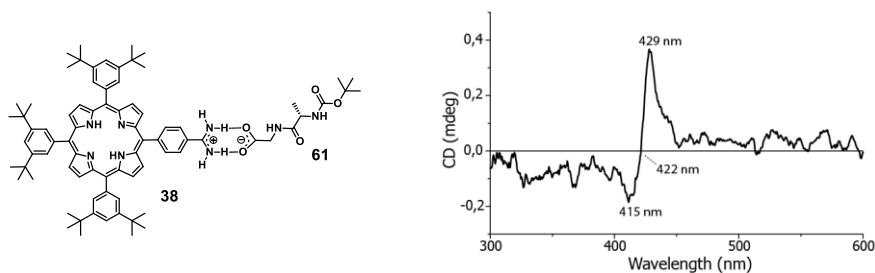
Figure 4.46 Circular dichroism spectrum for complex **38·61** (9.05 x 10^{-5} M) in CHCl$_3$. See Experimental Section for the synthesis of **61**.

In a similar way to dipeptide complexes, CD measurements for pentapeptide complexes (**38·59** and **38·60**) showed ICD signals which are attributed to a transmission of chirality from the enantiopure fullerene derivatives to the achiral porphyrin **38** through the amidinium-carboxylate pair. In the case of complex **38·59** in CHCl$_3$, CD spectra showed an ICD signal with a positive dichroic value at longer wavelength (431 nm), a negative value at shorter wavelength (400 nm) and a zero crossing point at 424 nm (Figure 4.47 A). The latter, very close to the λ of the Soret band of porphyrin (423 nm) as shown in figure 4.44 A. Similarly, measurements for **38·60** showed an ICD signal with a positive value at longer wavelength (429 nm) (Figure 4.47 B).
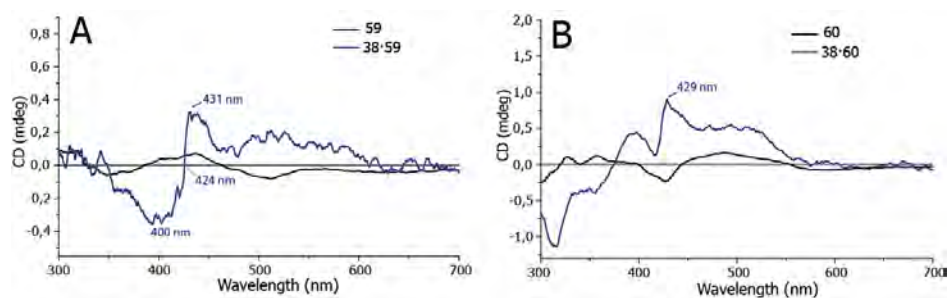
Figure 4.47 CD spectra for complexes **38·59** (A) and **38·60** (B) in CHCl$_3$ (8.03 x 10^{-5} M, blue lines). Spectra of the respective fullerene derivatives as references are also represented (8.03 x 10^{-5} M, black lines).

144

It is worth to mention that in both pentapeptide complexes, the CD responses are positive at longer wavelength (~430 nm), which differs from the results obtained in the case of dipeptide complexes that showed opposite signals. This similar response for pentapeptide complexes could be explained taking into account that the transmission of chirality in the pentapeptide complexes is mainly affected by the L-alanine unit due to the proximity of the latter to the hydrogen bonding pair; this accompanied with the negligible influence of the chiral center of fulleropyrrolidine owed to the larger distance to the carboxylate in comparison with dipeptides complexes (Figure 4.48).
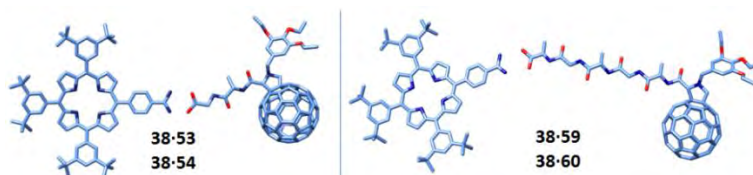
Figure 4.48 Molecular structures of complexes **38·53**, **38·54**, **38·59** and **38·60**. Alkyl chains have been omitted for clarity of the cartoon.

In order to corroborate this hypothesis, a CD experiment with a complex formed by porphyrin **38** and a pentapeptide moiety lacking the fulleropyrrolidine moiety **55** in CHCl$_3$ was performed. The formation of the complex gave rise to an ICD signal with a positive value at longer wavelength (429 nm), a negative value at shorter wavelength (417 nm) and a zero crossing point at 422 nm (Figure 4.49). This ICD signal is affected mainly by the L-alanine closer to the amidinium-carboxylate pair and is similar to that obtained for both pentapeptide complexes.
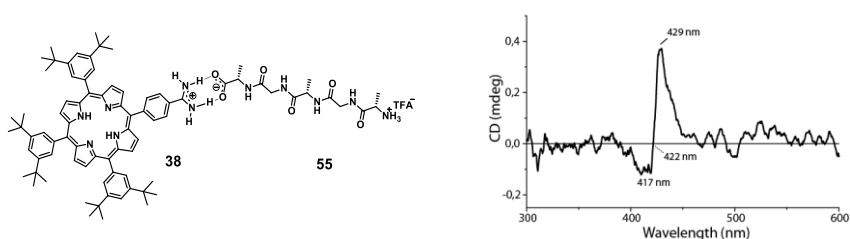
Figure 4.49 Circular dichroism spectrum for complex **38·55** (8.03 x 10^{-5} M) in CHCl$_3$.

145

Fluorescence titrations in CHCl$_3$ for complexes **38·53**, **38·54**, **38·59** and **38·60** were also performed. The emissions of the porphyrin were quenched upon addition of increasing amounts of fullerene derivatives which is in agreement with the formation of supramolecular dyads through the amidinium-carboxylate pair. This quenching was more pronounced in the case of dipeptide derivatives **38·53** and **38·54** (Figure 4.50 A and B, respectively) when compared to those of pentapeptide derivatives **38·59** and **38·60** (Figure 4.51 A and B, respectively). This observation could be presumably assigned to distance features between porphyrin and C$_{60}$ units, thus, a stronger quenching is observed with shorter distances between these two units, that is, in the case of dipeptide complexes **37·53** and **37·54**.
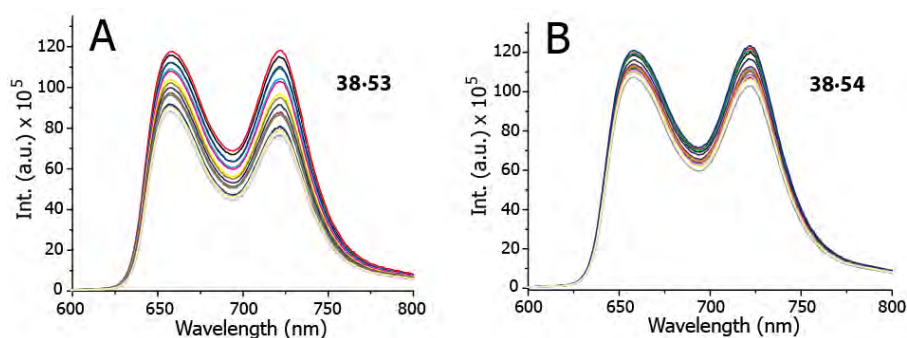
Figure 4.50 Fluorescence spectra of **38** (4.80 x 10^{-6} M) and variable concentration of **53** (A) and **54** (B) (0 - 3.02 x 10^{-5} M) in CHCl$_3$ (λ_{exc} = 433 nm).
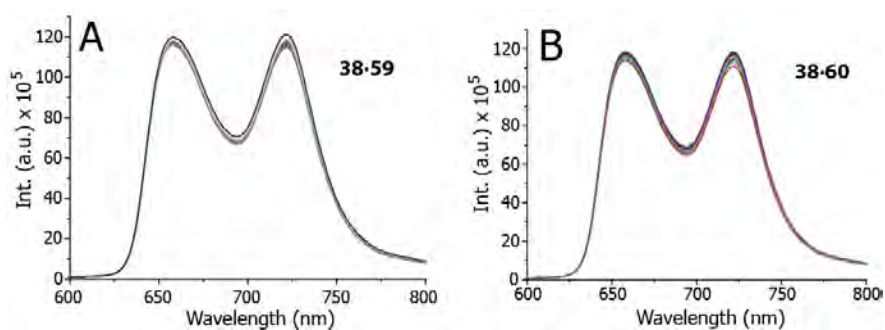
Figure 4.51 Fluorescence spectra of **38** (4.80 x 10^{-6} M) and variable concentration of **59** (A) and **60** (B) (0 - 2.69 x 10^{-5} M) in CHCl$_3$ (λ_{exc} = 433 nm).

In order to favor other kind of interactions such as $\pi-\pi$ interactions, we used a suitable solvent such as methylcyclohexane (MCH) and we studied the supramolecular organization using all the techniques previously described. In this regard, UV-Vis titrations experiments using solutions of **38** (2.01 x 10^-5 M) and adding increasing amounts of **53** (0 - 8.04 x 10^-5 M) showed that the Soret band of the porphyrin (420 nm) decreased and shifted to the red (431 nm) upon addition of **53** (Figure 4.52 A). Furthermore, the appearance of one pseudo-isosbestic point at 397 and one isosbestic point at 429 nm can be distinguished. All these observations could be attributed to the existence of the amidinium-carboxylate pair but also to $\pi-\pi$ interactions between porphyrin and C_{60} units in MCH.[114] UV-Vis titrations using the other diastereoisomer (**38·54**) showed a very similar behavior (Figure 4.52 B).
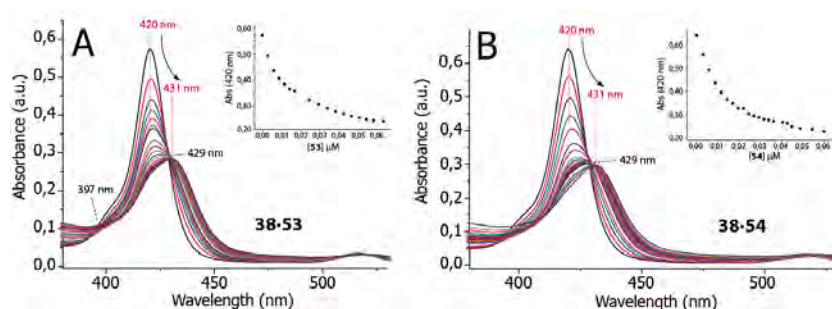
Figure 4.52 UV-Vis spectra of **38** (2.01 x 10^-5 M) and variable concentration of **53** (A) and **54** (B) (0 - 8.04 x 10^-5 M) in MCH. Insets show the variation in absorption at 420 nm with increasing amounts of **53** and **54**.

UV-Vis titrations in MCH for pentapeptide complexes (**38·59** and **38·60**) showed a decrease of the Soret band (420 nm), an increase in absorption around 440 nm and two isosbestic points at 394 and 431 nm (Figure 4.53 A and B). Taking into account these features and that the large batochromic shift ($\Delta \sim$ 11nm) was not observed, we believe that $\pi-\pi$ interactions between porphyrin and C_{60} units do not occur in this case. These results differs from those obtained for dipeptide complexes **38·53** and **38·54** in MCH in which $\pi-\pi$ interactions between porphyrin and C_{60} units take place. The results obtained for **38·59** and **38·60** in MCH compared to those obtained in CHCl₃

(Figure 4.44), showed changes that are clearly more pronounced; this is probably an indication of the formation of a new supramolecular ensemble in which $\pi-\pi$ interactions between porphyrin and C_{60} might be given.
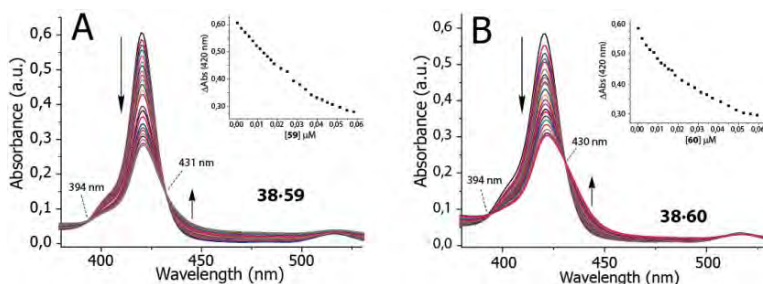
Figure 4.53 UV-Vis spectra of **38** (2.01 x 10^{-5} M) and variable concentration of **59** (A) and **60** (B) (0 - 5.45 x 10^{-5} M) in MCH. Insets show the variation in absorption at 420 nm with increasing amounts of **59** and **60**.

Circular dichroism (CD) measurements for **38·53** in MCH showed an induced circular dichroism (ICD) signal (Figure 4.54 A) that differs from that one obtained in CHCl$_3$ (Figure 4.45 A). The ICD signal obtained in MCH presents a positive Cotton effect at longer wavelength (442 nm), a zero crossing point at 432 nm and a negative Cotton effect at shorter wavelength (403 nm). In fact, the zero crossing point matches with the red shifted band of porphyrin upon addition of fullerene derivative in MCH (λ_{max} = 431 nm, Figure 4.52 A). This ICD signal is probably triggered by a transmission of chirality from the new supramolecular ensemble to porphyrin **38**, in which $\pi-\pi$ interactions between porphyrin and C_{60} units take place. Conversely, measurements for **38·54** showed an ICD signal with similar trends but opposite signs (Figure 4.54 B).
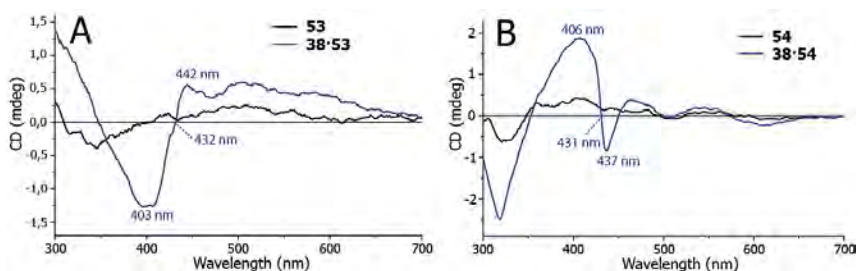
Figure 4.54 Circular dichroism (CD) spectra for complexes **38·53** (A) and **38·54** (B) in MCH (9.05 x 10^{-5} M, red lines). Spectra of the respective fullerene derivatives as references are also represented (9.05 x 10^{-5} M, black lines).

Circular dichroism measurements in MCH for pentapeptide complexes **38·59** and **38·60** showed ICD signals with positive value at 432 and 430 nm, respectively (Figure 4.55 A and B). These ICD signals are very similar to those obtained in $CHCl_3$ (Figure 4.47), but with a stronger response in MCH. For complex **38·59**, besides of the above mentioned positive signal, a negative signal at 419 nm and a zero crossing point at 424 nm were also observed. This ICD signal could be explained in terms of a transmission of chirality from a new supramolecular ensemble to the achiral porphyrin **38**. This differs from the case of dipeptide complexes in that $\pi-\pi$ interactions between porphyrin and C_{60} units are not involved and, hence, a similar response to that obtained in $CHCl_3$ for pentapeptide complexes are obtained.
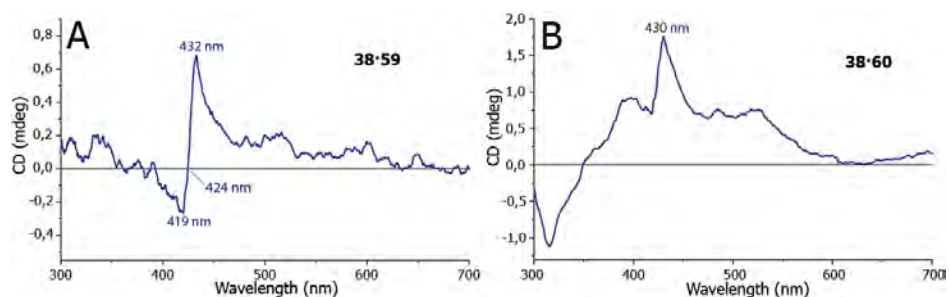
Figure 4.55 Circular dichroism (CD) spectra for complexes **38·59** (A) and **38·60** (B) in MCH (8.03 x 10^{-5} M, red lines). CD spectra of the respective fullerene derivatives **59** and **60** as references have a negligible CD response at the concentration worked for pentapeptide complexes.

Fluorescence titrations in MCH for dipeptide complexes **38·53** and **38·54** (Figure 4.56 A and B, respectively) were also performed. The emissions of the porphyrin were strongly quenched upon addition of increasing amounts of fullerene derivatives, which is in agreement with the formation of supramolecular dyads through the amidinium-carboxylate pair and the existence of $\pi-\pi$ interactions between porphyrins and C_{60} units. As a consequence, the quenching in MCH is stronger in comparison to that observed in $CHCl_3$ in which the stabilization of the supramolecular dyads is given exclusively through the amidinium-carboxylate pair (Figure 4.50). Interestingly, the emissions of the porphyrin for pentapeptide complexes **38·59** and **38·60** (Figure 4.57 A and B, respectively) showed a strong quenching as well. One would expect that due

to the lack of $\pi-\pi$ interactions between porphyrin and C_{60} units, the quenching would be lower; however, the strong quenching observed together with the results obtained in UV-Vis experiments in MCH, suggests the existence of a supramolecular ensemble in which probably $\pi-\pi$ interactions between porphyrin units are given.
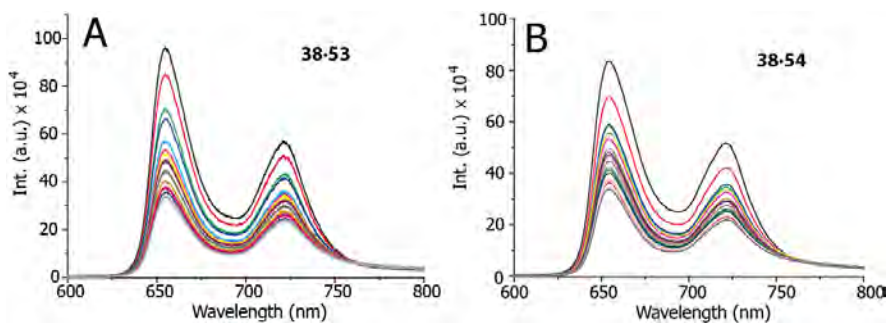
Figure 4.56 Fluorescence spectra of **38** (4.80 x 10^{-6} M) and variable concentration of **53** (A) and **54** (B) (0 - 3.02 x 10^{-5} M) in MCH (λ_{exc} = 433 nm).
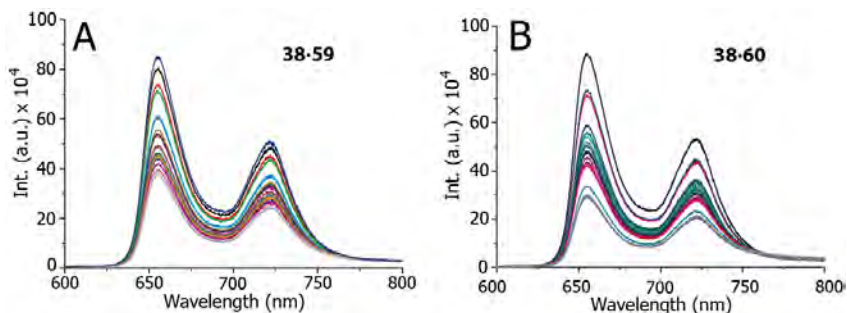
Figure 4.57 Fluorescence spectra of **38** (4.80 x 10^{-6} M) and variable concentration of **59** (A) and **60** (B) (0 - 2.69 x 10^{-5} M) in MCH (λ_{exc} = 433 nm).

Preliminary AFM studies for dipeptide complex **38·53** in CHCl$_3$ resulted in the formation of small isolated aggregates (Figure 4.58 A). However, in MCH a morphology consisting of a more aggregated network-like domains was observed; which is in agreement with the aforementioned results in which $\pi-\pi$ interactions play a key role in this solvent (Figure 4.58 B). Similar results were obtained for the other dipeptide complex **38·54** (Figure 4.58 C and D). Furthermore, these observations can be extent to the case of pentapeptide complexes **38·59** and **38·60** (Figure 4.59).
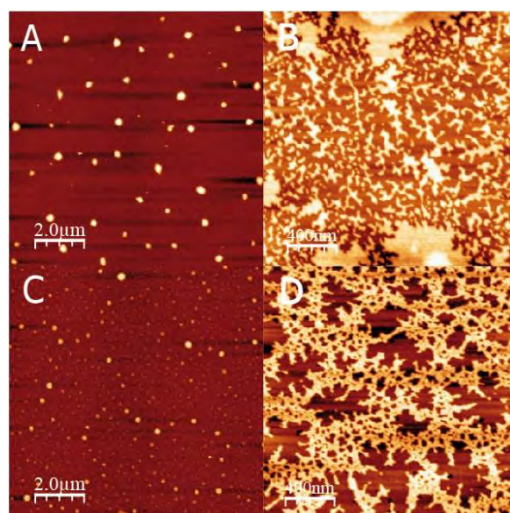
Figure 4. 58 AFM images obtained by drop-casting a solution of **38·53** in CHCl$_3$ (A) and MCH (B) (5.0 x 10^{-5} M) over freshly cleaved mica. AFM images of **38·54** in CHCl$_3$ (C) and MCH (D) are also shown (5.0 x 10^{-5} M).
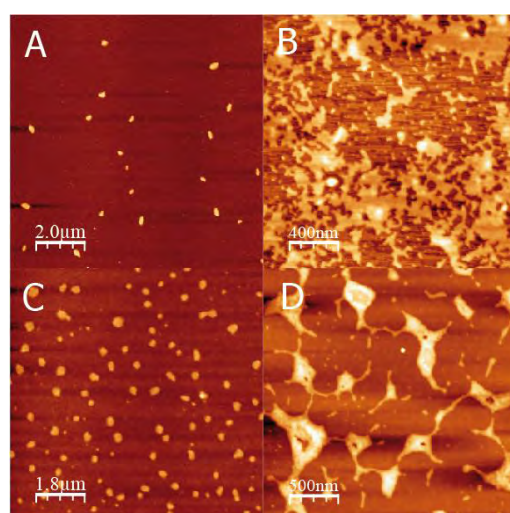
Figure 4.59 AFM images obtained by drop-casting a solution of **38·59** in CHCl$_3$ (A) and MCH (B) (5.0 x 10^{-5} M) over freshly cleaved mica. AFM images of **38·60** in CHCl$_3$ (C) and MCH (D) are also shown (5.0 x 10^{-5} M).

Taking into account all the above presented results, we believe that dipeptide complexes (**38·53** and **38·54**) are stabilized in CHCl$_3$ through the amidinium-

carboxylate pair. In MCH as solvent, besides of the latter, an additional stabilization through $\pi-\pi$ interactions between porphyrin and C_{60} units occurs in an antiparallel mode (Figure 4.60).
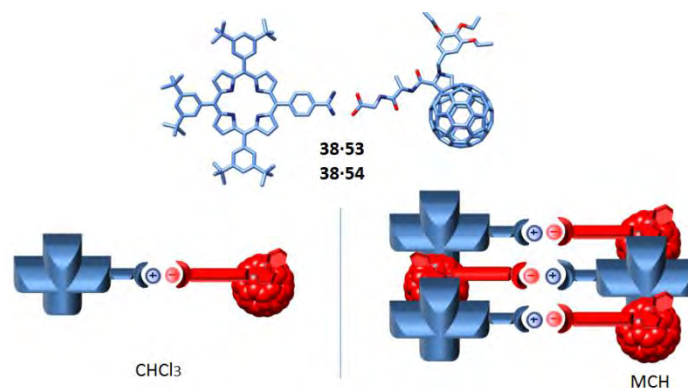
Figure 4.60 Schematic representation of supramolecular dipeptide complexes (**38·53** and **38·54**) in CHCl₃ and MCH. Alkyl chains have been omitted for clarity of the cartoon.

In the case of pentapeptide complexes (**38·59** and **38·60**) in CHCl₃, the stabilization is given by the amidinium-carboxylate pair as well. However, in MCH, taking into account the changes observed in UV-Vis, CD and fluorescence experiments, with respect to those obtained in CHCl₃, we believe that the formation of a new supramolecular ensemble is given. In this ensemble, porphyrins presumably interact between them separately from C_{60} units which are also $\pi-\pi$ interacting in a parallel mode (Figure 4.61). This proposal is in accordance with the lack of the large bathochromic shift that attests $\pi-\pi$ interactions between porphyrin and C_{60} units. The observed different CD response and the quenching of fluorescence in MCH also support this proposal.
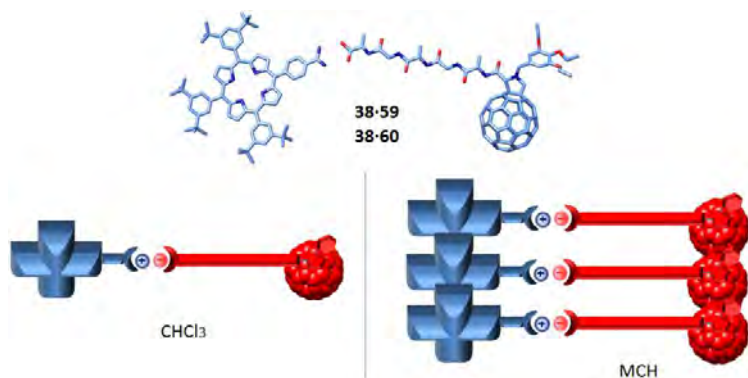
Figure 4.61 Schematic representation of supramolecular dipeptide complexes (**38·59** and **38·60**) in CHCl₃ and MCH. Alkyl chains have been omitted for clarity of the cartoon.

We are currently working on additional electron microscopy studies. Moreover, photophysical studies are being developed by Prof. D. M. Guldi in Germany.

5. Conclusions

5. CONCLUSIONS

The work developed in this study has provided valuable information on the key role of peptides in the construction of supramolecular assemblies at nano- and mesoscales. We have gained further knowledge in the morphology of the nanostructures generated when different electroactive cores are used; either planar or bulkier. Distance factors to β-sheet or peptide's chirality are also key issues.

We have also studied the supramolecular properties of exTTF-nanofibers for organizing C_{60} and PCBM molecules in order to create 1D n/p-nanohybrids and trigger the oriented crystallization of fullerene domains.

We have studied the formation of supramolecular dyads through a strong H-bond interaction pair that produces chiral induction effects. Distance factors to this pair as well as different diastereoisomers were also analyzed. The results of each section in the present study can be summarized as follows:

Section 4.1.
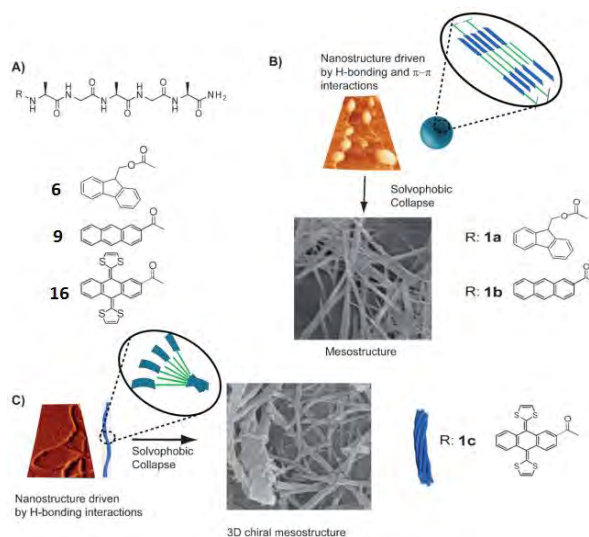
Concave vs planar geometries for the hierarchical organization of mesoscopic helical fibers.

- A new series of pentapeptide derivatives comprising planar (Fmoc and anthracene) and concave-shaped (exTTF) units have been synthesized. The study of their supramolecular nanostructures has shown the importance of the concave shape of exTTFs in the context of creating helical mesostructures.

- In TCE, planar derivatives (**6** and **9**) self-assemble by means of H-bonds and $\pi-\pi$ interactions into nanospheres or sheets, while exTTF derivative (**16**) self-assembles by H-bonds into a network of long chiral nanofibers with helical features. Importantly, exTTFs are not interacting with each other in the secondary structure.

- In CHCl$_3$/MCH, the subsequent self-assembly of the secondary structure into a tertiary structure by means of a solvophobic collapse, gives rise to straight fibers in the case of planar derivatives and helical mesostructures for the exTTF derivative. The latter supports the entwinement into one helical bias of several nanofibers to yield single handedness 3D fibers at mesoscale. These fibers were experimentally found to have an order that stems from stabilizing $\pi-\pi$ interactions between the non-planar exTTFs.

- Aged solutions of **16** showed distinct excited-state characteristics in terms of transient features and transient decays that contrast markedly from those seen for **16** in MeOH.

- The different nanostructures and morphologies have been confirmed by a variety of complementary techniques such as UV-Vis, CD, AFM, TEM, SEM, XRD and FTIR.

Section 4.2.

Supramolecular one dimensional n/p nanohybrids.
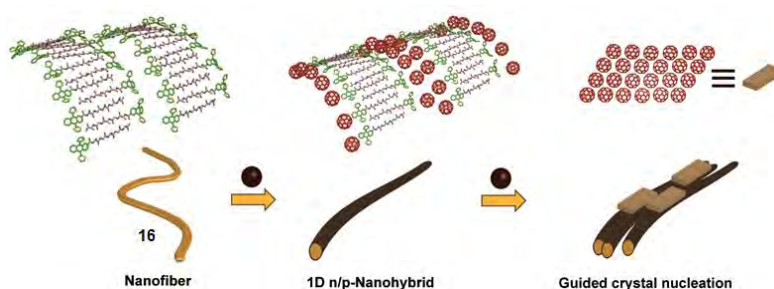
Nanofiber   1D n/p-Nanohybrid   Guided crystal nucleation

- The use of supramolecular exTTF nanofibers in TCE, in which exTTFs are not interacting between them, has led to the efficient formation of 1D *n/p*-nanohybrids through the concave-convex interaction between exTTFs and C_{60} units.

- The high tendency of C_{60} to aggregate is likely to favor the evolution from an initial state, in which close packed columns of C_{60}/PCBM are intercalated between exTTF-fibers, into a final state, where the C_{60}/PCBM crystalize onto *n/p*-nanohybrids. Implicit are 1D *n/p*-nanohybrids, in which donor and acceptor units are organized at the same length scale. It opens a promising avenue to guide the crystallization of C_{60} on top of exTTF-fibers and/or exTTF-gels to afford anisotropic C_{60} crystals.

- The construction of the presented 1D *n/p*-nanohybrids comes without the needs of using C_{60} derivatives covalently linked to functional substituents that would facilitate such growth.

- Photophysical studies showed that photoexcitation of the self-assembled nanohybrids proceeds via a transient excited state into a charge separated state.

- The different *n/p*-nanohybrid nanostructures and morphologies have been confirmed by a variety of complementary techniques such as UV-Vis, CD, AFM, TEM, SEM, XRD, FTIR and Raman.

Section 4.3.

Supramolecular pentapeptide-based fullerene nanofibers: effect of molecular chirality.

159
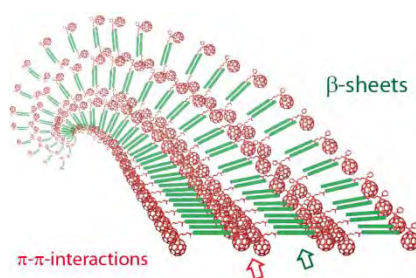
- A new series of pentapeptide derivatives comprising fullerene units have been synthesized. The study of their supramolecular nanostructures has shown the importance of chirality as well as the distance from the peptide backbone to the fullerene moiety.

- Their supramolecular nanostructures are stabilized through H-bonds forming β-sheets along with $\pi-\pi$ interactions between C_{60} units.

- A study over nanofiber's morphology showed that there is a correlation between the nanofibers obtained and chirality of the peptide. Thus, using a chiral peptide gives rise to twisted fibers, while the use of an achiral peptide with the same C_{60} moiety gives rise to straight fibers instead.

- A study over nanofiber's morphology showed that there is a correlation between the nanofibers and the distance from the peptide backbone and the C_{60} moiety. Thus, a short distance gives rise to straight, rigid and more aggregated fibers, while a larger distance affords twisted fibers instead.

- The different fullerene pentapeptide nanostructures and morphologies have been confirmed by a variety of complementary techniques such as UV-Vis, CD, AFM, TEM and FTIR.

Section 4.4.

Supramolecular porphyrin-C_{60} peptide dyads: morphology and chiral induction effects.
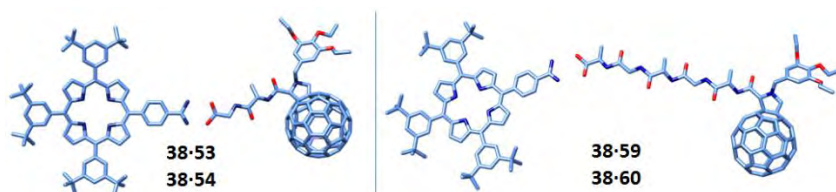
- A porphyrin endowed with an amidine group and two sets of enantiomerically pure fullerene derivatives functionalized with dipeptide (**53** and **54**) and pentapeptide (**59** and **60**) units comprising a carboxylic acid group as terminal group have been synthesized.

- The study of supramolecular dyads in $CHCl_3$ showed that the formation of the amidinium-carboxylate pair was efficiently achieved. This interaction gives rise to an induced circular dichroic (ICD) signal that in the case of dipeptide complexes is mainly affected by the chiral center over the fulleropyrrolidine, while in the case of pentapeptide complexes the ICD is mainly affected by the alanine units closer to the amidinium-carboxylate pair.

- The study of supramolecular dyads in MCH showed that besides of the formation of the amidinium-carboxylate pair, $\pi-\pi$ interactions were also involved. In the case of dipeptide complexes such $\pi-\pi$ interactions occur between porphyrin and C_{60} units in an antiparallel fashion, while in the case of pentapeptide complexes such interactions are probably given, in one side, between porphyrin units, and in the other side, between C_{60} moieties like in a parallel fashion. Due to these $\pi-\pi$ interactions, fluorescence was strongly quenched in both cases.

- Preliminary AFM studies corroborate the more aggregated structures in MCH that in $CHCl_3$.

6. Experimental section

6. EXPERIMENTAL SECTION

6.1. GENERAL REMARKS

Reagents and solvents were used as received from commercial sources unless stated otherwise.

- Preparative thin-layer chromatography was performed on E. Merck silica gel 60 F_{254} plates (1 mm).

- *NMR* spectra were recorded on a Bruker DPX-300 or Bruker AVIII-700 spectrometer. Unless otherwise indicated, chemical shifts are reported in ppm downfield from tetramethylsilane (TMS) as internal standard at room temperature using deuterated solvents. Multiplicities are denoted as follows: s = singlet, d = doublet, t = triplet, m = multiplet, br s = broad singlet, dd = double doublet. C denotes quaternary carbons.

- *FTIR* spectra were determined on a Bruker Tensor 27 (equipped with an ATR device) spectrometer. Only neat peaks are reported.

- *UV-Vis* spectra were recorded with a Shimadzu Spectrophotometer UV-3600 at room temperature.

- *Mass* spectra were realized by the mass spectra services at the Universidad Complutense de Madrid. MALDI-TOF experiments were taken on a Bruker-Ultraflex spectrometer using dithranol matrix. ESI-MS spectra were performed on a Bruker Apex Q IV mass spectrometer.

- *Circular Dichroism* spectra were performed in a Jasco J-815 CD spectrometer at room temperature.

- *Atomic Force Microscopy (AFM)* images were acquired under ambient conditions using SPM Nanoscope IIIa multimode working on tapping mode with a RTESPA tip

(Veeco) at a working frequency of ~235 kHz. The samples were prepared by drop-casting on a freshly cleaved mica surface and were dried under ambient conditions.

- *Transmission electron microscopy (TEM)* images were performed using a JEOL JEM 2100 electron microscope, operating at 200 kV accelerating voltage. The samples were prepared by drop-casting on carbon film 200 square mesh copper grids (CF200-Cu). High Resolution TEM (HRTEM) measurements were performed in a JEOL JEM 3000F, operating at 300 kV accelerating voltage.

- *Scanning electron microscopy (SEM)* images were acquired by using a JEOL JSM 6335F microscope working at 10 kV. Samples were deposited by drop-casting on silicon substrate, dried under ambient conditions and metallized with Au prior to observation.

- *Fluorescence* spectra were carried out in a Fluoromax 4 Horiba-4TCSPC spectroflurometer (Edinson, NJ) equipped with a xenon lamp.

- *Raman* spectra were acquired with a Renishaw in Via confocal Raman microscopy instrument, equipped with 532 nm on a glass microscope slide.

- *X-ray Diffraction (XRD)* was performed in a Panalytical X'Pert PRO diffractometer with Cu tube (lambda Kα=1.54187 Å) operated at 45 kV, 40 mA, Ni beta filter, programmable divergence and anti-scatter slits working in fixed mode, and fast linear detector (X'Celerator) working in scanning mode. Samples were deposited in a silicon zero background sampleholder and measured in reflection mode.

6.2.   SYNTHESIS OF COMPOUNDS

Section 4.1

L-alanyl-glycyl-L-alanyl-glycyl-L-alanine-NH₂ (5)
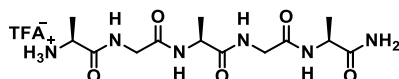
Standard solid phase using 9-fluorenylmethoxycarbonyl (Fmoc) chemistry on a 4-methyl-benzydrylamine (MBHA) resin (300 mg) was used to synthesize pentapeptide **5** (Scheme 4.3). Before the first amino acid coupling to the resin, the latter was swelled and rinsed with DMF and DCM. The amino acid couplings were performed, in general, by adding to the resin a DMF solution of the Fmoc-protected amino acid **1** or **2** (3eq., relative to the resin load = 1.0 - 1.2 mmol/g) previously activated with 3 eq. of *O*-benzotriazole-*N,N,N',N'*-tetramethyluronium hexafluorophosphate (HBTU) and 7 eq. of diisopropylethylamine (DIPEA). The resulting mixture was shaken for one hour by bubbling N_2 to chamber at room temperature. Then the resin was washed with DMF and DCM. Fmoc deprotection was performed by mixing the Fmoc-peptide-resine with a solution of piperidine (20%) in DMF for five minutes at room temperature. This process was repeated at least three times. After this, the resin was washed several times with DMF (x3) and DCM (x3). Every step (amino acid couplings and Fmoc deprotection) was checked by the Kaiser test taking few beads from the chamber. The cleavage of pentapeptide **5** from the resin was performed with a solution of trifluoroacetic acid and water (95:5) giving rise to the desired product **5** with an amine and an amide groups at the N-terminus and C-terminus positions, respectively. The resin was removed by filtration and washed with DCM. The filtrate was concentrated under reduced pressure and the peptide was precipitated by adding cold diethyl ether. The solid was filtered and washed with cold diethyl ether to obtain the peptide **5** as a white solid. Yield: 80% (108 mg). ¹H-NMR (300 MHz, D₂O): δ (ppm) 1.38 (d, *J* = 7.2 Hz, 3H, CH₃-Ala), 1.40 (d, *J* = 7.2 Hz, 3H, CH₃-Ala), 1.54 (d, *J* = 7.1 Hz, 3H, CH₃-Ala), 3.93 (s, 2H, CH₂-Gly), 4.01 (s, 2H, CH₂-Gly), 4.13 (q, *J* = 7.1 Hz, 1H, CH-Ala), 4.26-4.38

(m, 2H, 2CH-Ala). ^{13}C-NMR (75 MHz, D$_2$O): δ (ppm) 16.4 (CH$_3$-Ala), 16.5 (CH$_3$-Ala), 16.7 (CH$_3$-Ala), 42.2 (CH$_2$-Gly), 42.4 (CH$_2$-Gly), 49.1 (CH-Ala), 49.4 (CH-Ala), 49.9 (CH-Ala), 170.9 (C=O), 171.1 (C=O), 171.4 (C=O), 175.7 (C=O), 177.8 (C=O). HRMS (ESI-FT) *m/z*: [M$^+$] Calc. for C$_{13}$H$_{25}$N$_6$O$_5$: 345.1881; found: 345.1886.

Fmoc-L-alanyl-glycyl-L-alanyl-glycyl-L-alanine-NH$_2$ (6)
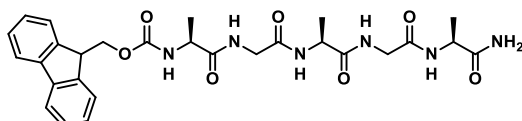
The synthesis of this compound was performed by SPPS (see schemes 4.3 and 4.4) using a MBHA resin (300 mg). Once compound **3** was achieved in the resin (scheme 4.3) the subsequent cleavage of the pentapeptide from the resin was performed with a solution of trifluoroacetic acid and water (95:5). The resin was removed by filtration and washed with DCM. The filtrate volume was concentrated under reduced pressure and the peptide was precipitated with cold diethyl ether. The precipitate **6** was filtered and washed with cold diethyl ether to obtain the peptide as a white solid. Yield: 58% (98 mg). ^{1}H-NMR (700 MHz, DMSO-*d$_6$*): δ (ppm) 1.35-1.23 (m, 9H, CH$_3$-Ala), 3.68-3.78 (m, 4H, CH$_2$-Gly), 4.00-4.36 (m, 6H, 3CH-Ala+CH$_2$O+C*H*-CH$_2$O-), 7.05 (s, 1H, NH$_2$), 7.29 (s, 1H, NH$_2$), 7.34 (dd, *J* = 7.4 Hz, *J* = 6.8 Hz, 2H, Ar-H), 7.44 (dd, *J* = 7.3 Hz, *J* = 6.8 Hz, 2H, Ar-H), 7.64 (d, 1H, *J* = 7.1 Hz, NH-Ala), 7.68-7.79 (m, 2H, Ar-H), 7.85 (d, 1H, *J* = 7.5 Hz, NH-Ala), 7.91 (d, *J* = 7.4 Hz, 2H, Ar-H), 8.03 (d, 1H, *J* = 6.7 Hz, NH-Ala), 8.10-8.27 (m, 2H, NH-Gly). ^{13}C-NMR (175 MHz, DMSO-*d$_6$*): δ (ppm) 18.3 (CH$_3$-Ala), 18.4 (CH$_3$-Ala), 18.7 (CH$_3$-Ala), 42.4 (CH$_2$-Gly), 42.5 (CH$_2$-Gly), 47.1 (CH-Ala), 48.5 (CH-Ala), 49.0 (CH-Ala), 50.6 (C*H*-CH$_2$O), 66.1 (CH$_2$O), 120.6 (Ar-H), 125.6 (C), 125.7 (C), 127.6 (Ar-H), 128.1 (Ar-H), 141.2 (Ar-H), 144.2 (C), 144.3 (C), 156.3 (-O-(C=O)-N-), 168.7 (C=O), 169.2 (C=O), 173.1 (C=O), 173.4 (C=O), 174.6 (C=O). HRMS (ESI-FT) *m/z*: [M+Na]$^+$ Calc. for C$_{28}$H$_{34}$N$_6$O$_7$Na: 589.2381; found: 589.2383. ATR-FTIR (TCE): 3300, 3069, 2972, 2929, 1682, 1651, 1630, 1541, 1449, 1258, 1230, 738 cm^{-1}.

Anthracene-2-carboxylic acid (8)[145]
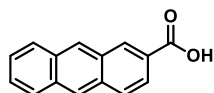
A mixture of 9,10-dioxo-9,10-dihydroanthracene-2-carboxylic acid **7** (120 mg, 0.48 mmol), zinc (311 mg, 4.8 mmol) and NH_4OH (20 mL) was refluxed 12 hours. Then, the mixture was cooled to room temperature and neutralized with HCl (2M) until pH = 6. The resulting mixture was filtered and the filtrate was extracted with CH_2Cl_2. The organic phase was dried over Na_2SO_4 and then the solution was filtered and concentrated under reduced pressure. The purification was performed by silica gel column chromatography using a mixture of CH_2Cl_2:MeOH (10:1) as eluent. The product was obtained as a yellow solid. Yield: 85% (91 mg). ^{1}H-NMR (300 MHz, MeOD-d_4): δ (ppm) 7.46-7.56 (m, 2H), 8.00-8.12 (m, 4H), 8.53 (s, 1H), 8.66 (s, 1H), 8.85 (s, 1H).

Anthracene-L-alanyl-glycyl-L-alanyl-glycyl-L-alanine-NH₂ (9)
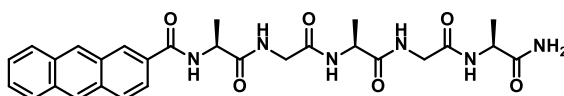
In a round-bottom flask, anthracene-2-carboxylic acid **8** (30 mg, 0.13 mmol) in anhydrous DMF (8 mL) was activated by adding HBTU (76 mg, 0.20 mmol) and DIPEA (0.16 mL, 0.94 mmol) under argon atmosphere. After 5 minutes of activation, a solution of pentapeptide **5** (74 mg, 0.16 mmol) in anhydrous DMF (2 mL) was added. The mixture was stirred at room temperature for 2 hours. Then, CH_2Cl_2 (30 mL) was added and the resulting mixture was washed with an aqueous solution of Na_2CO_3 (3 x 30 mL). The organic phase was dried over Na_2SO_4, filtered and concentrated under reduced pressure. The product was purified by silica gel column chromatography using a mixture of CH_2Cl_2:MeOH (10:1) as eluent. The product was obtained as a pale-yellow solid. Yield: 63% (46 mg). ^{1}H-NMR (700 MHz, MeOD-d_4): δ (ppm) 1.37 (d, *J* = 7.2

[145] J. Jiang, O. V. Lima, Y. Pei, Z. Jiang, Z. Chen, C. Yu, J. Wang, X. Cheng, E. Forsythe, L. Tan, *ACSNano* **2010**, *4*, 3773-3780.

Hz, 3H, CH$_3$-Ala), 1.49 (d, *J* = 7.5 Hz, 3H, CH$_3$-Ala), 1.59 (d, *J* = 7.0 Hz, 3H, CH$_3$-Ala), 3.84 (d, *J* = 16.7 Hz, 1H, CH$_2$-Gly), 3.89 (d, *J* = 16.7 Hz, 1H, CH$_2$-Gly), 3.97 (d, *J* = 16.7 Hz, 1H, CH$_2$-Gly), 4.02 (d, *J* = 16.7 Hz, 1H, CH$_2$-Gly), 4.31-4.38 (m, 2H, 2CH-Ala), 4.59 (q, *J* = 7.2 Hz, 1H, CH-Ala), 7.52-7.59 (m, 3H, Ar-H), 8.07-8.16 (m, 3H, Ar-H), 8.56 (s, 1H, Ar-H), 8.66 (s, 1H, Ar-H), 8.71 (s, 1H, Ar-H). ^{13}C-NMR (175 MHz, MeOD-*d*$_4$): δ (ppm) 16.0 (CH$_3$-Ala), 16.1 (CH$_3$-Ala), 16.7 (CH$_3$-Ala), 42.4 (CH$_2$-Gly), 42.5 (CH$_2$-Gly), 48.1 (CH-Ala), 48.2 (CH-Ala), 48.5 (CH-Ala), 122.8 (Ar-H), 125.6 (Ar-H), 126.1 (Ar-H), 127.1 (Ar-H), 127.4 (Ar-H), 127.9 (Ar-H), 128.0 (Ar-H), 128.3 (Ar-H), 130.1 (Ar-H), 130.4 (C), 132.1 (C), 132.2 (C), 132.3 (C), 133.0 (C), 169.1 (C=O), 170.0 (C=O), 170.7 (C=O), 174.5 (C=O), 175.2 (C=O), 176.3 (C=O). HRMS (ESI-FT) *m/z*: [M+Na]$^+$ Calc. for C$_{28}$H$_{32}$N$_6$O$_6$Na: 571.2281; found: 571.2275. ATR-FTIR (TCE): 3332, 2923, 2855, 1682, 1631, 1464, 1373, 1095, 826 cm^{-1}.

2-Methylthio-1,3-dithiolium tetrafluoroborate (11)[146]
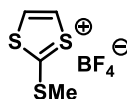
A solution of vinylene trithiocarbonate **10** (0.658 g, 4.90 mmol) in Me$_2$SO$_4$ (5 mL, 52.72 mmol) was heated at 95°C for 30 minutes or until dissolution was complete. The mixture was cooled to 0°C and glacial acetic acid (1 mL) was added. After stirring for 10 min, HBF$_4$·Et$_2$O (0.80 g, 4.90 mmol) was added and stirred for 15 minutes more. Then, cold diethyl ether (100 mL) was added giving rise to a precipitate that was collected by filtration and washed thoroughly with cold diethyl ether. Yield: 95% (1.100 g). ^{1}H-NMR (300 MHz, DMSO-*d*$_6$): δ (ppm) 3.17 (s, 3H), 8.73 (s, 2H).

2-Methylthio-1,3-dithiole (12)[146]

---
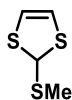
[146] A. J. Moore, M. R. Bryce, *Synthesis* **1991**, *1991*, 26-28.

NaBH$_4$ (0.178 g, 4.70 mmol) was added portionwise over to a stirred solution of salt **11** (1.100 g, 4.65 mmol) in absolute EtOH (30 mL) at 0°C. The mixture was stirred for 2 hours at room temperature. The solvent was removed under reduced pressure, washed with water and then extracted with CH$_2$Cl$_2$. The organic layer was dried over MgSO$_4$, filtered and taken to dryness affording the crude product **12** as a red oil of sufficient purity for next reaction. Yield: 95% (0.664 g). ^{1}H-NMR (300 MHz, CDCl$_3$): δ (ppm) 2.20 (s, 3H), 6.07 (s, 2H), 6.12 (s, 1H).

1,3-Dithiolium tetrafluoroborate (13)[146]
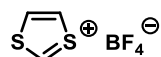
HBF$_4$·Et$_2$O (0.7 mL, 4.86 mmol) was added dropwise to a stirred solution of compound **12** (0.664 g, 4.42 mmol) in acetic anhydride (10 mL) at 0°C. After stirring for 15 minutes, diethyl ether (20 mL) was added and stirred for 30 minutes more. The solid was collected by filtration and washed thoroughly with diethyl ether obtaining **13** as a white solid. Yield: 90% (0.756 g). ^{1}H-NMR (300 MHz, DMSO-d_6): δ (ppm) 6.79 (s, 1H), 9.37 (s, 2H).

Dimethyl 1,3-dithiol-2-ylphosphonate (14)[146]
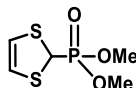
Trimethyl phosphite (0.62 mL, 5.3 mmol) and NaI (0.8 g, 5.34 mmol) were added successively to a stirred solution of salt **13** (1.0 g, 5.34 mmol) in acetonitrile (50 mL) at room temperature. The mixture was stirred for 2 hours, whereupon the solvent was evaporated under reduced pressure. Water (25 mL) was added to the residue and the mixture was extracted with CH$_2$Cl$_2$. The organic phase was dried over MgSO$_4$, filtered and the solvent removed under reduced pressure yielding the desired product **14** as a dark oil. Yield: 95% (1.077 g). ^{1}H-NMR (300 MHz, CDCl$_3$): δ (ppm) 3.75 (d, *J* = 10.5 Hz, 6H), 4.73 (d, *J* = 4.5 Hz, 1H), 5.98 (s, 2H).

9,10-Di(1,3-dithiol-2-ylidene)-9,10-dihydroanthracene-2-carboxylic acid (15)
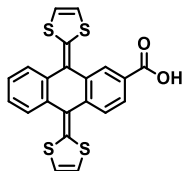
To a solution of phosphonate **14** (3.03 g, 14.3 mmol) in dry THF (100 mL) at -78°C, *n*-BuLi (12 mL, 19 mmol, 1.6 M in *n*-hexanes) was slowly added. The mixture was stirred at this temperature for 30 minutes followed by the addition of a suspension of anthraquinone-2-carboxylic acid **8** (600 mg, 2.38 mmol) in dry THF (40 mL). The mixture was allowed to reach room temperature and then stirred for further 6 hours. Solvent was evaporated under reduced pressure and the resultant oil crude was neutralized by addition of a solution of HCl (0.2M). Then, an extraction with CH_2Cl_2 was performed. The organic phase was dried over Na_2SO_4, filtered and concentrated under reduced pressure. The desired product **15** was purified by silica gel column chromatography using a mixture of CH_2Cl_2:MeOH (25:1) as eluent. The resulting solid was dissolved in MeOH and precipitated by the addition of *n*-hexane which was collected by filtration yielding an orange powder. Yield: 55% (556 mg). ^{1}H-NMR (DMSO-*d*$_6$, 300 MHz): δ (ppm) 6.77 (d, *J* = 2.4 Hz, 2H, dithiole-CH), 6.80 (br s, 2H, dithiole-CH), 7.33-7.41 (m, 2H, Ar-H), 7.65-7.72 (m, 2H, Ar-H), 7.76 (d, *J* = 7.8 Hz, 1H, Ar-H), 7.90 (dd, *J* = 7.80 Hz, *J* = 1.7 Hz, 1H, Ar-H), 8.24 (d, *J* = 1.7 Hz, 1H, Ar-H), 13.1 (s, 1H, COOH). ^{13}C-NMR (DMSO-*d*$_6$, 75 MHz): δ (ppm) 117.8 (dithiole-CH), 118.1 (dithiole-CH), 118.3 (dithiole-C), 119.9 (dithiole-C), 124.8 (Ar-H), 125.5 (Ar-H), 126.4 (Ar-H), 127.2 (Ar-H), 128.0 (Ar-H), 134.4 (C), 134.7 (C), 137.6 (C), 138.6 (C), 139.0 (C), 139.2 (C), 166.7 (C=O). MS (ESI) *m/z*: [M$^+$] Calc. for $C_{21}H_{12}O_2S_4$: 423.97; found: 423.94.

exTTF-L-alanyl-glycyl-L-alanyl-glycyl-L-alanine-NH$_2$ (16)
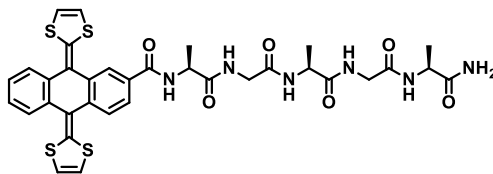
In a round-bottom flask, carboxylic acid **15** (30 mg, 0.07 mmol) in anhydrous DMF (8 mL) was activated by adding HBTU (40 mg, 0.11 mmol) and DIPEA (0.09 mL, 0.49 mmol) under argon atmosphere. After 5 minutes of activation, a solution of pentapeptide **5** (38 mg, 0.08 mmol) in anhydrous DMF (2 mL) was added. The mixture was stirred at room temperature for 2 hours. Then, CH$_2$Cl$_2$ (30 mL) was added and the resulting mixture was washed with an aqueous solution of Na$_2$CO$_3$ (3 x 30 mL). The organic phase was dried over Na$_2$SO$_4$, filtered and concentrated under reduced pressure. The product was purified by silica gel column chromatography using a mixture of CH$_2$Cl$_2$:MeOH (10:1) as eluent. The product was obtained as a yellow solid. Yield: 73% (39 mg). ^{1}H-NMR (700 MHz, MeOD-d_4) δ (ppm) 1.18 (d, J = 6.2 Hz, 3H, CH$_3$-Ala), 1.37 (d, J = 7.3 Hz, 3H, CH$_3$-Ala), 1.54 (d, J = 7.2 Hz, 3H, CH$_3$-Ala), 3.81-3.88 (m, 2H, CH$_2$-Gly), 3.91-4.05 (m, 2H, CH$_2$-Gly), 4.29-4.39 (m, 2H, 2CH-Ala), 4.48-4.53 (m, 1H, CH-Ala), 6.49-6.52 (m, 4H, dithiole-CH), 7.27-7.36 (m, 2H, Ar-H), 7.69-7.73 (m, 2H, Ar-H), 7.78 (d, J = 8.1 Hz, 1H, Ar-H), 7.85 (d, J = 8.1 Hz, 1H, Ar-H), 8.26 (s, 1H, Ar-H). ^{13}C-NMR (175 MHz, MeOD-d_4) δ (ppm) 15.9 (CH$_3$-Ala), 16.2 (CH$_3$-Ala), 16.6 (CH$_3$-Ala), 42.4 (CH$_2$-Gly), 42.5 (CH$_2$-Gly), 48.8 (CH-Ala), 49.9 (CH-Ala), 50.8 (CH-Ala), 117.1 (dithiole-CH), 117.3 (dithiole-CH), 120.4 (dithiole-C), 120.5 (dithiole-C), 124.2 (Ar-H), 124.5 (Ar-H), 124.6 (Ar-H), 124.7 (Ar-H), 125.8 (Ar-H), 130.3 (C), 135.1 (C), 135.2 (C), 135.7 (C), 137.6 (C), 138.7 (C), 168.5 (C=O), 169.9 (C=O), 170.7 (C=O), 174.5 (C=O), 175.2 (C=O), 176.3 (C=O). HRMS (ESI-FT) *m/z*: [M+Na]$^+$ Calc. for C$_{34}$H$_{34}$N$_6$O$_6$S$_4$Na: 773.1315; found: 773.1339. ATR-FTIR (TCE): 3281, 3069, 2920, 2851, 1691, 1627, 1545, 1513, 1449, 1263, 1223, 756, 702, 644 cm^{-1}.
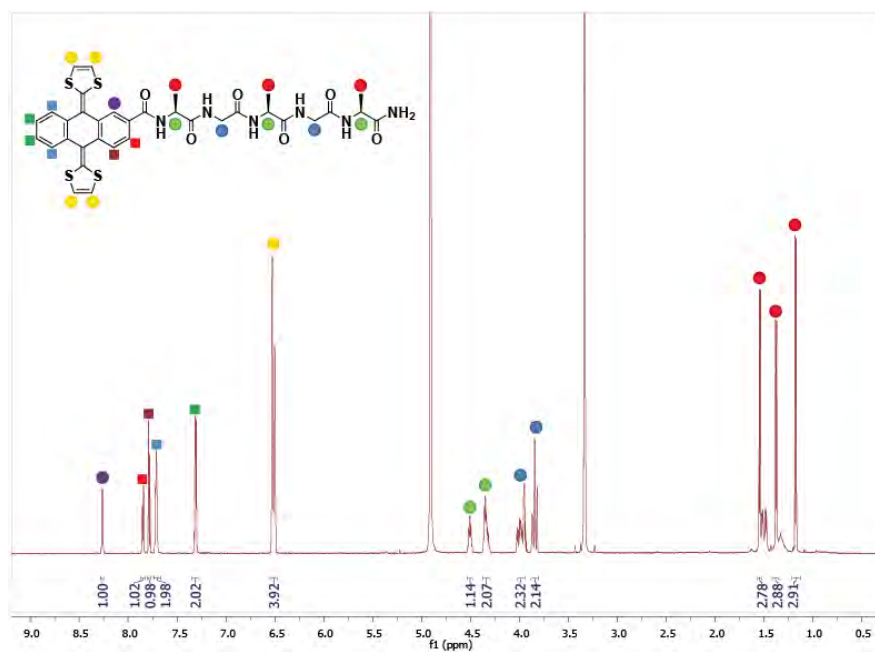
Figure 6.1 ^{1}H-NMR spectrum of compound **16** in MeOD-d_4.
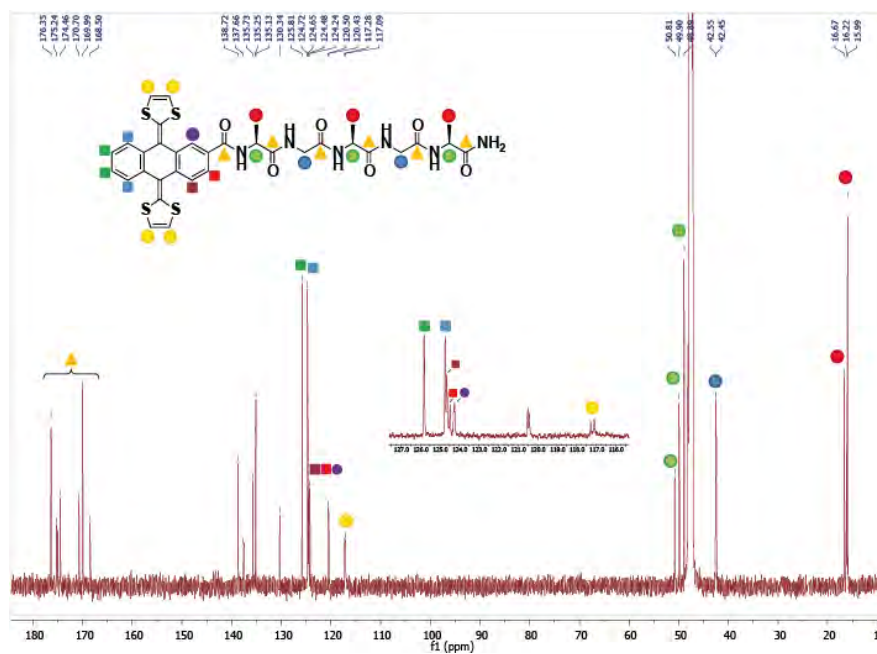
Figure 6.2 ^{13}C-NMR spectrum of compound **16** in MeOD-d_4.

174

Section 4.2

Methyl 4-benzoylbutyrate (19)[130]
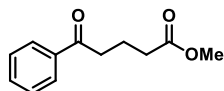
To a solution of 4-benzoylbutyric acid **18** (3 g, 15.6 mmol) in MeOH (40 mL), oxalyl chloride (2.97 g, 23.4 mmol) was added and then heated to reflux for 24 hours. The solvent was evaporated under reduced pressure and the residue was dissolved in CH_2Cl_2, then it was washed with aqueous Na_2CO_3. The organic phase was dried over $MgSO_4$, filtered and the solvent was evaporated under reduced pressure. The product **19** was obtained as a yellow oil and was used without further purification. Yield: 90% (2.89 g). ^{1}H-NMR (300 MHz, $CDCl_3$): δ (ppm) 2.08-2.11 (m, 2H), 2.45 (t, J = 7.1 Hz, 2H), 3.07 (t, J = 7.1 Hz, 2H), 3.69 (s, 3H, OCH_3), 7.45-7.48 (m, 1H, Ar-H), 7.65-7.70 (m, 2H, Ar-H), 7.97 (d, 2H, J = 8.1 Hz, Ar-H).

Methyl 4-benzoylbutyrate *p*-tosylhydrazone (20)[130]
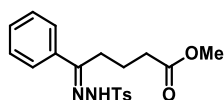
A mixture of methyl 4-benzoylbutyrate **19** (1.9 g, 9.2 mmol), *p*-toluenesulfonyl hydrazide (2.1 g, 11.0 mmol) and MeOH (70 mL) was refluxed for 6 hours. Then it was left to room temperature and stirred for 12 hours. Afterwards the mixture was cooled to -15°C and the forming precipitate was filtered and washed with cold MeOH affording the desired product **20**. Yield: 90% (3.1 g). ^{1}H-NMR (300 MHz, $CDCl_3$): δ (ppm) 1.68-1.71 (m, 2H), 2.31 (t, J = 6.0 Hz, 2H), 2.40 (s, 3H), 2.62-2.67 (m, 2H), 3.80 (s, 3H, OCH_3), 7.29 (d, J = 8.1 Hz, 2H), 7.35-7.41 (m, 3H), 7.62-7.66 (m, 2H), 7.94 (d, J = 8.1 Hz, 2H), 9.30 (s, 1H, NH).

1-[3-(Methoxycarbonyl)propyl]-1-phenyl[6,6]methanofullerene, PCBM (21)[130]
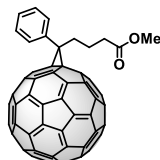
To a solution of tosylhydrazone **20** (169 mg, 0.45 mmol) in anhydrous pyridine (10 mL), sodium methoxide (28 mg, 0.521 mmol) was added and the resulting mixture was stirred at room temperature for 15 minutes under argon atmosphere. Then, a solution of C_{60} (250 mg, 0.35 mmol) in *o*-DCB (40 mL) was added and the mixture was heated to reflux for 48 hours. Under these conditions, only the [6,6]-closed isomer was obtained. The solvent was removed under reduced pressure and the desired product **21** was purified by silica gel column chromatography using first CS_2 to recover the unreacted C_{60}, and then using toluene as eluent. The solid obtained was dissolved in toluene and precipitated by the addition of cold diethyl ether which was collected by filtration yielding compounds **21** as brownish powder. Yield: 40% (128 mg). ^{1}H-NMR (300 MHz, CDCl$_3$/CS$_2$): δ (ppm) 2.14-2.27 (m, 2H), 2.54 (t, *J* = 7.6 Hz, 2H), 2.87-2.99 (m, 2H), 3.69 (s, 3H), 7.46-7.52 (m, 1H, Ar-H), 7.52-7.60 (m, 2H, Ar-H), 7.94 (d, *J* = 7.5 Hz, 2H, Ar-H).

Section 4.3

Glycyl-glycyl-glycyl-glycyl-glycine-NH₂ (22)
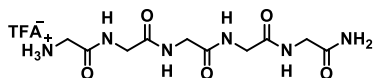
The synthesis of this compound was performed using the same methodology as compound **5** on a MBHA resin (300 mg) as well. The only difference relies on the use of Fmoc-glycine **2** in all coupling steps. The cleavage of pentapeptide **22** from the resin was performed with a solution of TFA:H_2O (95:5) giving rise to the desired product **22** with an amine and an amide groups at the N-terminus and C-terminus positions, respectively. The resin was removed by filtration and washed with DCM. The filtrate was concentrated under reduced pressure and the peptide was precipitated by adding cold diethyl ether. The precipitate was filtered and washed with cold diethyl ether to obtain the peptide as a white solid. Yield: 77% (96 mg). ^{1}H-NMR (300 MHz, D_2O): δ (ppm) 3.75 (s, 2H, CH_2-Gly), 3.78 (s, 2H, CH_2-Gly), 3.84 (s, 2H, CH_2-Gly), 3.86 (s, 2H, CH_2-Gly), 3.91 (s, 2H, CH_2-Gly). ^{13}C-NMR (75 MHz, D_2O): δ 40.4 (CH_2), 41.9 (CH_2), 42.3 (CH_2), 42.41 (CH_2), 42.46 (CH_2), 167.9 (C=O), 171.9 (C=O), 172.0 (C=O), 172.2 (C=O), 174.2 (C=O) ppm. MS (ESI) *m/z*: [M$^+$] Calc. for $C_{10}H_{19}N_6O_5^+$: 303.14; found: 303.10.

1-(3-Carboxypropyl)-1-phenyl[6,6]methanofullerene, PCBA (23)[130]
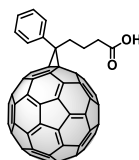
To a solution of PCBM **21** (100 mg, 0.11 mmol) in toluene (120 mL), HCl conc. (20 mL) and glacial acetic acid (50 mL) were added. This mixture was heated to reflux for 48 hours. Then, the solvent was removed until dryness. The crude was dissolved in the minimum volume of toluene and then cold diethyl ether was added to precipitate the product. The solid was washed with diethyl ether giving rise to the desired product **23** as a brownish solid. Yield: 90% (89 mg). ^{1}H-NMR (300 MHz, CDCl₃/CS₂): δ (ppm) 2.17-

2.28 (m, 2H), 2.50-2.62 (m, 2H), 2.88-3.01 (m, 2H), 7.45-7.59 (m, 3H, Ar-H), 7.93 (d, *J* = 6.9 Hz, 2H, Ar-H).

General procedure of the amidation reaction for obtaining compounds 24 and 25

HBTU (25 mg, 0.067 mmol) and DIPEA (0.04 mL, 0.234 mmol) were added to a solution of PCBA **23** (30 mg, 0.033 mmol) in a mixture of anhydrous DMF (4 mL), anhydrous toluene (4 mL) and CS_2 (2 mL). After 5 minutes of activation, a solution of pentapeptide **5** or **22** (0.040 mmol) in anhydrous DMF (2 mL) was added. The reaction was performed under argon atmosphere at room temperature. Upon 10 minutes of reaction the precipitation of a solid was observed. After 2 hours of stirring, the mixture was filtered and the solid was washed thoroughly with toluene, CS_2, diethyl ether and MeOH.

1-[3-(Amino-L-alanyl-glycyl-L-alanyl-glycyl-L-alanylcarbonyl)propyl]-1-phenyl[6,6] methanofullerene (24)
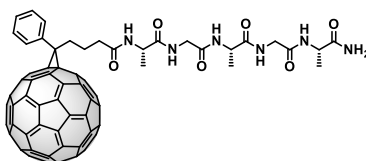
The synthesis was performed according to the procedure above described. The product **24** was obtained as a brownish solid. Yield: 62% (25 mg). ^{1}H-NMR (700 MHz, DMSO-d_6) δ (ppm) 1.23-1.29 (m, 9H, CH_3-Ala), 1.98-2.03 (m, 2H, CH_2-C$\underline{H_2}$-CH_2-(C=O)-), 2.32-2.38 (m, 2H, CH_2-CH_2-C$\underline{H_2}$-(C=O)-), 2.85-2.92 (m, 2H, C$\underline{H_2}$-CH_2-CH_2-(C=O)-), 3.64-3.77 (m, 4H, $2CH_2$-Gly), 4.15-4.23 (m, 3H, 3CH-Ala), 7.03 (s, 1H, NH_2), 7.27 (s, 1H, NH_2), 7.49 (t, *J* = 7.4 Hz, 1H, Ar-H), 7.56-7.60 (m, 2H, Ar-H), 7.82 (d, *J* = 7.4 Hz, 1H, NH-Ala), 8.01 (d, *J* = 6.6 Hz, 1H, NH-Ala), 8.05 (d, *J* = 7.4 Hz, 2H, Ar-H), 8.16-8.23 (m, 3H, NH-Ala+2NH-Gly). ^{13}C-NMR (175 MHz, DMSO-d_6) δ (ppm) 18.3 (CH_3-Ala), 18.4 (CH_3-Ala), 18.6 (CH_3-Ala), 23.2 (CH_2-C$\underline{H_2}$-CH_2-(C=O)-), 33.6 (C$\underline{H_2}$-CH_2-CH_2-(C=O)-), 35.2 (CH_2-CH_2-C$\underline{H_2}$-(C=O)-), 42.4 (CH_2-Gly), 42.6 (CH_2-Gly), 48.4 (CH-Ala), 49.0 (CH-Ala), 52.9 (C-methano), 80.7 (Csp^3-C_{60}), 128.7 (Ar-H), 128.8 (Ar-H), 132.6 (Ar-H), 136.9 (Ar), 137.1, 138.2, 140.5, 140.7, 142.0, 142.1, 142.3, 142.89, 142.92, 143.7, 143.8, 143.9, 144.2,

144.4, 144.6, 144.7, 145.0, 145.10, 145.12, 145.7, 146.4, 148.7, 149.9, 168.7 (C=O), 169.3 (C=O), 172.3 (C=O), 173.1 (C=O), 173.3 (C=O), 174.6 (C=O). HRMS (ESI-FT) *m/z*: [M + Na]$^+$ Calc. for $C_{84}H_{34}N_6O_6Na$: 1245.2432; found: 1245.2455. ATR-FTIR (TCE:DMSO(10%)): 3284, 2923, 2852, 1688, 1655, 1628, 1531, 1449, 1429, 1259, 1227, 1169, 701 cm^{-1}.
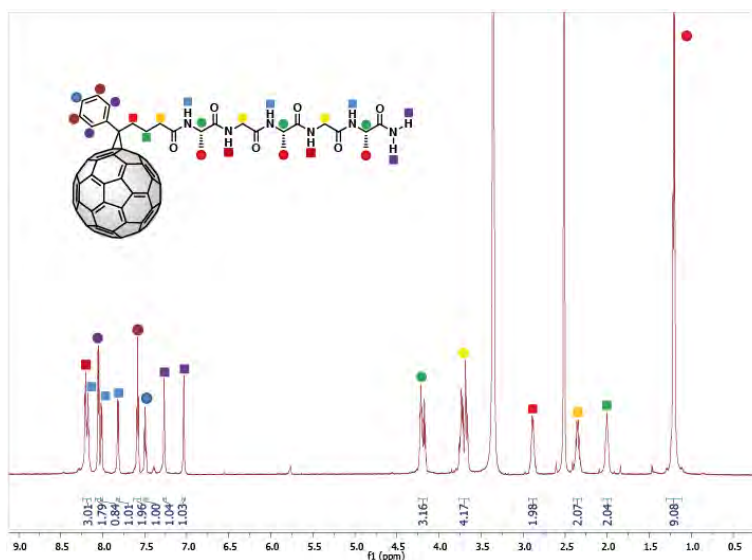
Figure 6.3 ^{1}H-NMR spectrum of compound **24** in DMSO-d_6.
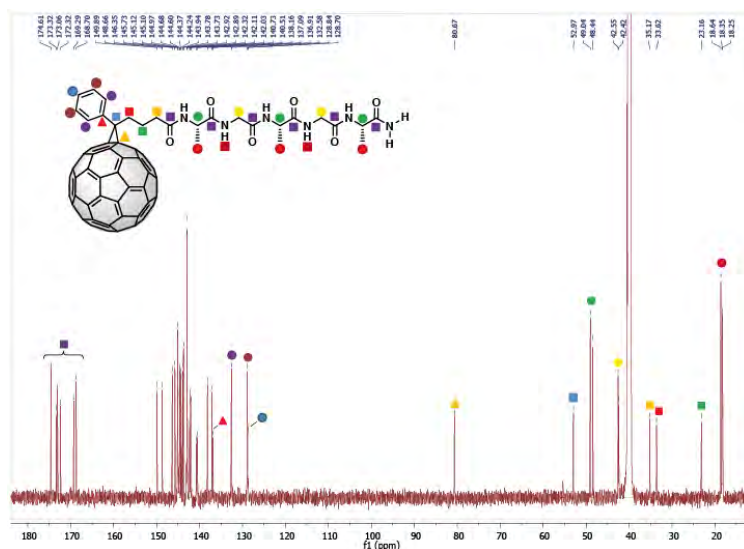
Figure 6.4 ^{13}C-NMR spectrum of compound **24** in DMSO-d_6.

1-[3-(Amino-glycyl-glycyl-glycyl-glycyl-glycylcarbonyl)propyl]-1-phenyl[6,6] methanofullerene (25)
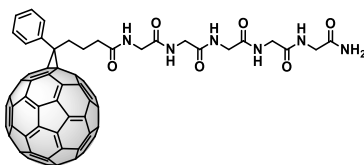
The synthesis was performed according to the procedure above described. The product **25** was obtained as a brownish solid. Yield: 59% (23 mg). ^{1}H-NMR (700 MHz, DMSO-d_6): δ (ppm) 1.98-2.04 (m, 2H, CH$_2$-CH_2-CH$_2$-(C=O)-), 2.35-2.39 (m, 2H, CH$_2$-CH$_2$-CH_2-(C=O)-), 2.87-2.91 (m, 2H, CH_2-CH$_2$-CH$_2$-(C=O)-), 3.63 (d, *J* = 5.3 Hz, 2H, CH$_2$-Gly), 3.70-3.80 (m, 8H, 4CH$_2$-Gly), 7.10 (s, 1H, NH$_2$), 7.22 (s, 1H, NH$_2$), 7.50 (t, *J* = 7.3 Hz, 1H, Ar-H), 7.56-7.61 (m, 2H, Ar-H), 8.06 (d, *J* = 6.9 Hz, 2H, Ar-H), 8.14-8.24 (m, 5H, 5NH-Gly). ^{13}C-NMR (175 MHz, DMSO-d_6) δ (ppm) 23.3 (CH$_2$-CH_2-CH$_2$-(C=O)-), 33.7 (CH_2-CH$_2$-CH$_2$-(C=O)-), 35.3 (CH$_2$-CH$_2$-CH_2-(C=O)-), 42.3 (CH$_2$-Gly), 42.4 (CH$_2$-Gly), 42.5 (CH$_2$-Gly), 42.6 (CH$_2$-Gly), 42.6 (CH$_2$-Gly), 53.0 (C-methano), 80.7 (Csp^3-C$_{60}$), 128.7 (Ar-H), 128.9 (Ar-H), 132.6 (Ar-H), 136.9, 137.1, 138.2, 140.4, 140.6, 142.1, 142.2, 142.89, 142.92, 143.7, 143.8, 143.9, 144.2, 144.4, 144.6, 144.7, 145.1, 145.8, 146.4, 148.7, 149.9, 169.4 (C=O), 169.8 (C=O), 169.8 (C=O), 169.9 (C=O), 171.3 (C=O), 172.6 (C=O). HRMS (ESI-FT) *m/z*: [M + Na]$^+$ Calc. for C$_{81}$H$_{28}$N$_6$O$_6$Na: 1203.1963; found: 1203.1933. ATR-FTIR (TCE:DMSO(10%)): 3294, 2922, 1687, 1651, 1631, 1539, 1432, 1236, 1190, 1025, 1011, 757, 702, 598 cm^{-1}.

***Tert*-butoxycarbonyl[6,6]methanofullerene (27)**[133]
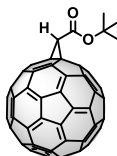
To a solution of C$_{60}$ (100 mg, 0.139 mmol) in dry toluene (100 mL), *tert*-butyldiazoacetate (0.02 mL, 0.139 mmol) was added. The mixture was refluxed for 4 hours and then the solvent was removed until dryness. Under these conditions the

formation of three isomers was achieved (two [5,6]-opened isomers and the [6,6]-closed one) and their isolation was performed by a silica gel column chromatography using CS_2 as eluent recovering in first place the unreacted C_{60} and then the isomers (with identical Rf values). The desired product ([6,6]-closed) was obtained by a thermal treatment refluxing the mixture of isomers in toluene for 24 hours. The mixture was cooled to room temperature and then the solvent was removed under reduced pressure giving rise to the product **27** as a brownish solid. Yield: 38% (44 mg). ^{1}H-NMR (300 MHz, CDCl$_3$/CS$_2$): δ (ppm) 1.73 (s, 9H), 4.72 (s, 1H).

Carboxy[6,6]methanofullerene (28)[147]
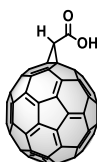
Fullerene *tert*-butyl ester derivative **27** (40 mg, 0.048 mmol) was dissolved in a mixture of CH_2Cl_2:CS_2 (3:1, 4 mL). Then, TFA (1.7 mL) was added and the resulting mixture was stirred for 3 hours at room temperature. A precipitate was formed and then it was filtered and washed with diethyl ether and CS_2 several times. The product **28** was obtained as a brownish solid. Yield: 87% (32 mg). ^{1}H-NMR (300 MHz, DMF-d_7/CS$_2$): δ (ppm) 5.28 (s, 1H).

1-(Amino-L-alanyl-glycyl-L-alanyl-glycyl-L-alanyl)carbonyl[6,6]-methanofullerene (29)
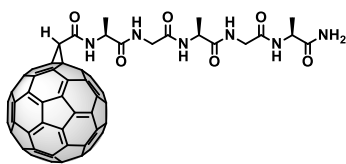
In a round bottom flask, HBTU (30 mg, 0.078 mmol) and DIPEA (0.05 mL, 0.273 mmol) were added to a solution of [6,6]-methanofullerene-C_{61}-carboxylic acid **28** (30 mg, 0.039 mmol) in a mixture of anhydrous DMF (4 mL) and anhydrous toluene (4 mL).

[147] L. Isaacs, F. Diederich, *Helv. Chim. Acta* **1993**, *76*, 2554-2464.

After 5 minutes of activation, a solution of pentapeptide **5** (22 mg, 0.047 mmol) in anhydrous DMF (2 mL) was added. The reaction was performed under argon atmosphere at room temperature. Upon 10 minutes of reaction the precipitation of a solid was observed. After 2 hours of stirring the mixture was filtered and the solid was washed thoroughly with toluene, CS_2, diethyl ether and MeOH. The product **29** was obtained as a brownish solid. Yield: 71% (30 mg). ^{1}H-NMR (700 MHz, DMSO-d_6) δ (ppm) 1.22 (d, *J* = 7.1 Hz, 3H, CH_3-Ala), 1.25 (d, *J* = 7.1 Hz, 3H, CH_3-Ala), 1.42 (d, *J* = 7.1 Hz, 3H, CH_3-Ala), 3.67-3.76 (m, 2H, CH_2-Gly), 3.79-3.87 (m, 2H, CH_2-Gly), 4.16-4.21 (m, 1H, CH-Ala), 4.24-4.30 (m, 1H, CH-Ala), 4.54-4.59 (m, 1H, CH-Ala), 5.38 (s, 1H, CH-methano), 7.04 (s, 1H, NH_2), 7.28 (s, 1H, NH_2), 7.85 (d, *J* = 7.5 Hz, 1H, NH-Ala), 8.12 (d, *J* = 6.8 Hz, 1H, NH-Ala), 8.22 (t, *J* = 5.8 Hz, 1H, NH-Gly), 8.47 (t, *J* = 5.7 Hz, 1H, NH-Gly), 9.39 (d, *J* = 7.0 Hz, 1H, NH-Ala). ^{13}C-NMR (175 MHz, DMSO-d_6) δ (ppm) 18.5 (CH_3-Ala), 18.7 (CH_3-Ala), 18.9 (CH_3-Ala), 40.5 (CH-methano), 42.4 (CH_2-Gly), 42.5 (CH_2-Gly), 48.5 (CH_3-Ala), 49.0 (CH_3-Ala), 49.5 (CH_3-Ala), 73.2 (Csp^3-C_{60}), 73.4 (Csp^3-C_{60}), 136.2, 140.0, 140.1, 140.6, 140.9, 142.0, 142.1, 142.2, 142.58, 142.59, 142.72, 142.74, 142.82, 142.83, 142.88, 142.90, 143.0, 143.2, 143.7, 143.86, 143.88, 143.97, 144.01, 144.17, 144.20, 144.3, 144.5, 144.8, 144.89, 144.94, 145.0, 145.1, 145.6, 145.7, 146.07, 146.14, 147.9, 148.2, 149.97, 150.04, 164.4 (C=O), 168.7 (C=O), 169.2 (C=O), 172.8 (C=O), 173.0 (C=O), 174.6 (C=O). HRMS (ESI-FT) *m/z*: [M + Na]$^+$ Calc. for $C_{75}H_{24}N_6O_6Na$: 1127.1650; found: 1127.1633. ATR-FTIR (TCE:DMSO(10%)): 3283, 2922, 2853, 1690, 1647, 1629, 1528, 1454, 1425, 1368, 1257, 1217, 1185, 766, 749 cm^{-1}.

Section 4.4

3,5-Di-*tert*-butyl(bromomethyl)benzene (31)[143]
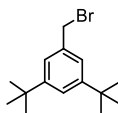
A mixture of 3,5-di-*tert*-butyltoluene **30** (120 mg, 0.59 mmol), NBS (182 mg, 0.89 mmol) and benzoyl peroxide (15 mg, 0.06 mmol) in CCl$_4$ (80 mL) was heated to reflux for 3h. The solution was cooled, filtered and concentrated under reduced pressure. The crude residue **31** was used without further purification in the next step. Yield: 80% (134 mg). ^{1}H-NMR (300 MHz, CDCl$_3$): δ (ppm) 1.35 (s, 18H), 4.60 (s, 2H), 7.14-7.23 (m, 3H).

3,5-Di-*tert*-butylbenzaldehyde (32)[143]
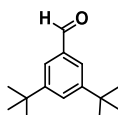
A mixture of compound **31** (125 mg, 0.44 mmol) and hexamethylenetetramine (HMTA) (256 mg, 1.83 mmol) in MeOH/H$_2$O (50 mL, 1:1) was refluxed for 4h. Concentrated aqueous HCl (15 mL) was added dropwise and the mixture refluxed for 30 minutes. The solution was cooled and extracted with CH$_2$Cl$_2$, then the organic phase was dried over Na$_2$SO$_4$, filtered and the solvent evaporated under reduced pressure. The residue was recrystallized from EtOH/H$_2$O to give to the product **32** as a white crystalline solid. Yield: 82% (79 mg). ^{1}H-NMR (300 MHz, CDCl$_3$): δ (ppm) 1.36 (s, 18H), 7.70-7.75 (m, 3H), 10.01 (s, 1H).

5-(4-Cyanophenyl)-10,15,20-tris(3,5-di-*tert*-butylphenyl)porphyrin (35)[142]
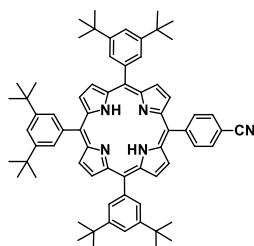
3,5-Di-*tert*-butylbenzaldehyde **32** (1 g, 4.60 mmol), 4-cyanobenzaldehyde **33** (200 mg, 1.54 mmol) and pyrrole **34** (0.43 mL, 6.14 mmol) were dissolved in dry CHCl₃ (500 mL). The mixture was degassed with argon for 30 minutes followed by the addition of Et₂O·BF₃ (0.27 mL, 2.1 mmol) to the solution. This mixture was stirred for 10 hours under argon atmosphere. Then, *p*-chloranil (1.52 g, 6.2 mmol) was added to the reaction mixture and heated at 60°C for 2 hours. The solvent was removed under reduced pressure and the desired product was purified by silica gel column chromatography with hexane/CH₂Cl₂ (2:1) as an eluent. The product **35** was obtained as a red solid. Yield: 16% (240 mg). ¹H-NMR (300 MHz, CDCl₃): δ (ppm) -2.71 (br s, 2H, pyrrole-NH), 1.52 (s, 54H, *t*Bu), 7.78 (t, *J* = 2.0 Hz, 1H, *t*Bu-ArH), 7.80 (t, *J* = 2.0 Hz, 2H, *t*Bu-ArH), 8.06 (d, *J* = 8.1 Hz, 2H, CN-ArH), 8.07 (d, *J* = 2.0 Hz, 2H, *t*Bu-ArH), 8.08 (d, *J* = 2.0 Hz, 4H, *t*Bu-ArH), 8.36 (d, *J* = 8.1 Hz, 2H, CN-ArH), 8.71 (d, *J* = 5.2 Hz, 2H, β-pyrrolic), 8.93 (s, 4H, β-pyrrolic), 8.92 (d, *J* = 5.2 Hz, 2H, β-pyrrolic).

Niquel(II) 5-(4-cyanophenyl)-10,15,20-tris(3,5-di-*tert*-butylphenyl)porphyrin (36)[142]
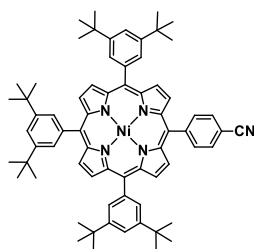
A solution of **35** (240 mg, 0.25 mmol) in CHCl₃ (25 mL) was mixed with a solution of Ni(AcO)₂·4H₂O (395 mg, 1.58 mmol) in MeOH (15 mL) and further refluxed for 12 hours. Afterward the solvent was removed under reduced pressure, the residue was

dissolved in a small volume of CH$_2$Cl$_2$, and then washed with aqueous NaHCO$_3$ (10%). The organic phase was dried over Na$_2$SO$_4$, filtered and evaporated under reduced pressure. The desired product was purified by silica gel column chromatography using CH$_2$Cl$_2$/hexane (1:2) as eluent. The product was obtained as a red solid. Yield: 92% (237 mg). ^{1}H-NMR (300 MHz, CDCl$_3$): δ (ppm) 1.45 (s, 54H, *t*Bu), 7.70-7.72 (m, 3H, *t*Bu-ArH), 7.84-7.87 (m, 6H, *t*Bu-ArH), 7.98 (d, *J* = 8.0 Hz, 2H, CN-ArH), 8.15 (d, *J* = 8.0 Hz, 2H, CN-ArH), 8.61 (d, *J* = 5.1 Hz, 2H, β-pyrrolic), 8.79-8.81 ppm (m, 6H, β-pyrrolic).

Niquel(II) 5-(4-carbamimidoylphenyl)-10,15,20-tris(3,5-di-*tert*-butylphenyl)-porphyrin hydrochloride (37)[142]
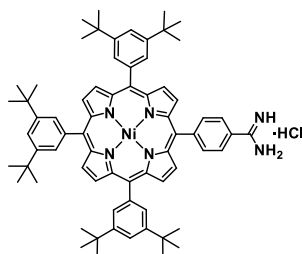
A solution of AlMe$_3$ in hexanes (1.20 mL, 2M) was added to a suspension of NH$_4$Cl (124 mg, 2.3 mmol) in dry toluene (10 mL). The resulting mixture was stirred for 2 hours at room temperature under argon atmosphere. Then, a solution of **36** (237 mg, 0.23 mmol) in dry toluene (10 mL) was added, and the resulting mixture was stirred at 80°C for 48 hours in the dark. The mixture was poured into a suspension of silica gel in CHCl$_3$ (10 g, 50 mL). The mixture was stirred and filtered. Then, the solvent was removed under reduced pressure and the desired compound was purified by silica gel chromatography using a mixture of CHCl$_3$:MeOH (2:1) as eluent. The product **37** was obtained as a red solid. Yield: 70% (175 mg). ^{1}H-NMR (300 MHz, CDCl$_3$): δ (ppm) 1.46 (s, 54H, *t*Bu), 7.71-7.73 (m, 3H, *t*Bu-ArH), 7.85-7.86 (m, 6H, *t*Bu-ArH), 8.17 (d, *J* = 8.1 Hz, 2H, amidinium-ArH), 8.31 (d, *J* = 8.1 Hz, 2H, amidinium-ArH), 8.61 (d, *J* = 5.0 Hz, 2H, β-pyrrolic), 8.80-8.84 (m, 6H, β-pyrrolic).

5-(4-Carbamimidoylphenyl)-10,15,20-tris(3,5-di-*tert*-butylphenyl)porphyrin (38)[142]
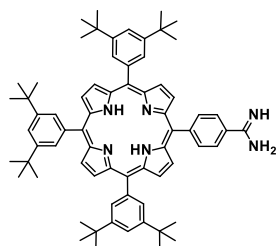
A mixture of HCl conc. (4 mL) and TFA (4 mL) were added to a solution of **37** (153 mg, 0.14 mmol) in CH$_2$Cl$_2$ (70 mL). The mixture was stirred at room temperature for 24 hours in the dark. Then, the mixture was washed with aqueous NaOH (10%) and the organic phase was dried over Na$_2$SO$_4$. Upon filtration and evaporation of the solvent under reduced pressure, compound **38** was obtained as a purple solid. Yield: 95% (132 mg). ^{1}H-NMR (300 MHz, CDCl$_3$): δ (ppm) -2.70 (s, 2H, pyrrole-NH), 1.50-1.53 (m, 54H, *t*Bu), 7.78-7.80 (m, 3H, *t*Bu-ArH), 8.06-8.10 (m, 6H, *t*Bu-ArH), 8.20 (d, *J* = 8.2 Hz, 2H, amidine-ArH), 8.41 (d, *J* = 8.2 Hz, 2H, amidine-ArH), 8.87-8.94 (m, 8H, β-pyrrolic).

Boc-L-alanyl-glycine-OMe (Boc-L-Ala-Gly-OMe) (41)[70]
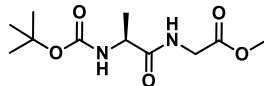
The carboxylic acid *N*-(*tert*-butoxycarbonyl)-L-alanine **39** (Boc-L-Ala-OH, 500 mg, 2.64 mmol) dissolved in anhydrous DMF (15 mL) was activated adding HBTU (1500 mg, 3.96 mmol) and DIPEA (2.3 mL, 13.2 mmol) under argon atmosphere. After 5 minutes of activation, a solution of glycine methyl ester hydrochloride **40** (398 mg, 3.17 mmol) in anhydrous DMF (5 mL) was added. The mixture was stirred for two hours at room temperature, period of time in which the formation of the product was followed by rinsing the TLC plate in a ninhydrin solution (0.2%, in ethanol). Afterwards it was extracted with CH$_2$Cl$_2$ and H$_2$O. The organic phase was dried over Na$_2$SO$_4$, filtered and concentrated under reduced pressure. The desired product was purified by silica gel column chromatography using a mixture CH$_2$Cl$_2$:MeOH (20:1) as eluent. The product **41** was obtained as a yellow solid. Yield: 90% (618 mg). ^{1}H-NMR (300 MHz, CDCl$_3$): δ

(ppm) 1.36 (d, *J* = 7.1 Hz, 3H, CH₃-Ala), 1.42 (s, 9H, 3CH₃-tBu), 3.72 (s, 3H, OCH₃), 4.02 (d, *J* = 5.4 Hz, 2H, CH₂-Gly), 4.15-4.30 (m, 1H, CH-Ala), 5.25 (d, *J* = 7.5 Hz, 1H, NH-Ala), 6.96 (br s, 1H, NH-Gly).

L-alanyl-glycine-OMe (L-Ala-Gly-OMe) (42)[70]
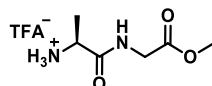
A solution of the *N*-protected dipeptide **41** (300 mg, 1.15 mmol) in a mixture of CH₂Cl₂:TFA (9:1, 2mL) was stirred for 30 minutes. The formation of the product was followed by rinsing the TLC plate in a ninhydrin solution (0.2%, in ethanol). Afterwards, the solvent was removed under reduced pressure giving rise to compound **42** as an oil that was used in the next reaction without further purification. Yield: 95% (299 mg). ¹H-NMR (300 MHz, MeOD-*d₄*): δ (ppm) 1.53 (d, *J* = 7.0 Hz, 3H, CH₃-Ala), 3.73 (s, 3H, OCH₃), 3.95-4.04 (m, 3H, CH-Ala + CH₂-Gly).

Methyl 3,4,5-tris(dodecyloxy)benzoate (44)[148]
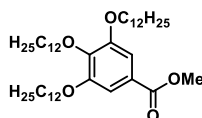
A mixture of methyl 3,4,5-trihydroxybenzoate **43** (3 g, 16.29 mmol), 1-bromododecane (13 g, 52.13 mmol) and potassium carbonate (11g, 81.45 mmol) in acetone (200 mL) was refluxed for 48 hours. Then it was cooled to room temperature and the solvent was removed under reduced pressure. An extraction with CH₂Cl₂ and H₂O was performed and the organic phase was dried over Na₂SO₄. The latter was filtered and the solvent was evaporated under reduced. The desired product **44** was purified by silica gel column chromatography using a mixture of CH₂Cl₂:hexane (1:1) as eluent and was obtained as a white solid. Yield: 84% (9.43 g). ¹H-NMR (300 MHz, CDCl₃): δ (ppm) 0.88 (t, *J* = 6.6 Hz, 9H, 3Alk-CH₃), 1.23-1.31 (m, 48H), 1.42-1.54 (m, 6H,

---

[148] V. Percec, M. Peterca, T. Tadjiev, X. Zeng, G. Ungar, P. Leowanawat, E. Aqad, M. R. Imam, B. M. Rosen, U. Akbey, R. Graf, S. Sekharan, D. Sebastiani, H. W. Spiess, P. A. Heiney, S. D. Hudson, *J. Am. Chem. Soc.* **2011**, *133*, 12197–12219.

3-OCH$_2$-CH$_2$-CH_2-), 1.77-1.89 (m, 6H, 3-OCH$_2$-CH_2-), 3.40 (s, 3H, OCH$_3$), 4.05 (t, *J* = 6.9 Hz, 6H, 3-OCH$_2$-), 7.07 (s, 2H, Ar-H).

(3,4,5-Tris(dodecyloxy)phenyl)methanol (45)[148]
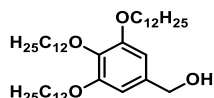
To a solution of **44** (1 g, 1.45 mmol) in dry THF (30 mL) at -20°C under argon atmosphere, LiAlH$_4$ (61 mg, 1.60 mmol) was added. This mixture was stirred in cold for 10 minutes and then it was left to room temperature for 1 hour. Afterwards MeOH (1 mL) was added in cold (0°C) followed by filtration. The filtrate was evaporated under reduced pressure. Then, an extraction with CH$_2$Cl$_2$ and H$_2$O was performed; the organic phase was dried over Na$_2$SO$_4$, filtered and the solvent was removed under reduced pressure giving rise to compound **45** as a white solid. Yield: 98% (939 mg). This product was used without further purification for the next reaction. ^{1}H-NMR (300 MHz, CDCl$_3$): δ (ppm) 0.88 (t, *J* = 6.7 Hz, 9H, 3CH$_3$), 1.21-1.31 (m, 48H), 1.43-1.53 (m, 6H, 3-OCH$_2$-CH$_2$-CH_2-), 1.77-1.86 (m, 6H, 3-OCH$_2$-CH_2-), 4.06 (t, *J* = 6.8 Hz, 6H, 3-OCH$_2$), 4.63 (s, 2H, CH_2-OH), 6.61 (s, 2H, Ar-H).

3,4,5-Tris(dodecyloxy)benzaldehyde (46)[148]
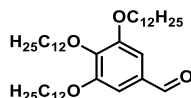
To a solution of alcohol **45** (960 mg, 1.45 mmol) in CH$_2$Cl$_2$ (60 mL), pyridinium chlorochromate (626 mg, 2.9 mmol) was added and the resulting mixture was stirred for 4 hours. Afterwards silica (1 g) was added and then solvent was removed under reduced pressure. The product was obtained by a silica gel column chromatography using a mixture of hexane:AcOEt (9:1) as eluent. The desired product was obtained as a white solid. Yield: 81% (774 mg). ^{1}H-NMR (300 MHz, CDCl$_3$): δ (ppm) 0.89 (t, *J* = 6.7 Hz, 9H, 3CH$_3$), 1.20-1.32 (m, 48H), 1.42-1.56 (m, 6H, 3-OCH$_2$-CH$_2$-CH_2-), 1.75-1.92 (m, 6H, 3-OCH$_2$-CH_2-), 4.01-4.09 (m, 6H, 3-OCH$_2$-), 7.09 (s, 2H, Ar-H), 9.83 (s, 1H, -CHO).

(*E*)-*Tert*-butyl 2-[(3,4,5-tris(dodecyloxy)benzylidene)amino]acetate (47)
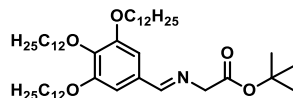
A mixture of glycine *tert*-butyl ester hydrochloride (186 mg, 1.11 mmol) and trimethylamine (0.15 mL, 1.11 mmol) in CH_2Cl_2 (10 mL) was stirred for 1 hour under argon atmosphere. Then the aldehyde **46** (730 mg, 1.11 mmol) dissolved in CH_2Cl_2 (4 mL) was added followed by the addition of anhydrous Na_2SO_4 (1.5 g, 10.6 mmol). The resulting mixture was stirred for 10 hours. Afterwards the solution was filtered and washed with water. The organic phase was dried over Na_2SO_4, filtered and the solvent was removed under reduced pressure giving rise to compound **47** as a white solid that was used in the next step without further purification. Yield: 93 % (797 mg). ^{1}H-NMR (300 MHz, CDCl$_3$): δ (ppm) 0.88 (t, *J* = 6.6 Hz, 9H, 3Alk-CH$_3$), 1.20-1.37 (m, 48H), 1.41-1.53 (m, 15H, 3-OCH$_2$-CH$_2$-*CH$_2$*- + 3CH$_3$ *t*-Bu), 1.75-1.85 (m, 6H, 3-OCH$_2$-*CH$_2$*-), 3.96-4.06 (m, 6H, 3-OCH$_2$-), 4.29 (s, 2H, N-CH$_2$-), 6.98 (s, 2H, Ar-H), 8.13 (s, 1H, N=CH-Ar). ^{13}C-NMR (75 MHz, CDCl$_3$): δ (ppm) 14.2 (Alk-CH$_3$), 22.7, 26.1, 28.1 (CH$_3$ *t*-Bu), 29.4, 29.6, 29.7, 29.8, 30.4, 32.0, 62.5 (N-CH$_2$-COOt-Bu), 69.2 (OCH$_2$-), 73.5 (OCH$_2$-), 81.4, 106.8 (Ar-H), 130.8, 140.9, 153.3, 165.2 (N=CH-Ar), 169.5 (C=O). MS (MALDI-TOF) *m/z*: [M+H]$^+$ Calc. for C$_{49}$H$_{90}$NO$_5$: 772.68; found: 772.57.

Tert-butyl 2-[(3,4,5-tris(dodecyloxy)benzyl)amino]acetate (48)
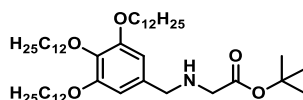
To a solution of **47** (450 mg, 0.58 mmol) in dry CH_2Cl_2 (15 mL) at 0°C, acetic acid (40 μL, 0.67 mmol) and sodium cyanoborohydride (46 mg, 0.67 mmol) were added and the resulting mixture was stirred for 1 hour at 0°C. Afterwards Na_2CO_3 (100 mg, 0.95 mmol) was added and the crude was washed with H_2O. The organic phase was dried over Na_2SO_4, filtered and evaporated until under reduced pressure. The desired product **48** was purified by silica gel column chromatography using CH_2Cl_2:MeOH (50:1) as eluent giving rise to a transparent oil. Yield: 65% (292 mg). ^{1}H-NMR (300

189

MHz, CDCl$_3$): δ (ppm) 0.88 (t, *J* = 6.6 Hz, 9H, 3Alk-CH$_3$), 1.22-1.35 (m, 48H), 1.41-1.52 (m, 15H, 3-OCH$_2$-CH$_2$-C*H$_2$*- + 3CH$_3$ *t*-Bu), 1.70-1.83 (m, 6H, 3-OCH$_2$-C*H$_2$*-), 3.31 (s, 2H, N-CH$_2$-COOt-Bu), 3.70 (s, 2H, Ar-CH$_2$-N), 3.89-4.00 (m, 6H, 3-OCH$_2$-), 6.52 (s, 2H, Ar-H). ^{13}C-NMR (75 MHz, CDCl$_3$): δ (ppm) 14.1 (Alk-CH$_3$), 22.7, 26.1, 28.2 (CH$_3$ *t*-Bu), 29.3, 29.41, 29.46, 29.49, 29.68, 29.72, 29.76, 29.78, 30.4, 32.0, 50.9, 53.6, 69.1 (OCH$_2$-), 73.4 (OCH$_2$-), 81.2, 106.7 (Ar-H), 134.7, 137.3, 153.2, 171.7 (C=O). MS (MALDI-TOF) *m/z*: [M]$^+$ Calc. for C$_{49}$H$_{91}$NO$_5$: 773.69; found: 773.56.

N-[3,4,5-tris(dodecyloxy)benzyl]-2-*tert*-butoxycarbonylpyrrolidino-[3,4:1,2][60] fullerene (49)
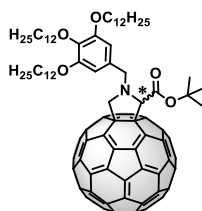
A mixture of compound **48** (100 mg, 0.13 mmol), paraformaldehyde (4 mg, 0.13 mmol) and C$_{60}$ (108 mg, 0.15 mmol) in toluene:*o*-DCB (1:1, 100 mL) was heated at 120°C for 10 hours. The reaction was cooled down to room temperature and the solvent was removed under reduced pressure. The purification of the desired product was performed by silica gel column chromatography using first CS$_2$ as eluent to recover the unreacted C$_{60}$ and then toluene to take out the product. Compound **49** was obtained as a brownish solid. Yield: 45% (88 mg). ^{1}H-NMR (300 MHz, CDCl$_3$): δ (ppm) 0.88 (t, *J* = 6.6 Hz, 9H, 3Alk-CH$_3$), 1.21-1.36 (m, 48H), 1.44-1.56 (m, 15H, 3-OCH$_2$-CH$_2$-C*H$_2$*- + 3CH$_3$ *t*-Bu), 1.76-1.89 (m, 6H, 3-OCH$_2$-C*H$_2$*-), 3.99-4.16 (m, 7H, 3-OCH$_2$- + 1H-CH$_2$ benzylic), 4.32 (d, *J* = 9.4 Hz, 1H, CH$_2$ pyrrolidine), 4.57 (d, *J* = 13.4 Hz, 1H, CH$_2$ benzylic), 4.97 (d, *J* = 9.4 Hz, 1H, CH$_2$ pyrrolidine), 5.01 (s, 1H, CH pyrrolidine), 6.92 (s, 2H, Ar-H). ^{13}C-NMR (75 MHz, CDCl$_3$): δ (ppm) 14.2 (Alk-CH$_3$), 22.7, 26.2, 28.4 (CH$_3$ *t*-Bu), 29.4, 29.5, 29.7, 29.8, 30.5, 32.0, 55.6 (CH$_2$ benzylic), 64.5 (CH$_2$ pyrrolidine), 69.3 (OCH$_2$), 69.6, 73.0, 73.5 (OCH$_2$), 76.3 (CH pyrrolidine), 83.0, 107.2 (Ar-H), 132.4, 135.5, 136.0, 136.5, 137.65, 137.68, 139.4, 139.9, 140.2, 140.3, 141.85, 141.86,

141.94, 142.00, 142.05, 142.12, 142.17, 142.20, 142.28, 142.31, 142.67, 142.70, 142.73, 143.1, 143.2, 144.5, 144.56, 144.60, 144.7, 145.3, 145.36, 145.44, 145.7, 145.9, 146.10, 146.12, 146.3, 146.42, 146.44, 146.6, 147.3, 147.5, 151.5, 153.4, 154.2, 155.0 169.1 (C=O). MS (MALDI-TOF) m/z: $[M]^+$ Calc. for $C_{110}H_{91}NO_5$: 1506.69; found: 1506.68.

N-[3,4,5-tris(dodecyloxy)benzyl]-2-carboxypyrrolidino-[3,4:1,2][60]fullerene (50)
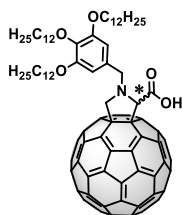
A solution of compound **49** (40 mg, 0.027 mmol) dissolved in a mixture CH_2Cl_2:TFA (1:1, 2 mL) was stirred for 2 hours. Afterwards, the solvent was removed under reduced pressure and the desired product was purified by silica gel column chromatography using a mixture of CH_2Cl_2:MeOH (50:1) as eluent. The product **50** was obtained as a brownish solid. Yield: 95% (37 mg). ^{1}H-NMR (300 MHz, CDCl$_3$): δ (ppm) 0.88 (t, J = 6.3 Hz, 9H, 3Alk-CH$_3$), 1.22-1.39 (m, 48H), 1.44-1.57 (m, 6H, 3-OCH$_2$-CH$_2$-CH_2-), 1.74-1.92 (m, 6H, 3-OCH$_2$-CH_2-), 3.96-4.15 (m, 7H, 3-OCH$_2$- + 1H-CH$_2$ benzylic), 4.36 (d, J = 9.8 Hz, 1H, CH$_2$ pyrrolidine), 4.59 (d, J = 13.3 Hz, 1H, CH$_2$ benzylic), 4.96 (d, J = 9.8 Hz, 1H, CH$_2$ pyrrolidine), 5.17 (s, 1H, CH pyrrolidine), 6.88 (s, 2H, Ar-H). ^{13}C-NMR (75 MHz, CDCl$_3$): δ (ppm) 14.3 (Alk-CH$_3$), 22.8, 26.4, 29.5, 29.7, 29.8, 29.9, 30.5, 32.0, 54.9 (CH$_2$ benzylic), 66.1 (CH$_2$ pyrrolidine), 69.2 (OCH$_2$), 69.4, 73.3, 73.5 (OCH$_2$), 75.5 (CH pyrrolidine), 107.5 (Ar-H), 131.7, 135.4, 136.0, 137.5, 139.7, 139.9, 140.3, 141.7, 141.8, 141.9, 142.0, 142.08, 142.12, 142.6, 142.7, 143.0, 143.1, 144.4, 144.5, 144.6, 145.2, 145.3, 145.4, 145.5, 145.6, 145.7, 146.1, 146.3, 146.4, 147.3, 147.4, 151.0, 153.4, 153.8, 154.8, 169.0 (C=O). MS (MALDI-TOF) m/z: $[M]^+$ Calc. for $C_{106}H_{83}NO_5$: 1450.63; found: 1450.61.

Fullerene-dipeptide-methyl ester diastereoisomers (51 and 52)
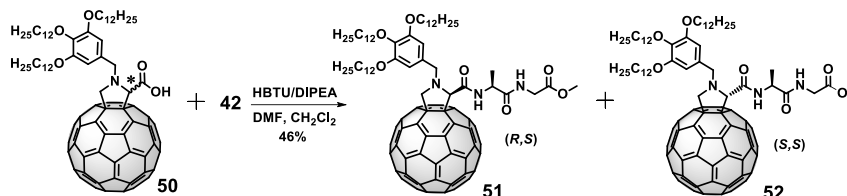
Carboxylic acid **50** (100 mg, 0.069 mmol) in a mixture of anhydrous DMF:CH$_2$Cl$_2$ (1:1, 10 mL) was activated by adding HBTU (39 mg, 0.102 mmol) and DIPEA (46 μL, 0.345 mmol) under argon atmosphere. After 5 minutes of activation, a solution of dipeptide **42** (23 mg, 0.083 mmol) in anhydrous DMF (2 mL) was added. The mixture was stirred at room temperature for 2 hours. Then, CH$_2$Cl$_2$ (30 mL) was added and the resulting mixture was washed with an aqueous solution of Na$_2$CO$_3$ (3 x 30 mL). The organic phase was dried over Na$_2$SO$_4$, filtered and concentrated under reduced pressure. The purification of the respective diastereoisomers **51** and **52** was performed by preparative thin layer chromatography using a mixture of CH$_2$Cl$_2$:MeOH (100:1) as eluent. The diastereoisomers were obtained in a ratio of (1:1) as brownish solids.

N-[3,4,5-tris(dodecyloxy)benzyl]-2-(R)-(methoxyglycyl-L-alanyl)carbonylpyrrolidino-[3,4:1,2][60]fullerene (51) (R,S)
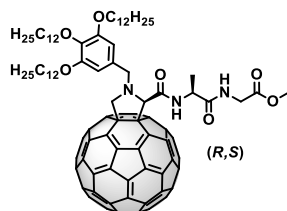
Diastereoisomer **51** was synthesized and purified as described previously. Yield: 46% (25 mg). ^{1}H-NMR (700 MHz, CDCl$_3$): δ (ppm) 0.88-0.91 (m, 9H, 3Alk-CH$_3$), 1.23-1.36 (m, 42H), 1.37-1.42 (m, 6H, 3-OCH$_2$-CH$_2$-CH$_2$-C$\underline{H_2}$-), 1.51-1.56 (m, 6H, 3-OCH$_2$-CH$_2$-C$\underline{H_2}$-), 1.57 (d, J = 7.0 Hz, 3H, CH$_3$-Ala), 1.79-1.84 (m, 2H, 1-OCH$_2$-C$\underline{H_2}$-), 1.86-1.91 (m, 4H, 2-OCH$_2$-C$\underline{H_2}$-), 3.70 (s, 3H, OCH$_3$), 3.75 (dd, J = 18.2, 5.0 Hz, 1H, CH$_2$-Gly), 3.80 (d, J = 12.9 Hz, 1H, CH$_2$ benzylic), 3.98 (dd, J = 18.2, 5.0 Hz, 1H, CH$_2$-Gly), 4.05 (t, J = 6.6 Hz, 2H, 1-OCH$_2$-), 4.13 (t, J = 6.6 Hz, 4H, 2-OCH$_2$-), 4.22 (d, J = 9.8 Hz, 1H, CH$_2$ pyrrolidine), 4.59

192

(d, *J* = 12.9 Hz, 1H, CH$_2$ benzylic), 4.69-4.74 (m, 1H, CH-Ala), 4.88 (d, *J* = 9.8 Hz, 1H, CH$_2$ pyrrolidine), 4.89 (s, 1H, CH-pyrrolidine), 6.49 (t, *J* = 5.0 Hz, 1H, NH-Gly), 6.85 (s, 2H, Ar-H), 7.89 (d, *J* = 8.1 Hz, 1H, NH-Ala). ^{13}C-NMR (175 MHz, CDCl$_3$): δ (ppm) 14.2 (Alk-CH$_3$), 17.7 (CH$_3$-Ala), 22.7, 26.2, 29.41, 29.42, 29.5, 29.68, 29.71, 29.73, 29.77, 29.78, 29.80, 29.81, 30.4, 31.0, 32.0, 41.4 (CH$_2$-Gly), 48.4 (CH-Ala), 52.5 (OCH$_3$), 53.5, 58.7 (CH$_2$ benzylic), 66.6 (CH$_2$ pyrrolidine), 68.9, 69.4 (OCH$_2$), 73.1, 73.6 (OCH$_2$), 79.4 (CH pyrrolidine), 107.2, 131.3, 135.4, 135.7, 136.2, 137.2, 138.1, 139.1, 140.23, 140.24, 140.4, 141.7, 141.8, 141.9, 141.95, 142.04, 142.07, 142.10, 142.2, 142.3, 142.67, 142.70, 142.8, 143.11, 143.14, 144.4, 144.5, 144.6, 144.7, 145.22, 145.24, 145.25, 145.38, 145.42, 145.5, 145.6, 145.78, 145.82, 145.9, 146.09, 146.12, 146.2, 146.3, 146.4, 146.45, 146.54, 147.3, 147.4, 150.8, 152.8, 153.3, 153.6, 155.0, 169.0 (C=O), 169.8 (C=O), 171.0 (C=O). HRMS (ESI-FT) *m/z*: [M-H]$^-$ Calc. for C$_{112}$H$_{92}$N$_3$O$_7$: 1590.6941; found: 1590.6884.

N-[3,4,5-tris(dodecyloxy)benzyl]-2-(*S*)-(methoxyglycyl-L-alanyl)carbonylpyrrolidino-[3,4:1,2][60]fullerene (52) (*S,S*)
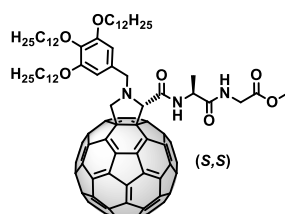
Diastereoisomer **52** was synthesized and purified as described previously. Yield: 46% (25 mg). ^{1}H-NMR (700 MHz, CDCl$_3$): δ (ppm) 0.88-0.92 (m, 9H, 3Alk-CH$_3$), 1.24-1.42 (m, 45H, 3Alk-CH$_3$ + CH$_3$-Ala), 1.37-1.43 (m, 6H, 3-OCH$_2$-CH$_2$-CH$_2$-C*H$_2$*-) 1.51-1.56 (m, 6H, 3-OCH$_2$-CH$_2$-C*H$_2$*-), 1.79-1.84 (m, 2H, 1-OCH$_2$-C*H$_2$*-), 1.86-1.91 (m, 4H, 2-OCH$_2$-C*H$_2$*-), 3.70 (d, *J* = 12.3 Hz, 1H, CH$_2$ benzylic), 3.79 (s, 3H, OCH$_3$), 4.03-4.06 (m, 2H, CH$_2$-Gly), 4.11-4.18 (m, 6H, 3-OCH$_2$-), 4.20 (d, *J* = 9.7 Hz, 1H, CH$_2$ pyrrolidine), 4.58 (d, *J* = 12.3 Hz, 1H, CH$_2$ benzylic), 4.72-4.75 (m, 1H, CH-Ala), 4.83 (s, 1H, CH pyrrolidine), 4.84 (d, *J* = 9.7 Hz, 1H, CH$_2$ pyrrolidine), 6.41-6.46 (m, 1H, NH-Gly), 6.95 (s, 2H, Ar-H), 8.30 (d, *J* = 7.8 Hz, 1H, NH-Ala). ^{13}C-NMR (175 MHz, CDCl$_3$): δ (ppm) 14.2 (Alk-CH$_3$), 18.8 (CH$_3$-Ala),

22.7, 26.2, 26.3, 29.4, 29.6, 29.69, 29.72, 29.75, 29.82, 30.4, 32.0, 41.3 (CH_2-Gly), 48.4 (CH-Ala), 52.6 (OCH_3), 59.2 (CH_2 benzylic), 66.6 (CH_2 pyrrolidine), 68.8, 69.3 (OCH_2), 73.2, 73.5 (OCH_2), 79.7 (CH pyrrolidine), 107.9, 131.5, 135.5, 135.7, 136.1, 136.8, 137.9, 139.5, 140.2, 140.25, 140.29, 141.5, 141.65, 141.72, 141.8, 141.99, 142.03, 142.06, 142.07, 142.12, 142.14, 142.3, 142.65, 142.68, 142.74, 143.1, 143.2, 144.4, 144.6, 144.7, 145.2, 145.4, 145.46, 145.50, 145.53, 145.6, 145.7, 145.8, 145.9, 146.06, 146.12, 146.2, 146.32, 146.35, 146.43, 146.7, 147.35, 147.43, 151.5, 152.9, 153.3, 153.4, 168.4 (C=O), 169.9 (C=O), 171.8 (C=O). HRMS (ESI-FT) *m/z*: [M-H]$^-$ Calc. for $C_{112}H_{92}N_3O_7$: 1590.6941; found: 1590.6870.

### *N*-[3,4,5-tris(dodecyloxy)benzyl]-2-(*R*)-(hydroxyglycyl-L-alanyl)carbonylpyrrolidino-[3,4:1,2][60]fullerene (53) (*R,S*)

A solution of **51** (25 mg, 0.016 mmol) dissolved in a mixture of dioxane:TFA:HCl conc (1:2:2, 5 mL) was heated for 3 hours at 60°C. Then CH_2Cl_2 (15 mL) was added and an extraction with an aqueous solution of Na_2CO_3 was performed. The organic phase was dried over Na_2SO_4 and then it was filtrated and concentrated under reduced pressure until dryness. The purification of the desired product **53** was performed by silica gel column chromatography using a mixture of CH_2Cl_2:MeOH (30:1) as eluent and was obtained as a brownish solid. Yield: 91% (23 mg). ^{1}H-NMR (700 MHz, $CDCl_3$): δ (ppm) 0.88-0.92 (m, 9H, 3Alk-CH_3), 1.23-1.35 (m, 42H), 1.35-1.41 (m, 6H, 3-OCH_2-CH_2-CH_2-*CH2*-), 1.47 (d, *J* = 6.8 Hz, 3H, CH_3-Ala), 1.51-1.55 (m, 6H, 3-OCH_2-CH_2-*CH2*-), 1.78-1.83 (m, 2H, 1-OCH_2-*CH2*-), 1.84-1.89 (m, 4H, 2-OCH_2-*CH2*-), 3.70-3.83 (m, 2H, 1H-CH_2-Gly + 1H-CH_2 benzylic), 3.98 (d, *J* = 17.0 Hz, 1H, CH_2-Gly), 4.04 (t, *J* = 6.6 Hz, 2H, 1-OCH_2-), 4.11 (t, *J* = 6.4 Hz, 4H, 2-OCH_2-), 4.22 (d, *J* = 9.2 Hz, 1H, CH_2 pyrrolidine), 4.50 (br s, 1H, CH_2 benzylic), 4.76-4.83 (m, 1H, CH-Ala), 4.88 (s, 2H, CH pyrrolidine + 1H-CH_2

pyrrolidine), 6.84 (s, 2H, Ar-H), 6.97 (s, 1H, NH-Gly), 8.09 (d, J = 6.7 Hz, 1H, NH-Ala). ^{13}C-NMR (175 MHz, CDCl$_3$): δ (ppm) 14.2 (Alk-CH$_3$), 18.0 (CH$_3$-Ala), 22.7, 26.2 (-OCH$_2$-CH$_2$-C*H$_2$*-), 26.2 (-OCH$_2$-CH$_2$-C*H$_2$*-), 29.4 (-OCH$_2$-C*H$_2$*-), 29.5, 29.6, 29.69, 29.74, 29.76, 29.79, 29.81, 30.4 (-OCH$_2$-C*H$_2$*-), 32.0, 41.5 (CH$_2$-Gly), 48.4 (CH-Ala), 58.2 (CH$_2$ benzylic), 66.2 (CH$_2$ pyrrolidine), 68.9 (C*sp^3*-C$_{60}$), 69.4 (-OCH$_2$-), 73.1 (C*sp^3*-C$_{60}$), 73.6 (-OCH$_2$-), 79.0 (CH pyrrolidine), 107.3 (Ar-H), 131.5, 135.3, 135.7, 136.3, 137.4, 137.8, 139.2, 140.0, 140.2, 140.3, 141.68, 141.73, 141.8, 141.8, 141.98, 142.04, 142.1, 142.2, 142.6, 142.7, 142.8, 143.11, 143.14, 144.4, 144.48, 144.54, 144.7, 145.2, 145.3, 145.4, 145.52, 145.54, 145.7, 145.8, 146.1, 146.2, 146.29, 146.33, 146.41, 146.44, 147.3, 147.4, 150.7, 152.9, 153.5, 154.8, 169.4 (C=O), 171.4 (C=O), 172.0 (C=O). HRMS (ESI-FT) *m/z*: [M-H]$^-$ Calc. for C$_{111}$H$_{90}$N$_3$O$_7$: 1576.6784; found: 1576.6762. ATR-FTIR (CHCl$_3$): 3299, 2924, 2853, 1731, 1658, 1508, 1438, 1229, 1163, 1114, 756, 726 cm^{-1}.
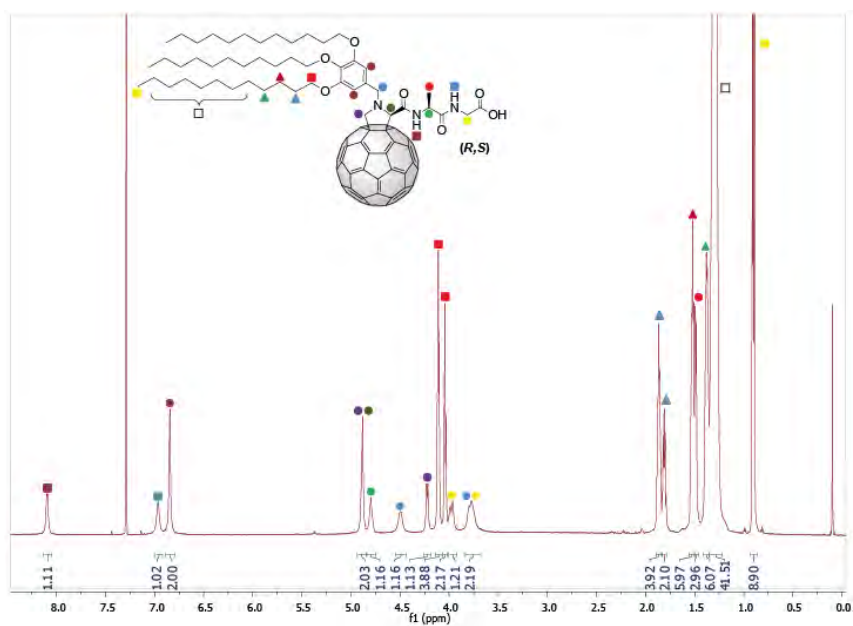
Figure 6.5 ^{1}H-NMR spectrum of compound **53** in CDCl$_3$.
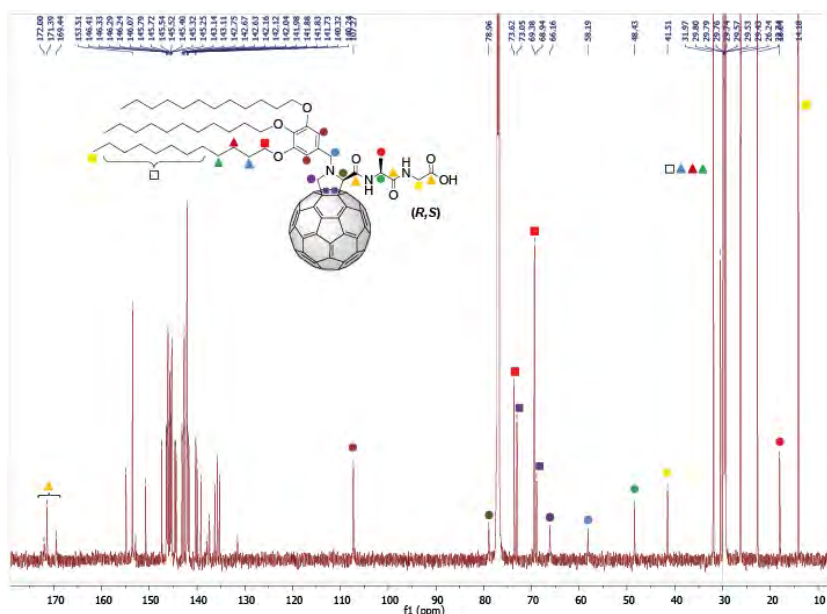
Figure 6.6 ^{13}C-NMR spectrum of compound **53** in CDCl$_3$.

N-[3,4,5-tris(dodecyloxy)benzyl]-2-(S)-(hydroxyglycyl-L-alanyl)carbonylpyrrolidino-[3,4:1,2][60]fullerene (54) (S,S)
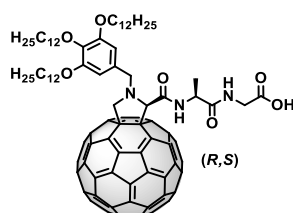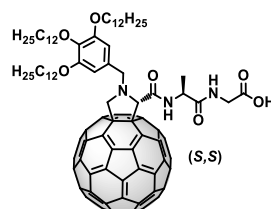

A solution of **52** (25 mg, 0.016 mmol) dissolved in a mixture of dioxane:TFA:HCl conc (1:2:2, 5 mL) was heated for 3 hours at 60°C. Then CH$_2$Cl$_2$ (15 mL) was added and an extraction with an aqueous solution of Na$_2$CO$_3$ was performed. The organic phase is dried over Na$_2$SO$_4$ and then it was filtrated and concentrated under reduced pressure until dryness. The purification of the desired product was performed by silica gel column chromatography using a mixture of CH$_2$Cl$_2$:MeOH (30:1) as eluent and was obtained as a brownish solid. Yield: 89% (22 mg). ^{1}H-NMR (700 MHz, CDCl$_3$): δ (ppm) 0.85-0.93 (m, 9H, 3Alk-CH$_3$), 1.23-1.41 (m, 51H, 48H-3Alk + CH$_3$-Ala), 1.47-1.58 (m, 6H,

196

3-OCH$_2$-CH$_2$-C*H$_2$*-), 1.78-1.84 (m, 2H, 1-OCH$_2$-C*H$_2$*-), 1.85-1.91 (m, 4H, 2-OCH$_2$-C*H$_2$*-), 3.60-3.69 (m, 1H, CH$_2$ benzylic), 3.92-4.23 (m, 9H, 3-OCH$_2$- + CH$_2$-Gly + 1H-CH$_2$ pyrrolidine), 4.52 (d, *J* = 10.4 Hz, 1H, CH$_2$ benzylic), 4.73-4.90 (m, 3H, CH-Ala + 1H-CH$_2$ pyrrolidine + CH pyrrolidine), 6.91 (s, 2H, Ar-H), 7.0-7.08 (m, 1H, NH-Gly), 8.35 (br s, 1H, NH-Ala). ^{13}C-NMR (175 MHz, CDCl$_3$): δ (ppm) 14.2 (Alk-CH$_3$), 18.8 (CH$_3$-Ala), 22.7, 26.2 (-OCH$_2$-CH$_2$-C*H$_2$*-), 26.3 (-OCH$_2$-CH$_2$-C*H$_2$*-), 29.4, 29.6, 29.7, 29.8, 30.5, 32.0, 41.5 (CH$_2$-Gly), 48.5 (CH-Ala), 59.2 (CH$_2$ benzylic), 66.5 (CH$_2$ pyrrolidine), 68.9, 69.3 (-OCH$_2$-), 73.1, 73.6 (-OCH$_2$-), 79.7 (CH pyrrolidine), 107.8 (Ar-H), 131.8, 135.4, 135.8, 136.1, 136.9, 137.7, 139.5, 140.1, 140.2, 140.30, 141.6, 141.7, 141.8, 141.9, 142.0, 142.1, 142.2, 142.7, 142.8, 143.1, 143.2, 144.4, 144.5, 144.6, 144.7, 145.2, 145.4, 145.45, 145.53, 145.7, 145.76, 145.82, 145.9, 146.07, 146.12, 146.2, 146.30, 146.35, 146.42, 146.6, 147.3, 147.4, 151.3, 152.8, 153.4, 155.1, 168.7 (C=O), 172.3 (C=O), 172.8 (C=O). HRMS (ESI-FT) *m/z*: [M-H]$^-$ Calc. for C$_{111}$H$_{90}$N$_3$O$_7$: 1576.6784; found: 1576.6744. ATR-FTIR (CHCl$_3$): 3351, 2920, 2850, 1728, 1656, 1508, 1435, 1222, 1161, 1109, 753, 722 cm^{-1}.

L-alanyl-glycyl-L-alanyl-glycyl-L-alanine-OH (55)[71]
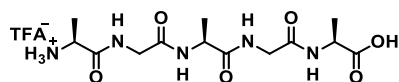
As mentioned in the discussion, standard solid phase using Fmoc chemistry on a Fmoc-Ala-Wang resin (300 mg) was used to synthesize pentapeptide **55** (Scheme 4.17). The resin was first swelled and rinsed with DMF and DCM. Deprotection of the Fmoc group was performed with a solution of piperidine (20%) in DMF for five minutes at room temperature. This process was repeated at least three times. Afterwards, the resin was washed several times with CH$_2$Cl$_2$ and DMF. The amino acid couplings were performed, in general, by adding to the resin a DMF solution of the Fmoc-protected amino acid **1** or **2** (3 eq., relative to the resin load = 1.0 - 1.2 mmol/g) previously activated with 3 eq. of HBTU and 7 eq. of DIPEA. After this, the resin was washed several times with DMF and DCM. Every step (amino acid couplings and Fmoc deprotection) was checked by the Kaiser test taking few beads from the chamber. The

cleavage of pentapeptide **55** from the resin was performed with a solution of trifluoroacetic acid and water (95:5) giving rise to the desired product with an amine and a carboxylic acid groups at the N-terminus and C-terminus positions, respectively. The resin was removed by filtration and washed with DCM. The filtrate was concentrated under reduced pressure and the peptide was precipitated by adding cold diethyl ether. The precipitate was filtered and washed with cold diethyl ether to obtain the peptide **55** as a white solid. Yield: 63% (87 mg). ^{1}H-NMR (300 MHz, MeOD-d_4): δ (ppm) 1.39 (d, J = 7.2 Hz, 3H, CH$_3$-Ala), 1.41 (d, J = 7.3 Hz, 3H, CH$_3$-Ala), 1.52 (d, J = 7.1 Hz, 3H, CH$_3$-Ala), 3.85-4.03 (m, 5H, CH-Ala + 2CH$_2$-Gly), 4.33 (q, J = 7.2 Hz, 1H, CH-Ala), 4.40 (q, J = 7.3 Hz, 1H, CH-Ala).

L-alanyl-glycyl-L-alanyl-glycyl-L-alanine-OMe (56)[71]
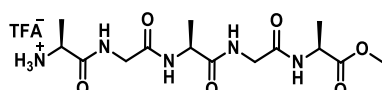
To a solution of the pentapeptide **55** (100 mg, 0.22 mmol) in MeOH (5 mL), a solution of trimethylsilyldiazomethane (1.5 mL, 3 mmol, 2M in hexane) was added dropwise. The mixture was stirred for 30 minutes and the solvent was removed until dryness. The remaining solid was dissolved in the minimum volume of methanol and the peptide was precipitated adding cold diethyl ether. After centrifugation the product **56** was obtained as a white solid that was used without further purification. Yield: 85% (88 mg). ^{1}H-NMR (300 MHz, MeOD-d_4): δ (ppm) 1.30 (d, J = 7.0 Hz, 3H, CH$_3$-Ala), 1.37-1.43 (m, 6H, 2CH$_3$-Ala), 3.72 (s, 3H, OMe), 3.82-3.98 (m, 5H, CH-Ala + 2CH$_2$-Gly), 4.27-4.36 (m, 1H, CH-Ala), 4.43 (q, J = 7.3 Hz, 1H, CH-Ala).

Fullerene-pentapeptide-methyl ester diastereoisomers (57 and 58)
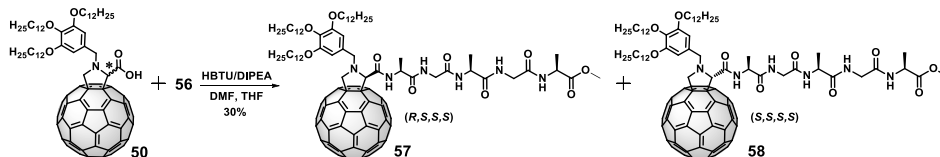
Carboxylic acid **50** (100 mg, 0.069 mmol) in a mixture of anhydrous DMF and dry THF (1:1, 10 mL) was activated by adding HBTU (39 mg, 0.102 mmol) and DIPEA (46 μL, 0.345 mmol) under argon atmosphere. After 5 minutes of activation, a solution of pentapeptide **56** (39 mg, 0.083 mmol) in anhydrous DMF (2 mL) was added. The mixture was stirred at room temperature for 2 hours. Then, CH_2Cl_2 (30 mL) was added and the resulting mixture was washed with an aqueous solution of Na_2CO_3 (3 x 30 mL). The organic phase was dried over Na_2SO_4, filtered and concentrated under reduced pressure. The purification of the respective diastereoisomers **57** and **58** was performed by preparative thin layer chromatography using a mixture of CH_2Cl_2:MeOH (30:1) as eluent. The diastereoisomers were obtained in a ratio of (1:1) as brownish solids.

N-[3,4,5-tris(dodecyloxy)benzyl]-2-(*R*)-(methoxy-L-alanyl-glycyl-L-alanyl-glycyl-L-alanyl)carbonylpyrrolidino-[3,4:1,2][60]fullerene (57) (*R,S,S,S*)
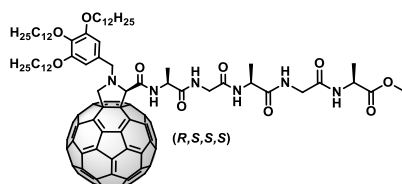
Diastereoisomer **57** was synthesized and purified as described previously. Yield: 30% (18 mg). ^{1}H-NMR (700 MHz, CDCl$_3$): δ (ppm) 0.88-0.92 (m, 9H, 3Alk-CH$_3$), 1.18-1.40 (m, 54H, 48H-Alk + 6H-CH$_3$-Ala), 1.41-1.46 (m, 3H, CH$_3$-Ala), 1.48-1.57 (m, 6H, 3-OCH$_2$-CH$_2$-*CH$_2$*-), 1.78-1.83 (m, 2H, 1-OCH$_2$-*CH$_2$*-), 1.84-1.90 (m, 4H, 2-OCH$_2$-*CH$_2$*-), 3.72 (s, 3H, OMe), 3.75-3.84 (m, 2H, CH$_2$-Gly), 3.85-3.91 (m, 1H, 1H-CH$_2$ benzylic), 3.95-4.14 (m, 8H, 3OCH$_2$ + CH$_2$-Gly), 4.27 (d, *J* = 9.5 Hz, 1H, CH$_2$ pyrrolidine), 4.50-4.59 (m, 2H, CH-Ala + 1H-CH$_2$ benzylic), 4.61-4.68 (m, 1H, CH-Ala), 4.72-4.81 (m, 1H, CH-Ala), 4.93-5.04 (m, 2H, CH pyrrolidine + 1H-CH$_2$ pyrrolidine), 6.87 (s, 2H, Ar-H), 7.28-7.50 (m, 4H, NH), 8.09 (br s, 1H, NH-Ala). ^{13}C-NMR (175 MHz, CDCl$_3$): δ (ppm) 14.2 (Alk-CH$_3$), 18.1 (CH$_3$-Ala), 18.4 (CH$_3$-Ala), 18.6 (CH$_3$-Ala), 22.7, 26.2, 29.4, 29.5, 29.68, 29.71, 29.73, 29.8, 30.4, 32.0, 43.1 (CH$_2$-Gly), 43.7 (CH$_2$-Gly), 48.0 (CH-Ala), 49.2 (CH-Ala), 49.6 (CH-Ala), 52.5 (OCH$_3$), 58.5 (CH$_2$ benzylic), 66.5 (CH$_2$ pyrrolidine), 69.1, 69.4 (OCH$_2$), 73.0, 73.6

(OCH$_2$), 79.1 (CH pyrrolidine), 107.3 (Ar-H), 131.6, 135.2, 135.8, 136.1, 137.2, 138.1, 139.1, 140.0, 140.3, 140.4, 141.6, 141.7, 141.8, 141.9, 142.0, 142.1, 142.2, 142.6, 142.69, 142.74, 142.8, 143.18, 143.24, 144.3, 144.4, 144.5, 144.7, 145.21, 145.25, 145.3, 145.4, 145.5, 145.67, 145.73, 146.1, 146.28, 146.31, 146.35, 146.40, 147.3, 147.5, 150.8, 153.3, 153.5, 153.6, 154.8, 168.1 (C=O), 168.3 (C=O), 170.0 (C=O), 172.3 (C=O), 172.4 (C=O), 173.6 (C=O). HRMS (ESI-FT) *m/z*: [M+Na]$^+$ Calc. for C$_{120}$H$_{106}$N$_6$O$_{10}$Na: 1813.7868; found: 1813.7863.

N-[3,4,5-tris(dodecyloxy)benzyl]-2-(S)-(methoxy-L-alanyl-glycyl-L-alanyl-glycyl-L-alanyl)carbonylpyrrolidino-[3,4:1,2][60]fullerene (58) (S,S,S,S)

Diastereoisomer **58** was synthesized and purified as described previously. Yield: 30% (18 mg). ^{1}H-NMR (700 MHz, CDCl$_3$): δ (ppm) 0.88-0.92 (m, 9H, 3Alk-CH$_3$), 1.15-1.40 (m, 54H, 48H-Alk + 6H-CH$_3$-Ala), 1.41-1.45 (m, 3H, CH$_3$-Ala), 1.48-1.56 (m, 6H, 3-OCH$_2$-CH$_2$-C*H$_2$*-), 1.78-1.83 (m, 2H, 1-OCH$_2$-C*H$_2$*-), 1.84-1.89 (m, 4H, 2-OCH$_2$-C*H$_2$*-), 3.69 (s, 3H, OMe), 3.90-4.18 (m, 12H, CH-Ala + 2CH$_2$-Gly + 3-OCH$_2$ + 1H-CH$_2$ benzylic), 4.20-4.28 (m, 1H-CH$_2$ pyrrolidine), 4.55-4.68 (m, 2H, CH-Ala + 1H-CH$_2$ benzylic), 4.70-4.79 (m, 1H, CH-Ala), 4.82-5.00 (m, 2H, CH pyrrolidine + 1H-CH$_2$ pyrrolidine), 6.91 (s, 2H, Ar-H), 7.39-7.80 (m, 4H, NH), 8.33 (br s, 1H, NH-Ala). ^{13}C-NMR (175 MHz, CDCl$_3$): δ (ppm) 14.2 (Alk-CH$_3$), 18.5 (CH$_3$-Ala), 19.1 (CH$_3$-Ala), 19.2 (CH$_3$-Ala), 22.7, 26.2, 26.3, 29.4, 29.6, 29.72, 29.74, 29.77, 29.79, 29.81, 29.83, 30.5, 32.0, 43.2 (CH$_2$-Gly), 43.3 (CH$_2$-Gly), 48.2 (CH-Ala), 48.7 (CH-Ala), 49.2 (CH-Ala), 52.6 (OCH$_3$), 57.6 (CH$_2$ benzylic), 65.8 (CH$_2$ pyrrolidine), 69.0, 69.3 (OCH$_2$), 73.2, 73.5 (OCH$_2$), 78.6 (CH pyrrolidine), 107.7 (Ar-H), 131.6, 135.3, 135.7, 136.2, 137.0, 137.8, 139.4, 139.8, 140.3, 141.8, 141.9, 142.0, 142.1, 142.6, 142.67, 142.73, 143.1, 143.2, 144.4, 144.48, 144.53, 144.7, 145.2, 145.3, 145.4, 145.5, 145.56, 145.62, 145.9, 146.1, 146.2, 146.27, 146.32, 146.6, 147.3, 147.4, 151.7, 153.2, 153.4, 155.1, 168.2 (C=O), 168.4 (C=O), 168.8 (C=O), 172.4 (C=O),

172.6 (C=O), 173.7 (C=O). HRMS (ESI-FT) *m/z*: [M+Na]$^+$ Calc. for $C_{120}H_{106}N_6O_{10}Na$: 1813.7868; found: 1813.7846.
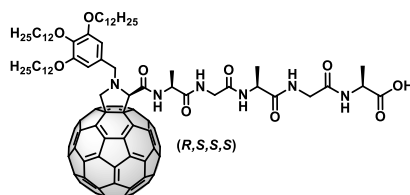
N-[3,4,5-tris(dodecyloxy)benzyl]-2-(R)-(hydroxy-L-alanyl-glycyl-L-alanyl-glycyl-L-alanyl)carbonylpyrrolidino-[3,4:1,2][60]fullerene (59) (R,S,S,S)

Methylester **57** (18 mg, 0.010 mmol) dissolved in a mixture of dioxane:TFA:HCl conc (1:2:2, 5 mL) was heated for 3 hours at 60°C. Then CH_2Cl_2 (15 mL) was added and an extraction with an aqueous solution of Na_2CO_3 was performed. The organic phase was dried over Na_2SO_4 and then it was filtrated and concentrated under reduced pressure until dryness. The purification of the desired product **59** was performed by silica gel column chromatography using a mixture of CH_2Cl_2:MeOH (10:1) as eluent and was obtained as a brownish solid. Yield: 40% (7 mg). ^{1}H-NMR (700 MHz, DMF-d_7/CS$_2$): δ (ppm) 1.08-1.16 (m, 9H, 3Alk-CH$_3$), 1.43-1.64 (m, 57H, 48H-Alk + 3CH$_3$-Ala), 1.71-1.78 (m, 6H, 3-OCH$_2$-CH$_2$-C*H$_2$*-), 1.93-1.98 (m, 2H, 1-OCH$_2$-C*H$_2$*-), 2.01-2.06 (m, 4H, 2-OCH$_2$-C*H$_2$*-), 3.90-3.96 (m, 1H, CH$_2$-Gly), 4.00-4.06 (m, 2H, CH$_2$-Gly), 4.09-4.14 (m, 1H, CH$_2$-Gly), 4.15-4.19 (m, 2H, -OCH$_2$-), 4.29-4.34 (m, 5H, 2-OCH$_2$- + 1H-CH$_2$ benzylic), 4.46-4.52 (m, 2H, CH-Ala), 4.60 (d, *J* = 9.3 Hz, 1H, CH$_2$ pyrrolidine), 4.72 (d, *J* = 13.2 Hz, 1H, CH$_2$ benzylic), 4.75-4.78 (m, 1H, CH-Ala), 5.31 (d, *J* = 9.1 Hz, 1H, CH$_2$ pyrrolidine), 5.35 (s, 1H, CH pyrrolidine), 7.26 (s, 2H, Ar-H), 8.02 (d, *J* = 6.9 Hz, 1H, NH-Ala), 8.33 (d, *J* = 6.6 Hz, 1H, NH-Ala), 8.39-8.42 (m, 1H, NH-Gly), 8.51-8.55 (m, 1H, NH-Gly), 9.30 (d, *J* = 6.1 Hz, 1H). ^{13}C-NMR (175 MHz, DMF-d$_7$/CS$_2$): δ (ppm) 14.4 (Alk-CH$_3$), 17.5 (CH$_3$-Ala), 17.7 (CH$_3$-Ala), 18.2 (CH$_3$-Ala), 23.16, 23.20, 26.7 (-OCH$_2$-CH$_2$-C*H$_2$*-), 29.4, 30.5, 31.0, 32.3, 32.4, 34.2, 42.5 (CH$_2$-Gly), 42.8 (CH$_2$-Gly), 48.1 (CH-Ala), 49.5 (CH-Ala), 49.7 (CH-Ala), 55.9 (CH$_2$ benzylic), 65.0 (CH$_2$ pyrrolidine), 68.9, 69.0, 69.9, 73.0, 73.6, 77.4 (CH pyrrolidine), 107.5 (Ar-H), 128.6, 132.9, 135.8, 136.0, 137.1, 137.3, 139.6, 139.7,

140.3, 141.9, 142.0, 142.18, 142.24, 142.3, 142.4, 142.69, 142.74, 142.8, 143.18, 143.23, 144.7, 144.81, 144.84, 145.36, 145.40, 145.46, 145.50, 145.54, 145.7, 145.9, 146.0, 146.15, 146.18, 146.3, 146.4, 146.5, 146.8, 147.38, 147.42, 147.5, 148.4, 153.4, 155.1, 155.7, 156.0, 168.8 (C=O), 167.9 (C=O), 169.4 (C=O), 172.7 (C=O), 172.8 (C=O), 174.1 (C=O). HRMS (ESI-FT) *m/z*: [M-H]$^-$ Calc. for $C_{119}H_{103}N_6O_{10}$: 1775.7741; found: 1775.7723. ATR-FTIR (CHCl$_3$): 3319, 2956, 2922, 2853, 1740, 1662, 1593, 1505, 1463, 1378, 1261, 1170, 1114, 1018, 802, 759, 721 cm^{-1}.

N-[3,4,5-tris(dodecyloxy)benzyl]-2-(*S*)-(hydroxy-L-alanyl-glycyl-L-alanyl-glycyl-L-alanyl)carbonylpyrrolidino-[3,4:1,2][60]fullerene (60) (*S,S,S,S*)
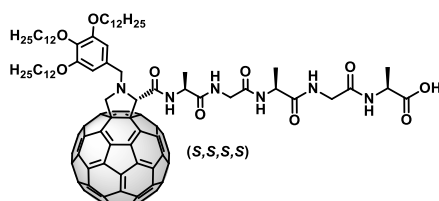

Methylester **58** (18 mg, 0.010 mmol) dissolved in a mixture of dioxane:TFA:HCl conc (1:2:2, 5 mL) was heated for 3 hours at 60°C. Then CH$_2$Cl$_2$ (15 mL) was added and an extraction with an aqueous solution of Na$_2$CO$_3$ was performed. The organic phase was dried over Na$_2$SO$_4$ and then it was filtrated and concentrated under reduced pressure until dryness. The purification of the desired product **60** was performed by silica gel column chromatography using a mixture of CH$_2$Cl$_2$:MeOH (10:1) as eluent and was obtained as a brownish solid. Yield: 73% (13 mg). ^{1}H-NMR (700 MHz, DMF-*d$_7$*/CS$_2$): δ (ppm) 1.10-1.16 (m, 9H, 3Alk-CH$_3$), 1.43 (d, *J* = 6.7 Hz, 3H, CH$_3$-Ala), 1.46 (d, *J* = 6.9 Hz, 3H, CH$_3$-Ala), 1.48-1.64 (m, 51H, 48H-Alk + CH$_3$-Ala), 1.72-1.79 (m, 6H, 3-OCH$_2$-CH$_2$-C*H$_2$*-), 1.93-1.98 (m, 2H, 1-OCH$_2$-C*H$_2$*-), 2.00-2.06 (m, 4H, 2-OCH$_2$-C*H$_2$*-), 3.82-3.87 (m, 1H, CH$_2$-Gly), 3.90-3.95 (m, 1H, CH$_2$-Gly), 4.00 (d, *J* = 12.2 Hz, 1H, CH$_2$ benzylic), 4.03-4.07 (m, 1H, CH$_2$-Gly), 4.12-4.18 (m, 2H, -OCH$_2$-), 4.20-4.27 (m, 2H, CH-Ala + 1H-CH$_2$-Gly), 4.28-4.37 (m, 4H, 2-OCH$_2$-), 4.48-4.56 (m, 2H, CH-Ala + 1H-CH$_2$ pyrrolidine), 4.76 (d, *J* = 12.2 Hz, 1H, CH$_2$ benzylic), 4.90-4.96 (m, 1H, CH-Ala), 5.06-5.12 (m, 2H, CH-pyrrolidine + 1H-CH$_2$ pyrrolidine), 7.23 (s, 2H, Ar-H), 7.80 (br s, 1H, NH), 8.48-8.76 (m,

3H, NH), 8.88 (br s, 1H, NH-Ala). ^{13}C-NMR (175 MHz, DMF-d_7/CS$_2$): δ (ppm) 14.6 (Alk-CH$_3$), 17.5 (CH$_3$-Ala), 18.1 (CH$_3$-Ala), 19.0 (CH$_3$-Ala), 23.4, 26.8 (-OCH$_2$-CH$_2$-C*H$_2$*-), 26.9 (-OCH$_2$-CH$_2$-C*H$_2$*-), 30.0, 30.38, 30.40, 30.43, 31.1, 32.5, 42.9 (CH$_2$-Gly), 48.6 (CH-Ala), 49.7 (CH-Ala), 55.1, 58.1 (CH$_2$ benzylic), 66.0 (CH$_2$ pyrrolidine), 68.9, 69.1, 73.0, 73.6, 79.2 (CH pyrrolidine), 108.1 (Ar-H), 132.5, 135.9, 136.0, 136.7, 137.3, 137.6, 139.5, 139.8, 140.4, 141.9, 142.0, 142.2, 142.3, 142.4, 142.5, 142.78, 142.82, 142.9, 143.2, 143.3, 144.7, 144.8, 144.9, 145.3, 145.4, 145.6, 145.7, 145.8, 145.89, 146.02, 146.06, 146.18, 146.21, 146.3, 146.4, 146.5, 146.6, 146.8, 147.4, 147.5, 147.6, 152.9, 153.4, 153.5, 154.3, 154.7, 156.1, 167.3 (C=O), 168.0 (C=O), 168.5 (C=O), 172.6 (C=O), 172.8 (C=O), 173.4 (C=O). HRMS (ESI-FT) *m/z*: [M-H]$^-$ Calc. for C$_{119}$H$_{103}$N$_6$O$_{10}$: 1775.7741; found: 1775.7770. ATR-FTIR (CHCl$_3$): 3312, 2955, 2921, 2852, 1739, 1660, 1590, 1504, 1462, 1377, 1260, 1169, 1113, 1019, 802, 761, 721 cm^{-1}.

Boc-L-alanyl-glycine (Boc-L-Ala-Gly) (61)[149]
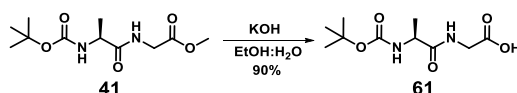
To a solution of dipeptide **41** (50 mg, 0.192 mmol) in a mixture of EtOH:H$_2$O, KOH (43 mg, 0.768 mmol) was added and the resulting mixture was heated to reflux for 30 minutes. Then, the mixture was cooled to room temperature and taken to neutral pH by adding aqueous HCl (1M). Afterwards, the solvent was evaporated under reduced pressure and an extraction with CH$_2$Cl$_2$ and water was performed. The organic phase was dried over Na$_2$SO$_4$, filtered and evaporated under reduced pressure. The product **61** was purified by a silica gel column chromatography using a mixture of CH$_2$Cl$_2$:MeOH (15:1) as eluent. The product was obtained as transparent oil. Yield: 90 % (43 mg). ^{1}H-NMR (300 MHz, MeOD-d_4): δ (ppm) 1.33 (d, *J* = 7.2, 3H, CH$_3$-Ala), 1.45 (s, 9H, *t*-Bu), 3.64-3.73 (m, 2H, CH$_2$-Gly), 4.04-4.15 (m, 1H, CH-Ala).

---

[149] J. Zhang, X. Li, Y. Jiang, J. Feng, X. Li, Y. Zhang, W. Xu, *Bioorg. Med. Chem.* **2014**, *22*, 3055-3064.

Bibliography

BIBLIOGRAPHY

[1] A. Mershin, K. Matsumoto, L. Kaiser, D. Yu, M. Vaughn, M. K. Nazeeruddin, B. D. Bruce, M. Graetzel, S. Zhang, *Sci. Rep.* **2012**, *2*, 234-240.

[2] J. Liu, *Phys. Chem. Chem. Phys.* **2012**, *14*, 10485-10496.

[3] J. Boekhoven, S. I. Stupp, *Adv. Mater.* **2014**, *26*, 1642-1659.

[4] J.-M. Lehn, *Angew. Chem. Int. Ed.* **1990**, *29*, 1304-1319.

[5] a) J.-M. Lehn, *Supramolecular Chemistry. Concepts and Perspectives*, Wiley-VCH, Weinheim, **1995**; b) J.-M. Lehn, J. L. Atwood, J. E. D. Davies, D. D. Macnicol, F. Vögtle, *Comprehensive Supramolecular Chemistry, Vol. 1-11*, Pergamon/Elsevier, Oxford, **1996**; c) P. D. Beer, P. A. Gale, D. K. Smith, *Supramolecular Chemistry*, Oxford University Press, Oxford, **1999**; d) J. W. Steed, J. L. Atwood, *Supramolecular Chemistry*, 2nd ed., John Wiley & Sons, Wiltshire, **2009**; e) N. Martín, J.-F. Nierengarten, *Supramolecular Chemistry of Fullerenes and Carbon Nanotubes*, Wiley-VCH, Weinheim, **2012**; f) J. W. Steed, P. A. Gale, *Supramolecular Chemistry: From Molecules to Nanomaterials*, John Wiley & Sons, **2012**; g) C. A. Schalley, *Analytical Methods in Supramolecular Chemistry*, 2nd ed., Wiley-VCH, Weinheim, **2012**.

[6] J. D. van der Waals, *Over de Continuiteit van den Gas- en Vloeistoftoestand*, PhD thesis, Leiden, **1873**.

[7] E. Fischer, *Ber. Deutsch. Chem. Ges.* **1894**, *27*, 2985-2993.

[8] a) T. S. Moore, T. F. Winmill, *J. Chem. Soc., Trans.* **1912**, *101*, 1635-1676; b) W. M. Latimer, W. H. Rodebush, *J. Am. Chem. Soc.*, **1920**, *42*, 1419–1433.

[9] J. W. Watson, F. H. C. Crick, *Nature* **1953**, *171*, 737-738.

[10] C. J. Pedersen, *J. Am. Chem. Soc.* **1967**, *89*, 7017-7036.

[11] B. Dietrich, J. M. Lehn, J. P. Sauvage, *Tetrahedron Lett.* **1969**, *10*, 2885-2888.

[12] D. J. Cram, T. Kaneda, R. C. Helgeson, G. M. Lehn, *J. Am. Chem. Soc.* **1979**, *101*, 6752-6754.

[13] M. Cesario, C. O. Dietrich-Buchecker, J. Guilhem, C. Pascard, J. P. Sauvage, *Chem. Commun.* **1985**, 244-247.

[14] K. S. Chichak, S. J. Cantrill, A. R. Pease, S.-H. Chiu, G. W. V. Cave, J. L. Atwood, J. F. Stoddart, *Science* **2004**, *304*, 1308-1312.

[15] H. Staudinger, *Berichte der deutschen chemischen Gesellschaft* **1920**, *53*, 1073-1085.

[16] T. Aida, E. W. Meijer, S. I. Stupp, *Science* **2012**, *335*, 813-817.

[17] a) G. Whitesides, J. P. Mathias, C. T. Seto, *Science* **1991**, *254*, 1312-1319; b) C. T. Seto, G. Whitesides, *J. Am. Chem. Soc.* **1993**, *115*, 905-916.

[18] a) S. I. Stupp, S. Son, H. C. Lin, L. S. Li, *Science* **1993**, *259*, 59-63; b) S. I. Stupp, V. LeBonheur, K. Walker, L. S. Li, K. E. Huggins, M. Keser, A. Amstutz, *Science* **1997**, *276*, 384-389.

[19] a) T. F. A. De Greef, M. M. J. Smulders, M. Wolffs, A. P. H. J. Shenning, R. P. Sijbesma, E. W. Meijer, *Chem. Rev.* **2009**, *109*, 5687-5754; b) Z. Chen, A. Lohr, C. R. Saha-Moller, F. Würthner, *Chem. Soc. Rev.* **2009**, *38*, 564-584.

[20] P. Cordier, F. Tournilhac, C. Soulié-Ziakovic, L. Leibler, *Nature* **2008**, *451*, 977-980.

[21] J. Hill, W. Jin, A. Kosaka, T. Fukushima, H. Ichihara, T. Shimonura, K. Ito, T. Hashizume, N. Ishii, T. Aida, *Science* **2004**, *304*, 1481-1483.

[22] S. I. Stupp, C. Palmer, *Chem. Mater.* **2014**, *26*, 507-518.

[23] R. P. Sijbesma, F. H. Beijer, L. Brunsveld, B. J. Folmer, J. H. Hirschberg, R. F. Lange, J. K. Lowe, E. W. Meijer, *Science* **1997**, *278*, 1601-1604.

[24] P. Jonkheijm, F. J. M. Hoeben, R. Kleppinger, J. van Herrikhuyzen, A. P. H. J. Schenning, E. W. Meijer, *J. Am. Chem. Soc.* **2003**, *125*, 15941-15949.

[25] F. J. M. Hoeben, L. M. Herz, C. Daniel, P. Jonkheijm, A. P. H. J. Schenning, C. Silva, S. C. J. Meskers, D. Beljonne, R. T. Phillips, R. H. Friend, E. W. Meijer, *Angew. Chem. Int. Ed.* **2004**, *43*, 1976-1979.

[26] F. J. M. Hoeben, A. P. H. J. Schenning, E. W. Meijer, *ChemPhysChem* **2005**, *6*, 2337-2342.

[27] V. K. Praveen, C. Ranjith, E. Bandini, A. Ajayaghosh, N. Armaroli, *Chem. Soc. Rev.* **2014**, *43*, 4222-4242.

[28] E. R. Zubarev, M. U. Pralle, E. D. Sone, S. I. Stupp, *J. Am. Chem. Soc.* **2001**, *123*, 4105-4106.

[29] B. W. Messmore, J. F. Hulvat, E. D. Sone, S. I. Stupp, *J. Am. Chem. Soc.* **2004**, *126*, 14452-14458.

[30] a) W. Jin, T. Fukushima, A. Kosaka, M. Niki, N. Ishii, T. Aida, *J. Am. Chem. Soc.* **2005**, *127*, 8284-8285; b) W. Zhang, W. Jin, T. Fukushima, A. Saeki, S. Seki, T. Aida, *Science* **2011**, *334*, 340-343.

[31] W. Jin, T. Fukushima, M. Niki, A. Kosaka, N. Ishii, T. Aida, *Proc. Natl. Acad. Sci.* **2005**, *102*, 10801-10806.

[32] Y. Yamamoto, T. Fukushima, W. Jin, A. Kosaka, T. Hara, T. Nakamura, A. Saeki, S. Seki, S. Tagawa, T. Aida, *Adv. Mater.* **2006**, *18*, 1297-1300.

[33] Y. Yamamoto, T. Fukushima, Y. Suna, N. Ishii, A. Saeki, S. Seki, S. Tagawa, M. Taniguchi, T. Kawai, T. Aida, *Science* **2006**, *314*, 1761-1764.

[34] Y. Yamamoto, G. Zhang, W. Jin, T. Fukushima, N. Ishii, A. Saeki, S. Seki, S. Tagawa, T. Minari, K. Tsukagoshi, T. Aida, *Proc. Natl. Acad. Sci.* **2009**, *106*, 21051-21056.

[35] J. D. Hartgerink, E. Beniash, S. I. Stupp, *Science* **2001**, *294*, 1684-1688.

[36] V. M. Tysseling-Mattiace, V. Sahni, K. L. Niece, D. Birch, C. Czeisler, M. G. Fehlings, S. I. Stupp, J. A. Kessler, *J. Neurosci.* **2008**, *28*, 3814-3823.

[37] K. Rajangam, H. A. Behanna, M. J. Hui, X. Han, J. F. Hulvat, J. W. Lomasney, S. I. Stupp, *Nano Lett.* **2006**, *6*, 2086-2090.

[38] A. Mata, Y. Geng, K. J. Henrikson, C. Aparicio, S. R. Stock, R. L. Satcher, S. I. Stupp, *Biomaterials* **2010**, *31*, 6004-6012.

[39] R. N. Shaha, N. A. Shahc, M. M. Del Rosario Lim, C. Hsieha, G. Nubere, S. I. Stupp, *Proc. Natl. Acad. Sci.* **2010**, *107*, 3293-3298.

[40] J. E. Goldberg, E. J. Berns, R. Bitton, C. J. Newcomb, S. I. Stupp, *Angew. Chem. Int. Ed.* **2011**, *50*, 6292-6295.

[41] S. E. Paramonov, H. W. Jun, J. D. Hartgerink, *J. Am. Chem. Soc.* **2006**, *128*, 7291-7298.

[42] T. Muraoka, H. Cui, S. I. Stupp, *J. Am. Chem. Soc.* **2008**, *130*, 2946-2947.

[43] J. D. Tovar, *Acc. Chem. Res.* **2013**, *46*, 1527-1537.

[44] V. Jayawarna, M. Ali, T. A. Jowitt, A. F. Miller, A. Saiani, J. E. Gough, R. V. Ulijn, *Adv. Mater.* **2006**, *18*, 611-614.

[45] Z. Yang, G. Liang, M. Ma, Y. Gao, B. Xu, *J. Mater. Chem.* **2007**, *17*, 850-854.

[46] R. Matmour, I. D. Cat, S. J. George, W. Adriaens, P. Leclère, P. H. H. Bomans, N. A. J. M. Sommerdijk, J. C. Gielen, P. C. M. Christianen, J. T. Heldens, J. C. M. van Hest, D. W. P. M. Löwik, S. D. Feyter, E. W. Meijer, A. P. H. J. Schenning, *J. Am. Chem. Soc.* **2008**, *130*, 14576-14583.

[47] M. Ma, Y. Kuang, Y. Gao, Y. Zhang, P. Gao, B. Xu, *J. Am. Chem. Soc.* **2010**, *132*, 2719-2728.

[48] S. R. Diegelmann, J. M. Gorham, J. D. Tovar, *J. Am. Chem. Soc.* **2008**, *130*, 13840-13841.

[49] S. R. Diegelmann, N. Hartman, N. Markovic, J. D. Tovar, *J. Am. Chem. Soc.* **2012**, *134*, 2028-2031.

[50] L. Tian, R. Szilluweit, R. Marty, L. Bertschi, M. Zerson, E.-C. Spitzner, R. Margerle, H. Frauenrath, *Chem. Sci.* **2013**, *3*, 1512-1521.

[51] H. Shao, T. Nguyen, N. C. Romano, D. A. Modarelli, J. R. Parquette, *J. Am. Chem. Soc.* **2009**, *131*, 16374-16376.

[52] D. T. Bong, T. D. Clark, J. R. Granja, M. R. Ghadiri, *Angew. Chem. Int. Ed.* **2001**, *40*, 988-1011.

[53] J. Montenegro, M. R. Ghadiri, J. R. Granja, *Acc. Chem. Res.* **2013**, *46*, 2955-2965.

[54] R. J. Brea, L. Castedo, J. R. Granja, M. A. Herranz, L. Sánchez, N. Martín, W. Seitz, D. M. Guldi, *Proc. Natl. Acad. Sci.* **2007**, *104*, 5291-5294.

[55] F. Wudl, G. M. Smith, E. J. Hufnagel, *J. Chem. Soc. D* **1970**, 1453-1454.

[56] J. Ferraris, D. O. Cowan, V. Walatka, J. H. Perlstei, *J. Am. Chem. Soc.* **1973**, *95*, 948-949.

[57] N. Martín, *Chem. Commun.* **2013**, *49*, 7025-7029.

[58] M. Bendikov, F. Wudl, D. F. Perepichka, *Chem. Rev.* **2004**, *104*, 4891-4995.

[59] F. G. Brunetti, J. L. López, C. Atienza, N. Martín, *J. Mater. Chem.* **2012**, *22*, 4188-4205.

[60] a) M. Wielopolski, C. Atienza, T. Clark, D. M. Guldi, N. Martín, *Chem. Eur. J.* **2008**, *14*, 6379-6390; b) A. Molina-Ontoria, G. Fernandez, M. Wielopolski, C. Atienza, L. Sánchez, A. Gouloumis, T. Clark, N. Martín, D. M. Guldi, *J. Am. Chem. Soc.* **2009**, *131*, 12218-12229.

[61] a) L. Sánchez, I. Pérez, N. Martín, D. M. Guldi, *Chem. Eur. J.* **2003**, *9*, 2457-2468; b) S. Castellanos, A. A. Vieira, B. M. Illescas, V. Sacchetti, C. Schubert, J. Moreno, D. M. Guldi, S. Hecht, N. Martín, *Angew. Chem. Int. Ed.* **2013**, *52*, 13985-13990.

[62] M. A. Herranz, N. Martín, S. Campidelli, M. Prato, G. Brehm, D. M. Guldi, *Angew. Chem. Int. Ed.* **2006**, *45*, 4478-4482.

[63] S. Wenger, P. A. Bouit, Q. L. Chen, J. Teuscher, D. Di Censo, R. Humphry-Baker, J. E. Moser, J. L. Delgado, N. Martín, S. M. Zakeeruddin, M. Grätzel, *J. Am. Chem. Soc.* **2010**, *132*, 5164-5169.

[64] E. M. Pérez, L. Sánchez, G. Fernández, N. Martín, *J. Am. Chem. Soc.* **2006**, *128*, 7172-7173; b) S. S. Gayathri, M. Wielopolski, E. M. Pérez, G. Fernández, L.

Sánchez, R. Viruela, E. Ortí, D. M. Guldi, N. Martín, *Angew. Chem. Int. Ed.* **2009**, *48*, 815-819.

[65] a) E. M. Pérez, N. Martín, *Chem. Soc. Rev.* **2008**, *37*, 1512-1519; b) D. Canevet, E. M. Pérez, N. Martín, *Angew. Chem. Int. Ed.* **2011**, *50*, 9248-9259; c) E. M. Pérez, N. Martín, *Chem. Soc. Rev.* **2015**, *44*, 6425-6433.

[66] H. Isla, M. Gallego, E. M. Pérez, R. Viruela, E. Ortí, N. Martín, *J. Am. Chem. Soc.* **2010**, *132*, 1772-1773.

[67] E. M. Pérez, A. L. Capodilupo, G. Fernández, L. Sánchez, P. M. Viruela, E. Ortí, M. Bietti, N. Martín, *Chem. Commun.* **2008**, *44*, 4567-4569.

[68] a) G. Fernández, E. M. Pérez, L. Sánchez, N. Martín, *Angew. Chem. Int. Ed.* **2008**, *47*, 1094-1097; b) H. Isla, E. M. Pérez, N. Martín, *Angew. Chem. Int. Ed.* **2014**, *53*, 5629-5633.

[69] C. R Nieto, R. García, M. A. Herranz, C. Ehli, M. Ruppert, A. Hirsch, D. M. Guldi, N. Martín, *J. Am. Chem. Soc.* **2012**, *134*, 9183-9192.

[70] F. G. Brunetti, C. R. Nieto, J. López-Andarias, C. Atienza, J. L. López, D. M. Guldi, N. Martín, *Angew. Chem. Int. Ed.* **2013**, *52*, 2180-2184.

[71] J. López-Andarias, J. L. López, C. Atienza, F. G. Brunetti, C. R. Nieto, D. M. Guldi, M. Martín, *Nat. Commun.* **2014**, *5*, 3763.

[72] A. de Juan, Y. Pouillon, L. Ruiz-Gonzalez, A. Torres-Pardo, S. Casado, N. Martín, Á. Rubio, E. M. Pérez, *Angew. Chem. Int. Ed.* **2014**, *53*, 5394-5400.

[73] J.L López, C. Atienza, W. Seitz, D. M. Guldi, N. Martín, *Angew. Chem. Int. Ed.* **2010**, *49*, 9876-9880.

[74] J. López-Andarias, M. J. Rodríguez, C. Atienza, J. L. López, T. Mikie, S. Casado, S. Seki, J. L. Carrascosa, N. Martín, *J. Am. Chem. Soc.* **2015**, *137*, 893-897.

[75] H. W. Kroto, J. R. Heath, S. C. O'Brien, R. F. Curl, R. E. Smalley, *Nature* **1985**, *318*, 162-163.

[76] a) *Fullerenes. Chemistry and reactions.*, (Ed. A. Hirsch and M. Brettreich), Wiley-VCH, **2005**; b) D. M. Guldi and N. Martin, *Fullerenes: From Synthesis to Optoelectronic Properties*, Springer, **2002**.

[77] Q. Xie, E. Pérez-Cordero, L. Echegoyen, *J. Am. Chem. Soc.* **1992**, *114*, 3978-3980.

[78] H. Ajie, M. M. Alvarez, S. J. Anz, R. D. Beck, F. Diederich, K. Fostiropoulos, D. R. Huffman, W. Kraetschmer, Y. Rubin, K. E. Schriver, D. Sensharma, R. L. Whetten, *J. Phys. Chem.* **1990**, *94*, 8630-8633.

[79] I. Hiroshi, H. Kiyoshi, A. Tsuyoshi, A. Masanori, T. Seiji, O. Tadashi, S. Masahiro and S. Yoshiteru, *Chem. Phys. Lett.* **1996**, *263*, 545-550.

[80] B. C. Thompson, J. M. J. Frechet, *Angew. Chem. Int. Ed.* **2008**, *47*, 58-77.

[81] a) J. L. Delgado, P. A. Bouit, S. Filippone, M. A. Herranz, N. Martín, *Chem. Commun.* **2010**, *46*, 4853-4865; b) J. E. Anthony, A. Facchetti, M. Heeney, S. R. Marder, X. Zhan, *Adv. Mater.* **2010**, *22*, 3876-3892.

[82] Y. Zhang, M. Wang, S. D. Collins, H. Zhou, H. Phan, C. Proctor, A. Mikhailovsky, F. Wuld, T.-Q. Nguyen, *Angew. Chem. Int. Ed.* **2014**, *53*, 244-249.

[83] D. M. Guldi, B. M. Illescas, C. Atienza, M. Wielopolski, N. Martín, *Chem. Soc. Rev.* **2009**, *38*, 1587-1597.

[84] A. S. Konev, A. F. Khlebnikov, P. I. Prolubnikov, A. S. Mereschenko, A. V. Povolotskiy, O. V. Levin, A. Hirsch, *Chem. Eur. J.* **2015**, *21*, 1237-1250.

[85] Y. Huang, E. J. Kramer, A. J. Heeger, G. C. Bazan, *Chem. Rev.* **2014**, *114*, 7006-7043.

[86] S. A. Mauger, L. Chang, S. Friedrich, C. W. Rochester, D. M. Huang, P. Wang, A. J. Moulé, *Adv. Funct. Mater.* **2013**, *23*, 1935-1946.

[87] S. S. Babu, H, Möhwald, T. Nakanishi, *Chem. Soc. Rev.* **2010**, *39*, 4021-4035.

[88] R. Bhosale, J. Misek, N. Sakai, S. Matile, *Chem. Soc. Rev.* **2010**, *39*, 138-149.

[89] Y. Hizume, T. Tashiro, R. Charvet, Y. Yamamoto, A. Saeki, S. Seki, T. Aida, *J. Am. Chem. Soc.* **2010**, *132***, 6628-6629.

[90] A. Muñoz, B. M. Illescas, M. Sánchez-Navarro, J. Rojo, N. Martín, *J. Am. Chem. Soc.* **2011**, *133*, 16758-16761.

[91] T. Nakanishi, *Chem. Commun.* **2010**, *46*, 3425-3436.

[92] S. S. Babu, A. Saeki, S. Seki, H. Möhwald, T. Nakanishi, *Phys. Chem. Chem. Phys.* **2011**, *13*, 4830-4834.

[93] Y. Shen, T. Nakanishi, *Phys. Chem. Chem. Phys.* **2014**, *16*, 7199-7204.

[94] T. Nakanishi, N. Miyashita, T. Michinobu, Y. Wakayama, T. Tsuruoka, K. Ariga, D. G. Kurth, *J. Am. Chem. Soc.* **2006**, *128*, 6328-6329.

[95] T. Nakanishi, Y. Shen, J. Wang, S. Yagai, M. Funahashi, T. Kato, P. Fernandes, H. Möhwald, D. G. Kurth, *J. Am. Chem. Soc.* **2008**, *130*, 9236-9237.

[96] C.-C. Chu, G. Raffy, D. Ray, A. D. Guerzo, B. Kauffmann, G. Wantz, L. Hirsch, D. M. Bassani, *J. Am. Chem. Soc.* **2010**, *132*, 12717-12723.

[97] R. Charvet, Y. Yamamoto, T. Sasaki, J. Kim, K. Kato, M. Takata, A. Saeki, S. Seki, T. Aida, *J. Am. Chem. Soc.* **2012**, *134*, 2524-2527.

[98] D. M. Guldi, A. Gouloumis, P. Vázquez, T. Torres, V. Georgakilas, M. Prato, *J. Am. Chem. Soc.* **2005**, *127*, 5811-5813.

[99] R. Charvet, S. Acharya, J. P. Hill, M. Akada, M. Liao, S. Seki, Y. Honsho, A. Saeki, K. Ariga, *J. Am. Chem Soc.* **2009**, *131*, 18030-18031.

[100] G. D. Pantos, J.-L. Wietor, J. K. M. Sanders, *Angew. Chem. Int. Ed.* **2007**, *46*, 2238-2240.

[101] E. Lee, J.-K. Kim, M. Lee, *J. Am. Chem. Soc.* **2009**, *131*, 18242-18243.

[102] T. Kawaguchi, J. Kumaki, A. Kitaura, K. Okoshi, H. Kusanagi, K. Kobayashi, T. Sugai, H. Shinohara, E. Yashima, *Angew. Chem. Int. Ed.* **2008**, *47*, 515-519.

[103] X. Zhang, M. Takeuchi, *Angew. Chem. Int. Ed.* **2009**, *48*, 9646-9651.

[104] T. Hasobe, A. S. D. Sandanayaka, T. Wadac, Y. Arakic, *Chem. Commun.* **2008**, *44*, 3372-3374.

[105] Z. Su, B. Yu, X. Jiang, J. Yin, *Macromulecules* **2013**, *46*, 3699-3707.

[106] S. I. Yang, J. Seth, J.-P. Strachan, S. Gentemann, D. Kim, D. Holten, J. S. Lindsey, D. F. Bocian, *J. Porphyrins Phthalocyanines* **1999**, *3*, 117-147.

[107] J. H. Fuhrhop, D. Mauzerall, *J. Am. Chem. Soc.* **1969**, *91*, 4174-4181.

[108] a) R. A. Reed, R. Purrello, K. Prendergast, T. G. Spiro, *J. Phys. Chem.* **1991**, *95*, 9720-9727. b) A. Harriman, G. Porter , N. Searle, *J. Chem. Soc., Faraday Trans. 2* **1979**, *75*, 1515-1521.

[109] Y. Sun, T. Drovetskaya, R. D. Bolskar, R. Bau, P. D. W. Boyd, C. A. Reed, *J. Org. Chem.* **1997**, *62*, 3642-3649.

[110] M. Kimura, Y. Saito, K. Ohta, K. Hanabusa, H. Shirai, N. Kobayashi, *J. Am. Chem. Soc.* **2002**, *124*, 5274-5275.

[111] a) J. Song, N. Aratani, H. Shinokubo and A. Osuka, *J. Am. Chem. Soc.* **2010**, *132*, 16356-16357; b) W. Meng, B. Breiner, K. Rissanen, J. D. Thoburn, J. K. Clegg, J. R. Nitschke, *Angew. Chem. Int. Ed.* **2011**, *50*, 3479-3483.

[112] D. Sun, F. S. Tham, C. A. Reed, L. Chaker, P. D. W. Boyd, *J. Am. Chem. Soc.* **2002**, *124*, 6604-6612.

[113] K. Tashiro, T. Aida, J.-Y. Zheng, K. Kinbara, K. Saigo, S. Sakamoto, K. Yamaguchi, *J. Am. Chem. Soc.* **1999**, *121*, 9477-9478.

[114] a) A. Hosseini, S. Taylor, G. Accorsi, N. Armaroli, C. A. Reed and P. D. W. Boyd, *J. Am. Chem. Soc.* **2006**, *128*, 15903-15913; b) Z.-Q. Wu, X.-B. Shao, C. Li, J.-L. Hou, K. Wang, X.-K. Jiang, Z.-T. Li, *J. Am. Chem. Soc.* **2005**, *127*, 17460-17468.

[115] A. Satake, Y. Kobuke, *Tetrahedron* **2005**, *61*, 13-41.

[116] F. D'Souza, P. M. Smith, M. E. Zandler, A. L. McCarty, M. Itou, Y. Araki, O. Ito, *J. Am. Chem. Soc.* **2004**, *126*, 7898-7907.

[117] a) J. L. Sessler, B. Wang, A. Harriman, *J. Am. Chem. Soc.* **1993**, *115*, 10418-10419; b) P. de Rege, S. Williams, M. Therien, *Science* **1995**, *269*, 1409-1413.

[118] L. Sánchez, M. Sierra, N. Martín, A. J. Myles, T. J. Dale, J. Rebek, W. Seitz, D. M. Guldi, *Angew. Chem. Int. Ed.* **2006**, *45*, 4637-4641.

[119] a) J. P. Kirby, J. A. Roberts, D. G. Nocera, *J. Am. Chem. Soc.* **1997**, *119*, 9230-9236; b) N. H. Damrauer, J. M. Hodgkiss, J. Rosenthal, D. G. Nocera, *J. Phys. Chem. B* **2004**, *108*, 6315-6321.

[120] a) N. Solladié, M. E. Walther, M. Gross, T. M. F. Duarte, C. Bourgogne, J.-F. Nierengarten, *Chem. Commun.* **2003**, 2412-2413; b) L. Moreira, J. Calbo, B. M. Illescas, J. Aragó, I. Nierengarten, B. D. Nicot, E. Ortí, N. Martín, J.-F. Nierengarten, *Angew. Chem. Int. Ed.* **2015**, *54*, 1255-1260.

[121] N. Solladié, M. E. Walther, H. Herschbach, E. Leize, A. V. Dorsselaer, T. M. F. Duarte, J.-F. Nierengarten, *Tetrahedron* **2006**, *62*, 1979-1987.

[122] J.-L. Hou, H.-P- Yi, X.-B. Shao, C. Li, Z.-Q. Wu, X.-K. Jiang, L.-Z. Wu, C.-H. Tung, Z.-T. Li, *Angew. Chem. Int. Ed.* **2006**, *45*, 796-800.

[123] S. González, N. Martín, D. M. Guldi, *J. Org. Chem.* **2002**, *68*, 779-791.

[124] J. C. M. van Hest, D. A. Tirell, *Chem. Commun.* **2001**, 1897-1904.

[125] K. J. Channon, G. L. Devlin, S. W. Magennis, C. E. Finlayson, A. K. Tickler, C. Silva, C. E. MacPhee, *J. Am. Chem. Soc.* **2008**, *130*, 5487-5491.

[126] a) a) A. Barth, C. Zscherp, *Q. Rev. Biophys.* **2002**, *35*, 369-430; b) Y. Cordeiro, J. Kraineva, M. P. B. Gomes, M. H. Lopes, V. R. Martins, L. M. T. R. Lima, D. Foguel, R. Winter, J. L. Silva, *Biophys. J.* **2005**, *89*, 2667–2676; c) H. Shao, J. R. Parquette, *Chem. Commun.* **2010**, *46*, 4285-4287.

[127] a) M. Zelzer, R. V. Ulijn, *Chem. Soc. Rev.* **2010**, *39*, 3351-3357; b) E. De Santis, M.G. Radnov, *Chem. Soc. Rev.* **2015**, DOI: 10.1039/c5cs00470e.

[128] A. M. Smith, R. J. Williams, C. Tang, P. Coppo, R. F. Collins, M. L. Turner, A. Saiani, R. V. Ulijn, *Adv. Mater.* **2008**, *20*, 37-41.

[129] E. D. T. Atkins, in *Supramolecular and Colloidal Structures in Biomaterials and Biosubtrates*, Wordscientific, UK, **1999**.

[130] J. C. Hummelen, B. W. Knight, F. LePeq, F. Wudl, *J. Org. Chem*. **1995**, *60*, 532-538.

[131] a) G. Fernández, E. M. Pérez, L. Sánchez, N. Martín, *J. Am. Chem. Soc.* **2008**, *130*, 2410-2411; b) G. Grimm, J. Santos, B. M. Illescas, A. Muñoz, D. M. Guldi, N. Martín, *J. Am. Chem. Soc.* **2010**, *132*, 17387-17389.

[132] a) J. Lenoble, N. Maringa, S. Campidelli, B. Donnio, D. Guillon, R. Deschenaux, *Org. Lett.* **2006**, *8*, 1851-1854; b) M. Makha, A. Purich, C. L. Raston, A. N. Sobolev, *Eur. J. Inorg. Chem*. **2006**, 507–517.

[133] L. Isaacs, A. Wehrsig, F. Diederich, *Helv. Chim. Acta*, **1993**, *76*, 1231-1250.

[134] a) E. E. Maroto, S. Filippone, A. Martín-Domenech, M. Suárez, N. Martín, *J. Am. Chem. Soc.* **2012**, *134*, 12936–12938; b) K. Swai, Y. Takano, M. Izquierdo, S. Filippone, N. Martín, Z. Slanina, N. Mizorogi, M. Waelchli, T. Tsuchiya, T. Akasaka, S. Nagase, *J. Am. Chem. Soc.* **2011**, *133*, 17746-17752.

[135] R. V. Bensasson, E. Bienvenue, M. Dellinger, S. Leach, P. Seta, *J. Phys. Chem.* **1994**, *98*, 3492-3500.

[136] W. Kratschmer, L. D. Lamb, K. Fostiropoulos, D. R. Huffmann, *Nature* **1990**, *347*, 354-358.

[137] G. Dan Pantos, J. L. Wietor, J. K. M. Sanders, *Angew. Chem. Int. Ed.* **2007**, *46*, 2238-2240.

[138] F. Diederich, J. Effing, U. Jonas, L. Jullien, T. Plesnivy, H. Ringsdorf, C. Thilgen, D. Weinstein, *Angew. Chem. Int. Ed.* **1992**, *31*, 1599-1602.

[139] a) J. Coro, H. Rodríguez, D. G. Rivera, M. Suárez, D. Molero, M. A. Herranz, R. Martínez-Álvarez, S. Filippone, N. Martín, *Eur. J. Org. Chem.* **2009**, *28*, 4810-4817; b) A. Ruiz, J. Coro, L. Almagro, J. A. Ruiz, D. Molero, E. E. Maroto, S. Filippone, M. A. Herranz, R. Martínez-Álvarez, J. C. Sancho-García, F. D. Meo, M. Suárez, N. Martín, *J. Org. Chem.* **2013**, *78*, 2819-2826.

[140] V. Castelletto, I. W. Hamley, *J. Phys. Chem. B* **2010**, *114*, 8002-8008.

[141] F. Aparicio, E. Matesanz, L. Sánchez, *Chem. Eur. J.* **2014**, *20*, 14599-14603.

[142] J. Otsuki, K. Iwsaki, Y. Nakano, M. Itou, Y. Araki, O. Ito, *Chem. Eur. J.* **2004**, *10*, 3461-3466.

[143] M. S. Newman, L. F. Lee, *J. Org. Chem.* **1972**, *37*, 4468-4469.

[144] J. Marco-Martínez, V. Marcos, S. Reboredo, S. Filippone, N. Martín, *Angew. Chem. Int. Ed.* **2013**, *52*, 5115-5119.

[145] J. Jiang, O. V. Lima, Y. Pei, Z. Jiang, Z. Chen, C. Yu, J. Wang, X. Cheng, E. Forsythe, L. Tan, *ACSNano* **2010**, *4*, 3773-3780.

[146] A. J. Moore, M. R. Bryce, *Synthesis* **1991**, *1991*, 26-28.

[147] L. Isaacs, F. Diederich, *Helv. Chim. Acta* **1993**, *76*, 2554-2464.

[148] V. Percec, M. Peterca, T. Tadjiev, X. Zeng, G. Ungar, P. Leowanawat, E. Aqad, M. R. Imam, B. M. Rosen, U. Akbey, R. Graf, S. Sekharan, D. Sebastiani, H. W. Spiess, P. A. Heiney, S. D. Hudson, *J. Am. Chem. Soc.* **2011**, *133*, 12197–12219.

[149] J. Zhang, X. Li, Y. Jiang, J. Feng, X. Li, Y. Zhang, W. Xu, *Bioorg. Med. Chem.* **2014**, *22*, 3055-3064.